

2019

Anticancer Mutual Prodrugs Activated by Hypoxia

Geraud N. Sansom
University of Wollongong

Follow this and additional works at: <https://ro.uow.edu.au/theses1>

University of Wollongong

Copyright Warning

You may print or download ONE copy of this document for the purpose of your own research or study. The University does not authorise you to copy, communicate or otherwise make available electronically to any other person any copyright material contained on this site.

You are reminded of the following: This work is copyright. Apart from any use permitted under the Copyright Act 1968, no part of this work may be reproduced by any process, nor may any other exclusive right be exercised, without the permission of the author. Copyright owners are entitled to take legal action against persons who infringe their copyright. A reproduction of material that is protected by copyright may be a copyright infringement. A court may impose penalties and award damages in relation to offences and infringements relating to copyright material.

Higher penalties may apply, and higher damages may be awarded, for offences and infringements involving the conversion of material into digital or electronic form.

Unless otherwise indicated, the views expressed in this thesis are those of the author and do not necessarily represent the views of the University of Wollongong.

Recommended Citation

Sansom, Geraud N., *Anticancer Mutual Prodrugs Activated by Hypoxia*, Doctor of Philosophy thesis, School of Chemistry and Molecular Bioscience, University of Wollongong, 2019. <https://ro.uow.edu.au/theses1/775>

Research Online is the open access institutional repository for the University of Wollongong. For further information contact the UOW Library: research-pubs@uow.edu.au

Anticancer Mutual Prodrugs Activated by Hypoxia

A thesis submitted in fulfilment of the requirements for the award of the degree

Doctor of Philosophy



The University of Wollongong

by

Geraud N. Sansom

Supervisor – Professor Michael Kelso
School of Chemistry and Molecular Bioscience

August, 2019

Declaration

I, Geraud N. Sansom, declare that this thesis, submitted in fulfilment of the requirements for the award of Doctor of Philosophy in the School of Chemistry and Molecular Bioscience, University of Wollongong, is wholly my own work unless otherwise referenced or acknowledged. The work has not been submitted for at any other academic institution.

Geraud N. Sansom

30/08/2019

Acknowledgments

I would like to dedicate this thesis to my loving mother, Sheila Sansom, who lost her 8-year battle with recurrent breast cancer on the 20th of February 2014, during my Honours year. She fought longer and harder than anyone could have expected, always pressing on, thinking about her three children and husband first. She was my inspiration to go into cancer research and I thank her for everything I have achieved so far.

I would like to thank the rest of my family: my father Philip, my older brother Sebastien and his wife Segolene, my younger brother Travers as well as Richard and Lisa for your support and patience throughout my PhD; and for all the video game distractions and fun times.

A huge thank you to my supervisor, Prof. Michael Kelso, for his guidance and the large amount of time he devoted to helping me with my PhD. I have learnt an insane amount through your support and hope to continue our amazing working relationship into my future career.

I would also like to thank the Kelso Research Group, past and present members: Richard, Alex, Ben, Ashraf, Ramesh, Ardeshir, Hiwa, Nehad, Nick, Poppy, Tim, Zander and Jess for all the joy they brought me in the lab and in life. Also, to all the international students that made my experience even more amazing: Aitziber, Jan, Florian, Caroline, Kristin and Carolin.

Thank you to all the other PhD students who made my time at UOW so memorable. For all the conversations about life and the universe at lunch. For the long and always interesting DnD nights. Friday night drinks and the Wollongong nightlife routine. Hikes with friends and all the nice time spent together.

Thank you to those who listened to me when I needed it most and helped me through one of the most challenging periods in my life. Thank you so much to everyone who helped me get through my PhD, I couldn't have done it alone.

Geraud Sansom.

Publications Arising from the Thesis

1. Kirk, N. S.; Sansom, G. N.; Sudta, P.; Suksamrarn, S.; Willis, A. C.; Bremner, J. B.; Kelso, M. J., Unexpected synthesis of 3-imino-2-(pyrrol-2-yl) isatogen derivatives affords facile access to a 2-pyrrolyl isatogen. *Synth. Commun.* 2017, 47 (1), 62-67.
2. Sansom, G. N.; Kirk, N. S.; Guise, C. P.; Anderson, R. F.; Smaill, J. B.; Patterson, A. V.; Kelso, M. J., Prototyping kinase inhibitor-cytotoxin anticancer mutual prodrugs activated by tumour hypoxia: A chemical proof of concept study. *Bioorg. Med. Chem. Lett.* 2019, 29 (10), 1215-1219.

Manuscripts in Preparation

3. Sansom, G. N.; Semken, J. L. K.; Richardson, C.; Smaill, J. B.; Patterson, A. V.; Anderson, R. F.; Kelso, M. J., Optimisation of nitroaromatic reduction potentials in kinase inhibitor - cytotoxin anticancer mutual prodrugs leads to discovery of new a new route to pyrroloquinoline fluorophores. To be submitted to *Tetrahedron Lett.*

Contents

Declaration	i
Acknowledgments	ii
Publications Arising from the Thesis	iii
Manuscripts in Preparation	iii
Contents	iv
Abbreviations	xii
List of Figures	xv
List of Schemes	xix
List of Tables	xxiv
Abstract	xxv
Chapter 1: Introduction	1
1.1 A Brief History of Cancer Treatments	1
1.2 Project Summary	4
1.3 Angiogenesis Inhibitors in Cancer Treatment	4
1.3.1 Semaxanib (SU5416) and Sunitinib (Sutent®)	5
1.3.2 Mechanisms of Angiogenesis Inhibition	6
1.4 Mechanism of Nitrogen Mustard Cytotoxicity	6
1.5 5-Fluorouracil (5-FU)	7
1.5.1 Mechanisms of 5-FU Cytotoxicity	7
1.5.2 Floxuridine	9
1.6 Prodrugs in Anticancer Chemotherapy	10
1.6.1 Mutual Prodrugs	10
1.6.2 Tumour-Selective Activation of Antitumour Prodrugs	11
1.7 Antibody-Drug Conjugates	11
1.7.1 Brentuximab vedotin (Adcetris®)	12
1.7.2 Trastuzumab emtansine (Kadcyla®)	12
1.8 Bioreductive Activation of Antitumour Prodrugs	13
1.8.1 Enzymatic Activation of Prodrugs by Reductases	14
1.9 Quinones as Hypoxia-Activated Prodrugs	15
1.9.1 Apaziquone	15
1.10 <i>N</i> -oxides as Hypoxia-Activated DNA Intercalator Prodrugs	16
1.10.1 Banoxantrone (AQ4N) – A Tertiary Amine- <i>N</i> -oxide	16

1.10.2 Tirapazamine (TPZ) – An Aromatic-N-oxide	17
1.11 Metal Complexes as Prodrugs Designed for Bioreductive Activation	18
1.11.1 Examples of Cobalt(III) Hypoxia Activated Prodrugs	19
1.11.2 Example of a Copper(II) Hypoxia Activated Prodrug	20
1.12 Nitroaromatics as Hypoxia-Activated Prodrugs	20
1.12.1 PR-104	20
1.12.2 Evofosfamide (TH-302)	22
1.12.3 Nitroaromatic Prodrug of a 4-Aminoaniline mustard	23
1.13 Molecularly Targeted Hypoxia Activated Prodrugs	23
1.13.1 Nitroaromatic Molecularly Targeted Hypoxia Activated Prodrugs	24
1.14 Design of Hypoxia-Activated Semaxanib Cytotoxin Mutual Prodrugs	25
1.15 Project Aims	27
Chapter 2: Synthesis of Semaxinib 4-Aminoaniline Mustard 1	28
2.1 Route Development	28
2.2 Amide Coupling	29
2.2.1 Spectroscopic Evidence for the Formation of 4	30
2.3 <i>Bis</i> -Alkylation of 4	30
2.3.1 Spectroscopic Evidence for the Formation of 5	32
2.4 <i>Bis</i> -TBS Protection of 5	32
2.4.1 Mechanism of <i>Bis</i> -TBS Protection	33
2.4.2 Spectroscopic Evidence for the Formation of 6	34
2.5 Knoevenagel Condensation of 6	35
2.5.1 Knoevenagel Reaction Mechanism	36
2.5.2 Optimising the Yield of (Z)- 8	37
2.5.3 Spectroscopic Evidence for the Formation of (Z)- 8	39
2.6 <i>Bis</i> -TBS Deprotection of (Z)- 8	40
2.6.1 Spectroscopic Evidence for the Formation of 9	41
2.7 <i>Bis</i> -Mesylation/Chlorination of 9 to give Mutual Prodrug 1	42
2.8 2D Spectroscopic Analysis of 1	43
2.8.1 ¹³ C APT NMR Analysis of 1	44
2.8.2 NOESY NMR Analysis of 1	45
2.8.3 gCOSY NMR Analysis of 1	45
2.8.4 gHSQC NMR Analysis of 1	46
2.8.5 gHMBC NMR Analysis of 1	47

2.9	Summary of the Scale-Up Synthesis of 1	48
Chapter 3: Synthesis of Semaxanib Floxuridine Mutual Prodrug 2		50
3.1	Route Development	50
3.2	TBS Protection of Floxuridine	51
3.2.1	Mechanism of Bis-TBS Protection	52
3.2.2	Spectroscopic Evidence for the Formation of 14	52
3.3	2,4-Dimethoxybenzoyl Protection of 14	53
3.3.1	Mechanism of 2,4-Dimethoxybenzoyl Protection of 14 with DMAP/DIPEA	55
3.3.2	Spectroscopic Evidence for the Formation of 20	55
3.4	Primary Alcohol Selective Deprotection in 20	56
3.4.1	Spectroscopic Evidence for the Formation of 21	58
3.5	Steglich Esterification of 21	58
3.5.1	Mechanism of Steglich Esterification	59
3.5.2	Spectroscopic Evidence for the Formation of 22	60
3.6	Knoevenagel Condensation of 22	61
3.6.1	Proposed Mechanism for the Formation of 25	62
3.6.2	Attempts to Optimise the Knoevenagel Reaction	63
3.6.3	Spectroscopic Evidence for the Formation of (Z)- 23	67
3.7	2,4-Dimethoxybenzoyl Deprotection of (Z)- 23	68
3.7.1	Spectroscopic Evidence for the Formation of 24	69
3.8	TBS Deprotection of 24 to Mutual Prodrug 2	70
3.9	2D Spectroscopic Analysis of 2	71
3.9.1	¹³ C APT Analysis of 2	72
3.9.2	gCOSY Analysis of 2	73
3.9.3	gHSQC Analysis of 2	74
3.9.4	gHMBC Analysis of 2	75
3.10	Summary of the Synthesis of 2	76
Chapter 4: Proof-of-Concept Chemical Reductions and <i>in vitro</i> Biological Evaluation		78
4.1	Proof-of-Concept Chemical Reductions	78
4.1.1	Mechanism of Chemical Nitroaromatic Reductions	78
4.1.2	Arylnitro Chemical Reduction Measurements	79
4.2	<i>In Vitro</i> Biological Evaluation of 1 and 2	80

4.3	Pulse Radiolysis One-Electron Reduction Potential Measurements	82
4.3.1	Reduction Potential Measurements with 2	84
4.3.2	Reduction Potential Measurements with 9	85
4.3.3	Conclusions	86
Chapter 5: Development of a New Divergent Route Towards Mutual Prodrugs		87
5.1	Synthetic Strategy	87
5.2	Esterification of 2-(2-nitrophenyl)acetic acid with Allyl Alcohol	88
5.3	Knoevenagel Reaction of 30 with 7	89
5.4	<i>N</i> -BOC Protection of (Z)- 31	90
5.5	Deallylation of 32 to Acid 33	92
5.5.1	Mechanism of Palladium-Catalysed Deallylation of 32	92
5.6	Esterification of 33 with Floxuridine	93
5.6.1	Mechanism of <i>N</i> -Acyl Urea and Anhydride Formation	95
5.6.2	Mechanism of HOBt/HOAt Ester Formation	96
5.6.3	Mechanism for the Formation of 2,3' Anhydrofloxuridine Derivative	97
5.7	Trial Esterification Reactions with 33 and Benzyl Alcohol	98
5.8	Trial Amide Couplings with 33 and Benzylamine	99
5.9	Conclusions and Future Directions	99
Chapter 6: Optimisation of Prodrug Nitroaromatic Reduction Potentials		101
6.1	Overview and Synthetic Strategy	101
6.2	Synthesis of Ally Esters 36-41	103
6.3	Discovery of a Nucleophilic Aromatic Substitution Route to Novel Pyrrol oquinoline Fluorophores	104
6.4	Optimisation of Knoevenagel Reaction Conditions	107
6.4.1	Knoevenagel Reaction with Allyl Ester 39	107
6.4.2	Knoevenagel Reaction with Allyl Ester 40	108
6.4.3	Knoevenagel Reaction with Allyl Ester 41	109
6.5	Pulse Radiolysis One-Electron Reduction Potential Measurements	109
6.5.1	Reduction Potential of Unsubstituted Parent (Z)- 31	109
6.5.2	Reduction Potential (Z)- 42	112
6.5.3	Reduction Potential of (Z)- 43	112
6.5.4	Reduction Potential of (Z)- 44	112
6.5.5	Reduction Potential Measurement of (Z)- 46	113

6.5.6	Summary of One-Electron Reduction Potential Measurements	113
6.6	Chemical Reductions with Fe/CH ₃ COOH	114
6.7	Conclusions and Future Directions	116
6.7.1	Future Work on Hypoxia Activated Mutual Prodrugs	116
6.7.2	Future Work on Pyrroloquinoline Fluorophores	117
Chapter 7: Experimental		118
7.1	General Methods	118
7.1.1	Chromatography	118
7.1.2	Melting Points	118
7.1.3	Polarimetry	118
7.1.4	Infrared Spectroscopy	118
7.1.5	Nuclear Magnetic Resonance Spectroscopy	118
7.1.6	Mass Spectrometry	119
7.2	Synthesis of <i>N</i> -(4-aminophenyl)-2-(2-nitrophenyl)acetamide 4	119
7.3	Synthesis of <i>N</i> -(4-(bis(2-hydroxyethyl)amino)phenyl)-2-(2-nitrophenyl)acetamide 5	119
7.4	Synthesis of <i>N</i> -(4-(bis(2-((<i>tert</i> -butyldimethylsilyl)oxy)ethyl)amino)phenyl)-2-(2-nitrophenyl)acetamide 6	120
7.5	Synthesis of methyl 2-formyl-3,5-dimethyl-1 <i>H</i> -pyrrole-1-carboxylate 7	121
7.6	Synthesis of (<i>Z</i>)- <i>N</i> -(4-(bis(2-((<i>tert</i> -butyldimethylsilyl)oxy)ethyl)amino)phenyl)-3-(3,5-dimethyl-1 <i>H</i> -pyrrol-2-yl)-2-(2-nitrophenyl)acrylamide (<i>Z</i>)- 8	121
7.7	Synthesis of (<i>Z</i>)- <i>N</i> -(4-(bis(2-hydroxyethyl)amino)phenyl)-3-(3,5-dimethyl-1 <i>H</i> -pyrrol-2-yl)-2-(2-nitrophenyl)acrylamide 9	122
7.8	Synthesis of (<i>Z</i>)- <i>N</i> -(4-(bis(2-chloroethyl)amino)phenyl)-3-(3,5-dimethyl-1 <i>H</i> -pyrrol-2-yl)-2-(2-nitrophenyl)acrylamide 1	123
7.9	Synthesis of 1-((2 <i>R</i> ,4 <i>S</i> ,5 <i>R</i>)-4-((<i>tert</i> -butyldimethylsilyl)oxy)-5-(((<i>tert</i> -butyldimethylsilyl)oxy)methyl)tetrahydrofuran-2-yl)-5-fluoropyrimidine-2,4(1 <i>H</i> ,3 <i>H</i>)-dione 14	123
7.10	Synthesis of 1-((2 <i>R</i> ,4 <i>S</i> ,5 <i>R</i>)-4-((<i>tert</i> -butyldimethylsilyl)oxy)-5-(((<i>tert</i> -butyldimethylsilyl)oxy)methyl)tetrahydrofuran-2-yl)-3-(2,4-dimethoxybenzoyl)-5-fluoropyrimidine-2,4(1 <i>H</i> ,3 <i>H</i>)-dione 20	124

7.11	Synthesis of 1-((2 <i>R</i> ,4 <i>S</i> ,5 <i>R</i>)-4-((<i>tert</i> -butyldimethylsilyl)oxy)-5-(hydroxymethyl)tetrahydrofuran-2-yl)-3-(2,4-dimethoxybenzoyl)-5-fluoropyrimidine-2,4(1 <i>H</i> ,3 <i>H</i>)-dione 21	125
7.12	Synthesis of ((2 <i>R</i> ,3 <i>S</i> ,5 <i>R</i>)-3-((<i>tert</i> -butyldimethylsilyl)oxy)-5-(3-(2,4-dimethoxybenzoyl)-5-fluoro-2,4-dioxo-3,4-dihydropyrimidin-1(2 <i>H</i>)-yl)tetrahydrofuran-2-yl)methyl 2-(2-nitrophenyl)acetate 22	126
7.13	Synthesis of ((2 <i>R</i> ,3 <i>S</i> ,5 <i>R</i>)-3-((<i>tert</i> -butyldimethylsilyl)oxy)-5-(3-(2,4-dimethoxybenzoyl)-5-fluoro-2,4-dioxo-3,4-dihydropyrimidin-1(2 <i>H</i>)-yl)tetrahydrofuran-2-yl)methyl (<i>Z</i>)-3-(3,5-dimethyl-1 <i>H</i> -pyrrol-2-yl)-2-(2-nitrophenyl)acrylate (<i>Z</i>)- 23	127
7.14	Synthesis of ((2 <i>R</i> ,3 <i>S</i> ,5 <i>R</i>)-3-((<i>tert</i> -butyldimethylsilyl)oxy)-5-(5-fluoro-2,4-dioxo-3,4-dihydropyrimidin-1(2 <i>H</i>)-yl)tetrahydrofuran-2-yl)methyl (<i>Z</i>)-3-(3,5-dimethyl-1 <i>H</i> -pyrrol-2-yl)-2-(2-nitrophenyl)acrylate 24	129
7.15	Synthesis of ((2 <i>R</i> ,3 <i>S</i> ,5 <i>R</i>)-5-(5-fluoro-2,4-dioxo-3,4-dihydropyrimidin-1(2 <i>H</i>)-yl)-3-hydroxytetrahydrofuran-2-yl)methyl (<i>Z</i>)-3-(3,5-dimethyl-1 <i>H</i> -pyrrol-2-yl)-2-(2-nitrophenyl)acrylate 2	130
7.16	Characterisation of Side Product 3,5-dimethyl-1-(methylsulfonyl)-1 <i>H</i> -pyrrole-2-carbaldehyde 26	130
7.17	Characterisation of Side Product 4,6-dimethylpyrrolo[1,2- <i>b</i>]isothiazole 1,1-dioxide 27	131
7.18	Characterisation of Side Product 4,6-dimethylpyrrolo[1,2- <i>b</i>]isothiazole 1,1-dioxide 28	131
7.19	Proof of Concept Chemical Reductions with Fe(0) in CH ₃ COOH	131
7.20	Proof of Concept Chemical Reductions with FeCl ₃ 6H ₂ O/Zn	132
7.21	Proof of Concept Chemical Reductions with NaBH ₄ /Pd-C	132
7.22	<i>In Vitro</i> Biological Evaluation of 1 and 2	132
7.23	Synthesis of allyl 2-(2-nitrophenyl)acetate 30	133
7.24	Synthesis of allyl (<i>Z</i>)-3-(3,5-dimethyl-1 <i>H</i> -pyrrol-2-yl)-2-(2-nitrophenyl)acrylate (<i>Z</i>)- 31	134
7.25	Synthesis of <i>tert</i> -butyl (<i>Z</i>)-2-(3-(allyloxy)-2-(2-nitrophenyl)-3-oxoprop-1-en-1-yl)-3,5-dimethyl-1 <i>H</i> -pyrrole-1-carboxylate 32	135
7.26	Synthesis of (<i>Z</i>)-3-(1-(<i>tert</i> -butoxycarbonyl)-3,5-dimethyl-1 <i>H</i> -pyrrol-2-yl)-2-(2-nitrophenyl)acrylic acid 33	136

7.27	Synthesis of <i>tert</i> -butyl (<i>Z</i>)-2-(3-(benzyloxy)-2-(2-nitrophenyl)-3-oxopro- p-1-en-1-yl)-3,5-dimethyl-1 <i>H</i> -pyrrole-1-carboxylate 34	136
7.28	Synthesis of <i>tert</i> -butyl (<i>Z</i>)-2-(3-(benzylamino)-2-(2-nitrophenyl)-3-oxopr- op-1-en-1-yl)-3,5-dimethyl-1 <i>H</i> -pyrrole-1-carboxylate 35	137
7.29	Allyl Esterification General Method 1	138
7.30	Synthesis of Allyl 2-(3-fluoro-2-nitrophenyl)acetate 36	138
7.31	Synthesis of Allyl 2-(4-fluoro-2-nitrophenyl)acetate 37	138
7.32	Synthesis of Allyl 2-(5-fluoro-2-nitrophenyl)acetate 38	139
7.33	Synthesis of Allyl 2-(2-fluoro-6-nitrophenyl)acetate 39	139
7.34	Synthesis of Allyl 2-(2-nitro-4-(trifluoromethyl)phenyl)acetate 40	140
7.35	Synthesis of Allyl 2-(2-nitro-5-(trifluoromethyl)phenyl)acetate 41	140
7.36	Knoevenagel Condensation General Method 2	140
7.37	Synthesis of Allyl 8-fluoro-1,3-dimethylpyrrolo[1,2- <i>a</i>]quinoline-5-carbo- xylate 48	141
7.38	Synthesis of Allyl (<i>Z</i>)-3-(3,5-dimethyl-1 <i>H</i> -pyrrol-2-yl)-2-(3-fluoro-2-nitr- ophenyl)acrylate (<i>Z</i>)- 42	141
7.39	Synthesis of Allyl (<i>Z</i>)-3-(3,5-dimethyl-1 <i>H</i> -pyrrol-2-yl)-2-(4-fluoro-2-nitr- ophenyl)acrylate (<i>Z</i>)- 43	142
7.40	Synthesis of Allyl (<i>Z</i>)-3-(3,5-dimethyl-1 <i>H</i> -pyrrol-2-yl)-2-(5-fluoro-2-nitr- ophenyl)acrylate (<i>Z</i>)- 44	143
7.41	Synthesis of Allyl 1,3-dimethyl-6-nitropyrrolo[1,2- <i>a</i>]quinoline-5-carboxy- late 49	144
7.42	Synthesis of Allyl (<i>Z</i>)-3-(3,5-dimethyl-1 <i>H</i> -pyrrol-2-yl)-2-(2-nitro-4-(trifl- uoromethyl)phenyl)acrylate (<i>Z</i>)- 46	145
7.43	Synthesis of Allyl 1,3-dimethyl-7-(trifluoromethyl)pyrrolo[1,2- <i>a</i>]quinoli- ne-5-carboxylate 52	147
7.44	Fe/CH ₃ COOH Reduction General Method 3	147
7.45	Synthesis of (<i>Z</i>)-3-((3,5-dimethyl-1 <i>H</i> -pyrrol-2-yl)methylene)-6-fluoroind- olin-2-one 53	147
7.46	Synthesis of (<i>Z</i>)-3-((3,5-dimethyl-1 <i>H</i> -pyrrol-2-yl)methylene)-5-fluoroind- olin-2-one 54	148
7.47	Synthesis of (<i>Z</i>)-3-((3,5-dimethyl-1 <i>H</i> -pyrrol-2-yl)methylene)indolin-2-o- ne 3	148
	References	149

Appendix 1: X-ray Crystallographic Data for 48	172
Appendix 2: NMR Spectra	173

Abbreviations

5-FU	5-Fluorouracil
¹³ C APT	Attached carbon test (spectroscopy)
ADC	Antibody-drug conjugate
AQ4N	Banoxantrone
ATP	Adenosine triphosphate
BOC	<i>Tert</i> -butoxycarbonyl
BOP	Benzotriazol-1-yloxytris(dimethylamino)phosphonium hexafluorophosphate
BTZ [•]	Benzotriazinyl radical
Bz	Benzoyl
BzCl	Benzoyl chloride
CH ₂ THF	5,10-Methylenetetrahydrofolate
CIS	Cisplatin
CSF-1R	Colony-stimulating factor receptor type 1
dATP	Deoxyadenosine triphosphate
dCTP	Deoxycytidine triphosphate
dGTP	Deoxyguanosine triphosphate
DCC	<i>N,N'</i> -Dicyclohexylcarbodiimide
DCU	Dicyclohexylurea
DEAD	Diethyl azodicarboxylate
DHFU	Dihydrofluorouracil
DIC	<i>N,N'</i> -diisopropylcarbodiimide
DIPEA	<i>N,N</i> -diisopropylethylamine
DMAP	4-Dimethylaminopyridine
DMF	Dimethylformamide
DMSO	Dimethyl sulfoxide
DNA	Deoxyribonucleic acid
dNTP	Deoxynucleotide
DPD	Dihydropyrimidine dehydrogenase
DR	Deactivation ratio
dTMP	Deoxythymidine monophosphate
dTTP	Deoxythymidine triphosphate

dUMP	Deoxyuridine monophosphate
dUTP	Deoxyuridine triphosphate
dUTPase	Pyrophosphatase
EDCI	1-Ethyl-3-(3-dimethylaminopropyl)carbodiimide
EGFR	Epidermal growth factor receptors
eq.	Equivalence
FBAL	α -Fluoro- β -alanine
FDA	US Food and Drug Administration
FdUDP	Fluorodeoxyuridine diphosphate
FdUMP	Fluorodeoxyuridine monophosphate
FdUTP	Fluorodeoxyuridine triphosphate
FLT3	Fms-like tyrosine kinase-3 receptor
FUDR	Fluorodeoxyuridine
FUTP	Fluorouridine triphosphate
gCOSY	Gradient-selected correlation spectroscopy
gHMBC	Gradient-selected heteronuclear multiple bond coherence
gHSQC	Gradient-selected heteronuclear single quantum coherence
HATU	Hexafluorophosphate azabenzotriazole tetramethyl uronium
HBTU	Hexafluorophosphate benzotriazole tetramethyl uranium
HCR	Hypoxic cytotoxicity ratio
HER2	Human epidermal growth factor receptor 2
HOBt	Hydroxybenzotriazole
KIT	Stem cell factor receptor
MMAE	Monomethyl auristan E
M.P.	Melting point
NMR	Nuclear magnetic resonance
NOESY	Nuclear Overhauser effect spectroscopy
NQO1	NAD(P)H quinone dehydrogenase 1
O.R.	Optical Rotation
PARP	Poly(ADP-ribose) polymerase
Pet. Spirit	Petroleum spirit (B.P 40-60 °C)
POR	Cytochrome p450 oxidoreductase
RET	Glial cell-line-derived neurotrophic factor receptor
RNA	Ribonucleic acid

SR 4317	1,2,4-Benzotriazin-3-amine 1-oxide
TBAF	Tetrabutylammonium fluoride
TBDMSCl	<i>Tert</i> -butyldimethylsilyl chloride
TBS	<i>Tert</i> -butyldimethylsilyl
TBDPSCl	<i>Tert</i> -Butyl(chloro)diphenylsilane
TeQ ²⁺	Tetraquat
TFA	Trifluoroacetic acid
TFFH	Tetramethylfluoroformamidium hexafluorophosphate
TH-302	Evofosfamide
THF	Tetrahydrofuran
TK	Thymidine kinase
TQ ²⁺	Triquat
TLC	Thin layer chromatography
TP	Thymidine phosphorylase
TPZ	Tirapazamine
TS	Thymidylate synthase
UDG	Uracil-DNA-glycosylase
UOW	University of Wollongong
VEGF	Vascular endothelial growth factor
VEGFR	Vascular endothelial growth factor receptor

List of Figures

Figure 1.1 Chemical structure of Mitomycin C.	1
Figure 1.2 Chemical structure of methotrexate.	2
Figure 1.3 Chemical structures of paclitaxel, camptothecin and irinotecan.	2
Figure 1.4 Chemical structure of doxorubicin.	3
Figure 1.5 Chemical structures of vinblastine and vincristine.	3
Figure 1.6 Chemical structures of imatinib and lapatinib.	4
Figure 1.7 Tumour growth and metastasis is promoted by angiogenesis driven by signalling VEGF. (Figure modified from ref. 20).	5
Figure 1.8 Structures of semaxanib and sunitinib.	6
Figure 1.9 Active metabolites of 5-FU, fluorodeoxyuridine monophosphate (FdUMP), fluorodeoxyuridine triphosphate (FdUTP) and fluorouridine triphosphate (FUTP).	8
Figure 1.10 Fluorodeoxyuridine triphosphate (FdUTP) inhibition of thymidine synthase (TS) leading to DNA damage and disrupted DNA replication and repair. (Figure modified from 54).	9
Figure 1.11 Antibody drug conjugates comprise a monoclonal antibody, linker and drug. The mechanism of action involves: 1) specific binding of the antibody to an internalising antigen, followed by endocytosis; 2) transfer to the lysosome; 3) lysosomal cleavage of the linker to release the active drug; 4) drug transfer to the cytoplasm/nucleus leading to cell death and diffusion to neighbouring tumour cells to cause bystander killing effects.	11
Figure 1.12 Structure of the ADC Brentuximab vedotin (Adcetris®).	12
Figure 1.13 Structure of trastuzumab emtansine (Kadcyla®).	13
Figure 1.14 Oxygen and pH gradients present in solid tumours arising from an aberrant vasculature. Cells closest to the nearby blood vessels (red) consume all available oxygen leaving cells furthest away to experience continuous hypoxia (blue).	14
Figure 1.15 Examples of cobalt(III) prodrugs containing nitrogen mustard or <i>seco</i> -CPyI-TMI cytotoxins as ligands.	19
Figure 1.16 Example of a copper(II) cyclen nitrogen mustard prodrug.	20
Figure 1.17 Molecularly Targeted Hypoxia Activated Prodrugs (bioreductive moiety shown in green).	24

- Figure 1.18** Postulated therapeutically beneficial “viscous cycle” created by hypoxia-activated semaxanib|cytotoxin mutual prodrugs. 27
- Figure 2.1** Aromatic region of the 500 MHz ^1H NMR spectrum of **4** in d_6 -DMSO. 30
- Figure 2.2** Aliphatic region of the 500 MHz ^1H NMR spectrum of **5** in d_6 -DMSO. 32
- Figure 2.3** Aliphatic region of the 500 MHz ^1H NMR spectrum of **6** in d_6 -DMSO. 34
- Figure 2.4** The pyrrole NH forms a hydrogen bond to the amide carbonyl in (*Z*)-**8**. 39
- Figure 2.5** Aliphatic region of the 500 MHz ^1H NMR spectrum of **9** (bottom) showing loss of the TBS signals present in (*Z*)-**8** (Top). Both spectra were recorded in CDCl_3 . 41
- Figure 2.6** Aliphatic region of the 500 MHz ^{13}C APT NMR spectrum of **9** (bottom) recorded in CDCl_3 showing loss of the three TBS carbon signals present in (*Z*)-**8** (Top). 41
- Figure 2.7** Aromatic region of the 500 MHz ^1H -NMR spectrum of **1** recorded in CDCl_3 . 43
- Figure 2.8** Aliphatic region of the 500 MHz ^1H - NMR spectrum of **1** recorded in CDCl_3 . 44
- Figure 2.9** Aromatic region of the 500 MHz ^{13}C APT NMR spectrum of **1** recorded in CDCl_3 . The peaks at 166.88 and 149.75 ppm were evident in the gHMBC spectrum. 44
- Figure 2.10** Aliphatic region of the 500 MHz ^{13}C APT NMR spectrum of **1** recorded in CDCl_3 . 45
- Figure 2.11** NOESY correlations of **1** recorded in CDCl_3 (500 MHz) 45
- Figure 2.12** $^3J_{\text{H-H}}$ correlations observed in the 500 MHz gCOSY NMR spectrum (with diagonal suppression) of **1** recorded in CDCl_3 . 46
- Figure 2.13** Aromatic region of the 500 MHz gHSQC spectrum of **1** recorded in CDCl_3 . 46
- Figure 2.14** Aliphatic region of the 500 MHz gHSQC spectrum of **1** recorded in CDCl_3 . 47
- Figure 2.15** Aromatic region of the 500 MHz gHMBC spectrum of **1** recorded in CDCl_3 , $^2J_{\text{H-C}}$ correlations are shown in blue and $^3J_{\text{H-C}}$ correlations in red. 47

- Figure 2.16** Aliphatic region of the 500 MHz gHMBC spectrum of **1** recorded in CDCl₃. 48
- Figure 3.1** Appearance of the TBS signals in the 500 MHz ¹H NMR spectrum of **14**. The spectrum was recorded in CDCl₃. 53
- Figure 3.2** The presence of electron donating *o,p*-methoxy groups was predicted to reduce electrophilicity of the benzoyl carbonyl group, stabilising it towards nucleophiles and avoiding inadvertent deprotection during the Knoevenagel reaction. 53
- Figure 3.3** Section of the 500 MHz ¹H NMR spectrum of **20** (CDCl₃) showing the presence of 2,4-dimethoxybenzoyl signals. 56
- Figure 3.4** Typical yields of recovered starting material, the desired mono-alcohol **21** and two side products formed during TCA deprotection of **20**. 57
- Figure 3.5** Removal of one TBS group halved the number of TBS signals detected in ¹H-NMR (CDCl₃) of **21** (relative to **20**). 58
- Figure 3.6** Steglich esterification produced diagnostic aromatic signals in the 500 MHz ¹H-NMR spectrum (CDCl₃) of **22**. 61
- Figure 3.7** Published series of pyrrole *N*-heteroaryl fused vinyl sultams related to compound **28** and their versatile chemistry.¹⁵⁹ 66
- Figure 3.8** Downfield region of the 500 MHz ¹H-NMR (CDCl₃) spectrum of (*Z*)-**23** showing all of the expected signals, including the highly deshielded pyrrole N-H signal indicating the presence of an H-bond to the ester carbonyl oxygen. 67
- Figure 3.9** Downfield region of the 500 MHz ¹H-NMR (CDCl₃) spectrum of **24**. 70
- Figure 3.10** Aromatic region of the 500 MHz ¹H-NMR spectrum of **2** recorded in CDCl₃. 71
- Figure 3.11** Aliphatic region of the 500 MHz ¹H-NMR spectrum of **2** recorded in CDCl₃. 72
- Figure 3.12** Aromatic and Aliphatic regions of the 500 MHz ¹³C-NMR spectrum of **2** recorded in CDCl₃. 73
- Figure 3.13** Selected correlations observed in the 500 MHz gCOSY spectrum of **2** (with diagonal suppression) recorded in CDCl₃. 74
- Figure 3.14** Aromatic region of the 500 MHz gHSQC spectrum of **2** recorded in CDCl₃. 74

- Figure 3.15** Aliphatic region of the 500 MHz gHSQC spectrum of **2** recorded in CDCl₃. 75
- Figure 3.16** Aromatic region of the 500 MHz gHMBC spectrum of **2** recorded in CDCl₃. 75
- Figure 3.17** Aliphatic region of the 500 MHz gHMBC spectrum of **2** recorded in CDCl₃. 76
- Figure 4.1** Proof-of-concept chemical reduction reactions performed with mutual prodrugs **1** and **2**. 78
- Figure 4.2** Schematic of pulse radiolysis experiments.¹⁷⁹ 83
- Figure 4.3** Changes in UV-vis absorption with sequential doses of γ -irradiation of **2** in an evacuated solution containing formate ions (25 mM) at pH 7 (after initial removal of a small contaminant concentration of O₂). 84
- Figure 4.4** Chemical structure of viologen triquat (TQ²⁺) used to establish redox equilibrium. 85
- Figure 4.5** Changes in UV-visible absorption with sequential doses of γ -irradiation of **9** in an evacuated solution containing formate ions (25 mM) at pH 7. 86
- Figure 5.1** Mechanism of deallylation of **32** using a palladium(0) catalyst and morpholine. 93
- Figure 6.1** Nitroaromatic one-electron reduction potentials of a series of substituted mono- and dinitrobenzene derivatives from the literature.¹⁹⁰ 101
- Figure 6.2** Unexpected side product formed in the attempted Knoevenagel reaction of **7** with 4-F allyl ester **37**. A) Crystal used to obtain the X-ray structure. B) Crystals dissolved in pet. spirit displayed bright blue fluorescence under 365 nm UV light. 104
- Figure 6.3** X-ray crystal structure of unexpected fluorescent side product **48** (courtesy of Dr Christopher Richardson, UOW). Key correlations observed in the 2D NOESY spectrum of **48** are indicated. Crystallographic data are provided in Appendix 1. 105
- Figure 6.4** Spectral changes following pulse radiolysis (3 Gy in 200 ns) of (*Z*)-**31**, 75 μ M in deaerated aqueous solution containing *tert*-butanol (2 M) and phosphate buffer (5 mM, pH 7), 5 μ s and 200 μ s after the pulse. Spectra corrected for the absorption of the pre-pulsed spectrum, dashed line. 110

- Figure 6.5** Chemical structures of triquat (TQ²⁺) and tetraquat (TeQ²⁺) standards used to establish redox equilibria for one-electron pulse radiolysis reduction potential measurements. 111
- Figure 6.6** Proposed mutual prodrug based on the FDA-approved drug sunitinib, incorporating an additional *para* (relative to the nitro) trifluoromethyl substituent. 116
- Figure 7.1** Summary of the protocol used for *in vitro* testing of hypoxia-activated cytotoxicity of mutual prodrugs **1** and **2**. 133

List of Schemes

- Scheme 1.1** Formation of aziridinium ions by nitrogen mustards leads to reactions with nucleophiles (Nu), including guanine bases of DNA, resulting in formation of cytotoxic interstrand DNA crosslinks. 7
- Scheme 1.2** Liver metabolism of 5-FU produces three inactive metabolites; dihydrofluorouracil (DHFU), α -fluoro- β -ureidopropionic acid and α -fluoro- β -alanine (FBAL). 7
- Scheme 1.3** Metabolism of floxuridine to 5-FU and FdUMP. 9
- Scheme 1.4** Metabolic activation of a 5-FU|cytarabine mutual prodrug yields two active drugs (5-FU and cytarabine) and two “waste” (linker) fragments.⁶⁰ 10
- Scheme 1.5** Quinones can undergo an irreversible two-electron reduction *in vivo* catalysed by NQO1, or oxygen sensitive reversible one-electron reduction catalysed by POR. 15
- Scheme 1.6** Apaziquone can undergo two-electron reductive activation via NQO1, resulting in a hydroquinone, or oxygen-sensitive one-electron reduction to the semiquinone radical by POR. Both adducts are able to damage DNA. 16
- Scheme 1.7** AQ4N is a prodrug variant of mitoxantrone that masks the alkyl amines as *N*-oxides. AQ4N undergoes two-electron bioreductive activation catalysed by nitric oxide synthase to give the intercalator AQ4. This process is inhibited by molecular oxygen, giving rise to hypoxia-selective activation. 17
- Scheme 1.8** Mechanism of hypoxia-selective activation of TPZ leading to DNA cleavage and tumour cell death. 18

Scheme 1.9 Mechanism of activation of the pre-prodrug PR-104. The major PR-104 metabolite in solid tumour patients was the <i>O</i> -glucuronide metabolite (PR-104G) formed by glucuronidation of PR-104A.	21
Scheme 1.10 Mechanism of hypoxia- activation of TH-302.	22
Scheme 1.11 Tumour-selective nitroaromatic prodrug reported by Denny <i>et al.</i> ¹²⁵	23
Scheme 1.12 Mechanism of hypoxia selective activation of TH-4000 to a radical anion followed by fragmentation to release the tyrosine kinase inhibitor TH-4000E.	25
Scheme 1.13 (a) Anti-angiogenic 2-(2-nitrophenyl)acetate derivatives related to sunitinib. ¹³⁸ (b) Prototype mutual prodrugs 1 and 2 and their proposed mechanism of bioreductive activation to selectively release indoline-2-one multi-kinase inhibitor semaxanib 3 and 4-aminoaniline mustard or floxuridine cytotoxins within hypoxic regions of tumours.	26
Scheme 2.1 Pilot synthesis of mutual prodrug 1 developed by former PhD student Nicholas Kirk.	28
Scheme 2.2 Literature precedent for amide coupling of 2-(2-nitrophenyl)acetic acid to electron rich aryl amines. ¹²⁵	29
Scheme 2.3 Amide coupling of 2-(2-nitrophenyl)acetic acid to <i>p</i> -phenylenediamine with HBTU to give 4 .	30
Scheme 2.4 Three literature precedents for the <i>bis</i> -alkylation of aromatic amines. ¹⁴⁰⁻¹⁴²	31
Scheme 2.5 <i>Bis</i> -alkylation of 4 with neat 2-bromoethanol yielded 5 on multi-gram scale.	32
Scheme 2.6 Literature precedent for <i>bis</i> -TBS protection of a <i>bis</i> -ethanolamine structurally related to 5 .	33
Scheme 2.7 <i>Bis</i> -TBS protection of 5 .	33
Scheme 2.8 Mechanism for the <i>Bis</i> -TBS protection of 5 .	34
Scheme 2.9 Knoevenagel condensation with 6 trialled on small scale by Nicholas Kirk. ¹³⁹	36
Scheme 2.10 Proposed mechanism for the formation of (<i>Z</i>)- 8 by the Knoevenagel condensation of 6 with pyrrole aldehyde 7 .	36
Scheme 2.11 Proposed mechanism for the formation of pyrrolizinone side product 11 from the desired product (<i>Z</i>)- 8 during the Knoevenagel reaction.	37

Scheme 2.12 Proposed mechanism for the formation of <i>N</i> -aryl oxindole side product 13 from the desired product (<i>Z</i>)- 8 during the Knoevenagel reaction.	38
Scheme 2.13 Literature precedents for <i>bis</i> -TBS deprotection of <i>bis</i> -alcohols using TBAF or EtN ₃ •3HF. ¹⁴⁸⁻¹⁴⁹	40
Scheme 2.14 <i>Bis</i> -TBS-deprotection of (<i>Z</i>)- 8 to afford 9 .	40
Scheme 2.15 Literature precedents for the conversion of <i>bis</i> -alcohols to aniline mustards. ^{148, 150}	42
Scheme 2.16 Two-step conversion of 9 to the target semaxinib 4-aminoaniline mustard mutual prodrug 1 .	43
Scheme 2.17 Summary of the scaled-up synthesis of 1 . Total quantities of compounds synthesised across all reactions are indicated.	49
Scheme 3.1 Pilot synthesis of semaxinib floxuridine Mutual Prodrug 2 scoped during my Honours research in 2014 at UOW. The yields shown represent the highest yields obtained in each step.	50
Scheme 3.2 Literature precedent for <i>bis</i> -TBS protection of thymidine. ¹⁵³	51
Scheme 3.3 Mechanism for the <i>bis</i> -TBS protection of the 1° and 2° alcohols of floxuridine using TBDMSCl and imidazole.	52
Scheme 3.4 Literature precedent for the benzoyl protection of <i>bis</i> -TBS protected thymidine.	54
Scheme 3.5 Mechanism for <i>N</i> -2,4-dimethoxybenzoylation of 14 with 2,4-dimethoxybenzoyl chloride in the presence of catalytic DMAP and DIPEA.	55
Scheme 3.6 Literature precedent reporting selective 1° alcohol TBS-deprotection of uridine. ¹⁵¹	57
Scheme 3.7 Literature precedent demonstrating esterification of TBS-protected thymidine. ¹⁵⁶	58
Scheme 3.8 Steglich esterification of 21 with 2-(2-nitrophenyl)acetic acid gave 22 in excellent yield.	59
Scheme 3.9 Mechanism for the DCC-mediated Steglich esterification of 21 with 2-(2-nitrophenyl)acetic acid to form 22 .	60
Scheme 3.10 A) Knoevenagel condensation of 22 with pyrrole aldehyde 7 gave (<i>Z</i>)- 23 and (<i>E</i>)- 23 in modest yields. B) Starting material 22 and side products 11 and 25 were also isolated from the reaction.	62

Scheme 3.11 Proposed mechanism for the formation of methoxide during the Knoevenagel reaction and subsequent formation of the major side-product 25 .	63
Scheme 3.12 Attempts to synthesise alternative <i>N</i> -protected pyrrole-2-aldehydes for use in the Knoevenagel reaction.	65
Scheme 3.13 <i>N</i> -Mesyl pyrrole aldehyde 26 did not undergo the desired Knoevenagel reaction but instead formed a <i>N</i> -heteroaryl fused vinyl sultam, the first example of a compound from this class.	65
Scheme 3.14 Literature precedent for benzoyl deprotection of a structurally related uridine derivative. ¹⁶¹	68
Scheme 3.15 Model 2,4-dimethoxybenzoyl deprotection reaction with 20 delivered 14 in quantitative yield.	68
Scheme 3.16 Literature precedent showing TBS-deprotection of a deoxyuridine derivative. ¹⁶²	70
Scheme 3.17 Summary of the completed synthesis of 2 . Total quantities of each compound produced over the course of my PhD are shown.	77
Scheme 5.1 Proposed divergent strategy that could allow rapid access to a diverse range of amide and ester-linked mutual prodrugs.	87
Scheme 5.2 Intramolecular cyclisation to a pyrrolizin-3-one occurs upon activation of the carboxylic acid when attempting amide or ester coupling reactions with the pyrrole nitrogen unprotected.	88
Scheme 5.3 Established methods from the Kelso Lab for the synthesis of allyl ester 30 . Method A) K ₂ CO ₃ , allyl bromide, acetone, rt, 74%. Method B) allyl alcohol, cat. H ₂ SO ₄ , reflux, 88%.	89
Scheme 5.4 Knoevenagel reactions of 30 with 7 afforded (<i>Z</i>)- 31 41% and (<i>E</i>)- 31 33% when performed on a 1 g scale (Kelso Lab PhD student Pichit Sudta). When I performed the reaction (once) under the same conditions at 8 g scale, lower yields ((<i>Z</i>)- 31 20%, (<i>E</i>)- 31 21%) were obtained.	90
Scheme 5.5 <i>N</i> -BOC protection of (<i>Z</i>)- 31 using potassium hydride affords 32 in 75% yield when performed on a small scale (Pichit Sudta).	90
Scheme 5.6 Literature precedent for the <i>N</i> -BOC protection of diverse pyrroles using BOC ₂ O and DMAP in the absence of strong base. ¹⁸³	91
Scheme 5.7 Optimised <i>N</i> -BOC protection of (<i>Z</i>)- 31 using BOC ₂ O and DMAP in acetonitrile.	91

Scheme 5.8 Deallylation of 32 with Pd(PPh ₃) ₄ and morpholine provided acid 33 .	92
Scheme 5.9 Mechanism of <i>N</i> -acyl urea and symmetrical anhydride formation during carbodiimide-mediated ester coupling reactions with 33 .	95
Scheme 5.10 Explanation for why HOAt/HOBt esters of 33 were isolated from attempted HATU/HBTU-mediated ester couplings with floxuridine.	96
Scheme 5.11 Mechanism of the Mitsunobu reaction of 33 with floxuridine and subsequent intramolecular cyclisation leading to a bridge-bicyclic side product.	97
Scheme 5.12 Literature example of a Mitsunobu reaction that resulted in formation of a bridged-bicyclic floxuridine derivative. ¹⁸⁹	98
Scheme 5.13 Proposed future strategy allowing practical access to diverse amide and ester-linked mutual prodrugs containing addition electron withdrawing substituents on the nitroaryl ring to increase the reduction potential.	100
Scheme 6.1 Proposed synthesis of allyl ester model prodrugs (<i>Z</i>)- 42-45 containing electron withdrawing fluorine and trifluoromethyl groups on the nitroaryl ring.	103
Scheme 6.2 Literature report of intermolecular nucleophilic aromatic substitution of indole onto 4-nitrophthalonitrile. ¹⁹³	106
Scheme 6.3 Literature report on the synthesis of azole (pyrrole or imidazole)-fused quinolones related to 48 . ¹⁹⁴	106
Scheme 6.4 Knoevenagel reaction of 39 with 7 at room temperature produced intramolecular nucleophilic aromatic substitution product 49 .	108
Scheme 6.5 Knoevenagel reaction of 40 with 7 produced a mixture of the desired alkenes (<i>Z</i>)- 46 and (<i>E</i>)- 46 , along with side products 50 and 51 .	108
Scheme 6.6 Knoevenagel reaction of 41 produced nucleophilic aromatic substitution product 52 as the major product.	109
Scheme 6.7 Resonance forms of (<i>Z</i>)- 46 that allow free rotation around the alkene bond.	116
Scheme 6.8 Proposed synthesis of proteins labelled with pyrroloquinoline fluorescent tags using the chemistry developed in Chapters 5 and 6.	117

List of Tables

Table 2.1 Knoevenagel reactions between 2-(2-nitrophenyl)acetic esters and amides developed previously in the Kelso Lab. ¹³⁸	35
Table 2.2 Representative selection of conditions trialled in attempts to optimise the Knoevenagel reaction.	38
Table 3.1 Optimisation of 2,4-dimethoxybenzoyl protection of 14 to give 20 .	55
Table 3.2 Knoevenagel reactions performed in the presence of methoxide scavengers.	64
Table 3.3 2,4-Dimethoxybenzoyl deprotection of (Z)- 23 .	69
Table 3.4 Optimisation of Purification of TBAF deprotection of 24 .	71
Table 4.1 Chemical reduction reactions performed on mutual prodrugs 1 and 2	79
Table 4.2 <i>In vitro</i> evaluation of the hypoxia-selective cytotoxicity of drug treatments.	81
Table 5.1 Attempted esterification reactions with 33 and floxuridine.	94
Table 5.2 Trial esterification reactions with 33 and benzyl alcohol.	98
Table 5.3 Trial amide coupling reactions with 33 and benzylamine.	99
Table 6.1 Synthesis of allyl esters 36-41 .	104
Table 6.2 Knoevenagel reactions with allyl esters 36-38 .	107
Table 6.3 Summary of pulse radiolysis one-electron reduction potential measurements.	114
Table 6.4 Summary of chemical reductions of allyl ester <i>cis</i> derivatives.	115

Abstract

The effectiveness of current anticancer drugs such as nitrogen mustards, 5-fluorouracil and sunitinib is hampered by dose-limiting side effects. Targeted prodrugs designed to be selectively activated in hypoxic regions of solid tumours and locally deliver active cytotoxins are potentially very useful for improving the efficacy and side effect profiles of anticancer chemotherapeutics. This project investigated rationally designed hypoxia-activated antitumour amide- and ester-linked kinase inhibitor–cytotoxin prodrug conjugates. These mutual prodrugs combined an angiogenesis inhibitor, semaxanib (SU5416), together with a cytotoxin into a single molecule, with the cytotoxin being either a 4-aminoaniline nitrogen mustard or floxuridine (an FDA-approved antimetabolite). The compounds contained an aryl nitro triggering group designed to undergo bioreductive activation selectively in hypoxic regions of tumours to the aniline derivative. Formation of the aniline group then initiates a spontaneous intramolecular cyclisation reaction to simultaneously eject the two active anticancer drugs.

The first goal of the project was to devise and implement viable synthetic routes towards semaxanib|4-aminoaniline mutual prodrug **1** and semaxanib|floxuridine mutual prodrug **2**. The synthesis of mutual prodrug **1** was optimised and scaled-up based on a previous small-scale synthesis completed by PhD student Nicholas Kirk. The synthesis of **1** was accomplished in 6 steps providing 190 mg of **1** prepared in pure form. The synthesis of mutual prodrug **2** was completed in 7 steps to give a total of 302 mg of pure **2**.

Chemical reductions of **1** and **2** confirmed that intramolecular cyclisation occurs spontaneously after nitro to amine/hydroxylamine conversion. Preliminary cell testing and reduction potential measurements with **1** and **2** performed by collaborators at the University of Auckland showed favourable deactivation of the prodrugs relative to their parent cytotoxins in an aerobic environment. Unfortunately, the compounds were unable to undergo bioreductive activation under hypoxic conditions, which was attributed to the low aryl nitro one-electron reduction potentials (measured by collaborators using pulse radiolysis).

Whilst these biological studies were being undertaken, an alternative and more divergent strategy for future syntheses of mutual prodrugs was investigated. The new strategy

addressed the key shortcomings in the synthesis of **1** and **2**, specifically the low yielding Knoevenagel condensations. The new route allowed the Knoevenagel reaction to be performed in higher yield earlier in the synthesis on a simpler allyl ester. Subsequent pyrrole *N*-*tert*-butoxycarbonyl (BOC) protection and deallylation reaction gave an advanced carboxylic acid common intermediate **32** that could potentially be coupled directly to diverse cytotoxins containing free amino or alcohol groups. Model ester and amide couplings reactions were then successfully developed and optimised for future use with cytotoxins and intermediate **32**.

A second series of model prodrugs were designed and synthesised in an attempt to address the poor bioactivation observed with **1** and **2**. These new target compounds were semaxanib derivatives containing electron withdrawing groups added to the nitroaryl ring to increase the one-electron reduction potentials. The compound also contained an allyl ester to serve as a simpler model substitute for ester-linked cytotoxins. From this series, 4 model prodrugs were synthesised containing either fluorine or trifluoromethyl electron withdrawing groups at various positions around the aryl nitro ring. Each compound was chemically reduced at the aryl nitro group and shown to undergo spontaneous intramolecular cyclisation to the expected indolin-2-one. Pulse radiolysis measurements showed that addition of the electron withdrawing groups does indeed increase in the one-electron reduction potentials. In the course of these studies, an interesting side reaction was discovered involving intramolecular nucleophilic aromatic substitution and cyclisation of a pyrrole moiety onto an aryl nitro group. The compounds produced, novel pyrroloquinolines, have great scope for future investigations as protein fluorescent tags.

Chapter 1: Introduction

1.1 A Brief History of Cancer Treatments

Before 1950, cancer treatments were based solely on the surgical removal of solid tumours. Radiation treatments became common after 1960 following the invention of linear accelerators but, like surgery, these suffered from an inability to treat metastatic cancers. The introduction of anticancer chemotherapy can be traced back to the discovery of nitrogen mustards; the first effective chemical treatments for cancer.¹ Nitrogen mustards were developed in 1942 by Louis Goodman and Alfred Gilman, who were employed by the United States Department of Defence to investigate the therapeutic potential of toxins developed as chemical warfare agents.² Nitrogen mustards are reactive alkylating agents that exhibit cytotoxic anticancer effects through covalent attachment to DNA.³

In the 1950s, Mitomycin C was isolated by Japanese microbiologists in fermentation cultures of *Streptomyces caespitosus* (Figure 1.1).⁴ Mitomycin C is a potent DNA crosslinker that undergoes reductive activation to mitosene, which can successively *N*-alkylate two DNA bases leading to crosslinks and cell death.⁵

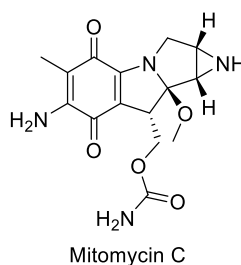


Figure 1.1 Chemical structure of Mitomycin C.

Shortly after World War II, a second approach to anticancer chemotherapy was identified by Sydney Farber, who used folic acid to treat patients with leukaemia. Subsequent investigations with folate analogues led to aminopterin and eventually amethopterin (methotrexate, Figure 1.2). These antimetabolites block folate-requiring enzymes to suppress proliferation of malignant cells.⁶⁻⁷

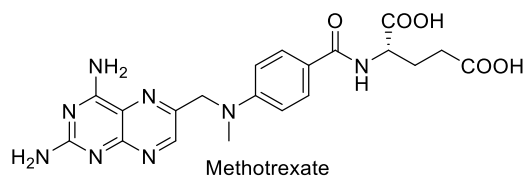


Figure 1.2 Chemical structure of methotrexate.

The effectiveness of natural products as cancer treatments was explored by Gordon Zubrod and led to the discovery of the taxanes in 1964 and camptothecins in 1966 (Figure 1.3). The drug Paclitaxel (Taxol), obtained from the bark of the Pacific Yew tree, was developed from this work by Bristol Myers Squibb and it was approved for use in 1991 for the treatment of ovarian cancer.⁸ Taxol belongs to the class known as mitotic inhibitors; compounds that either inhibit or promote the assembly of microtubules. Camptothecin, derived from a Chinese ornamental tree, inhibits topoisomerase I, an enzyme responsible for DNA unwinding and strand passage. Early clinical trials with camptothecin identified a problem with nephrotoxicity leading to the development of irinotecan, a less toxic analogue that was granted US Food and Drug Administration (FDA) approval in 1996 for the treatment of colon cancer.⁹

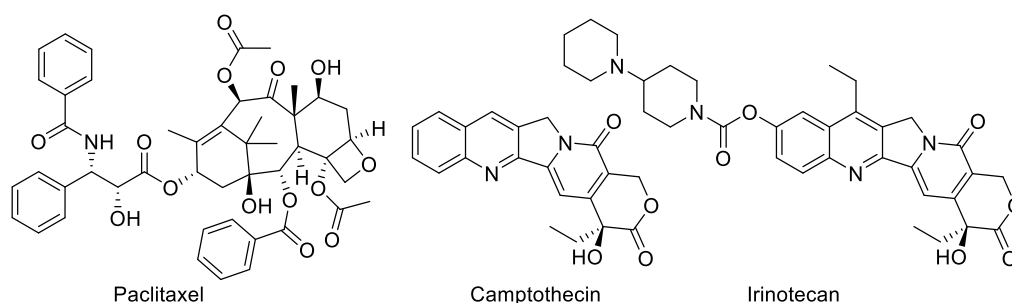


Figure 1.3 Chemical structures of paclitaxel, camptothecin and irinotecan.

Anthracyclines are a class of chemotherapy drugs that were first isolated from the actinobacteria *Streptomyces peucetius* in the 1960s.¹⁰ They were originally investigated for their antibiotic effects due to their ability to intercalate between base pairs of DNA/RNA strands. Investigations into their anticancer effects then led to the development of doxorubicin (Figure 1.4). Doxorubicin interacts with DNA by intercalation, inhibiting the progression of topoisomerase II and preventing cell replication.¹¹

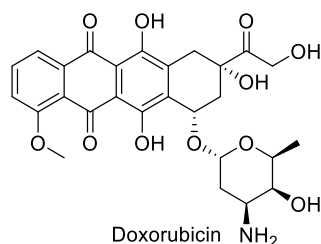


Figure 1.4 Chemical structure of doxorubicin.

Vinca alkaloids are a set of anti-mitotic and anti-microtubule alkaloids that were originally isolated from the periwinkle plant *Catharanthus roseus* (basionym *Vinca rosea*). Anticancer effects of the class were first identified in the late 1950s after a drug-screening program.¹² Important agents from this class are vinblastine and vincristine, which were both approved for use in multiple cancer indications during the 1960s (Figure 1.5). These agents exhibit their mechanism of action by binding to tubulin, stopping cells from separating their chromosomes during the metaphase of cell division and eventually leading to cell apoptosis.¹³

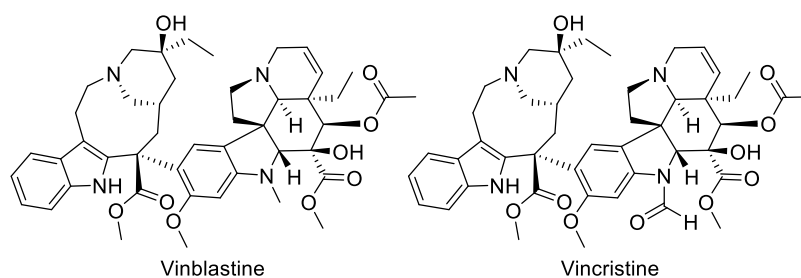


Figure 1.5 Chemical structures of vinblastine and vincristine.

Tyrosine-kinase inhibitors, a more recent class of anticancer drugs, were first investigated in 1988.¹⁴ Tyrosine-kinase enzymes are responsible for the activation via phosphorylation of many proteins involved in signal transduction cascades. In the context of cancer, epidermal growth factor receptors (EGFR) are one of the main targets as they promote tumour angiogenesis, growth and metastases. Tyrosine-kinase inhibitors became of significant interest after the discovery of low molecular weight inhibitors that could discriminate between EGFR and other tyrosine kinase receptors, including human epidermal growth factor receptor 2 (HER2) and the insulin receptor.¹⁵ Two examples of drugs from this class are imatinib and lapatinib (Figure 1.6).

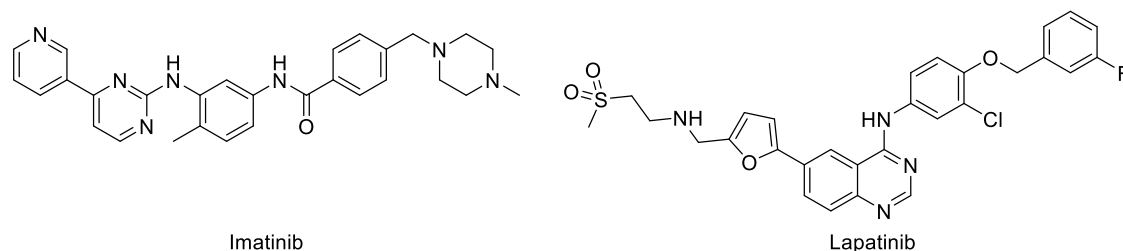


Figure 1.6 Chemical structures of imatinib and lapatinib.

Monoclonal antibodies are a recent class of cancer treatments. These protein-based therapeutics are antibodies made by identical immune cells that are all clones of a parent cell, meaning that they bind to the same antigen. Recent advances have been made in the targeting of specific antigens overexpressed, mutated or selectively expressed in specific tumour types.¹⁶

1.2 Project Summary

New cancer treatments have been steadily moving towards a more personalised approach that limits side effects and maximises efficacy. It was envisioned at the start of my PhD project that by combining two chemotherapeutics into a single mutual prodrug, which was able to be selectively activated within solid tumours to locally release both active drugs, could alleviate some of the debilitating side effects of current cancer treatment whilst maximising potential benefits. One way to achieve tumour selective prodrug activation is through exploitation of the unique micro environment of solid tumours. In our case, we aimed to exploit the hypoxic microenvironment of solid tumours to trigger mutual prodrug activation. The following sections rationalise the choice of anticancer agents for inclusion in the mutual prodrugs and their method of activation.

1.3 Angiogenesis Inhibitors in Cancer Treatment

Angiogenesis is the normal physiological process of new blood vessel growth from a pre-existing vasculature. It occurs mainly during growth and development but is also important during wound healing. As in normal tissues, tumours require an adequate supply of oxygen and nutrients and an ability to remove waste products.¹⁷ When solid tumours increase in size and density their vascular requirements increase, leading to pro-angiogenic gene expression driven by increasing tumour hypoxia.¹⁸ Tumour angiogenesis is activated when hypoxic tumour cells release vascular endothelial growth factors (VEGFs) (Figure 1.7). High levels of VEGF is able to stimulate angiogenesis from

a dormant, mature vasculature.¹⁹ VEGF results first in vasodilation and increased permeability of capillaries, enabling extravasation of plasma proteins to form a provisional matrix upon which endothelial cells can migrate and develop new vasculature.

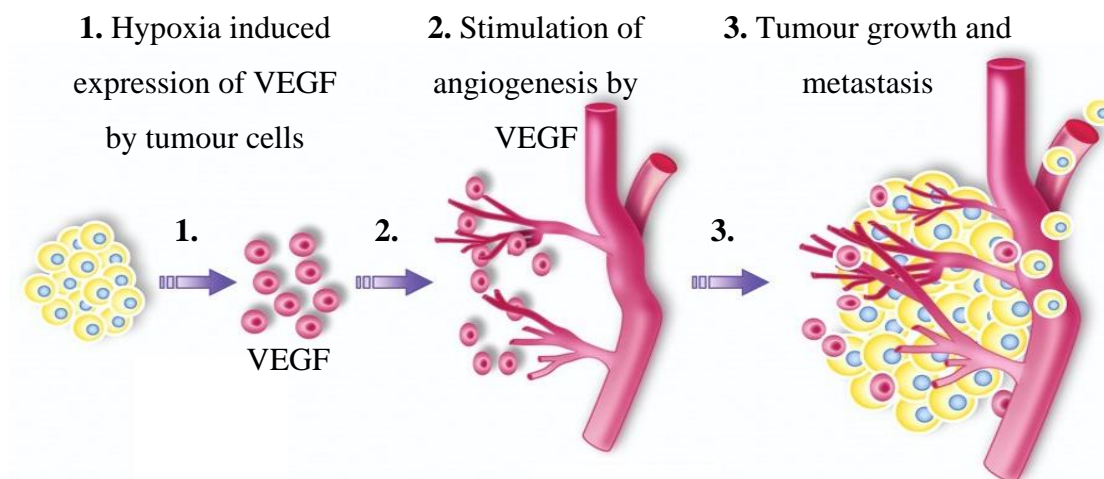


Figure 1.7 Tumour growth and metastasis is promoted by angiogenesis driven by signalling VEGF. (Figure modified from ref. 20).

Angiogenesis in normal tissues is tightly regulated by a balance between pro- and anti-angiogenic signals. When angiogenesis occurs in a tissue, the new vessels rapidly mature and switch off further angiogenesis. Tumour induced angiogenesis, however, does not result in new endothelial cell maturation, allowing continued growth of new tumour blood vessels.²¹

1.3.1 Semaxanib (SU5416) and Sunitinib (Sutent®)

Semaxanib (SU5416) is a tyrosine-kinase and angiogenesis inhibitor from Sugen Inc. (acquired by Pfizer in 2003) that reached Phase III clinical trials for the treatment of advanced colorectal cancer.²² Trials with semaxanib were halted in February 2002 so that the company could focus efforts on a superior successor compound sunitinib (Sutent®) (Figure 1.8). Sunitinib was subsequently approved by the FDA for use as a single agent treatment for renal cell carcinoma and imatinib-resistant gastrointestinal stromal tumours.²³ More recently it was approved for the treatment of pancreatic neuroendocrine tumours.²⁴

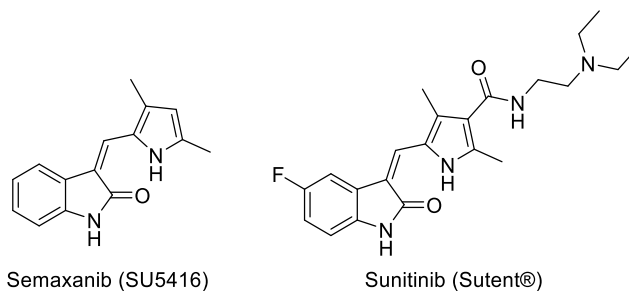


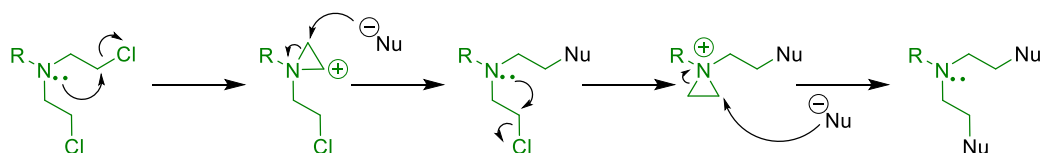
Figure 1.8 Structures of semaxanib and sunitinib.

1.3.2 Mechanisms of Angiogenesis Inhibition

Sunitinib and semaxanib inhibit angiogenesis by ATP- competitive inhibition of receptor tyrosine kinases. Semaxanib is a selective inhibitor of the tyrosine kinase activity of the VEGF-2 receptor,²⁵ while sunitinib shows much broader activity against VEGF-1, VEGF-2, VEGF-3, Fms-like tyrosine kinase-3 receptor (FLT3), stem cell factor receptor (KIT), colony-stimulating factor receptor type 1 (CSF-1R) and the glial cell-line-derived neurotrophic factor receptor (RET).²⁶ VEGF released by hypoxic tumour cells binds to VEGF receptors (VEGFRs) on the surface of endothelial cells, causing dimerization and activation of intracellular kinase domains. The activation process requires concurrent binding of intracellular adenosine triphosphate (ATP). Sunitinib and semaxanib enter cells by passive diffusion and compete with ATP for the VEGFR ATP-binding site.²⁷ Once sunitinib or semaxanib are bound, VEGF cannot activate its intracellular kinase domain, leading to inhibition of downstream signalling and ultimately angiogenesis. Sunitinib also inhibits VEGF-dependent proliferation and migration of endothelial cells to disrupt capillary tube formation.²⁸

1.4 Mechanism of Nitrogen Mustard Cytotoxicity

Nitrogen mustards form highly reactive aziridinium ions via intramolecular cyclisation of an amine to expel a leaving group (often chloride) located two carbons atoms away (Scheme 1.1). The aziridinium ring is highly strained and susceptible to ring opening by the nucleophilic guanine bases of DNA. This alkylation reaction can be repeated to result in the formation of interstrand DNA crosslinks.²⁹⁻³⁰ Alkylation of DNA alone is not in itself cytotoxic and it is the interstrand crosslinks of double stranded DNA that drives the cytotoxicity of nitrogen mustards.³¹⁻³²



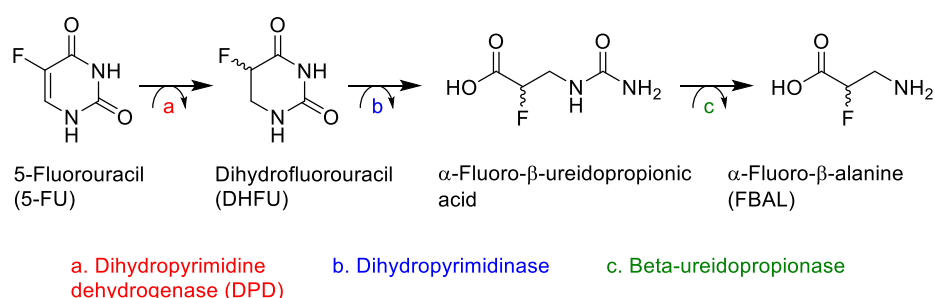
Scheme 1.1 Formation of aziridinium ions by nitrogen mustards leads to reactions with nucleophiles (Nu), including guanine bases of DNA, resulting in formation of cytotoxic interstrand DNA crosslinks.

1.5 5-Fluorouracil (5-FU)

5-FU was first synthesised in 1957 and continues to be a mainstay treatment for many types of cancers. It is approved for use both alone and in combination with other drugs for the treatment of basal cell carcinoma, breast cancer, colorectal cancer, gastric adenocarcinoma, pancreatic cancer and squamous cell carcinomas of the head and neck.³³ Approximately 2 million patients worldwide are administered 5-FU each year.³⁴

1.5.1 Mechanisms of 5-FU Cytotoxicity

After IV administration, 5-FU rapidly enters cells via the same facilitated transport mechanism responsible for uracil uptake.³⁵ More than 80% of administered 5-FU is metabolised in the liver by dihydropyrimidine dehydrogenase (DPD) to inactive (racemic) dihydrofluorouracil (DHFU), which is further converted to α -fluoro- β -ureidopropionic acid and α -fluoro- β -alanine (FBAL) (Scheme 1.2).³⁶ All three metabolites are inactive and excreted in urine within 24 hours. Approximately 60-90% of administered 5-FU ends up as FBAL.³⁷



Scheme 1.2 Liver metabolism of 5-FU produces three inactive metabolites; dihydrofluorouracil (DHFU), α -fluoro- β -ureidopropionic acid and α -fluoro- β -alanine (FBAL).

Once inside cells, 5-FU is converted to active metabolites by the same pathways available to its endogenous counterpart uracil. Active metabolites include fluorodeoxyuridine monophosphate (FdUMP), fluorodeoxyuridine triphosphate (FdUTP) and fluorouridine triphosphate (FUTP) (Figure 1.9). The active 5-FU metabolite FUTP is extensively incorporated into RNA, where it disrupts normal RNA function by inhibiting the processing of pre-RNA into mature ribosomal RNA. It also disrupts post-transcriptional modification of transfer RNAs and the activity of small nuclear RNA/protein complexes, resulting in inhibition of pre-messenger RNA splicing.³⁸⁻⁴³

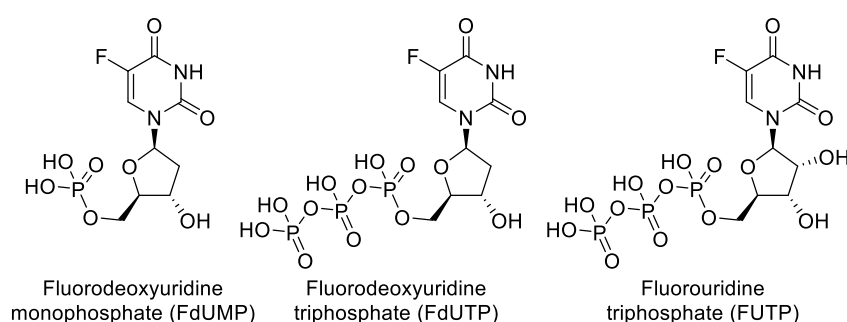


Figure 1.9 Active metabolites of 5-FU, fluorodeoxyuridine monophosphate (FdUMP), fluorodeoxyuridine triphosphate (FdUTP) and fluorouridine triphosphate (FUTP).

Part of the antitumour mechanism of 5-FU involves inhibition of thymidylate synthase (TS) (Figure 1.10). TS is crucial for cell survival as it catalyses the reductive methylation of deoxyuridine monophosphate (dUMP) to deoxythymidine monophosphate (dTMP), with reduced folate 5,10-methylenetetrahydrofolate (CH_2THF) acting as a cofactor. FdUMP produced from 5-FU binds to the nucleotide binding site of TS to form a stable ternary complex between the enzyme and CH_2THF that blocks dUMP binding and inhibits dTMP synthesis.⁴⁴⁻⁴⁵ Depletion of dTMP results in reduced deoxythymidine triphosphate (dTTP), which in turn affects levels of deoxyadenosine triphosphate (dATP), deoxyguanosine triphosphate (dGTP) and deoxycytidine triphosphate (dCTP) through various feedback mechanisms.⁴⁶ The resulting imbalance in the dATP/dTTP ratio is thought to disrupt DNA synthesis and repair, resulting in lethal DNA damage and cell death.⁴⁷⁻⁴⁸ Deoxynucleotide (dNTP) imbalance also leads to higher concentrations of deoxyuridine triphosphate (dUTP) within cells.⁴⁹⁻⁵⁰ Both dUTP and the 5-FU metabolite FdUTP can be misincorporated into DNA and disrupt its function. The concentration of dUTP is highly dependent on levels of pyrophosphatase (dUTPase), which acts to limit intracellular accumulation.⁵¹⁻⁵²

Repair of damaged DNA by the nucleotide excision repair enzyme uracil-DNA-glycosylase (UDG) is ineffective in the presence of high FdUTP/dTTP ratios.⁵³ Misincorporation excision and repair instead leads to further errors in DNA, eventually breaking the DNA strand and triggering cell death.

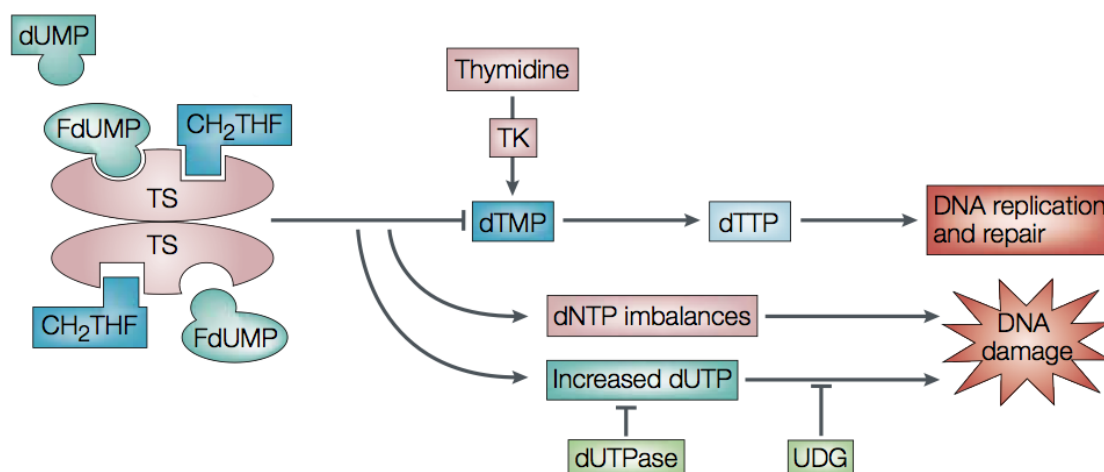
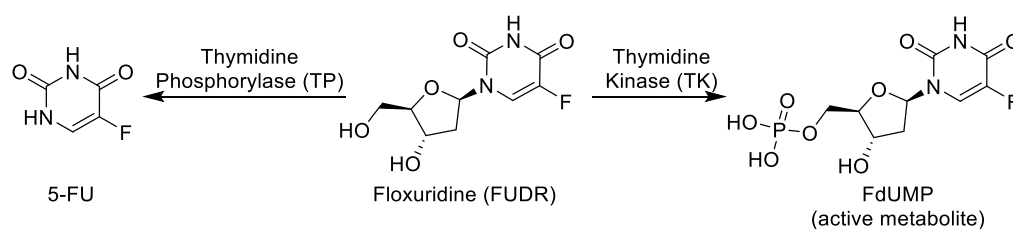


Figure 1.10 Fluorodeoxyuridine triphosphate (FdUTP) inhibition of thymidine synthase (TS) leading to DNA damage and disrupted DNA replication and repair. (Figure modified from 54).

1.5.2 Floxuridine

Fluorodeoxyuridine (FdUR), a prodrug form and metabolite of 5-FU, is an FDA approved drug sold commercially as floxuridine (Scheme 1.3). Floxuridine is more efficiently metabolized to active species in the liver than 5-FU and is sometimes administered via the hepatic artery to treat liver metastases of colorectal cancers.⁵⁵ Meta-analysis of randomised trials indicated that this route is superior in terms of response rates and survival compared to intravenous administration.⁵⁶ Floxuridine is metabolised to either 5-FU (via thymidine phosphorylase, TP) or to the active metabolite FdUMP (via thymidine kinase, TK).



Scheme 1.3 Metabolism of floxuridine to 5-FU and FdUMP.

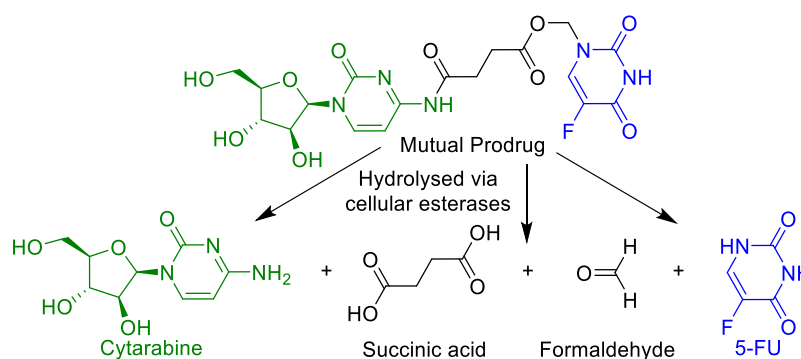
1.6 Prodrugs in Anticancer Chemotherapy

Prodrugs are pharmacologically inert molecules that are converted to active drugs *in vivo* after undergoing metabolic reactions. They are often used to render drug molecules inactive until specific enzymes or biological environments within the body convert them to the active parent. Anticancer prodrugs often contain a non-toxic group covalently attached to the active agent to enhance stability, solubility or another drug property and/or enhance selectivity for tumour cells.⁵⁷

1.6.1 Mutual Prodrugs

Mutual prodrugs are comprised of two or more drugs that are chemically linked such that they are released from each other simultaneously after some triggering reaction *in vivo*.⁵⁸ The drugs can either be connected directly or via a linker. A potential advantage of mutual prodrugs is that they address issues relating to co-administration of structurally unrelated molecules and their distribution to the target tissue(s), since they are co-transported as a single molecule.⁵⁹

One reported example is the 5-FU|Cytarabine mutual prodrug described by Menger *et al.* (1997).⁶⁰ This prodrug combines (via a succinate linker) 5-FU and cytarabine, a front-line anticancer agent used mainly in the treatment of leukaemia (Scheme 1.4).⁶¹ The mutual prodrug was designed to undergo amidase-mediated hydrolysis *in vivo*. The linking of the two drugs together creates the inactive prodrug. It has been proposed that a “dual-hit” from a mutual prodrug of this type can be more cytotoxic to tumour cells than the two individual drugs used in combination. Attachment of the acyl group to the exocyclic amine also serves to decrease inactivation of cytarabine by cytidine deaminase.⁶²



Scheme 1.4 Metabolic activation of a 5-FU|cytarabine mutual prodrug yields two active drugs (5-FU and cytarabine) and two “waste” (linker) fragments.⁶⁰

1.6.2 Tumour-Selective Activation of Antitumour Prodrugs

A shortcoming of traditional anticancer cytotoxins (such as 5-FU and nitrogen mustards) is their relatively low selectivity for tumour cells over normal tissues. Consequently, treatments with these agents are hampered by dose-limiting toxic side effects. One possible solution to this problem is to create prodrugs that selectively reveal the active drug(s) only in the immediate tumour microenvironment. This can lead to improved pharmacodynamics and reduced side effects by lowering exposure of normal tissues to the toxic active agent(s). Prodrugs of this type are often comprised of trigger, linker and effector units, with the linker unit functioning to release the effector (active drug) after the triggering moiety undergoes a metabolic reaction selectively within tumours.⁶³

1.7 Antibody-Drug Conjugates

Antibody-drug conjugates (ADC) are a major class of modern, tumour-selective anticancer prodrugs. The design of an ADC involves linking a highly potent cytotoxin to a monoclonal antibody via a linker that can be selectively cleaved within tumour cells to release the active cytotoxin (Figure 1.11).⁶⁴

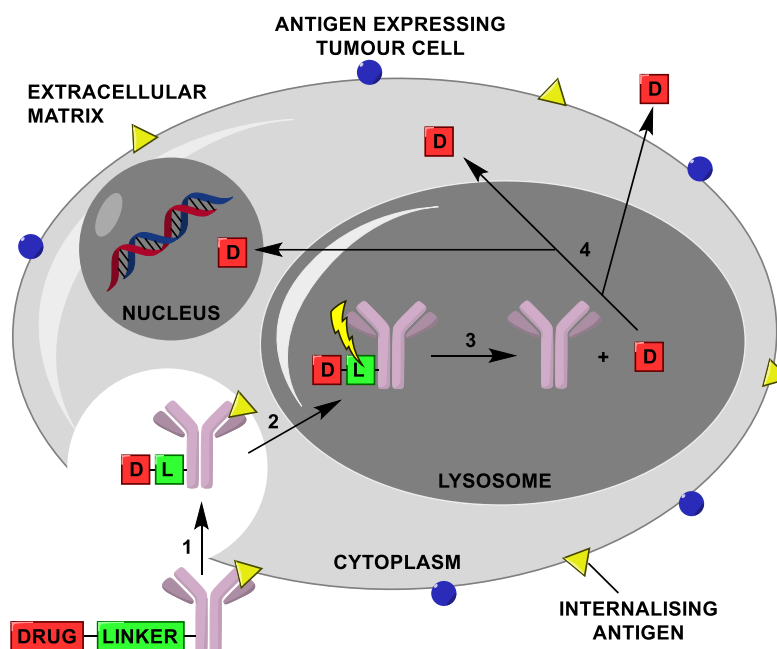


Figure 1.11 Antibody drug conjugates comprise a monoclonal antibody, linker and drug. The mechanism of action involves: 1) specific binding of the antibody to an internalising antigen, followed by endocytosis; 2) transfer to the lysosome; 3) lysosomal cleavage of the linker to release the active drug; 4) drug transfer to the cytoplasm/nucleus leading to cell death and diffusion to neighbouring tumour cells to cause bystander killing effects.

Ideally, the antibody targets an internalising antigen exclusively expressed on the surface of tumour cells, leading to tumour-selective drug uptake.⁶⁵ Linkers are typically composed of a lysosome-sensitive peptide, which upon endocytosis and fusion with lysosomes, is cleaved by lysosomal proteases to release the active cytotoxin within tumour cells.⁶⁶

1.7.1 Brentuximab vedotin (Adcetris®)

Brentuximab vedotin (Adcetris®) is an FDA-approved ADC used in the treatment of relapsed or refractory Hodgkin lymphoma and systemic anaplastic large cell lymphoma.⁶⁷ Brentuximab vedotin consists of the chimeric monoclonal antibody brentuximab (cAC10), a maleimide attachment group, a cathepsin-cleavable linker (valine-citrulline), a fragmenting spacer and the cytotoxin monomethyl auristan E (MMAE) (Figure 1.12).⁶⁸ The brentuximab antibody selectively targets the CD30 cell-surface antigen (expressed by both anaplastic large cell lymphoma and Hodgkin lymphoma) leading to tumour selective uptake.⁶⁹ The antitumour activity arises from MMAE, an exquisitely potent antimetabolic.⁷⁰

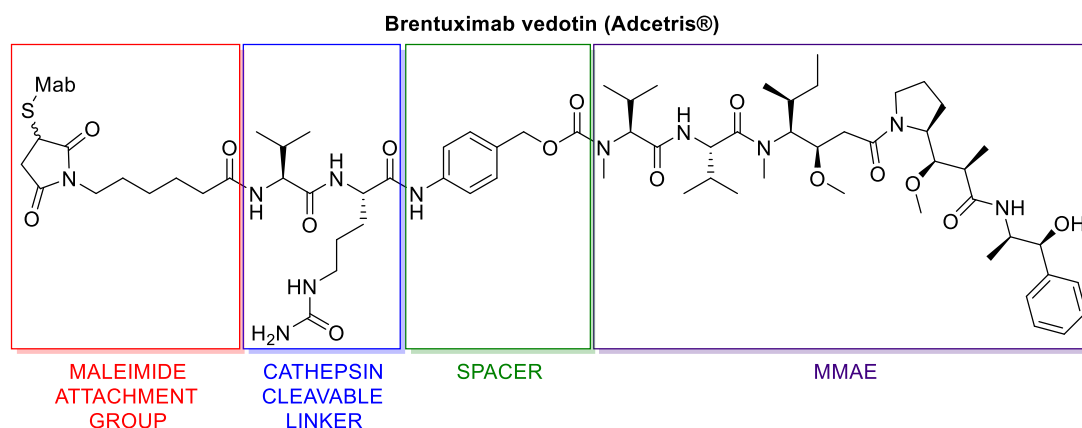


Figure 1.12 Structure of the ADC Brentuximab vedotin (Adcetris®).

1.7.2 Trastuzumab emtansine (Kadcyla®)

Trastuzumab emtansine (Kadcyla®) is an FDA-approved ADC for the treatment of HER2-positive metastatic breast cancer.⁷¹ The drug consists of the monoclonal antibody trastuzumab, a succinimide linker and mertansine, a modified maytansine analogue that contains a thioether (Figure 1.13). The trastuzumab antibody targets HER2, which is overexpressed in 20-30% of breast cancers.⁷² Trastuzumab (Herceptin®) itself was approved by the FDA for use in HER2-positive metastatic breast cancer in 1998.⁷³

Trastuzumab binds to the IV domain of the extracellular segment of the HER2 receptor causing cell arrest in the G1 phase of the cell cycle and reduced cell proliferation.⁷⁴ After tumour selective endocytosis and fusion with a lysosome, the (HER2)-trastuzumab-DM1 complex is degraded to release mertansine,⁷⁵ a potent anti-microtubule agent that triggers apoptosis.⁷⁵

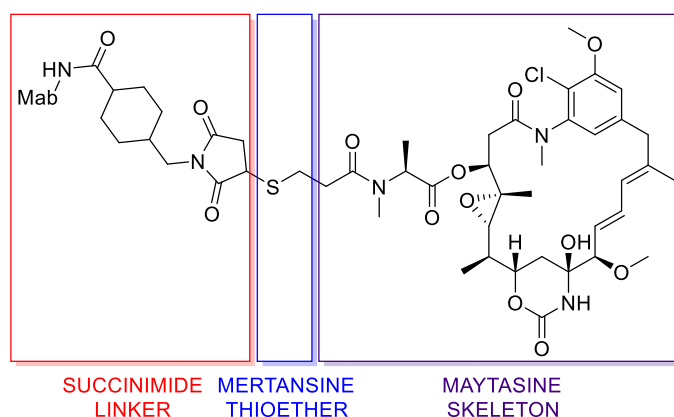


Figure 1.13 Structure of trastuzumab emtansine (Kadcyla®).

1.8 Bioreductive Activation of Antitumour Prodrugs

Rapidly dividing solid tumours quickly outgrow their existing blood supply and develop poorly perfused hypoxic regions.⁷⁶ The vasculature that develops after tumour angiogenesis initiated by hypoxia tends to be aberrant and less ordered than in normal tissues, meaning that pockets of hypoxia remain.⁷⁷ Tumour cells closest to vessels consume the majority of available oxygen, whilst those further away are left in a continuous state of hypoxia. Oxygen partial pressures in hypoxic regions can drop below 2 mm Hg, or 20 times lower than in deoxygenated blood (Figure 1.14). A concomitant drop in pH occurs due to increased lactic acid production from cells undergoing anaerobic metabolism.⁷⁸ Prodrugs that can exploit the uniquely hypoxic regions of solid tumours to locally release active cytotoxins, especially those capable of diffusing and killing nearby oxygenated tumour cells (i.e. bystander effects),⁷⁹ are conceptually a very attractive way of achieving tumour-selective chemotherapy.⁸⁰

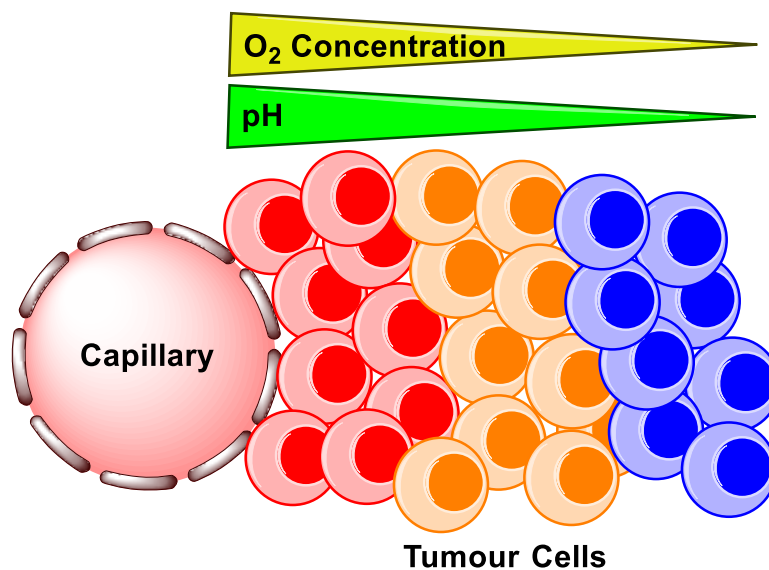


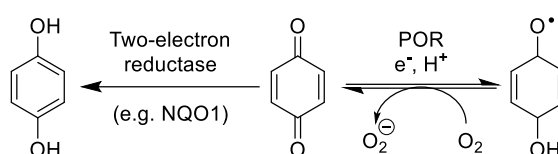
Figure 1.14 Oxygen and pH gradients present in solid tumours arising from an aberrant vasculature. Cells closest to the nearby blood vessels (red) consume all available oxygen leaving cells furthest away to experience continuous hypoxia (blue).

1.8.1 Enzymatic Activation of Prodrugs by Reductases

Over the last 30 years, many hypoxia-activated prodrugs have been designed to exploit enzymes for tumour selective prodrug activation. For example, prodrug activation can be initiated by a one-electron reduction carried out by flavin-dependant oxidoreductases. The one-electron adducts that are formed can be back-scavenged by molecular oxygen in normoxic tissues to regenerate the prodrug. In hypoxic tissues, the one-electron adduct either fragments via a radical dependant mechanism or is further reduced by a stepwise addition of electrons. Sequencing of the human genome identified ninety annotated human flavoproteins that are responsible the catalysing redox processes in primary metabolic pathways, such as the citric acid cycle, β -oxidation and degradation of amino acids.⁸¹ Identification of specific flavoproteins that are the most amenable to tumour-specific activation of prodrugs has proven to be difficult due to the functional redundancy of this family of proteins.⁸² Nevertheless, some of the more important bioreductive enzymes identified include cytochrome p450 oxidoreductase (POR), NAD(P)H quinone dehydrogenase 1 (NQO1), xanthine oxidase/xanthine dehydrogenase and cytochrome b₅ reductase.⁸³

1.9 Quinones as Hypoxia-Activated Prodrugs

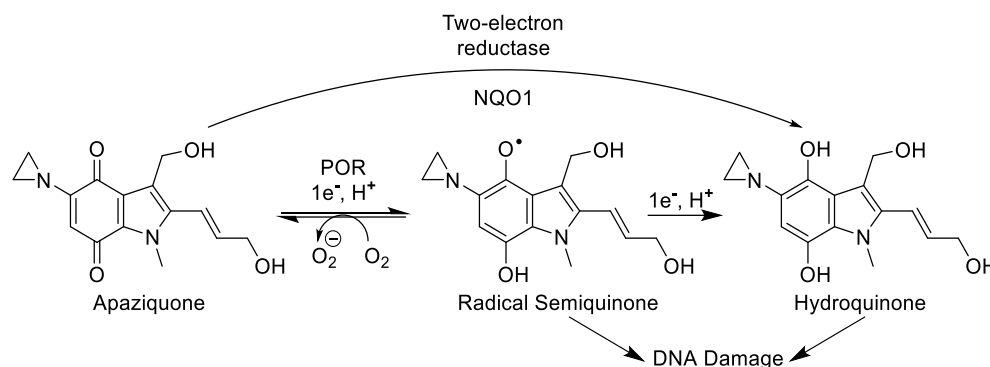
Quinones occur in many biologically active molecules, including vitamin K and doxorubicin. The quinone group has long been of interest in hypoxia activated prodrugs due to the ease with which it undergoes one-electron reduction, primarily catalysed by POR, which converts it to a semiquinone radical anion (Scheme 1.5).⁸⁴ This radical anion is back-scavenged by molecular oxygen, making it highly suited to hypoxia-activated prodrugs. One issue with quinones, however, is their propensity to undergo irreversible two electron reductions to hydroquinones in reactions catalysed by NQO1.



Scheme 1.5 Quinones can undergo an irreversible two-electron reduction *in vivo* catalysed by NQO1, or oxygen sensitive reversible one-electron reduction catalysed by POR.

1.9.1 Apaziquone

Two electron quinone reductions have been explored for the activation of the prodrug apaziquone (Scheme 1.6), which can be selectively activated by a NQO1 catalysed two-electron reduction.⁸⁵ Both the semiquinone radical and hydroquinone adducts can alkylate DNA.⁸⁶ Meta-analysis of NQO1 polymorphism C609T demonstrated an increased risk of multiple types of cancers.⁸⁷ Levels of NQO1 are significantly higher in tumours with nodal metastases compared to those without metastasis, resulting in some tumour selective activation of apaziquone.⁸⁸ Results from two phase III clinical trials of apaziquone were reported in 2017 (sponsored by Spectrum Pharmaceuticals and Allergan) for the treatment of superficial non-muscle invasive bladder cancer in patients undergoing transurethral resection of bladder tumours. Unfortunately, both trials missed the primary endpoint of a statistically significant reduction in disease recurrence at two years following tumour resection and a single dose of apaziquone versus placebo (NCT00461591 and NCT00598806). In 2017, a new phase III trial with an increased single dose of apaziquone (8 mg from previous trials of 4 mg) began recruiting with results to be reported in 2021 (NCT03224182).



Scheme 1.6 Apaziquone can undergo two-electron reductive activation via NQO1, resulting in a hydroquinone, or oxygen-sensitive one-electron reduction to the semiquinone radical by POR. Both adducts are able to damage DNA.

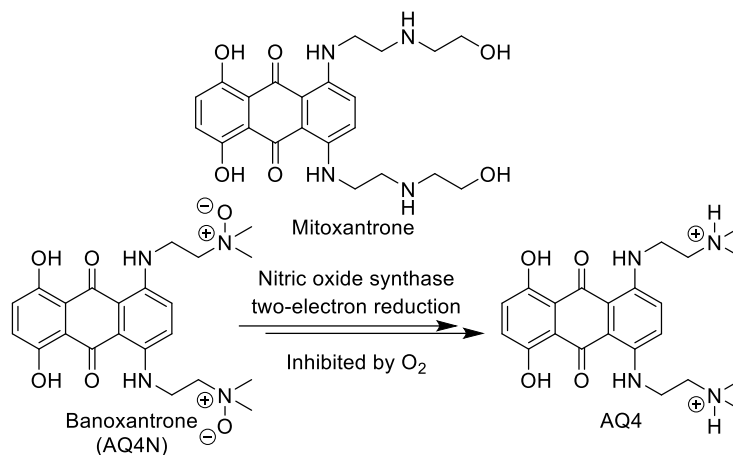
1.10 *N*-oxides as Hypoxia-Activated DNA Intercalator Prodrugs

Anticancer agents containing *N*-oxides were described as early as the 1960s.⁸⁹ The two main subclasses of *N*-oxides can act as hypoxia activated prodrugs; i.e. tertiary amine-*N*-oxides and aromatic-*N*-oxides. Tertiary amine-*N*-oxides typically rely on loss of target-binding interactions when in the *N*-oxide prodrug form. Upon hypoxia-triggered reduction, the newly revealed amine shows increased affinity for the target. Aromatic-*N*-oxides are reduced in a one-electron process that generates cytotoxic nitroxide radicals, which cause radical-mediated oxidative DNA strand cleavage.⁹⁰ Hypoxia-selectivity is achieved by the initial radical species being back-oxidised by molecular oxygen, thus limiting toxicity in oxygenated tissues.

1.10.1 Banoxantrone (AQ4N) – A Tertiary Amine-*N*-oxide

Mitoxantrone is a DNA intercalator that disrupts DNA synthesis and DNA repair in both cancerous and healthy cells, leading to severe side effects (Scheme 1.7). Mitoxantrone is also a potent type II topoisomerase inhibitor and can interfere with RNA. At physiological pH, the alkyl amine groups are protonated and form key interactions with the negatively charged DNA backbone. The experimental drug banoxantrone (AQ4N) is a prodrug of mitoxantrone that shows reduced binding to DNA due to the presence of tertiary amine-*N*-oxides. AQ4N is unique among hypoxia-activated prodrugs because its alkyl-*N*-oxides undergo bioreduction catalysed by nitric oxide synthase in a two-electron process.⁹¹ Reduction of AQ4N is thought to be inhibited by molecular oxygen through competitive inhibition at the heme iron atom, leading to hypoxia-selective activation.⁹² AQ4N undergoes two identical bioreduction of its amine *N*-oxides to first give AQ4M

(single bioreduction) and finally its active drug AQ4, a potent inhibitor of type II topoisomerase.⁹³



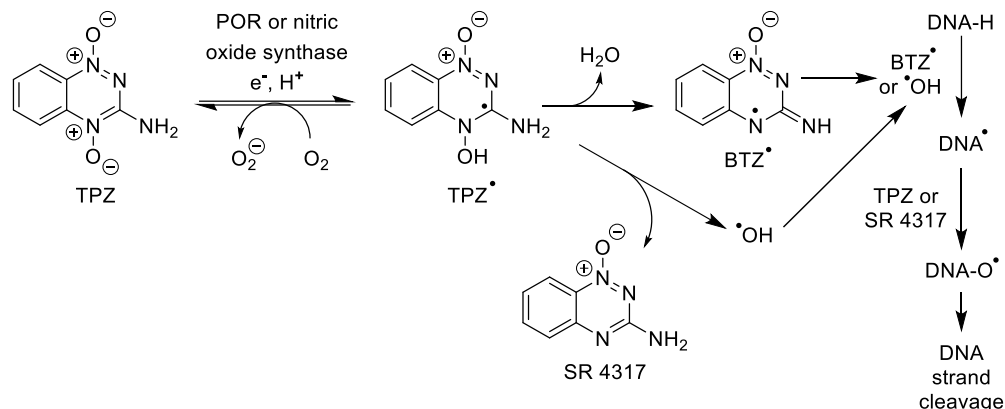
Scheme 1.7 AQ4N is a prodrug variant of mitoxantrone that masks the alkyl amines as *N*-oxides. AQ4N undergoes two-electron bioreductive activation catalysed by nitric oxide synthase to give the intercalator AQ4. This process is inhibited by molecular oxygen, giving rise to hypoxia-selective activation.

Encouraging results were seen with AQ4N in two phase I clinical trials, with no dose-limiting side effects observed.⁹⁴⁻⁹⁵ A phase II trial of AQ4N in combination with radiotherapy and temozolomide in glioblastoma multiforme (NCT00394628) was commenced in 2006 but results were not reported.

1.10.2 Tirapazamine (TPZ) – An Aromatic-*N*-oxide

The most extensively-studied aromatic di-*N*-oxide hypoxia-activated prodrug is Tirapazamine (TPZ) (Scheme 1.8).⁹⁶ TPZ undergoes one-electron reduction by either POR or nitric oxide synthase to form a TPZ^{•-} radical anion.⁹⁷⁻⁹⁸ The radical anion can then be back-oxidised by molecular oxygen or protonated to form the TPZ[•] radical, which undergoes rearrangement with loss of water to form a benzotriazinyl radical (BTZ[•]). Alternatively, TPZ[•] releases a hydroxyl radical ([•]OH) to produce 1,2,4-benzotriazin-3-amine 1-oxide (SR 4317). Once formed, the BTZ[•] and hydroxyl radicals can induce reactive DNA radicals through hydrogen abstraction at the C1', C4' or C5' positions of the deoxyribose sugar backbone.⁹⁹ Under hypoxic conditions, either TPZ or SR 4317 can substitute for molecular oxygen in the subsequent oxygenation of

the C1', C4' or C5' radicals.⁹⁹ The oxygenated radicals then trigger sequence-independent DNA strand cleavage and tumour cell death.¹⁰⁰



Scheme 1.8 Mechanism of hypoxia-selective activation of TPZ leading to DNA cleavage and tumour cell death.

TPZ was studied in three phase III clinical trials (NCT00094081, NCT00017459 and NCT00262821) but the results of only one has been published. In this trial, TPZ was tested in combination with cisplatin (CIS) and irradiation in cervical carcinoma. TPZ/CIS therapy was tolerated at the modified starting dose, however, the combination failed to show superiority over CIS chemoradiotherapy in terms of progression-free survival or overall survival.¹⁰¹ Although these results were discouraging, it was highlighted that the clinical trials did not employ biomarkers to identify patients expected to benefit most from the therapy. One explanation that has been offered for the lack of success of TPZ and other hypoxia-activated prodrugs in clinical studies is the inadvertent inclusion of patients whose tumours show low levels of hypoxia. A hypoxia-imaging sub-study within a larger randomised phase II trial comparing TPZ/CIS plus radiation to CIS plus radiation for advanced head and neck cancer demonstrated a significant benefit for TPZ, providing the first clinical evidence that TPZ acts by specifically targeting hypoxic tumour cells.¹⁰² The study supported use of [¹⁸F]-fluoromisonidazole positron emission tomography imaging as a means of stratifying patients with hypoxic tumours in future clinical studies.⁸²

1.11 Metal Complexes as Prodrugs Designed for Bioreductive Activation

Metal complexes have been intensively studied as hypoxia-activated prodrugs.¹⁰³ Cobalt is a suitable metal for selective delivery of chemotherapeutics to regions of tumour

hypoxia owing to the higher lability of reduced Co(II) complexes relative to Co(III). It was originally proposed that as the reduction potential of Co(III) complexes is usually between -0.20 to -0.40 V, they could be reduced to Co(II) within hypoxic cancer cells, with selectivity obtained by the Co(II) complex being back-oxidised by molecular oxygen within normoxic cells. The complex could break apart in hypoxic tumour cells releasing attached cytotoxins.¹⁰⁴ Pulse radiolysis studies, however, revealed that selectivity was mostly achieved through competitive binding of oxygen to one-electron reductants in cells rather than through Co(II)/Co(III) redox cycling.¹⁰⁵

1.11.1 Examples of Cobalt(III) Hypoxia Activated Prodrugs

An early example of a cobalt(III) hypoxia-activated prodrug was SN24771 (Figure 1.15).¹⁰⁶ When the nitrogen mustard is bound to the cobalt complex it is unable to alkylate DNA. In cell culture assays, SN24771 showed 5- to 30-fold higher toxicity towards hypoxic cells versus normoxic cells.^{80,106} Although SN24771 showed significant hypoxia selectivity *in vitro*, no selectivity was observed *in vivo* and development of the compound was abandoned.¹⁰⁷ It is thought that the limited stability of the cobalt(III) complex itself likely contributed to the poor activity *in vivo*.

In an attempt to improve the kinetic stability of the cobalt(III) oxidation state, complexes containing tetradentate ligands such as cyclam and cyclen were investigated.¹⁰⁸ One complex contained a potent DNA minor groove alkylator 1-(chloromethyl)-5-hydroxy-1*H*-pyrrolo[3,2-*f*]quinolin-3(2*H*)-yl(5,6,7-trimethoxy-1*H*-indol-2-yl)methanone (*seco*-CPyI-TMI) bound to cobalt(III), along with the cyclam (Figure 17). The racemic *seco*-CPyI-TMI cobalt complex showed 81 to 212-fold higher cytotoxicity under hypoxic conditions relative to 20% oxygen in a panel of 10 human tumour cell lines.¹⁰⁸

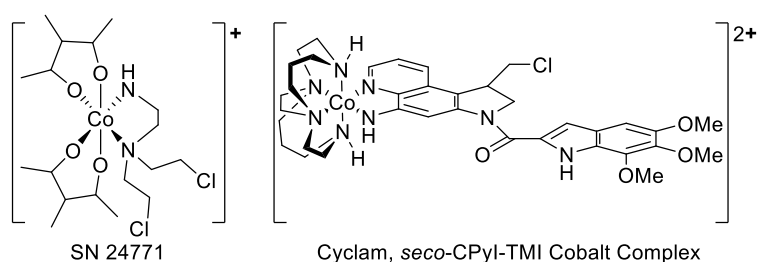


Figure 1.15 Examples of cobalt(III) prodrugs containing nitrogen mustard or *seco*-CPyI-TMI cytotoxins as ligands.

1.11.2 Example of a Copper(II) Hypoxia Activated Prodrug

The limited aqueous solubility of Co(III) complexes and their stability problems led to exploration of other metals in hypoxia-activated prodrugs. Reduction of a copper(II) complex containing a cyclen nitrogen mustard derivative to copper(I) was shown to release the active cytotoxin (Figure 1.16). This complex showed 24-fold selectivity for hypoxic human tumour cells *in vitro* and good water solubility.¹⁰⁹ Hypoxia-activated copper complexes are still in early development and are yet to be studied in the clinic.

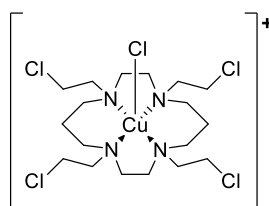


Figure 1.16 Example of a copper(II) cyclen nitrogen mustard prodrug.

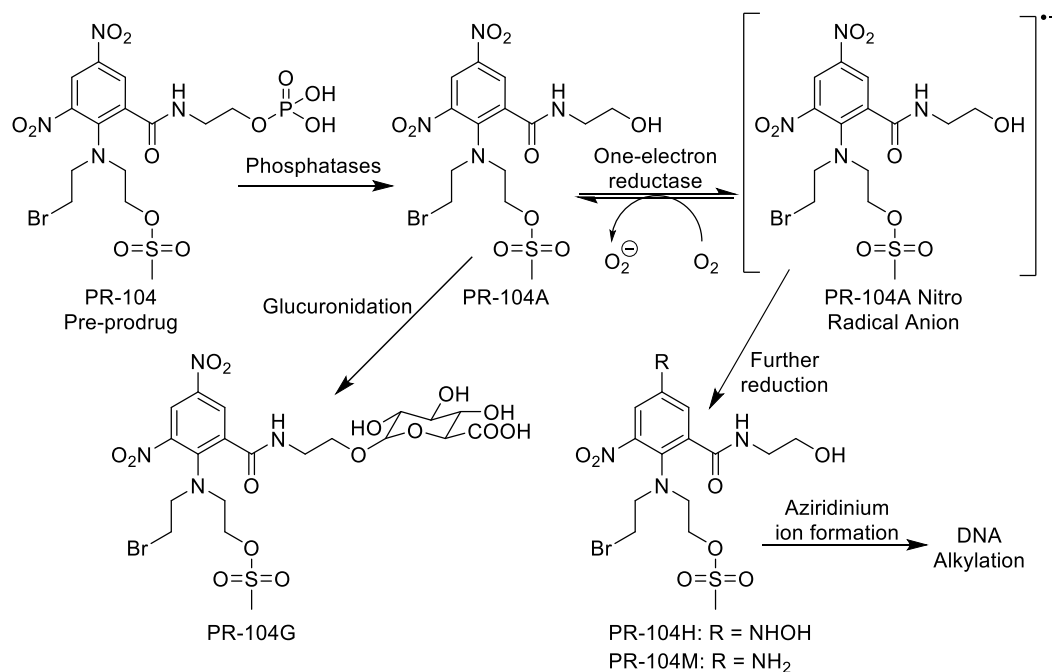
1.12 Nitroaromatics as Hypoxia-Activated Prodrugs

Nitroaromatics as a class of hypoxia activated prodrugs have been extensively studied, with multiple examples progressing to clinical trials. There are two main subtypes of nitroaromatic prodrugs; those that rely on differences between electronic properties of the nitro groups versus the amine/hydroxylamine reduction products and those that involve fragmentation reactions that occur after nitro reduction.

1.12.1 PR-104

The most widely studied nitroaromatic prodrug of the first type is PR-104 (Scheme 1.9). This dinitrobenzamide mustard relies on the nitro groups pulling electron density away from the nitrogen mustard to prevent formation of the DNA-reactive aziridinium ions (Section 1.4). Bioreductive activation to the hydroxylamine or aniline results in a large increase in reactivity and cytotoxicity of the nitrogen mustard.¹¹⁰ PR-104 is actually a pre-prodrug, where it must undergo two separate activation steps before revealing the active cytotoxin. The sidechain phosphate group increases aqueous solubility but is quickly metabolised by plasma phosphatases giving the prodrug PR-104A. Selectivity for cancer cells is achieved by reduction of the nitroaromatic group by one-electron reductases forming the PR-104A nitro radical anion, which in normoxic cells is back-scavenged by molecular oxygen to form superoxide. In hypoxic tumour cells, further reduction delivers the active cytotoxin. Reduction of PR-104A gives PR-104H

(hydroxylamine) after addition of 4-electrons and PR-104M (amine) after 6-electron reduction. Using a combination of siRNA transfection and antisense expression it was determined that the main reductase responsible for the initial reduction is POR, although other flavoenzymes may also contribute.¹¹¹



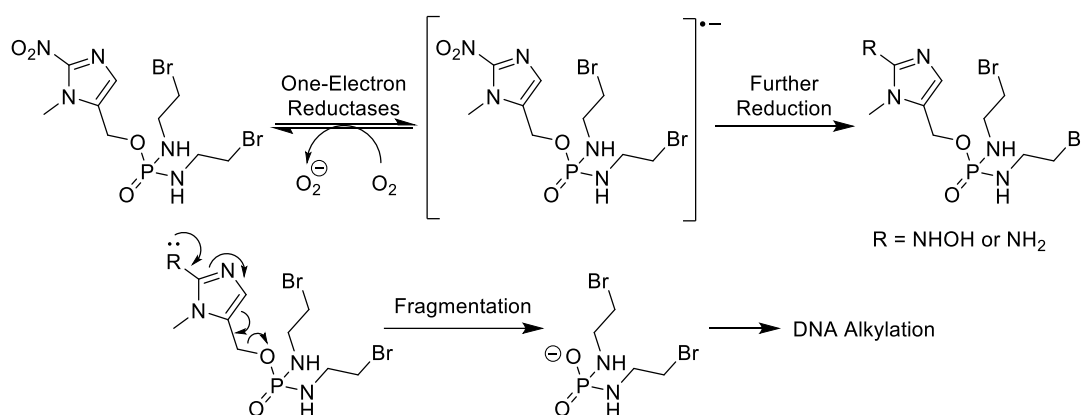
Scheme 1.9 Mechanism of activation of the pre-prodrug PR-104. The major PR-104 metabolite in solid tumour patients was the *O*-glucuronide metabolite (PR-104G) formed by glucuronidation of PR-104A.

During animal studies, PR-104 showed significant efficacy, especially in AKR1C3-expressing xenografts, where it decreased disease progression and tumour metastases and prolonged overall mouse survival.¹¹²⁻¹¹³ Phase I/II trials with PR-104 were initiated for relapsed small cell lung cancer (NCT00544674), non-small cell lung cancer (NCT00862134), hepatocellular carcinoma (NCT00862082) and refractory/relapsed acute leukemia (NCT01037556). Unfortunately, each trial of PR-104 was discontinued after PR104 showed significant toxicity, including myelosuppression and gastrointestinal effects.¹¹⁴ It is thought that the intestinal cytotoxicity occurs through biliary excretion of the *O*-glucuronide metabolite (PR-104G), the major PR-104 metabolite identified in solid tumour patients (Figure 11).¹¹⁵ Once in the gut, β -glucuronidase activity of the gut flora regenerates PR-104A and bacterial nitroreductases trigger reduction of PR-104A to its active cytotoxins in the intrinsically hypoxic environment of the intestines.¹¹⁶

Myelosuppression is thought to occur through effects on hematopoietic stem/progenitor cells residing within hypoxic bone marrow niches.¹¹⁷

1.12.2 Evofosfamide (TH-302)

Nitroimidazoles (e.g. misonidazole) were originally developed as oxygen mimetics that could act as radiosensitizers in hypoxic tumour cells to cause oxidative DNA damage in the presence of ionising radiation.¹¹⁸ The compounds showed limited selective toxicity towards hypoxic tumour cells in the absence of radiation due to their ability to fragment into DNA alkylating species.¹¹⁹ This observation led to development of Evofosfamide (TH-302), a nitroimidazole conjugated to a bromoisophosphoramidate mustard (Scheme 1.10).¹²⁰ Following initial reduction by a one-electron reductase, oxygen back-oxidises the nitro radical anion to form superoxide. In hypoxic tumour cells, further reduction leads to the hydroxylamine and amine derivatives, both of which push electrons into the imidazole ring leading to fragmentation and release of an activated bromoisophosphoramidate mustard.



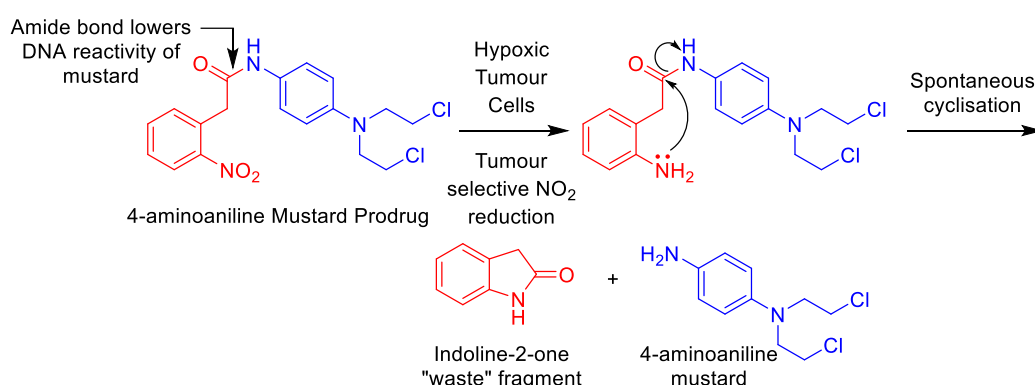
Scheme 1.10 Mechanism of hypoxia-activation of TH-302.

In vitro studies with TH-302 showed up to 300-fold higher cytotoxicity toward hypoxic tumour cells versus aerobic cells,¹²¹ and initial results of phase I/II studies showed limited safety concerns.¹²²⁻¹²³ Treatment of advanced or metastatic pancreatic carcinoma with a combination of gemcitabine and TH-302 showed significantly improved progression-free survival compared to gemcitabine alone. These promising results led to two phase III trials in soft tissue sarcoma (NCT01440088) and pancreatic adenocarcinoma (NCT01746979). In the soft tissue sarcoma trials, TH-302 in combination with doxorubicin showed little difference in median progression free survival to doxorubicin

alone (6.3 months versus 6.0 months).¹²⁴ The disappointing results of these trials caused Threshold Pharmaceuticals to halt clinical development of TH-302.

1.12.3 Nitroaromatic Prodrug of a 4-Aminoaniline mustard

In an early example reported by the Denny group, a bioreductively-activated nitrogen mustard prodrug was conceived that linked a 4-aminoaniline mustard to a 2-(2-nitrophenyl)acetic triggering moiety.¹²⁵ Hypoxia-selective 6-electron reduction of the aryl NO₂ group in the molecule was designed to trigger a cyclisation reaction that yielded the active mustard and an indolin-2-one waste fragment (Scheme 1.11). The presence of the amide bond in the prodrug served to lower the reactivity of the mustard towards DNA, with nucleophilic reactivity greatly increasing after amide cleavage. In normoxic tissues, the 1-electron reduction product (nitro radical anion) would be back-scavenged by molecular oxygen to regenerate the inert prodrug.



Scheme 1.11 Tumour-selective nitroaromatic prodrug reported by Denny *et al.*¹²⁵

1.13 Molecularly Targeted Hypoxia Activated Prodrugs

DNA is the most common target for hypoxia activated prodrugs, such as cytotoxic cross-linking agents. These drugs induce DNA damage in proliferating normal tissues and, therefore, are associated with high levels of toxicity.¹²⁶ It was envisioned that selectively activation triggered by tumour hypoxia would limit off-target toxicity. Diffusion of activated prodrugs into the surrounding area has been shown to cause bystander damage to neighbouring cells.¹²⁷ A more elegant approach is the development of molecularly targeted hypoxia activated prodrugs, delivering a ligand for protein inhibition which is more toxic to hypoxic tissues than normal cells.¹²⁸ The small molecules inhibitors released by hypoxia activated prodrugs are aimed at exploiting biochemical responses to

hypoxia by targeting proteins associated with tumourigenesis and survival, leading to greater selectivity over healthy tissue.¹²⁹

1.13.1 Nitroaromatic Molecularly Targeted Hypoxia Activated Prodrugs

An early example of a molecularly targeted hypoxia activated prodrugs incorporated a poly(ADP-ribose)polymerase (PARP) inhibitor, developed by Parveen and co-workers (Figure 1.17).¹³⁰ PARP1 has been implicated in the repair of damaged DNA, repairing single-stranded DNA breaks and therefore, inhibiting PARP was proposed to increase radiosensitivity. This has led to a series of similarly designed molecularly targeted hypoxia activated prodrugs such as CH-01 (targeting Chk1/Aurora A,),¹³¹ BCCA621C (targeting DNA-protein kinase),¹³² SN29966 (targeting EGFR)¹³³ and TH-4000 (targeting EGFR).¹³⁴

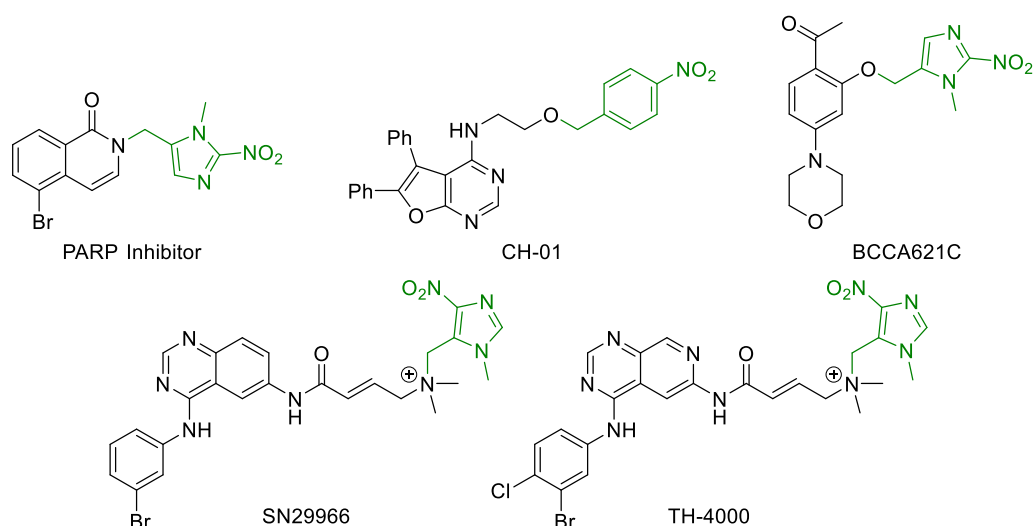
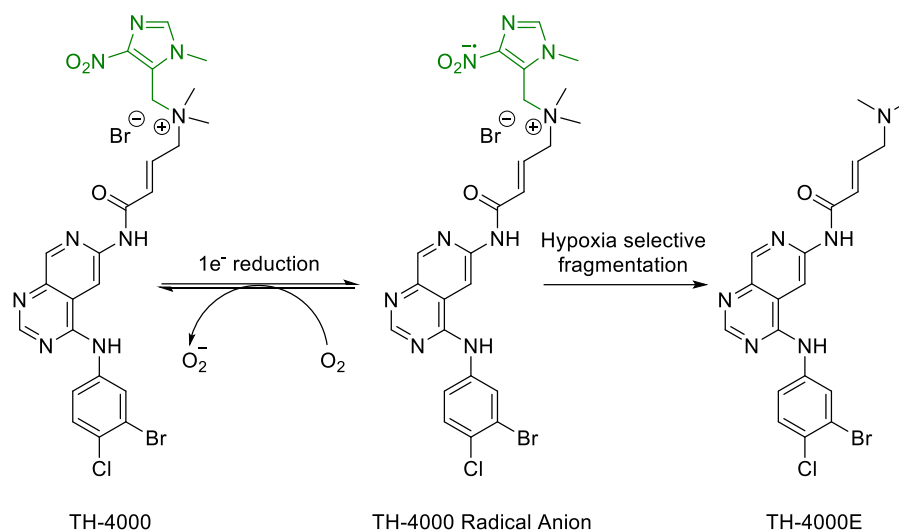


Figure 1.17 Molecularly Targeted Hypoxia Activated Prodrugs (bioreductive moiety shown in green).

The most clinically advanced molecularly targeted hypoxia activated prodrug is TH-4000, originally developed as a result of a structure activity relationship study of SR29966, which is a hypoxia activated epidermal growth factor receptor tyrosine kinase inhibitor.¹³⁵ TH-4000 employs a 4-nitroimidazole bioreductive group, which under hypoxic conditions, undergoes conjugate elimination to release the active tyrosine kinase inhibitor TH-4000E (Scheme 1.12). Fragmentation is proposed via the radical formed after single electron reduction, not requiring reduction to the corresponding amine or hydroxylamine.



Scheme 1.12 Mechanism of hypoxia selective activation of TH-4000 to a radical anion followed by fragmentation to release the tyrosine kinase inhibitor TH-4000E.

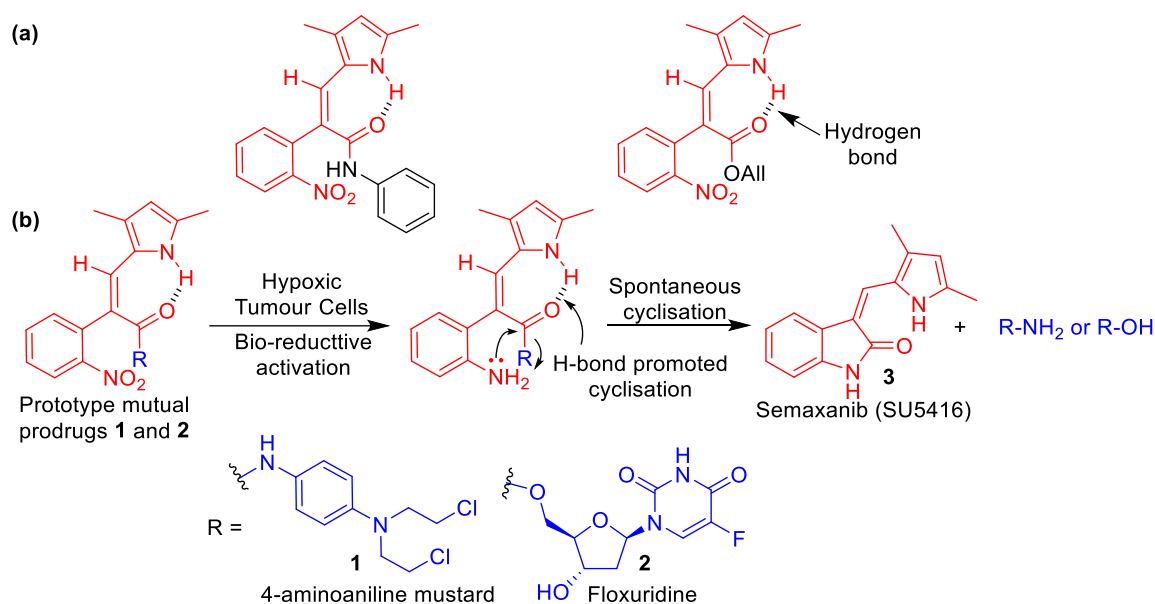
Phase I clinical trials of TH-4000 showed TH-4000 was more effective than commonly used tyrosine kinase inhibitors such as erlotinib against non-small-cell lung carcinoma xenografts with wild-type and mutant EGFR.¹³⁶⁻¹³⁷ On the basis of these results, TH-4000 was advanced into two parallel phase II clinical trials against EGFR-mutant, T790M-negative patients with advanced NSCLC (NCT02454842) and metastatic squamous cell carcinoma of the head and neck or skin (NCT02449681). Unfortunately, both clinical trials have now been terminated due to a lack of efficacy with results yet to be published.

1.14 Design of Hypoxia-Activated Semaxanib|Cytotoxin Mutual Prodrugs

Many of the concepts presented to this point were integrated into the design of two prototype hypoxia-activated antitumour mutual prodrugs comprised of semaxanib (Section 1.3.1) linked to either 4-aminoaniline nitrogen mustard or floxuridine (Section 1.5.2) cytotoxins. The prodrugs were specifically designed to invoke the hypoxia-activated 2-(2-nitrophenyl)acetic triggering mechanism reported by Denny *et al.*¹²⁵ (Section 1.12.3). However, instead of releasing an indoline-2-one as a “waste” fragment, they would release this moiety as part of the angiogenesis inhibitor semaxanib (Section 1.3.1). The other active drug released from the mutual prodrugs would be either the 4-aminoaniline mustard or floxuridine cytotoxin. The aryl nitro group acts as the triggering moiety, designed to undergo selective reduction to the corresponding aniline in hypoxic regions of solid tumours. Spontaneous cyclisation analogous to that reported

by Denny *et al* would then fragment the prodrugs to reveal the two active drugs (Scheme 1.13(b)).¹²⁵

The Kelso Research Group at the University of Wollongong (UOW) reported the synthesis and anti-angiogenic properties of 2-(2-nitrophenyl)acetate derivatives related to the drug semaxanib (Scheme 1.13(a)).¹³⁸ It was noted that a hydrogen bond was invariably present between the pyrrole-NH and carbonyl oxygen atoms in the 2-(2-nitrophenyl)acetic amides and esters (Scheme 1.13(a)), suggesting the scaffold may be pre-organised and activated for rapid indoline-2-one cyclisation following reduction to the aniline.¹³⁸



Scheme 1.13 (a) Anti-angiogenic 2-(2-nitrophenyl)acetate derivatives related to sunitinib.¹³⁸ (b) Prototype mutual prodrugs **1** and **2** and their proposed mechanism of bio-reductive activation to selectively release indoline-2-one multi-kinase inhibitor semaxanib **3** and 4-aminoaniline mustard or floxuridine cytotoxins within hypoxic regions of tumours.

It is conceivable that clinical use of mutual prodrugs of this type could mitigate side effects resulting from either or both drugs, while at the same time increasing localised tumour concentrations of the active agents to improve pharmacodynamics. The mutual prodrug **2** may also lessen the hepatic metabolism issues associated with 5-FU therapy. It is speculated that a therapeutically beneficial prodrug activation “viscous cycle” might

also be established within solid tumours, where continuous administration of the prodrug over time could create increasingly hypoxic tumours through the anti-angiogenic action of semaxanib, possibly enhancing prodrug activation and efficacy as a course of treatment progresses (Figure 1.18).

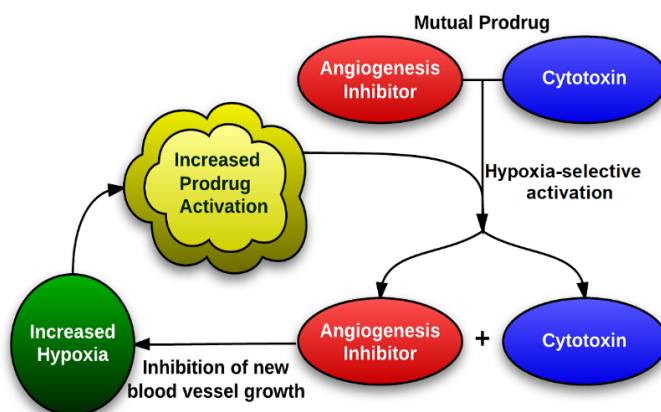


Figure 1.18 Postulated therapeutically beneficial “viscous cycle” created by hypoxia-activated semaxanib|cytotoxin mutual prodrugs.

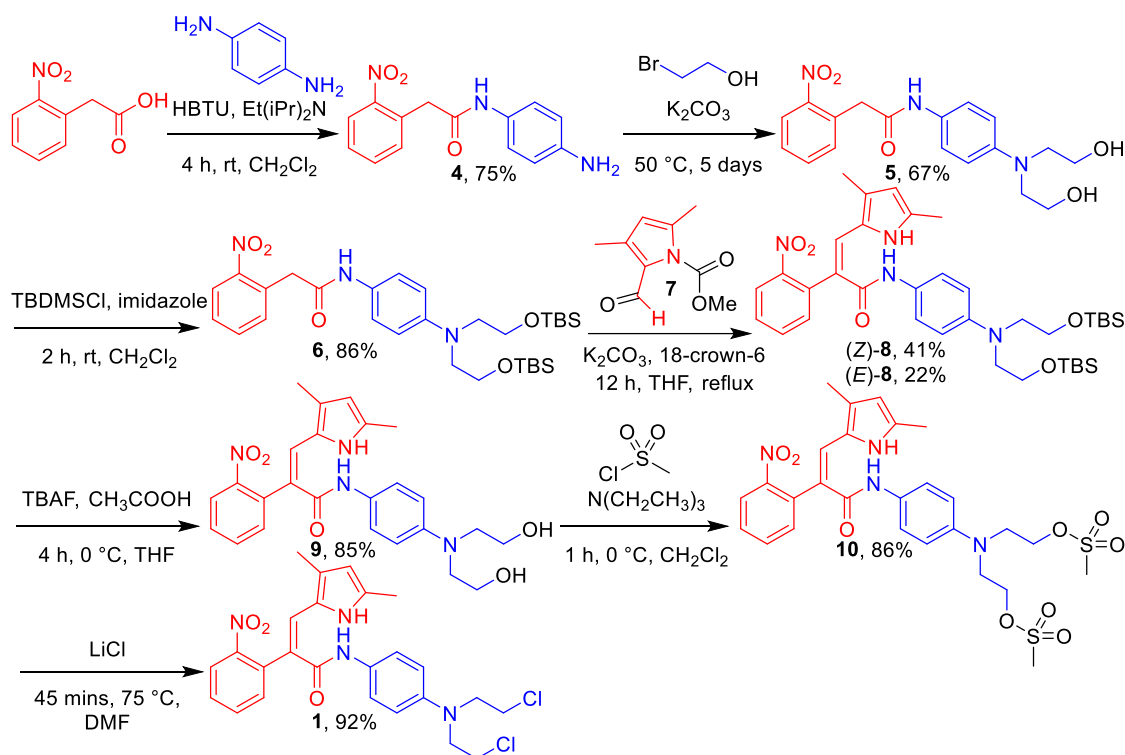
1.15 Project Aims

The primary aims of this thesis work were to develop viable routes for the synthesis of useable quantities (>100 mg) of the semaxanib|cytotoxin mutual prodrugs **1** and **2**. A second aim was to perform chemical reductions (i.e. $\text{NO}_2 \rightarrow \text{NH}_2$) on the prodrugs to establish whether the molecules spontaneously cyclise and fragment to yield the two constituent anticancer drugs. The third aim was to submit the compounds to collaborators at the University of Auckland for pulse-radiolysis experiments and cell testing to measure the nitroaromatic reduction potentials and hypoxia-selective cytotoxicity, respectively.

Chapter 2: Synthesis of Semaxinib|4-Aminoaniline Mustard 1

2.1 Route Development

The synthesis of semaxinib|4-aminoaniline mustard mutual prodrug **1** had previously been scoped on small scale in A/Prof. Michael Kelso's laboratory at UOW by former PhD student Nicholas Kirk (Scheme 2.1).¹³⁹ Kirk's pilot synthesis was used as the foundation for developing a scale-up synthesis capable of delivering sufficient material for chemical and biological testing, as well as optimising the yields and procedures for publication.

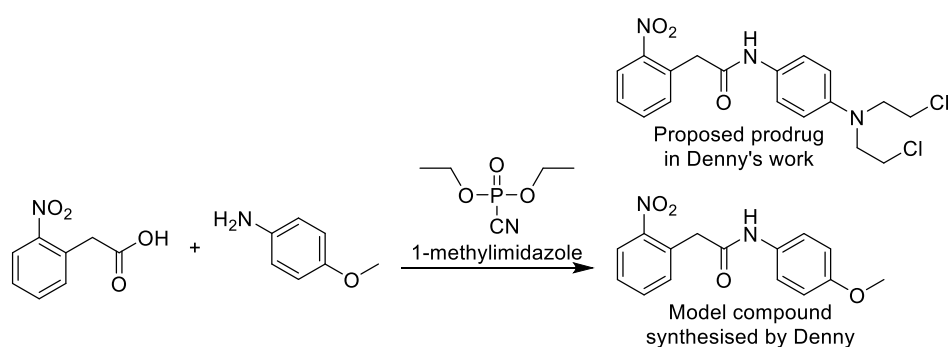


Scheme 2.1 Pilot synthesis of mutual prodrug **1** developed by former PhD student Nicholas Kirk.

The first step in Kirk's synthesis involved coupling 2-(2-nitrophenyl)acetic acid to *p*-phenylenediamine to give amide **4**. This was followed by *bis*-alkylation of the aniline nitrogen with 2-bromoethanol to yield **5**. The *bis*-alcohol **5** was protected with *tert*-butyldimethylsilyl (TBS) groups to afford **6**. With both alcohols protected, a key Knoevenagel condensation of *N*-methylcarbamoyl pyrrole-2-carbaldehyde **7** with **6** gave (Z)-**8**.¹³⁸ Silyl deprotection afforded the *bis*-alcohol **9** and *bis*-mesylation followed by chlorination delivered **1**.

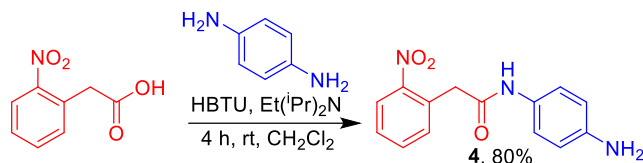
2.2 Amide Coupling

The closest literature precedent for the coupling of *p*-phenylenediamine to 2-(2-nitrophenyl)acetic acid came from Denny *et al*'s work exploring 2-(2-nitrophenyl)acetic acid|4-aminoaniline mustard prodrugs (Section 1.12.3).¹²⁵ In their work, the target nitrogen mustard prodrug was not actually synthesised and a model compound was prepared instead. Denny *et al* coupled 2-(2-nitrophenyl)acetic acid to *p*-anisidine using diethyl cyanophosphate and 1-methylimidazole (Scheme 2.2). Diethyl cyanophosphate is an older, toxic amide coupling reagent so alternative reagents were investigated.



Scheme 2.2 Literature precedent for amide coupling of 2-(2-nitrophenyl)acetic acid to electron rich aryl amines.¹²⁵

Nicholas Kirk investigated the use of hexafluorophosphate benzotriazole tetramethyl uronium (HBTU), diisopropylethylamine in dichloromethane for the coupling to obtain **4**. The reaction was high yielding (75%) but the workup procedure needed to be optimised for larger scale. In Kirk's procedure, upon completion of the reaction the organic layer was extracted with 1 M HCl and the aqueous layer collected, washed with dichloromethane, neutralised with 1 M NaOH, filtered and solids recrystallised from hot ethanol. I found that increasing the concentration of HCl and NaOH to 5 M greatly simplified the isolation procedure and produced purer **4**. Use of 5 M HCl caused the product to precipitate in the acidic aqueous extract, which could be filtered and neutralised with 5 M NaOH. The improved reaction and workup procedure was performed twice on multigram scale (10.1 g and 10.2 g of 2-(2-nitrophenyl)acetic acid), delivering pure **4** in slightly increased yield (80%, Scheme 2.3). A total of 23.8 g of **4** was synthesised in the two reactions.



Scheme 2.3 Amide coupling of 2-(2-nitrophenyl)acetic acid to *p*-phenylenediamine with HBTU to give **4**.

2.2.1 Spectroscopic Evidence for the Formation of **4**

Clear evidence for the formation of **4** was observed by ^1H nuclear magnetic resonance (NMR) spectroscopy in deuterated dimethyl sulfoxide (d_6 -DMSO) (Figure 2.1). The appearance of two new 2H doublets at 7.16 ppm and 6.48 ppm corresponded to the addition of the *para*-substituted aromatic ring. Additionally, the appearance of four new aromatic peaks in the ^{13}C NMR and observing the expected $\text{M}+\text{H}^+$ ion at m/z 272.1035 by high resolution mass spectrometry confirmed the structure of **4**.

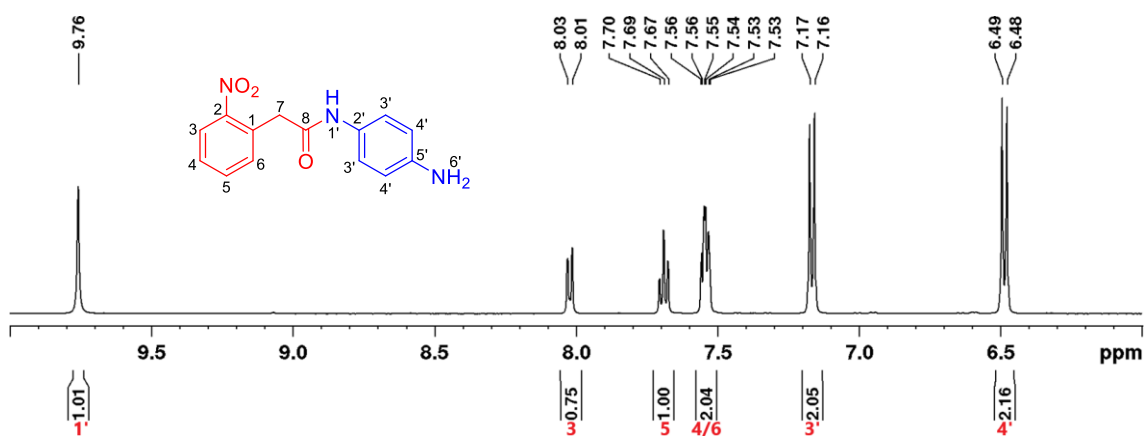
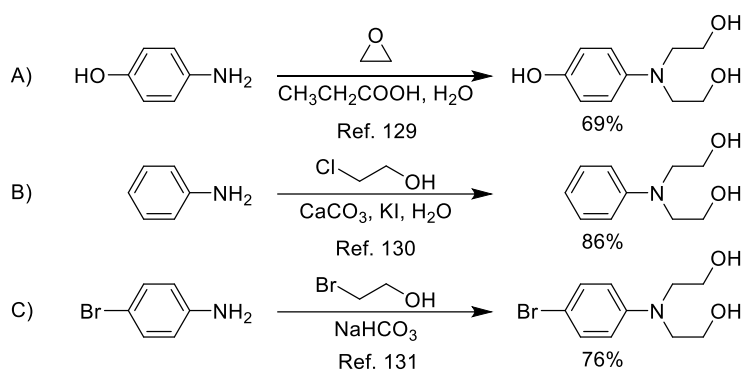


Figure 2.1 Aromatic region of the 500 MHz ^1H NMR spectrum of **4** in d_6 -DMSO.

2.3 Bis-Alkylation of **4**

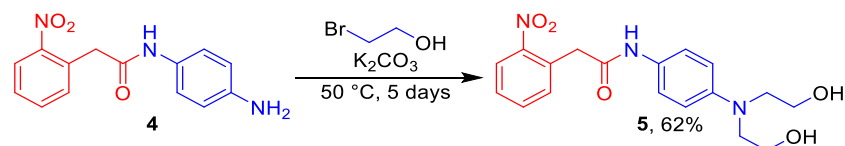
Alkylation and *bis*-alkylation of aromatic amines is a common reaction with several examples in the literature using many different reagents. In one representative example, alkylation of 4-methoxyaniline with ethylene oxide in the presence of propionic acid and water gave 69% of the *bis*-alkylated product (Scheme 2.4, A).¹⁴⁰ In this reaction, the acid first protonates ethylene oxide to activate it towards nucleophilic attack by the aniline and release of ring strain provides a strong driving force for ring opening.

A second example used 2-chloroethanol, calcium carbonate and potassium iodide in water to give *N,N*-bis-alkylated aniline in 86% yield (Scheme 2.4, B).¹⁴¹ The reaction likely proceeds via Finkelstein conversion of 2-chloroethanol to 2-iodoethanol, followed by nucleophilic substitution by the aniline nitrogen and loss of iodide as a leaving group. In a third example, alkylation of 4-bromoaniline using 2-bromoethanol and sodium bicarbonate gave 76% of the *bis*-alkylated product (Scheme 2.4, C).¹⁴² 2-Bromoethanol was used neat as the reagent and solvent in this reaction.



Scheme 2.4 Three literature precedents for the *bis*-alkylation of aromatic amines.¹⁴⁰⁻¹⁴²

Bis-alkylation of **4** was explored by Nicholas Kirk using neat 2-bromoethanol and potassium carbonate (Scheme 2.5). The reaction was problematic, however, being limited in scale by both the workup and purification procedures. Kirk's workup involved concentrating the mixture under reduced pressure and extracting with ethyl acetate and brine solutions. Purification required complex and lengthy column chromatography. When performed on a large scale (11.6 g **4**), I noted that several impurities were being formed during the concentration step leading to reduced yield (28%). To circumvent this, I found that the product could be precipitated directly from the 2-bromoethanol reaction mixture by addition of excess brine. The crude precipitate was then easily filtered and recrystallised ($-20\text{ }^\circ\text{C}$) from hot ethanol. The simplified workup procedure allowed more practical and rapid access to larger quantities of **5**. The reaction was successfully performed two more times (4.0 g and 6.6 g **4**) and gave acceptable yields (62% and 53%, respectively), affording a total of 12.3 g of **5** across the three reactions.



Scheme 2.5 Bis-alkylation of **4** with neat 2-bromoethanol yielded **5** on multi-gram scale.

2.3.1 Spectroscopic Evidence for the Formation of **5**

Evidence for the formation of **5** was clearly observed in the ^1H NMR spectrum (Figure 2.2), where a new quartet had appeared at 3.51 ppm, along with a triplet at 3.37 ppm, both with integration 4H. The two new signals corresponded to addition of two chemically equivalent ethanol groups to the aryl NH_2 group of **4**. When recorded in d_6 -DMSO, the alcohols appeared as a 2H triplet at 4.70 ppm due to coupling from the adjacent CH_2 , which in turn appeared as an apparent quartet due to coupling from both the alcohol and adjacent CH_2 groups. The singlet at 4.05 ppm with an integration of 2H corresponded to the benzylic CH_2 . The appearance of two new aliphatic signals at 58.1 and 53.3 ppm in the ^{13}C NMR supported addition of the two ethanol chains. Observation of the expected $\text{M}+\text{H}^+$ ion at m/z 360.1559 by high resolution mass spectrometry confirmed formation of **5**.

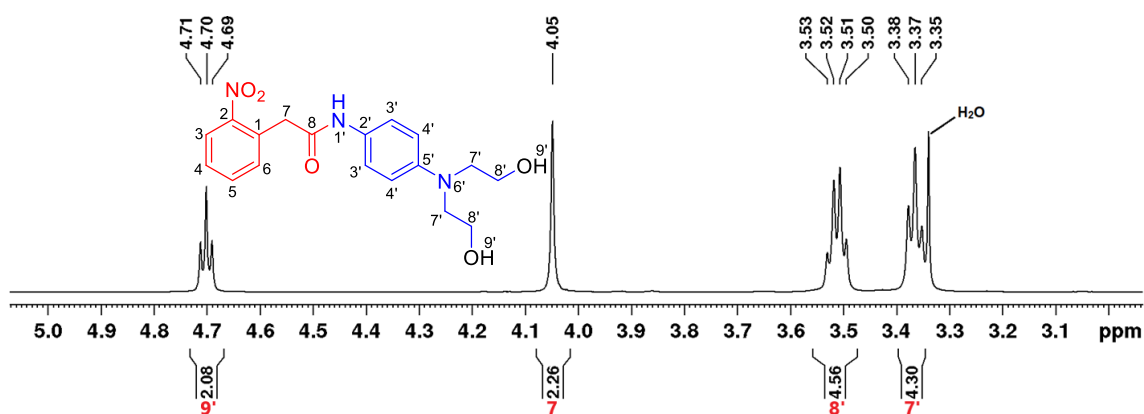
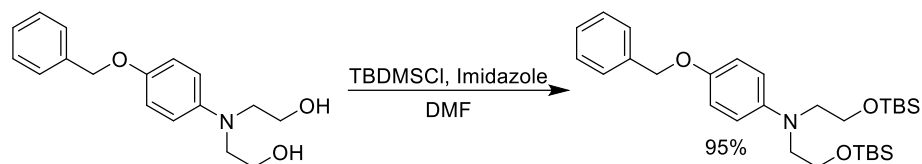


Figure 2.2 Aliphatic region of the 500 MHz ^1H NMR spectrum of **5** in d_6 -DMSO.

2.4 Bis-TBS Protection of **5**

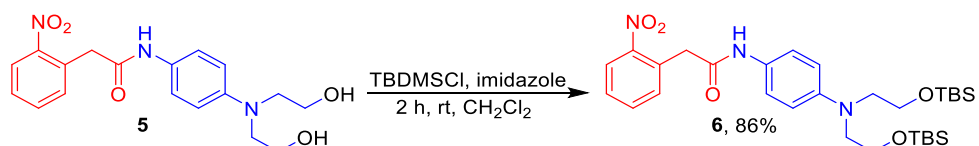
Protection of the two alcohol groups was found by Nicholas Kirk to be essential for success of the ensuing Knoevenagel condensation, presumably because the reaction requires an absence of acidic protons. The protecting group selected was TBS as it is simple to install and later remove under mild conditions. It is also base stable, which is important as the Knoevenagel reaction is performed under basic conditions. There are

many literature precedents for the protection of structurally similar *bis*-ethanolamines with TBS groups. One representative example is shown in Scheme 2.6, where *tert*-butyldimethylsilyl chloride (TBDMSCl) and imidazole in dimethylformamide (DMF) were used to produce 95% of the desired *bis*-TBS-protected diol.¹⁴³



Scheme 2.6 Literature precedent for *bis*-TBS protection of a *bis*-ethanolamine structurally related to **5**.

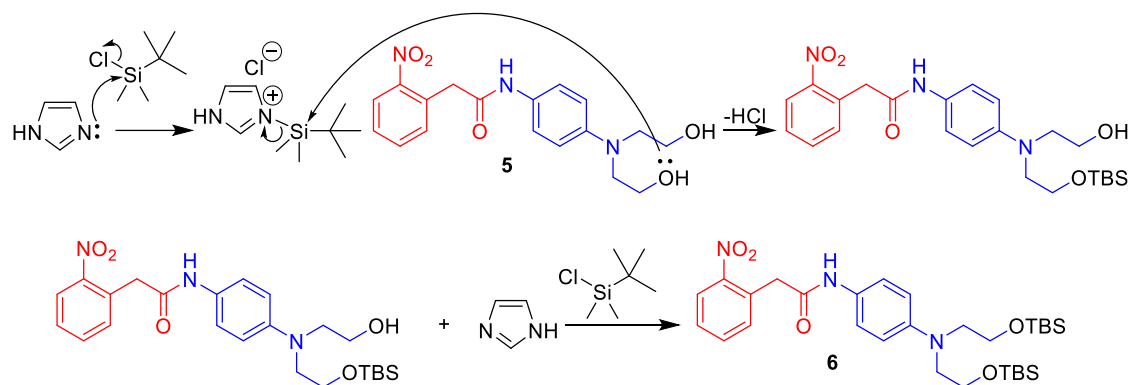
The method of converting **5** to **6** developed by Nicholas Kirk using TBDMSCl/imidazole in dichloromethane reportedly gave good yields (86%). Kirk used recrystallisation from pet. spirit for product purification, which was easily adaptable to scale-up. I performed Kirk's procedure three times on increasing scale (3.0 g, 4.2 g and 4.5 g of **5**) and obtained a consistent yield (86%, Scheme 2.7) of **6** in each case, yielding a total of 16.0 grams of **6** from the three reactions.



Scheme 2.7 *Bis*-TBS protection of **5**.

2.4.1 Mechanism of *Bis*-TBS Protection

The mechanism for the *bis*-TBS-protection of **5** uses the catalyst imidazole to first form an activated imidazolium-chloride salt from TBDMSCl (Scheme 2.8). Activation of the silicon atom for nucleophilic attack by alcohols in this way significantly increases the rate of reaction.¹⁴⁴ After the first protecting group is added, the process then repeats on the second alcohol due to the excess of TBDMSCl/imidazole present, yielding *bis*-TBS protected **6**.



Scheme 2.8 Mechanism for the *Bis*-TBS protection of **5**.

2.4.2 Spectroscopic Evidence for the Formation of **6**

Addition of two TBS groups was supported by the appearance of two large singlets in the far upfield region of the ^1H NMR spectrum (Figure 2.3). The first singlet at 0.85 ppm was highly shielded and integrated for 18 protons, corresponding to the two *tert*-butyl moieties of the TBS groups. The singlet at 0 ppm integrating for 12 protons corresponded to the four methyl groups; two each attached to the two silicon atoms. Additionally, the appearance of three new aliphatic peaks at 26.0, 18.4 and -5.2 ppm in the ^{13}C NMR spectrum supported successful addition of two chemically equivalent TBS groups. Finally, observation of the expected $\text{M}+\text{H}^+$ ion at m/z 588.3289 by mass spectrometry confirmed formation of **6**.

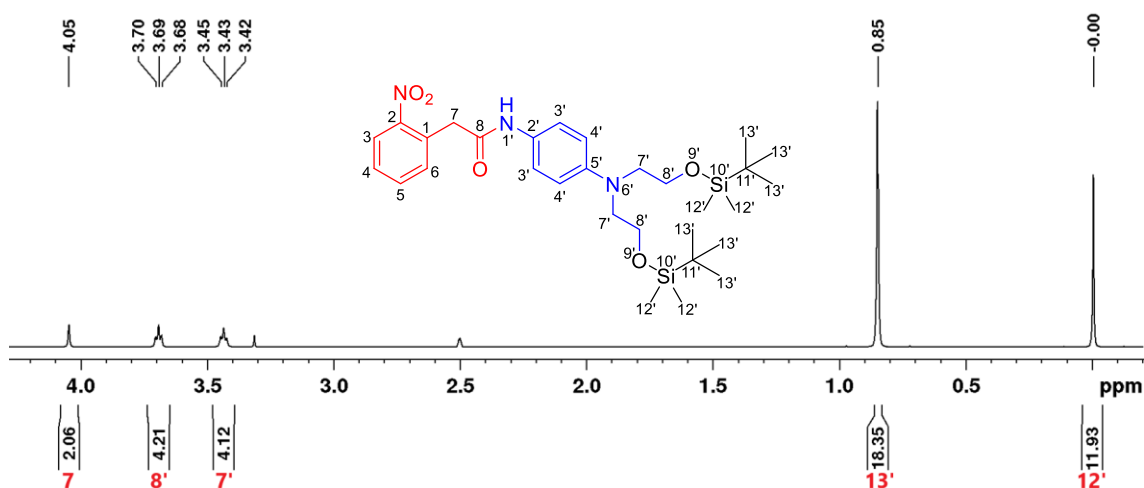
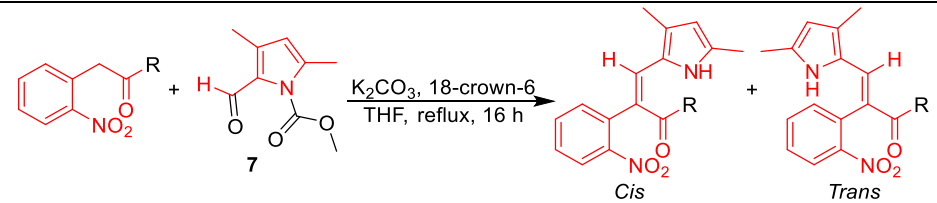


Figure 2.3 Aliphatic region of the 500 MHz ^1H NMR spectrum of **6** in d_6 -DMSO.

2.5 Knoevenagel Condensation of **6**

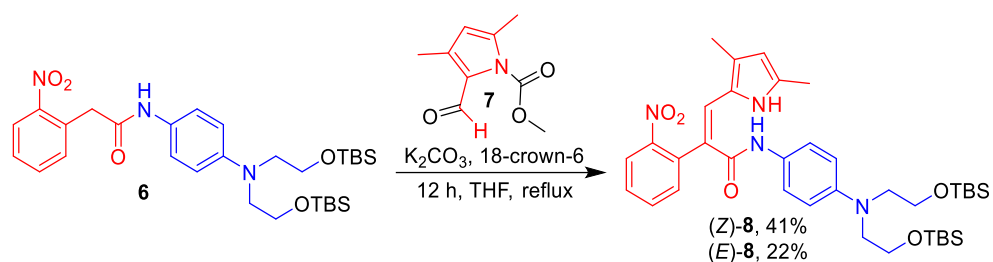
The key step in Nicholas Kirk's synthesis of **1** was a Knoevenagel condensation between **6** and *N*-protected pyrrole aldehyde **7**. Closely related Knoevenagel reactions were developed in the Kelso Lab at UOW by Kirk and others for the synthesis of 2-(2-nitrophenyl)acetic esters and amides (Table 2.1).¹³⁸ Optimisation of the reactions by previous students showed that condensations with pyrrole-2-carbaldehydes required addition of a methyl carbamate protecting group to the pyrrole nitrogen. Use of potassium carbonate with 18-crown-6 in tetrahydrofuran (THF) at reflux was found to work with a variety of esters and amides, typically giving a ~1:1 mixture of *cis/trans* isomers for esters and almost exclusively *cis* products for amides, albeit in lower yields.

Table 2.1 Knoevenagel reactions between 2-(2-nitrophenyl)acetic esters and amides developed previously in the Kelso Lab.¹³⁸



R	<i>Cis</i> , Yield %	<i>Trans</i> Yield %
OEt	42	35
OMe	36	40
OAll	41	33
NHEt	21	0
NHPh	22	<5
NHBn	16	<5

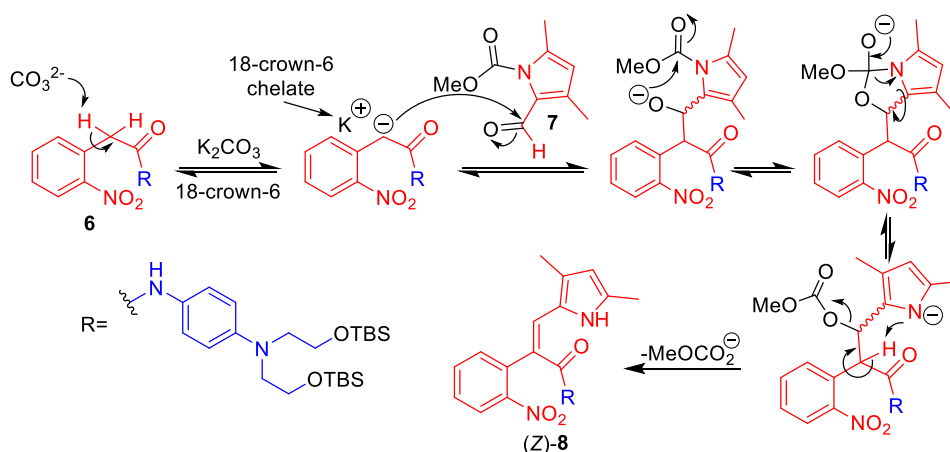
Nicholas Kirk was the first to trial condensing **6** with aldehyde **7** using the above conditions (K_2CO_3 , 18-crown-6, THF, reflux), and he obtained (*Z*)-**8** in modest yield (41% *cis* and 22% *trans*, Scheme 2.9). This yield was achieved only once by Kirk in eight small-scale attempts and post-analysis of his NMR data indicated that the product was of low purity.



Scheme 2.9 Knoevenagel condensation with **6** trialled on small scale by Nicholas Kirk.¹³⁹

2.5.1 Knoevenagel Reaction Mechanism

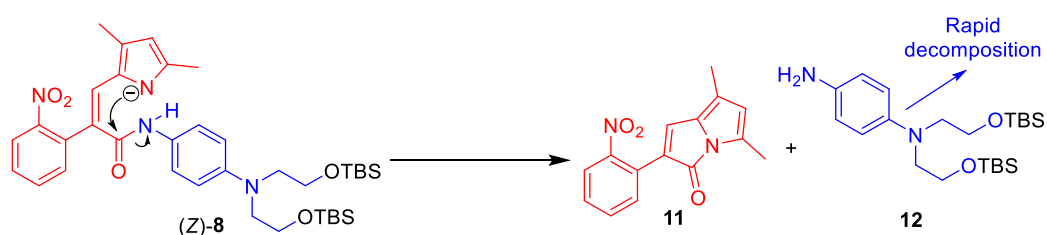
A plausible mechanism for the condensation reaction that accounts for *in situ* pyrrole-*N*-deprotection is outlined in Scheme 2.10. Potassium carbonate initiates the reaction by abstracting a proton from the 2-(2-nitrophenyl)-acetic amide portion of **6** to generate a benzylic carbanion, with the K^+ counterion chelated by 18-crown-6. The ‘naked’ carbanion then adds to the aldehyde group of **7** with the resulting oxyanion attacking the neighbouring carbonyl carbon of the *N*-methylcarbamate to form a 5-membered oxazolidine ring. Collapse of the oxyanion leading to cleavage of the C-N bond and loss of pyrrolate as the leaving group (in preference to cleavage of the C-O bond and loss of methoxide) then ensues. The basic pyrrolate anion abstracts the remaining benzylic proton and methyl carbonate is eliminated to provide alkene (Z)-**8** as a mixture of *cis* and *trans* isomers. It is possible that an intramolecular hydrogen bond between the nascent pyrrole N-H and amide carbonyl oxygen favours formation of the *cis*-product.



Scheme 2.10 Proposed mechanism for the formation of (Z)-**8** by the Knoevenagel condensation of **6** with pyrrole aldehyde **7**.

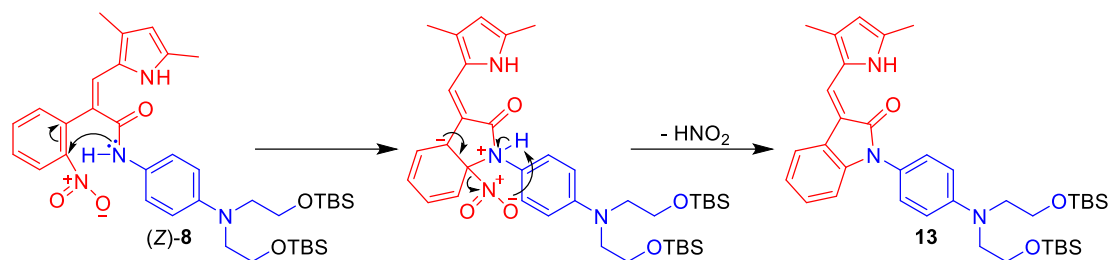
2.5.2 Optimising the Yield of (Z)-8

The Knoevenagel reaction was the lowest yielding step in Kirk's synthesis of **1** so considerable effort was invested into attempts to optimise the reaction conditions. The reaction would typically proceed for about 3 hours and then no further product would form (by thin layer chromatography, TLC analysis) despite a large amount of the starting materials **6** and **7** remaining. When the reaction was left for longer than 3 hours, two new side products started to form. The first side product was identified as pyrrolizinone **11**, which was hypothesised to form from the desired product (Z)-**8** after proton abstraction from the pyrrole nitrogen under the basic reaction conditions. Cyclisation of the pyrrolate anion onto the amide carbonyl would lead to cleavage of the amide bond and release of the 4-aminoaniline derivative **12** (Scheme 2.11). Compound **12** was not able to be isolated from the reaction as the electron rich 4-aminoaniline was unstable and rapidly decomposed. Deliberate formation of pyrrolizinones using a related procedure was later optimised by Nicholas Kirk to produce a variety of 5,7-dimethyl-2-aryl-3*H*-pyrrolizin-3-ones that showed potent anti-angiogenic activity.¹⁴⁵



Scheme 2.11 Proposed mechanism for the formation of pyrrolizinone side product **11** from the desired product (Z)-**8** during the Knoevenagel reaction.

The second side product observed in the Knoevenagel reaction was *N*-aryl oxindole **13**, apparently formed by nucleophilic displacement of the aryl nitro group by the amide nitrogen (Scheme 2.12). Whilst uncommon, intramolecular cyclisation of amides onto aryl nitro groups has been reported.¹⁴⁶



Scheme 2.12 Proposed mechanism for the formation of *N*-aryl oxindole side product **13** from the desired product (Z)-**8** during the Knoevenagel reaction.

It was thought that the basic conditions and heating of the Knoevenagel reaction was causing (Z)-**8** to undergo these side reactions. Attempts to optimise the yield of (Z)-**8** were performed using small scale reactions (~30 mg) with a variety of carbonate bases/crown ethers and solvents (Table 2.2). The products were not isolated but each reaction was analysed for the presence of (Z)-**8** by TLC comparison to a standard, with the presence of the product further confirmed by mass spectrometry. Of all the bases trialled, only potassium carbonate and caesium carbonate delivered (Z)-**8** in THF or acetonitrile. Despite these and many other attempts, no improvements to Kirk's original conditions were identified.

Table 2.2 Representative selection of conditions trialled in attempts to optimise the Knoevenagel reaction.

Base/Crown Ether	DMF	CH ₃ CN	THF
Cs ₂ CO ₂	No Reaction	Low Yield	No Reaction
K ₂ CO ₃ /18-crown-6	No Reaction	Medium Yield	Highest Yield
Na ₂ CO ₃ /15-crown-5	No Reaction	No Reaction	No Reaction
Li ₂ CO ₃ /12-crown-4	No Reaction	No Reaction	No Reaction

It was postulated that grinding the potassium carbonate into a fine powder instead of using the slightly granular form might accelerate the reaction and allow more of (Z)-**8** to form before the side reactions commenced. When tested side-by-side, use of granular

potassium carbonate and the finely ground form did not change the yield of (Z)-**8**. In the end, I was able to implement Kirk's original method on a large enough scale to generate sufficient quantities of pure material for this study. Performing the reaction three times using 1.0, 2.2 and 5.0 g of **6** produced a total of 1.7 g of (Z)-**8** in 21% yield. The *trans* product, which was only observed in trace quantities, had previously been investigated in a series of isomerisation reactions by Kirk but encouraging results were not obtained. Isomerisation of (E)-**8** could be partially achieved using catalytic H₂SO₄ in THF, producing a 19% yield of the desired (Z)-**8** with 62% recovery of (E)-**8**. Base-promoted isomerisation using triethylamine or *N,N*-diisopropylethylamine (DIPEA) was not successful, instead producing the oxindole derivative **13** as the major product.

2.5.3 Spectroscopic Evidence for the Formation of (Z)-**8**

The Knoevenagel condensation gave a complex mixture of desired and side products that had to be individually isolated and characterised. During the characterisation it was important to confirm that the *cis* and not the *trans* isomer was being isolated. The desired *cis*-product was hypothesised to contain an intramolecular hydrogen bond between the pyrrole N-H and the amide C=O (Figure 2.4). This postulation was based on previous observations by X-ray crystallography of this H-bond in the related 2-(2-nitrophenyl)acetic esters and amides (Table 2.1).¹³⁸ Based on this earlier work, the pyrrole N-H was expected to appear in the ¹H NMR spectrum between 11-13 ppm for the *cis*-product and 6-7 ppm for the *trans* product. For compound (Z)-**8**, the pyrrole N-H signal appeared at 12.10 ppm, confirming the desired *cis*-product had been isolated. Assignment of *cis* stereochemistry was further confirmed by the appearance of a nuclear overhauser effect spectroscopy (NOESY) correlation between the alkene hydrogen and the nearby *ortho*-proton of the 2-nitrophenyl ring, which is not possible in the *trans* isomer.

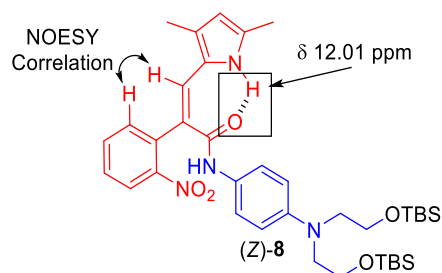
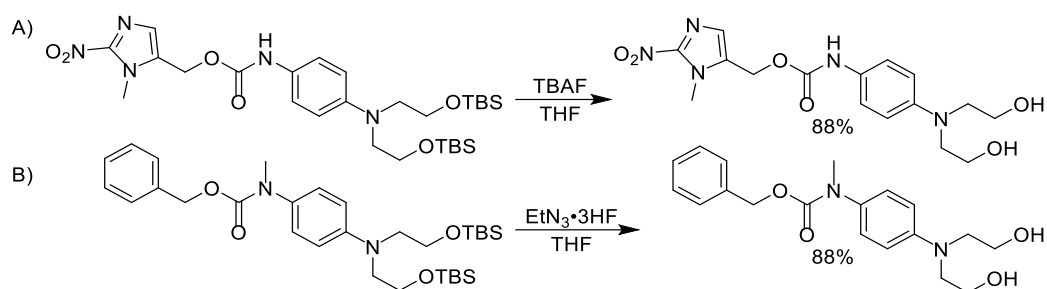


Figure 2.4 The pyrrole NH forms a hydrogen bond to the amide carbonyl in (Z)-**8**.

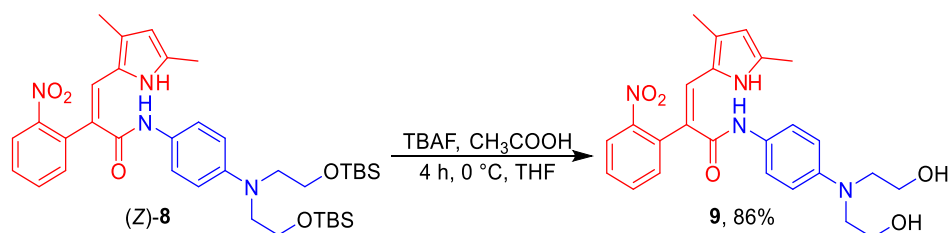
2.6 Bis-TBS Deprotection of (Z)-8

With the key Knoevenagel condensation complete, the second last step in the synthesis involved removing the TBS protecting groups from the two alcohols before final conversion to alkyl chlorides. The most common methods for removing TBS groups from alcohols uses fluoride ions, driven by formation of the very strong Si-F bond (565 kJ.mol⁻¹).¹⁴⁷ The literature provided a relevant precedent where two TBS groups were simultaneously removed from a nitroimidazole carbamate prodrug structurally related to our target molecule. Use of tetrabutylammonium fluoride (TBAF) in this precedent gave a high yield of the *bis*-alcohol (88%, Scheme 2.13, A).¹⁴⁸ A second precedent was identified in a paper reporting the synthesis of a self-immolative nitrogen mustard prodrug, wherein two TBS groups were deprotected using triethylamine trihydrofluoride in 88% yield (Scheme 2.13, B).¹⁴⁹ Both methods appeared promising but as triethylamine trihydrofluoride produces highly toxic HF, TBAF was chosen as the preferred reagent for the reaction.



Scheme 2.13 Literature precedents for *bis*-TBS deprotection of *bis*-alcohols using TBAF or EtN₃·3HF.¹⁴⁸⁻¹⁴⁹

Nicholas Kirk found that adding acetic acid to buffer the reaction was essential for obtaining a high yield of **9** (85%). Using Kirk's method, I successfully performed the reaction four times on increasing scale (0.2 g, 0.4 g, 0.5 g and 0.7 g of (Z)-**8**) with consistent yields (86%, Scheme 2.14) to generate a total of 0.95 g of pure **9**.



Scheme 2.14 *Bis*-TBS-deprotection of (Z)-**8** to afford **9**.

2.6.1 Spectroscopic Evidence for the Formation of **9**

Removal of the two TBS-protecting groups was clearly evident from the ^1H and ^{13}C NMR spectra of **9**, where loss of the two large singlets in the ^1H NMR spectrum at 0.89 and 0.04 ppm (Figure 2.5) and the three peaks in the ^{13}C NMR at 26.0, 18.4 and -5.2 ppm (Figure 2.6) was observed. There was also a slight downfield shift in the ^1H NMR signals of the *bis*-ethanolamine CH_2 groups, which moved from 3.73 and 3.48 in (*Z*)-**8** to 3.79 and 3.52 ppm, respectively, in **9**.

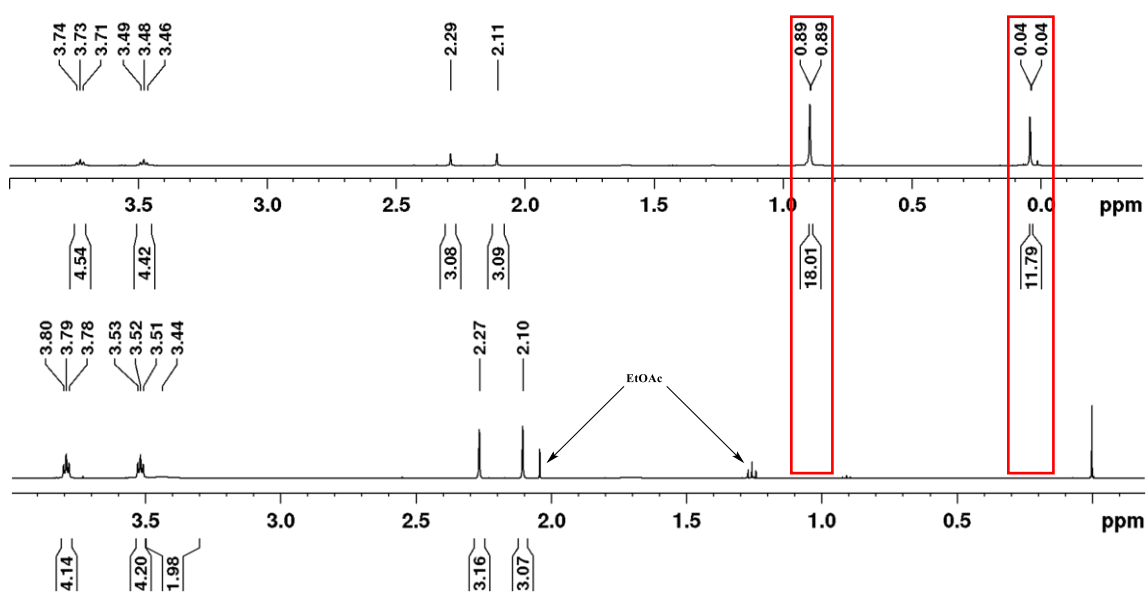


Figure 2.5 Aliphatic region of the 500 MHz ^1H NMR spectrum of **9** (bottom) showing loss of the TBS signals present in (*Z*)-**8** (Top). Both spectra were recorded in CDCl_3 .

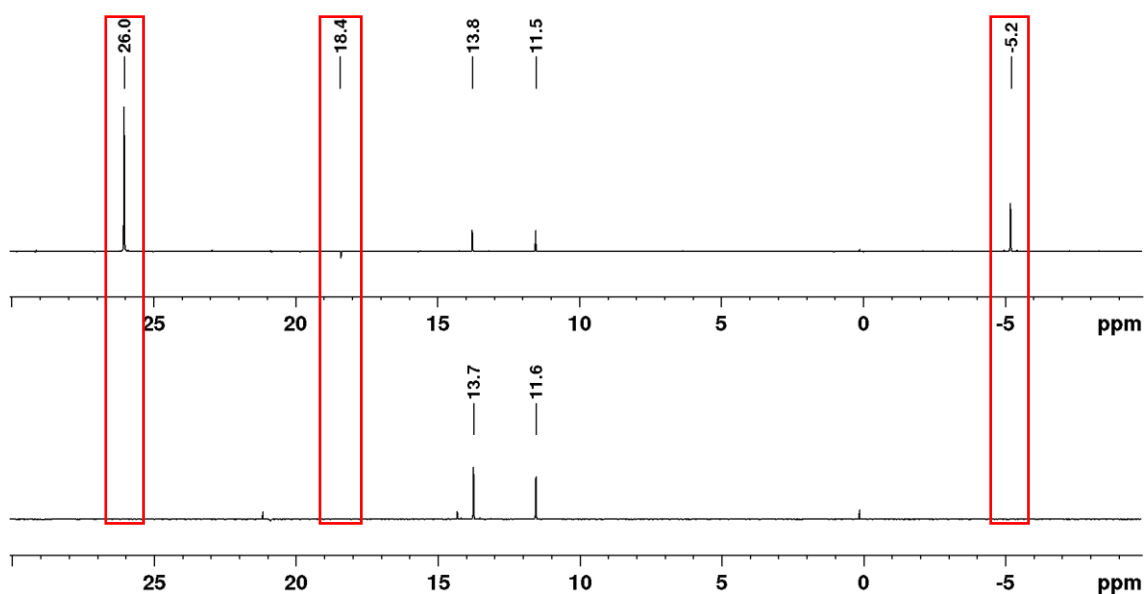
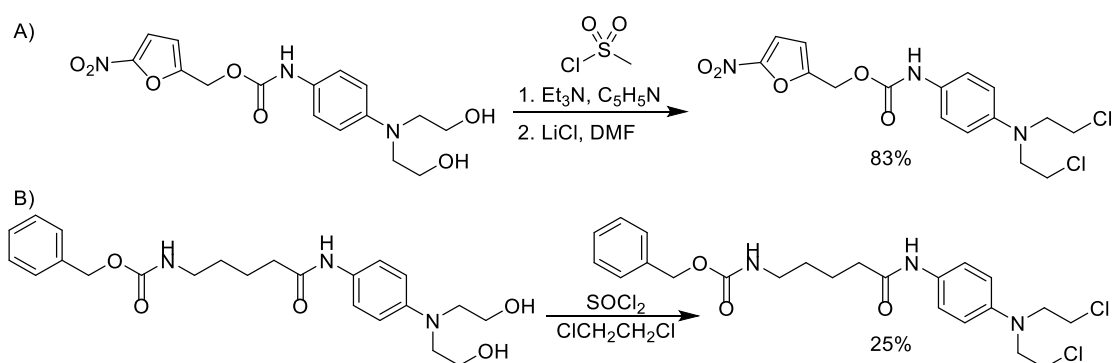


Figure 2.6 Aliphatic region of the 500 MHz ^{13}C APT NMR spectrum of **9** (bottom) recorded in CDCl_3 showing loss of the three TBS carbon signals present in (*Z*)-**8** (Top).

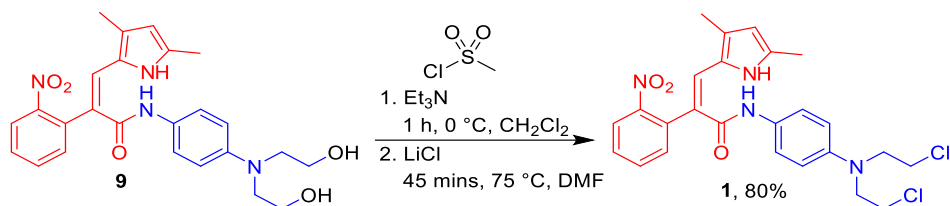
2.7 *Bis*-Mesylation/Chlorination of **9** to give Mutual Prodrug **1**

The final step in the synthesis of **1** involved converting the two alcohol groups of **9** to primary alkyl chlorides. Nitrogen mustards are a well-studied class of compounds and several methods have been reported for the conversion of *bis*-alcohols to *bis*-chlorides. In the above-mentioned synthesis of a nitroimidazole carbamate prodrug (Section 2.6), conversion to the mustard was carried out in two steps. Mesylation was carried out first in pyridine using mesyl chloride and triethylamine and subsequent chlorination with lithium chloride in DMF gave the mustard in 83% over the 2 steps (Scheme 2.15, A).¹⁴⁸ In another example, aniline mustards were synthesised from *bis*-alcohols using thionyl chloride in dichloroethane in 25% yield (Scheme 2.15, B).¹⁵⁰



Scheme 2.15 Literature precedents for the conversion of *bis*-alcohols to aniline mustards.^{148, 150}

Nicholas Kirk attempted the *bis*-chlorination of **9** using the 2-step mesylation/chlorination procedure. He was able to achieve a yield of 79% over the two steps and noted that the *bis*-mesylate could not be isolated due to its low stability. I repeated Kirk's conditions twice using 150 mg and 300 mg of **9** and obtained **1** in consistent yield (80%, Scheme 2.16). The reaction required immediate and very careful isolation and transfer of the crude *bis*-mesylate into the second chlorination reaction. In an attempt to simplify the procedure for further scale-up, single step conversions with phosphoryl chloride and thionyl chloride were trialled on small scales with remaining quantities of **9** but both reactions gave multiple products, including insoluble polymer. Using Kirk's original method, I was able to obtain sufficient quantities of **1** (210 mg in total) to explore the chemical reductions (Section 4.1) and biological testing (Section 4.2) aims of the thesis.



Scheme 2.16 Two-step conversion of **9** to the target semaxinib|4-aminoaniline mustard mutual prodrug **1**.

2.8 2D Spectroscopic Analysis of **1**

NMR data for **9** and **1** were almost identical, consistent with the minor changes expected after transforming the two primary alcohols into primary alkyl chlorides. Within the aromatic region of the ^1H -NMR spectrum, all signals were accounted for (Figure 2.7). Of key interest was the pyrrole N-H peak, which was observed at 12.04 ppm due to the intramolecular hydrogen bond it forms to the carbonyl oxygen of the amide. Only slight changes were observed in the aliphatic ^1H NMR chemical shifts of the mustard CH_2 groups, which moved from 3.79 and 3.52 in **9** to 3.70 and 3.60 ppm in **1** (Figure 2.8).

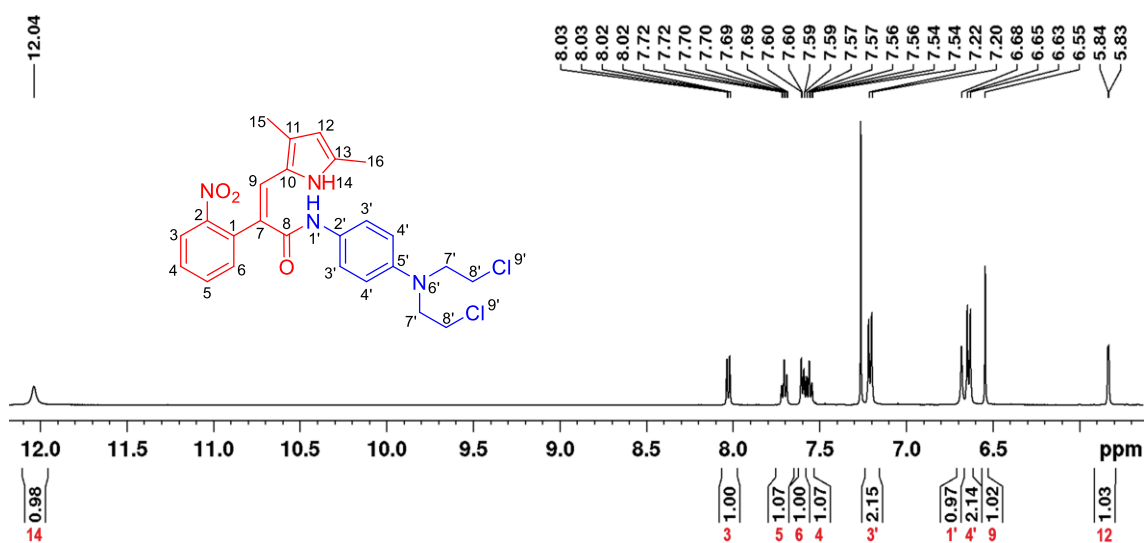


Figure 2.7 Aromatic region of the 500 MHz ^1H -NMR spectrum of **1** recorded in CDCl_3 .

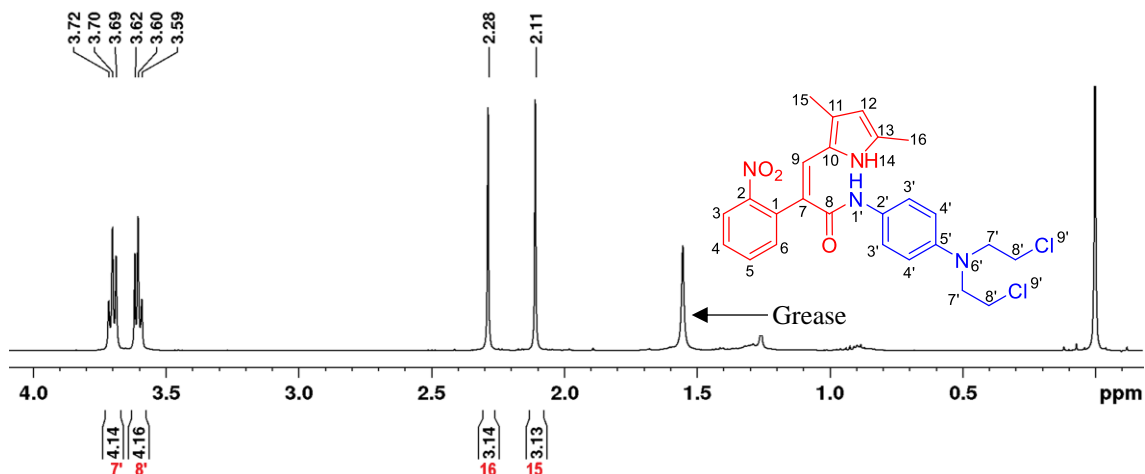


Figure 2.8 Aliphatic region of the 500 MHz ^1H -NMR spectrum of **1** recorded in CDCl_3 .

2.8.1 ^{13}C APT NMR Analysis of **1**

The ^{13}C NMR of **1** was complex owing to the 21 different carbon types, including 10 quaternary carbons and required an attached proton test (APT) ^{13}C NMR spectrum to aid assignment of each signal (Figure 2.9 and Figure 2.10). The carbons with attached protons were assigned using a combination of gradient-selected heteronuclear single quantum coherence (gHSQC), gradient-selected correlation spectroscopy (gCOSY) and NOESY spectra. The quaternary carbons C2 and C8 were assigned from a gradient-selected heteronuclear multiple bond coherence (gHMBC) spectrum.

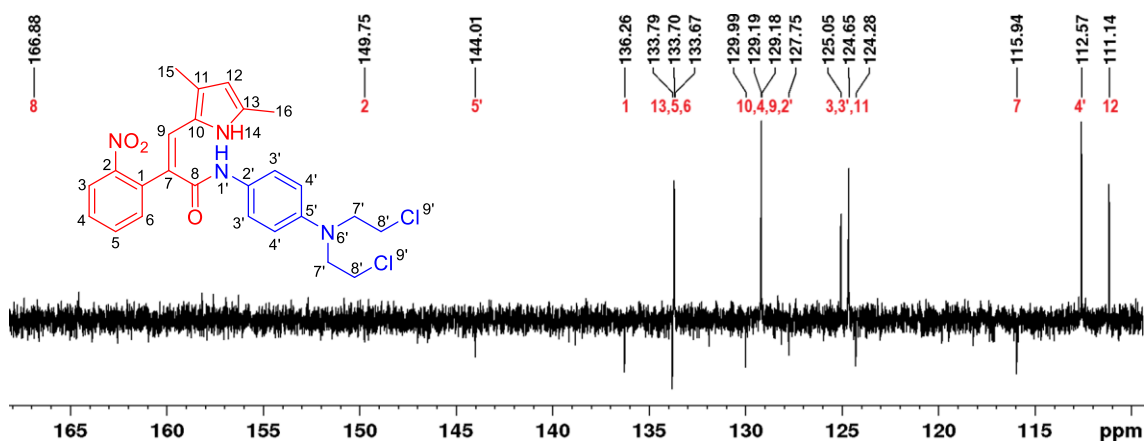


Figure 2.9 Aromatic region of the 500 MHz ^{13}C APT NMR spectrum of **1** recorded in CDCl_3 . The peaks at 166.88 and 149.75 ppm were evident in the gHMBC spectrum.

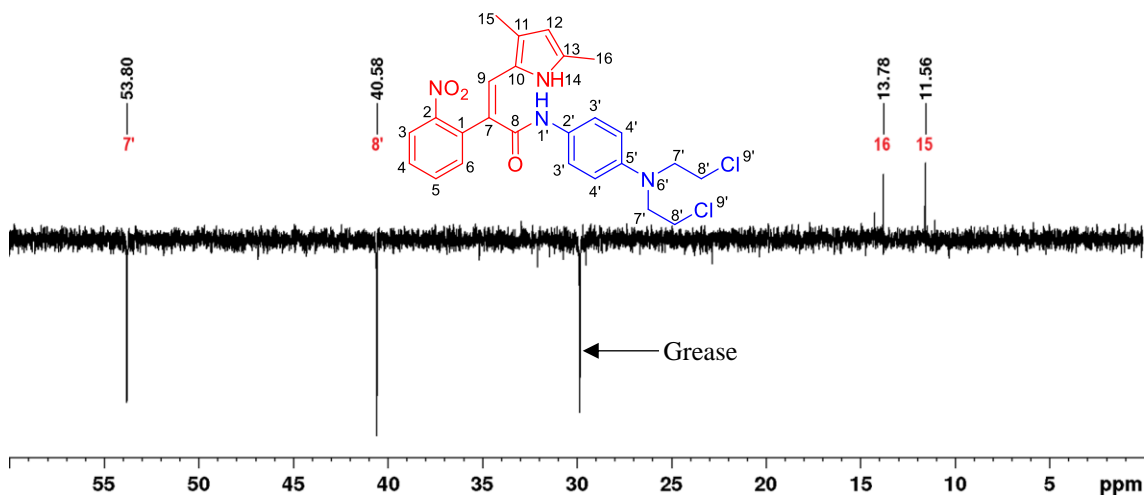


Figure 2.10 Aliphatic region of the 500 MHz ^{13}C APT NMR spectrum of **1** recorded in CDCl_3 .

2.8.2 NOESY NMR Analysis of **1**

The NOESY spectrum of **1** showed only two visible NOE correlations (Figure 2.11); one between a methyl group on the pyrrole and its adjacent alkene proton. This NOE provided definitive assignments for the two chemically similar methyl groups on the pyrrole. The other NOE observed was between one of the pairs of methylene protons on the nitrogen mustard and the adjacent protons of the 4-aminoaniline ring. This NOE allowed definitive assignment of both pairs of methylene protons on the nitrogen mustard as well as the two pairs of equivalent phenylenediamine protons.

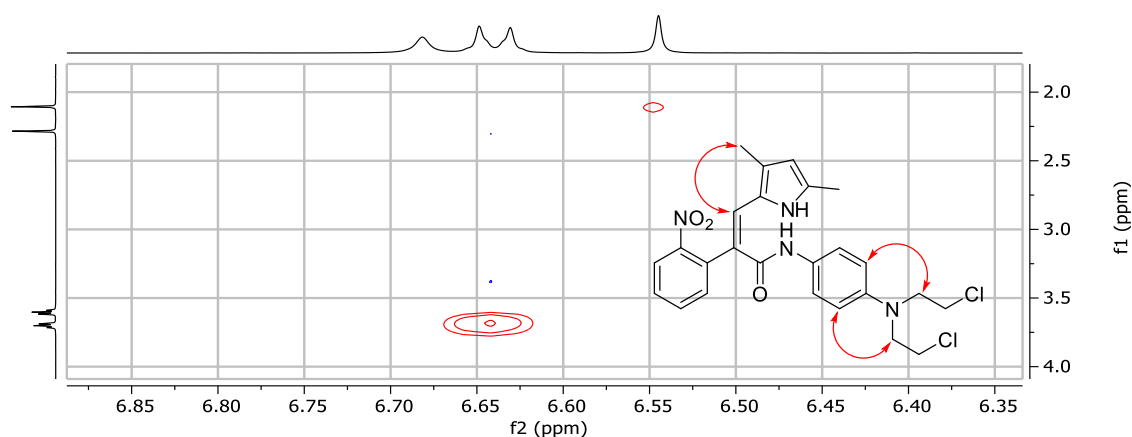


Figure 2.11 NOESY correlations of **1** recorded in CDCl_3 (500 MHz)

2.8.3 gCOSY NMR Analysis of **1**

After applying a diagonal suppression to the gCOSY spectrum of **1**, five $^3J_{\text{H-H}}$ correlations were observed (Figure 2.12). These correlations were as expected for the pairs of vicinal

protons in **1**. The correlations allowed definitive assignment of the protons around the nitrobenzene ring by starting at the heavily deshielded doublet at 8.03, ppm corresponding to the proton adjacent to the nitro group and walking the correlations around the aromatic ring. Also observed was a correlation between the two pairs of chemically equivalent protons on the 4-aminoaniline ring and a correlation between the two pairs of methylene protons on the nitrogen mustard.

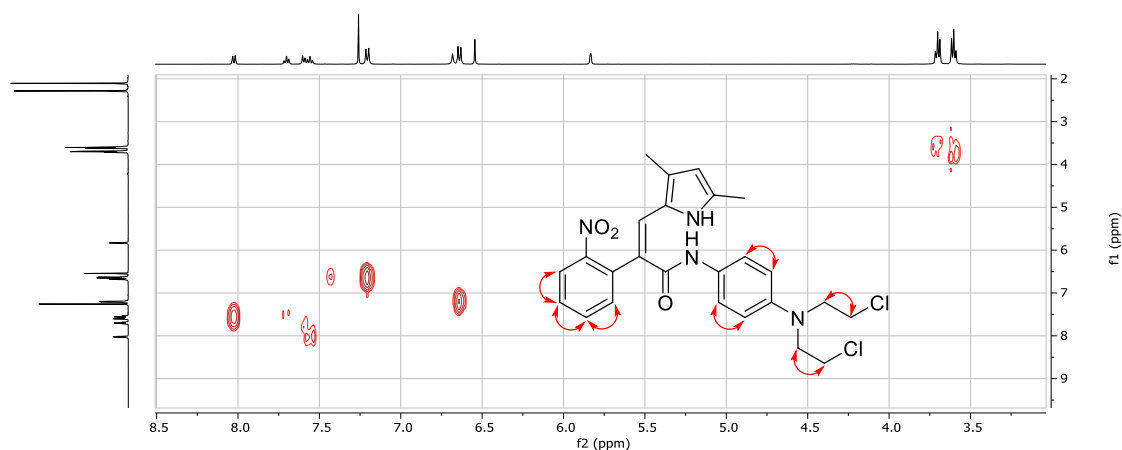


Figure 2.12 $^3J_{\text{H-H}}$ correlations observed in the 500 MHz gCOSY NMR spectrum (with diagonal suppression) of **1** recorded in CDCl_3 .

2.8.4 gHSQC NMR Analysis of **1**

The aromatic region of the gHSQC spectrum of **1** revealed eight different C-H correlations (red, Figure 2.13). The correlations between these carbons and their attached protons allowed assignment of each of these carbon atoms based upon their attached proton signals.

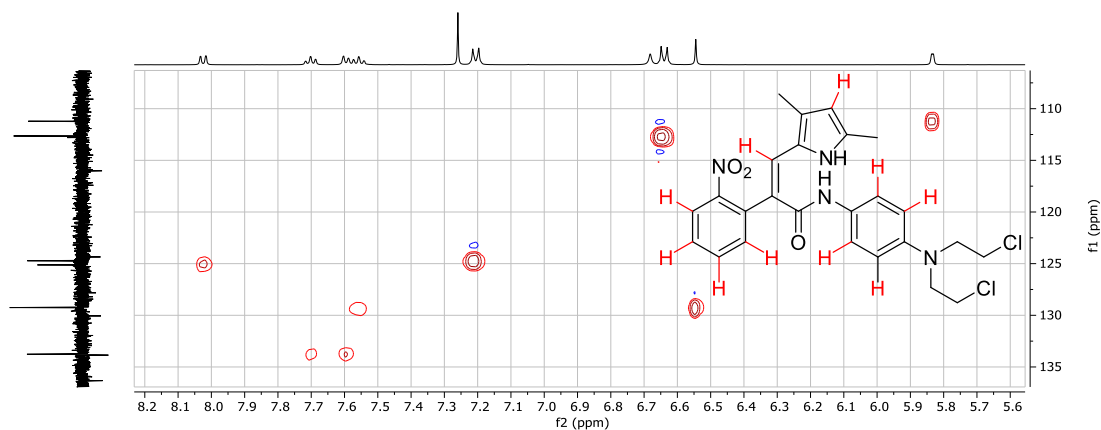


Figure 2.13 Aromatic region of the 500 MHz gHSQC spectrum of **1** recorded in CDCl_3 .

The aliphatic region of the gHSQC spectrum of **1** contained four correlations; two corresponding to CH₂ (blue) signals and two arising from CH₃ carbons (red, Figure 2.14). The two CH₂ signals corresponded to the pairs of methylene protons on the nitrogen mustard arms and allowed assignment of their respective carbons. The two CH₃ signals corresponded to the two methyl groups on the pyrrole.

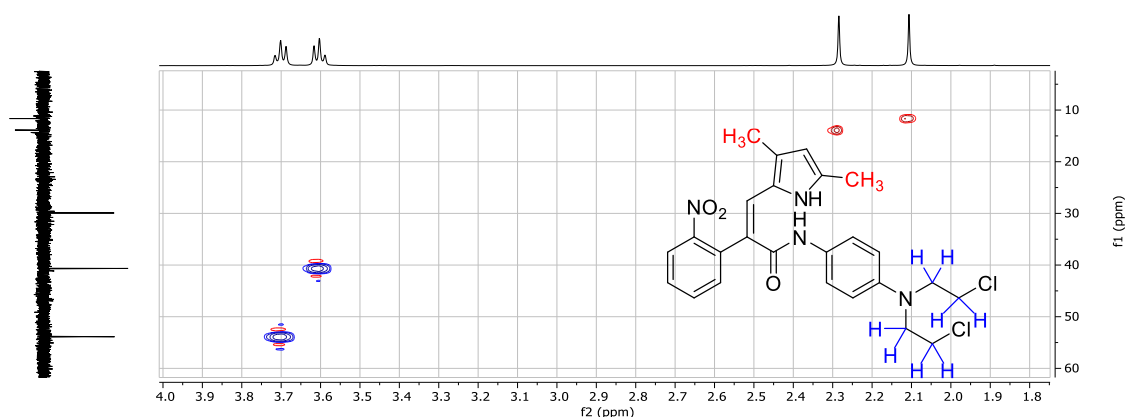


Figure 2.14 Aliphatic region of the 500 MHz gHSQC spectrum of **1** recorded in CDCl₃.

2.8.5 gHMBC NMR Analysis of **1**

The aromatic region of the gHMBC spectrum of **1** displayed many correlations (Figure 2.15), especially within each of the phenyl rings. Most of the correlations were ³J_{H-C} (red) although several ²J_{H-C} correlations (blue) were also present. The large number and variety of multi-bond correlations present allowed definitive assignment of each of the as yet unassigned quaternary carbons within the molecule.

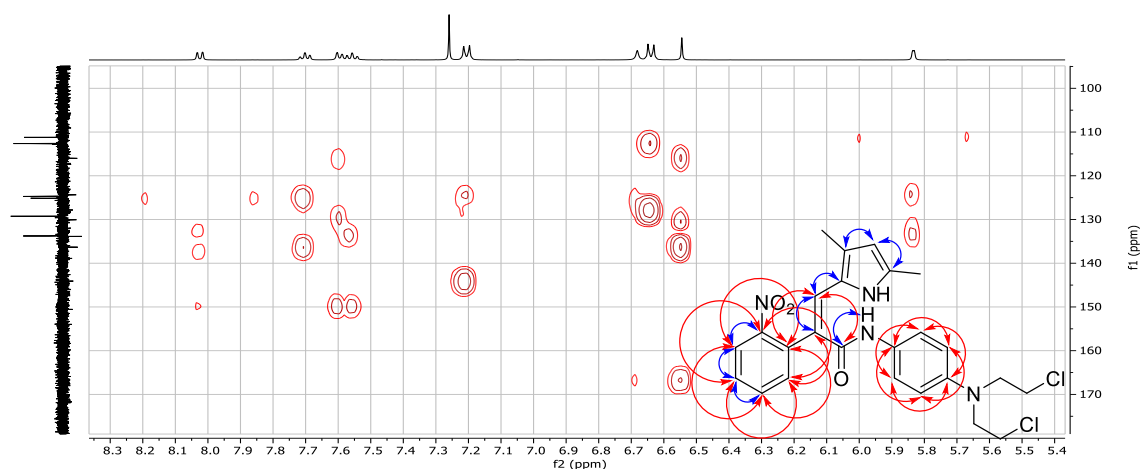


Figure 2.15 Aromatic region of the 500 MHz gHMBC spectrum of **1** recorded in CDCl₃, ²J_{H-C} correlations are shown in blue and ³J_{H-C} correlations in red.

The aliphatic region of the gHMBC spectrum also contained several $^3J_{\text{H-C}}$ and $^2J_{\text{H-C}}$ correlations (Figure 2.16). Both methyl groups on the pyrrole showed a $^2J_{\text{H-C}}$ correlation to their adjacent quaternary carbons, along with $^3J_{\text{H-C}}$ correlations to the next carbon. The two pairs of methylene protons on the nitrogen mustard exhibited $^2J_{\text{H-C}}$ correlations within each chain and $^3J_{\text{H-C}}$ correlations through the nitrogen atom into the other chain. A $^3J_{\text{H-C}}$ correlation was also observed between the methylene protons next to the nitrogen and the quaternary carbon of the attached 4-aminoaniline ring. This correlation allowed unambiguous assignment of this tertiary carbon from the other chemically similar tertiary carbon on the 4-aminoaniline ring.

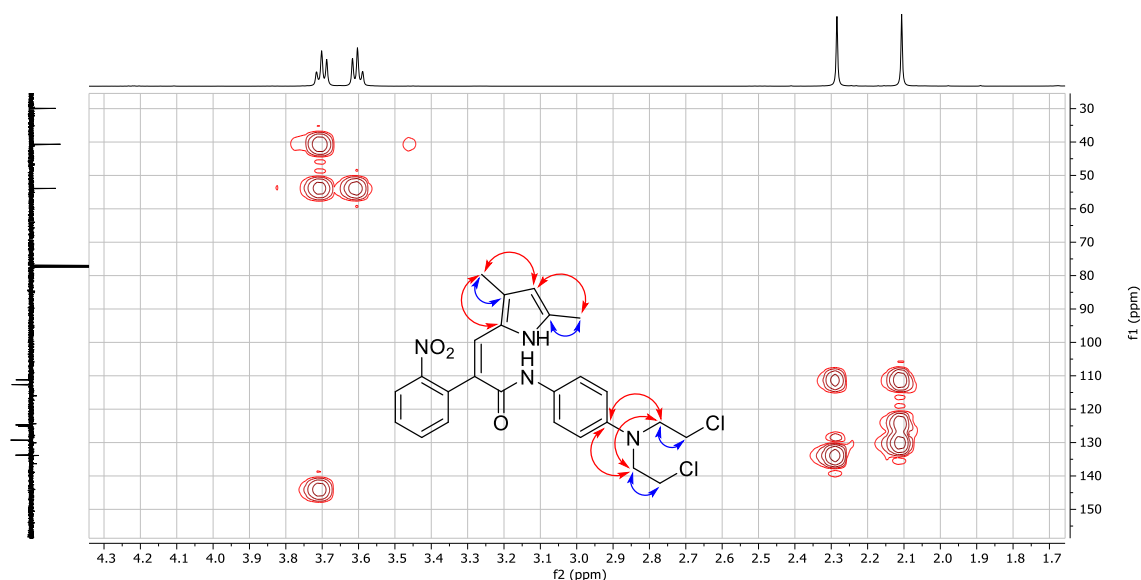
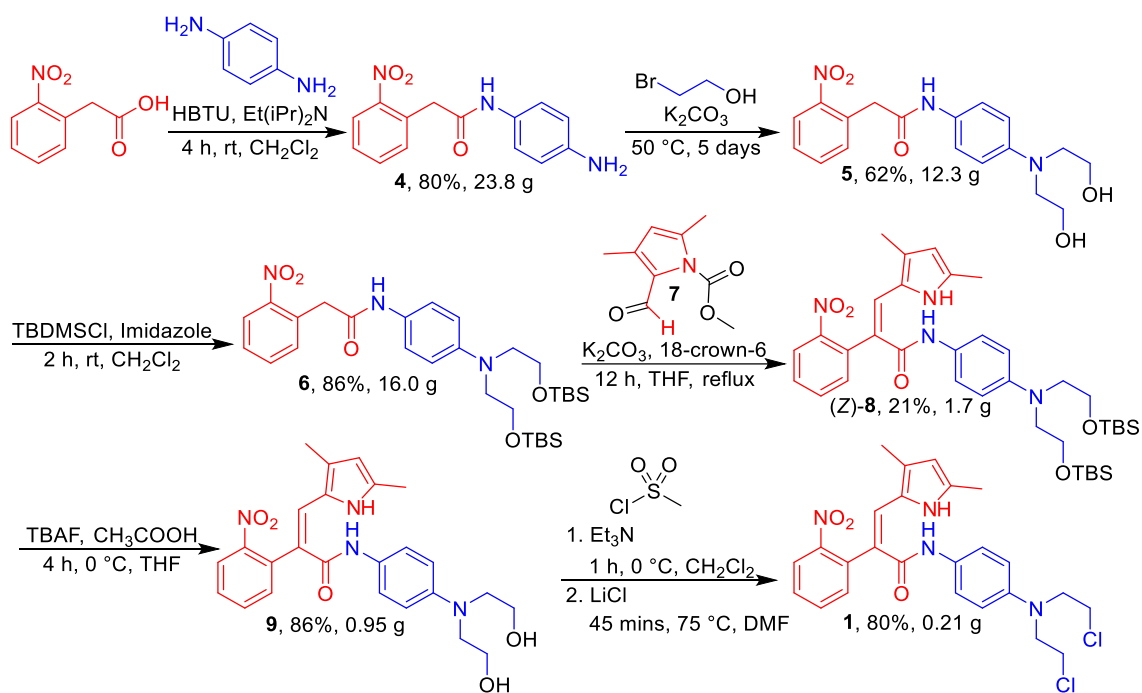


Figure 2.16 Aliphatic region of the 500 MHz gHMBC spectrum of **1** recorded in CDCl_3 .

2.9 Summary of the Scale-Up Synthesis of **1**

The total synthesis of **1**, having been originally scoped on small scale by Nicholas Kirk, was repeated here, improved in parts and successfully scaled up to provide adequate quantities of the semaxinib|4-aminoaniline mustard mutual prodrug **1** for chemical (Section 4.1) and biological testing (Section 4.2). The synthesis was completed in 6 steps in an overall yield of 6.2% (Scheme 2.17), producing a total of 190 mg of pure **1**. The synthesis still poses challenges that could be addressed in the future, if needed. Firstly, *bis*-alkylation of **4** with 2-bromoethanol was a long reaction (5 days) that produced only a moderate yield of **5** (62%). One way to potentially improve this reaction would be to use ethylene oxide in place of 2-bromoethanol, although as a toxic gas this presents its own challenges. The other problematic step in the synthesis was the Knoevenagel

condensation, where a maximum yield of only 21% of the *cis* isomer was obtained after extensive optimisation efforts. Work described in Chapter 5 showed that moving the Knoevenagel reaction to earlier in the synthesis is a promising alternative.

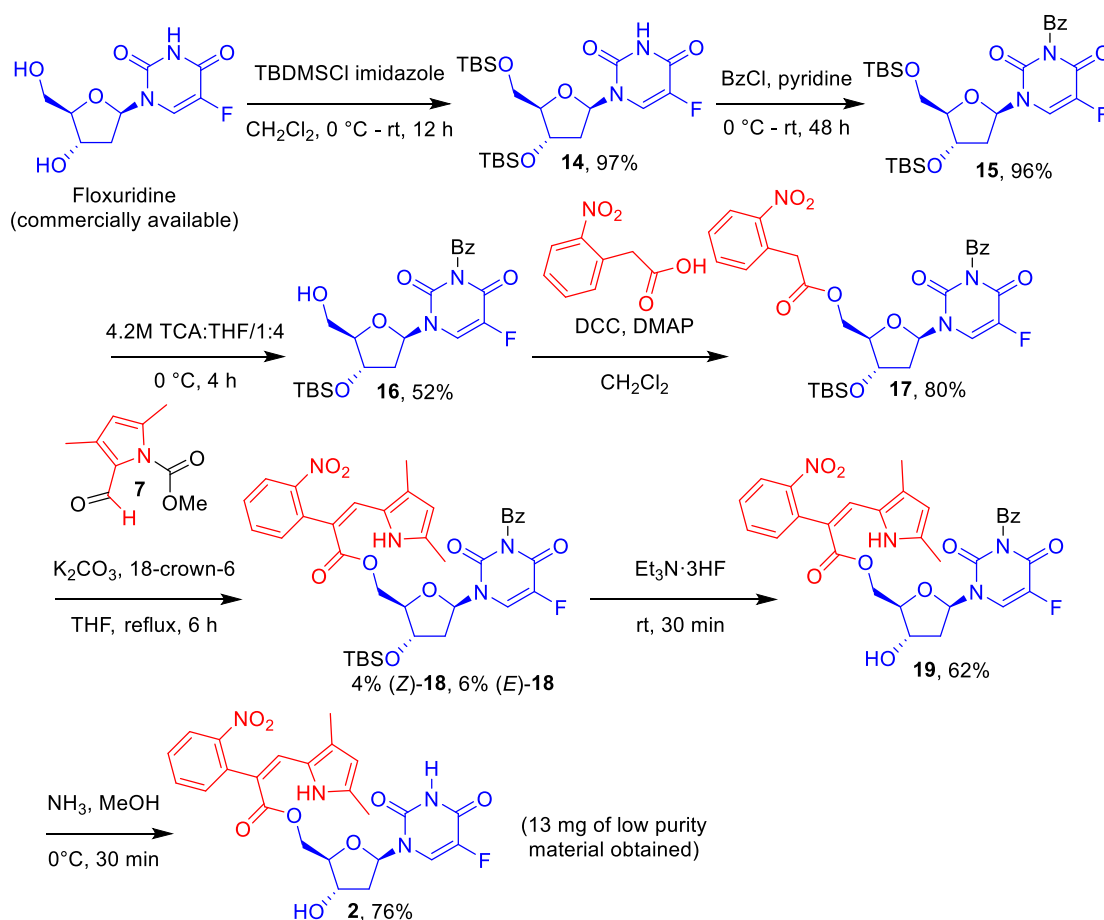


Scheme 2.17 Summary of the scaled-up synthesis of **1**. Total quantities of compounds synthesised across all reactions are indicated.

Chapter 3: Synthesis of Semaxanib|Floxuridine Mutual Prodrug **2**

3.1 Route Development

I had previously explored a pilot route towards the semaxanib|floxuridine mutual prodrug **2** during my 2014 Honours research project in the Kelso Research Lab at UOW (Scheme 3.1). The route I pursued started from the commercially available drug floxuridine, which was *bis*-silyl protected at its 1° and 2° alcohols using TBDMSCl and imidazole to obtain **14** in 97% yield. Subsequent benzoylation of the imide nitrogen of **14** with benzoyl chloride (BzCl) in pyridine gave **15** in 96% yield. The third step involved selective silyl-deprotection of the less sterically hindered 1° alcohol (aqueous trichloroacetic acid, 4.2 M in THF 1:4)¹⁵¹ to give **16** (52% yield). Esterification of the floxuridine derivative **16** with 2-(2-nitrophenyl)acetic acid gave ester **17** (80% yield).

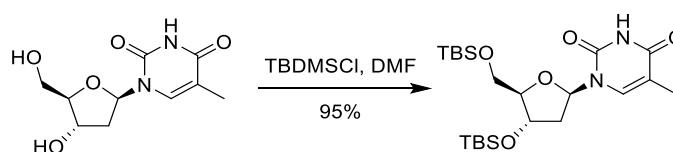


Scheme 3.1 Pilot synthesis of semaxanib|floxuridine Mutual Prodrug **2** scoped during my Honours research in 2014 at UOW. The yields shown represent the highest yields obtained in each step.

Submitting **17** to the novel Knoevenagel condensation with *N*-methylcarbamoyl pyrrole aldehyde **7** gave the *cis/trans* isomers (*Z*)-**18** and (*E*)-**18** in only 4% and 6% yields, respectively.¹³⁸ The final steps involved sequential removal of the TBS (Et₃N.3HF, 62% yield) and benzoyl (NH₃/MeOH, 76% yield) protecting groups to give **2** (13 mg), albeit in low purity. The major goal in this chapter of my PhD studies was to improve and scale up the synthesis so that sufficient quantities of **2** could be obtained in pure form for chemical and biological studies (Chapter 4).

3.2 TBS Protection of Floxuridine

The first step in the synthesis was the *bis*-TBS protection of commercially sourced floxuridine. The closest literature precedent for this reaction came from the reported *bis*-TBS-protection of thymidine,¹⁵² an almost identical compound differing only in replacement of the fluorine atom with a methyl group (Scheme 3.2).



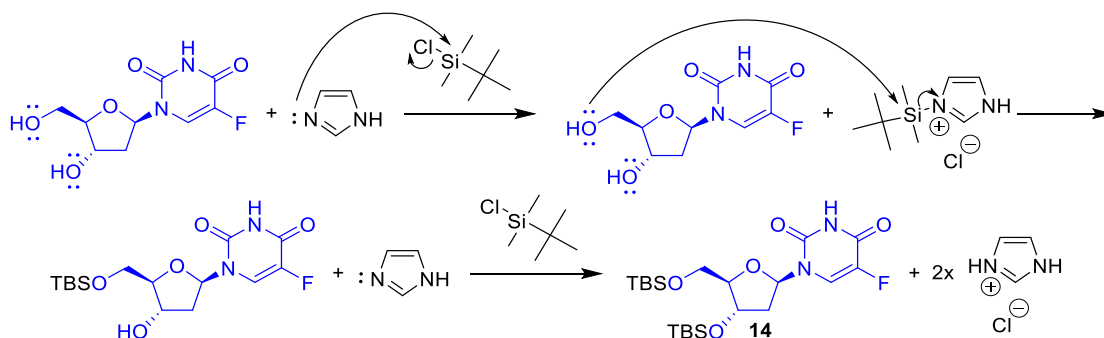
Scheme 3.2 Literature precedent for *bis*-TBS protection of thymidine.¹⁵³

During my Honours year, the *bis*-TBS-protection of floxuridine was carried out at room temperature in CH₂Cl₂ for 24 hours using 3 equivalents (eq.) of TBDMSCl and 3.5 eq. of imidazole relative to floxuridine. The reaction was carried out once with 0.2 g and twice with 5.0 g floxuridine and high yields were consistently obtained (97%).

In my PhD studies I had focused on scaling up the reaction to allow access to ample quantities of later intermediates in the synthesis. The reaction was successfully scaled up to a maximum of 25 g of floxuridine, which gave 46.8 g of pure **14** (97% yield). Purification at this scale using column chromatography was unattractive so multiple recrystallisation conditions were trialled. Recrystallisation at -20 °C after dissolution in boiling pet. spirit and slow cooling was found to give pure **14**. The reaction was performed a total of four times on increasing scale (5.0 g, 8.2 g, 25.0 g, 25.2 g floxuridine) with a consistently high yields obtained (84%, 77%, 97% and 78% yield, respectively), providing a total of 105 g of **14** over the course of my PhD.

3.2.1 Mechanism of Bis-TBS Protection

In this reaction, the imidazole acts as a nucleophilic catalyst that attacks the silicon atom using its pyridine-like nitrogen and displaces the chloride (Scheme 3.3). The more nucleophilic primary alcohol of floxuridine then attacks the silicon atom of the TBS-imidazolium cation, generating the TBS-protected primary alcohol and imidazole·HCl. The reaction then repeats on the secondary alcohol to provide the *bis*-TBS-protected **14**.



Scheme 3.3 Mechanism for the *bis*-TBS protection of the 1° and 2° alcohols of floxuridine using TBDMSCl and imidazole.

3.2.2 Spectroscopic Evidence for the Formation of **14**

Consistent with the addition of two TBS protecting groups, two new large singlets and two doublets were observed in the upfield region of the ^1H NMR spectrum of **14** (Figure 3.1). The two singlets at 0.92 and 0.88 ppm integrated for 9 protons each, corresponding to the chemically non-equivalent *tert*-butyl moieties of the two TBS groups. The two apparent doublets at 0.12 and 0.07 ppm integrated for 6 protons each, corresponding to the two methyl groups attached to the two silicon atoms. The apparent doublets arise from the nearby chirality of the ribose ring, causing the methyl groups to be diastereotopic; i.e. each methyl group is in a unique chemical environment. These apparent doublets are therefore actually four individual singlets arising from the four chemically non-equivalent methyl groups attached to the silicon atoms. Additionally, the appearance of eight new aliphatic peaks at 26.0, 25.8, 18.5, 18.1, -4.5, -4.7, -5.4 and -5.5 ppm in the ^{13}C NMR spectrum supported incorporation of two chemically non-equivalent TBS protecting groups. As seen in the ^1H spectrum, the two pairs of methyls attached to the silicon atoms are diastereotopic, experiencing different chemical environments due to the nearby chirality of the ribose ring, leading to all four methyl signals appearing. Observation of

the expected $M+H^+$ ion at m/z 475.2460 by high resolution mass spectrometry confirmed formation of **14**.

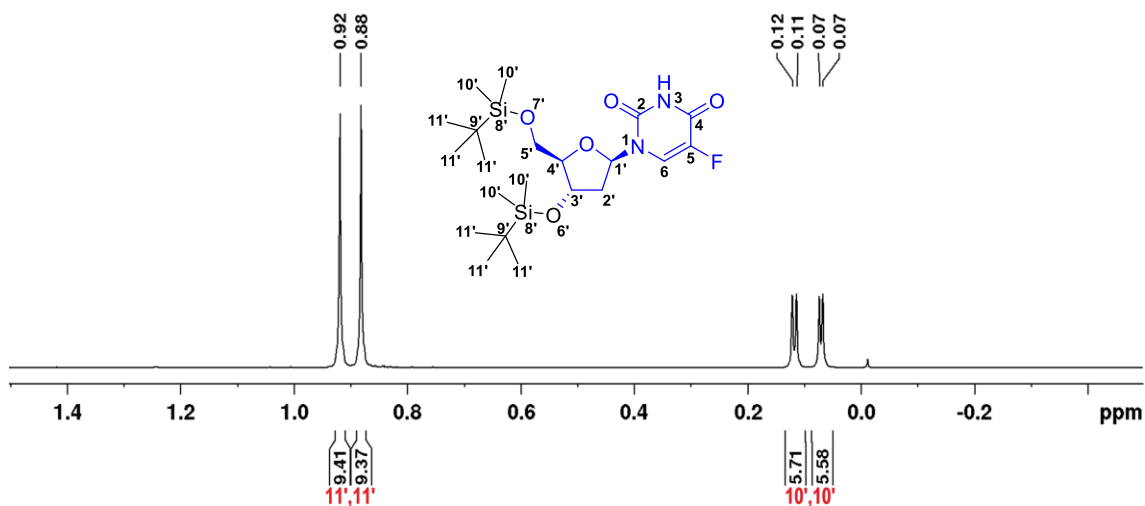


Figure 3.1 Appearance of the TBS signals in the 500 MHz ^1H NMR spectrum of **14**. The spectrum was recorded in CDCl_3 .

3.3 2,4-Dimethoxybenzoyl Protection of **14**

The lowest yielding step in my Honours year synthesis of **2** was the Knoevenagel condensation, which gave only 4% of the desired (*Z*)-**18**. This was partly attributed to unwanted deprotection of the benzoyl group during the reaction. It was thought that this may be overcome by addition of two *o,p*-methoxy electron donating groups to the aromatic ring. Electron donation from the *o,p*-methoxy groups was predicted to lessen the electrophilic character of the benzoyl carbonyl carbon, leading to reduced susceptibility to inadvertent deprotection by nucleophiles (Figure 3.2).

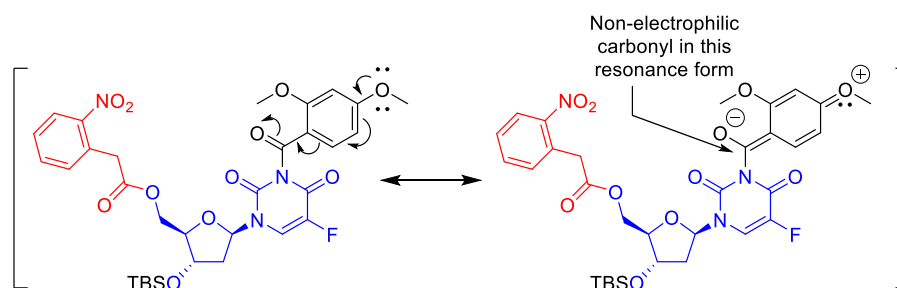
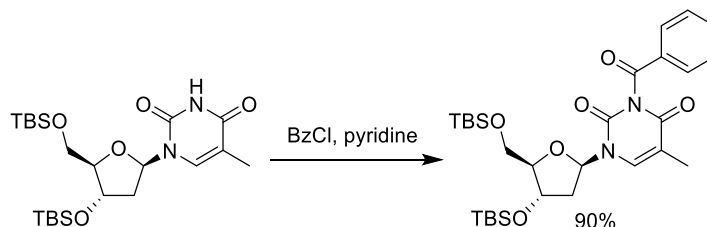


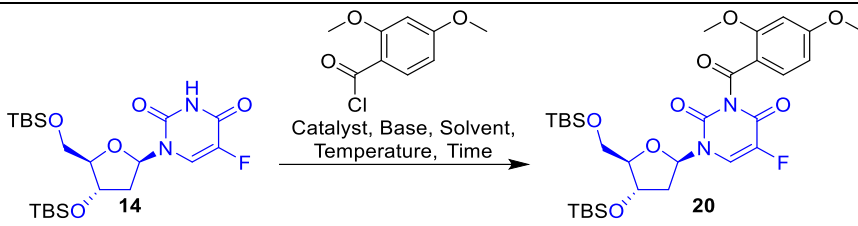
Figure 3.2 The presence of electron donating *o,p*-methoxy groups was predicted to reduce electrophilicity of the benzoyl carbonyl group, stabilising it towards nucleophiles and avoiding inadvertent deprotection during the Knoevenagel reaction.

The closest literature precedent for installation of the *o,p*-dimethoxybenzoyl group came from the previously mentioned paper reporting *bis*-TBS-protection of thymidine (Section 3.2),¹⁵² wherein the authors subsequently installed a benzoyl group onto the imide nitrogen in 90% yield (Scheme 3.4).



Scheme 3.4 Literature precedent for the benzoyl protection of *bis*-TBS protected thymidine.

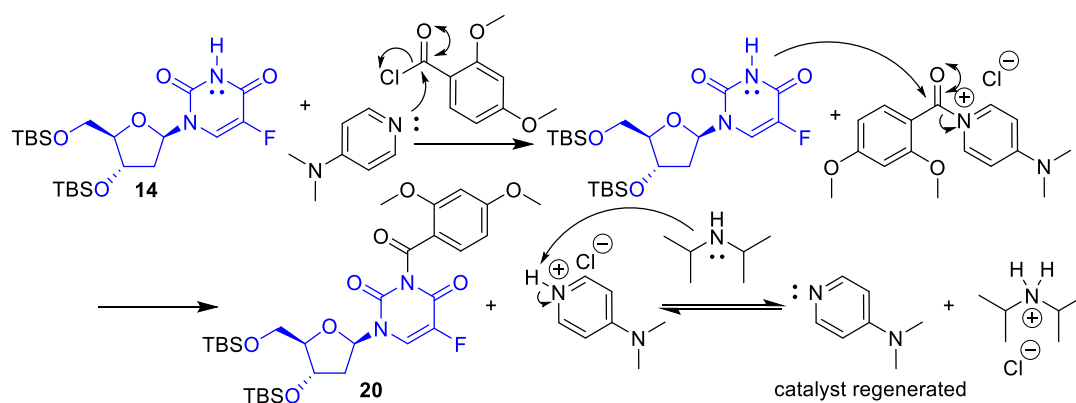
During my Honours year, benzoyl protection of **14** to give **15** was carried out at room temperature in pyridine over 48 hours using 4 eq. of benzoyl chloride. Although high yielding (97%), the product was difficult to isolate due to the large amount of pyridine that needed to be removed. Similar conditions using pyridine as the solvent/base/catalyst were initially investigated in my PhD for the reaction of **14** to give the new 2,4-dimethoxybenzoyl protected **20** (Table 3.1). Isolated yields were lower than expected (Entry 1), possibly due to difficulties in isolating the product, along with the lower electrophilicity of 2,4-dimethoxybenzoyl chloride due to the presence of the two electron donating methoxy groups. Heating the reaction (Entries 2 and 3) gave only minor improvements. It was postulated that switching from *N,N*-diisopropylethylamine (DIPEA)/pyridine to a DIPEA/4-dimethylaminopyridine (DMAP) combination in dichloromethane might both improve the yield and aid purification, especially on a large scale. The new conditions afforded **20** in 87% yield (Entry 4) and the purification was simplified as the DMAP, DIPEA and unreacted 2,4-dimethoxybenzoyl chloride were all removed by HCl_(aq) and sat. NaHCO_{3(aq)} washes during workup. It was noted that distillation of the 2,4-dimethoxybenzoyl chloride was essential for the reaction to proceed in good yield. 2,4-Dimethoxybenzoyl chloride was freshly prepared from 2,4-dimethoxybenzoic acid by reaction with oxalyl chloride in dichloromethane using catalytic DMF, followed by distillation.¹⁵⁴ Over the course of my PhD, the optimised reaction was repeated a total of eight times (0.1 g, 0.5 g, 0.6 g, 4.9 g, 5.0 g, 9.1 g, 10.0 g, 22.8 g of **14**), affording a total of 59.2 g of **20** in consistently high yields.

Table 3.1 Optimisation of 2,4-dimethoxybenzoyl protection of **14** to give **20**.


Entry	Catalyst	Base	Solvent	Temp °C	Time (h)	Yield (%)
1	Pyridine	DIPEA	Pyridine	r.t.	48	46
2	Pyridine	DIPEA	Pyridine	45	48	48
3	Pyridine	DIPEA	Pyridine	65	48	51
4	DMAP	DIPEA	CH ₂ Cl ₂	45	24	87

3.3.1 Mechanism of 2,4-Dimethoxybenzoyl Protection of **14** with DMAP/DIPEA

In this reaction, the nucleophilic pyridine nitrogen of the DMAP catalyst reacts with the electrophilic 2,4-dimethoxybenzoyl chloride to produce an activated *N*-acylpyridinium salt (Scheme 3.5). The imide nitrogen then acts as a nucleophile, attacking the carbonyl carbon of the *N*-acylpyridinium species to displace DMAP and produce **20** and DMAP·HCl. DIPEA then neutralises the DMAP·HCl to regenerate the DMAP catalyst.



Scheme 3.5 Mechanism for *N*-2,4-dimethoxybenzoylation of **14** with 2,4-dimethoxybenzoyl chloride in the presence of catalytic DMAP and DIPEA.

3.3.2 Spectroscopic Evidence for the Formation of **20**

The ¹H NMR spectrum of **20** (Figure 3.3) showed three new aromatic signals and two new singlets consistent with two methoxy groups. A doublet at 8.07 ppm was coupled to a doublet of doublets at 6.59 ppm, which was also coupled to a doublet at 6.38 ppm. These

signals corresponded to the three protons around the newly installed dimethoxybenzoyl group. Two large singlets observed at 3.85 ppm and 3.76 ppm, both integrating at 3H, indicated the presence of two methoxy groups. In addition to these peaks, all of the original peaks from the TBS-protected floxuridine **14** were observed in the spectrum of **20** except for the imide N-H. The appearance of nine new peaks in the ^{13}C NMR spectrum supported successful addition of the 2,4-dimethoxybenzoyl protecting group. Finally, observation of the expected $\text{M}+\text{H}^+$ ion at m/z 639.2933 by high resolution mass spectrometry confirmed formation of **20**.

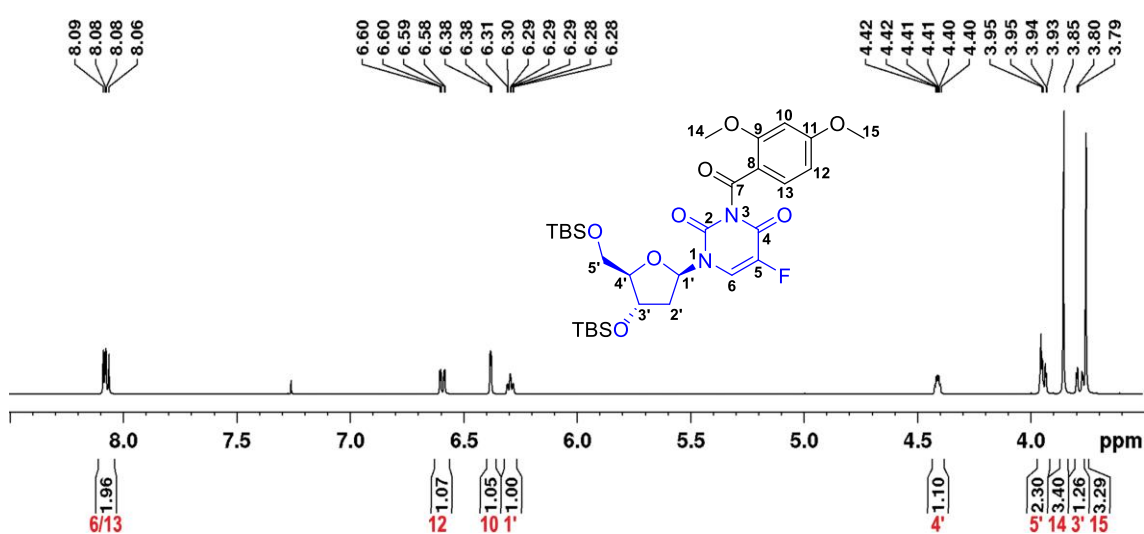


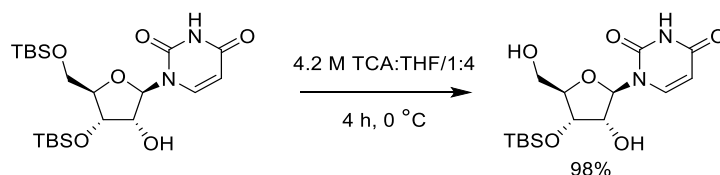
Figure 3.3 Section of the 500 MHz ^1H NMR spectrum of **20** (CDCl_3) showing the presence of 2,4-dimethoxybenzoyl signals.

3.4 Primary Alcohol Selective Deprotection in **20**

To achieve the desired Steglich esterification (Section 3.5), it was envisaged that selective TBS deprotection of the less hindered 1° alcohol of **20** to provide the required **21** could be achieved using aqueous trichloroacetic acid (TCA, 4.2 M) in THF (1:4).¹⁵¹ The use of THF as co-solvent with H_2O has been reported to improve the selectivity of 5'-desilylation and also to reduce unwanted depurination side products.¹⁵⁵ The milder reagent trichloroacetic acid ($pK_a = 0.66$) was reported to be superior to trifluoroacetic acid (TFA) ($pK_a = 0.23$) in terms of 5'-desilylation selectivity with 2',5'-disilylated nucleosides.¹⁵¹

These conditions had previously been successful for the benzoyl protected compound **15** during my Honours work (52%). The key literature precedent that led to use of these conditions described the selective TBS deprotection of the corresponding *bis*-TBS

protected uridine (Scheme 3.6). Although very similar in structure, it was predicted that the extra 2'-hydroxyl group in the protected uridine would add more steric hindrance around its 2° alcohol, thus driving preferential deprotection of the 1° alcohol leading to the very high yield (98%). Based on this, lower selectivity was expected for the mono-deprotection of the less hindered **20**.



Scheme 3.6 Literature precedent reporting selective 1° alcohol TBS-deprotection of uridine.¹⁵¹

The first attempted mono-deprotection of **20** gave **21** in 50% yield. The structures of the side products were tentatively identified using ¹H-NMR, with the reaction producing 20% of recovered starting material **20**, ~6% of the unwanted 2° mono alcohol and 25% of the *bis*-deprotected compound (Figure 3.4).

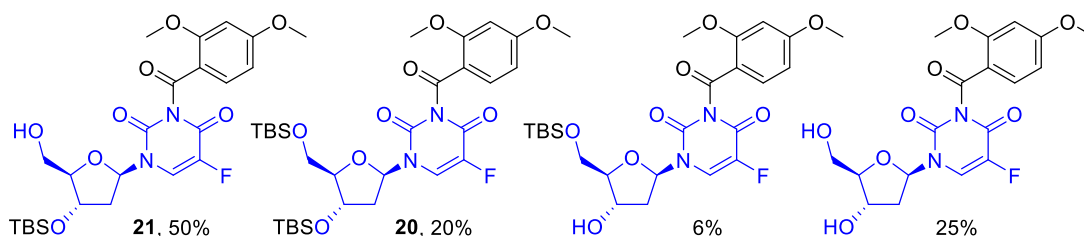


Figure 3.4 Typical yields of recovered starting material, the desired mono-alcohol **21** and two side products formed during TCA deprotection of **20**.

The deprotection of **20** was completed using 40 eq. of TCA in 1:4 H₂O/THF a total of seven times on increasing scale (0.1 g, 0.4 g, 0.8 g, 2.3 g, 3.9 g, 17.9 g and 29.7 g of **20**). The respective yields obtained were 50%, 39%, 47%, 42%, 46%, 31% (over 2 steps) and 37% (over 2 steps). The two larger scale reactions were carried out using crude **20** and purified only after TBS deprotection for practical reasons. Hence, their yields were consistent with the other reactions. A total of 17.3 g of **21** was synthesised over the course of my PhD.

3.4.1 Spectroscopic Evidence for the Formation of **21**

Removal of one TBS protecting group was evident in the $^1\text{H-NMR}$ spectrum of **21** from loss of half of the TBS peaks originally present for **20** (Figure 3.5). The disappearance of the corresponding three peaks in the $^{13}\text{C-NMR}$ spectrum of **21** also supported successful removal of one TBS protecting group. Additionally, the $^1\text{H-NMR}$ data showed a slight chemical shift in the methylene signal adjacent to the revealed primary alcohol (**20** δ 3.95 ppm, **21** δ 3.93 ppm) supporting that it was indeed the primary alcohol that had undergone selective deprotection. Finally, observation of the expected $\text{M}+\text{H}^+$ ion at m/z 525.2068 by high resolution mass spectrometry confirmed the structure of **21**.

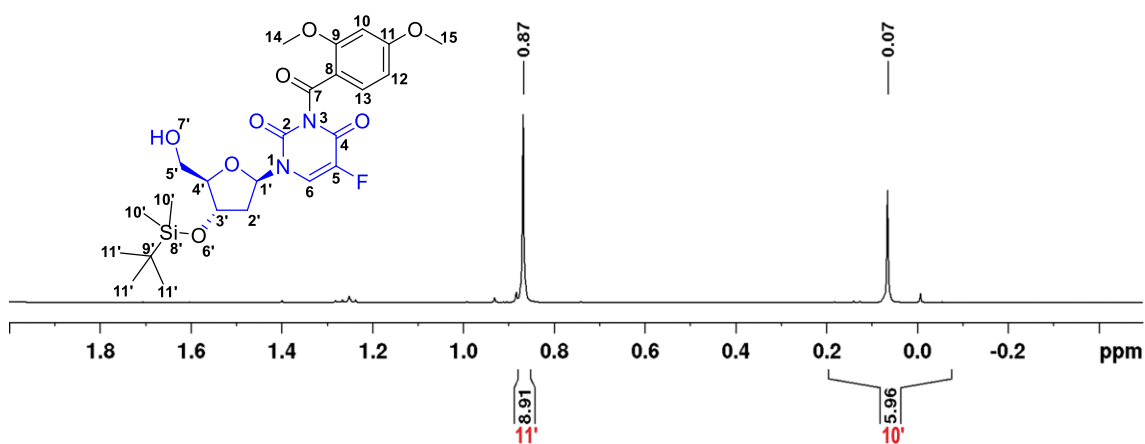
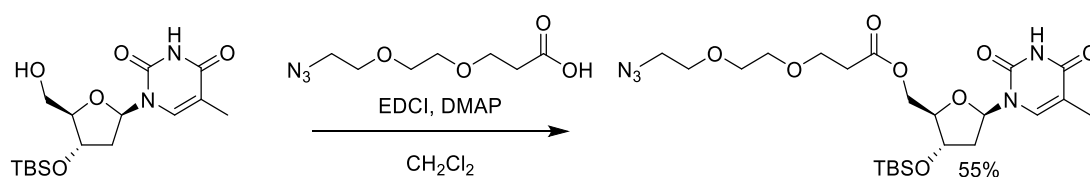


Figure 3.5 Removal of one TBS group halved the number of TBS signals detected in $^1\text{H-NMR}$ (CDCl_3) of **21** (relative to **20**).

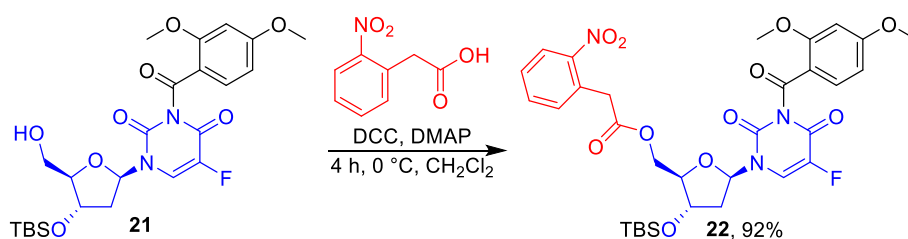
3.5 Steglich Esterification of **21**

In the literature there are only a few examples of esterification reactions with nucleosides and none with the fluorinated floxuridine. One relevant example, however, coupled a structurally similar TBS-protected thymidine and an alkyl carboxylic acid using 1-ethyl-3-(3-dimethylaminopropyl)carbodiimide (EDCI) and DMAP in dichloromethane (55%, Scheme 3.7).



Scheme 3.7 Literature precedent demonstrating esterification of TBS-protected thymidine.¹⁵⁶

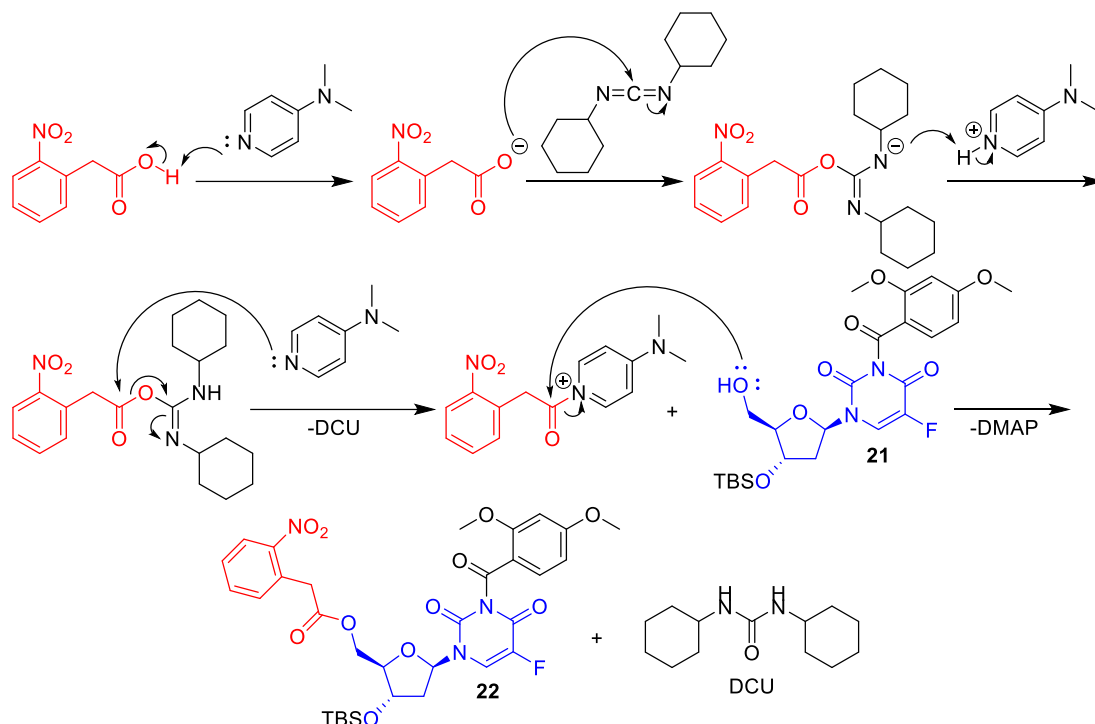
I found during my 2014 Honours studies that 2-(2-nitrophenyl)acetic acid could be esterified with the related benzoyl-protected compound **16** under similar Steglich esterification conditions using dicyclohexylcarbodiimide (DCC; instead of EDCI) to provide ester **17** in 80% yield (Scheme 3.1).¹⁵⁷ When the same (DCC) conditions were trialled on compound **21** during my PhD, the product **22** was formed in very high yield (Scheme 3.8). The reaction was carried out a total of five times on increasing scale 0.05 g (43%), 0.2 g (82%), 1.7 g (66%), 4.7 g (92%), 9.3 g (87%). In all cases the reaction proceeded well, with lower yields in some reactions observed only because of purification challenges due to the large amount of dicyclohexylurea (DCU) by-product formed. A process for removing the urea by-product was identified whereby cooling the mixture upon completion of the reaction to $-20\text{ }^{\circ}\text{C}$ overnight in a freezer caused the DCU to precipitate. The mixture could then simply be filtered and washed with cold dichloromethane before standard extraction and purification. This key improvement to the workup procedure led to consistently high yields at multi-gram scale. In total 17.8 g of pure **22** was synthesised.



Scheme 3.8 Steglich esterification of **21** with 2-(2-nitrophenyl)acetic acid gave **22** in excellent yield.

3.5.1 Mechanism of Steglich Esterification

The Steglich esterification uses DCC as the coupling reagent and DMAP as a nucleophilic catalyst (Scheme 3.9). The reaction begins with the neutralisation of the carboxylic acid with DMAP acting as the base. Once neutralised, the carboxylate nucleophile attacks DCC, whose nascent anion is then protonated by the pyridinium salt of DMAP to regenerate the catalyst. DMAP then displaces DCC from the carboxylic acid to form a highly reactive acyl pyridinium salt, with DCU formed in this process as a by-product. The nucleophilic alcohol then attacks the carbonyl group of the acyl pyridinium ion to form the ester bond and regenerate the DMAP catalyst.



Scheme 3.9 Mechanism for the DCC-mediated Steglich esterification of **21** with 2-(2-nitrophenyl)acetic acid to form **22**.

3.5.2 Spectroscopic Evidence for the Formation of **22**

Addition of the 2-(2-nitrophenyl)acetic acid group to **21** produced several new signals in the aromatic region of the ^1H NMR spectrum of **22** (Figure 3.6), including two new doublets of doublets and two new triplets of doublets. These splitting patterns arise from the *ortho* and *meta* coupling of each of the new aromatic protons in the 2-(2-nitrophenyl)acetic acid phenyl ring. The downfield doublet of doublets at 8.17 ppm is de-shielded due to the presence of the *ortho* nitro group. The benzylic methylene protons were obscured by the ribose C-O signals in the ^1H -NMR spectrum but they were evident from the integration and signals in the ^{13}C NMR spectrum. In the ^{13}C NMR spectrum eight new peaks (relative to **21**) were observed, supporting successful introduction of the 2-(2-nitrophenyl)acetic group. Finally, observation of the expected $\text{M}+\text{H}^+$ ion at m/z 688.2338 by high resolution mass spectrometry confirmed the structure of **22**.

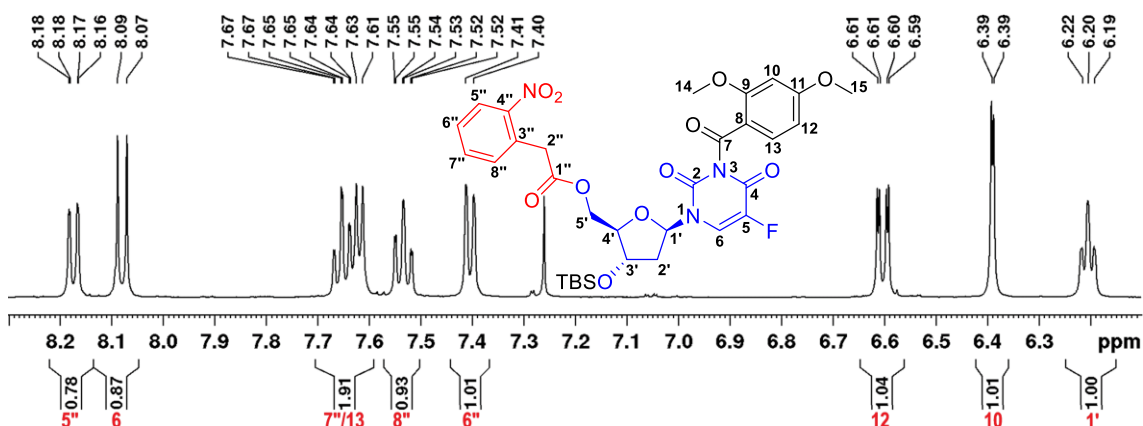
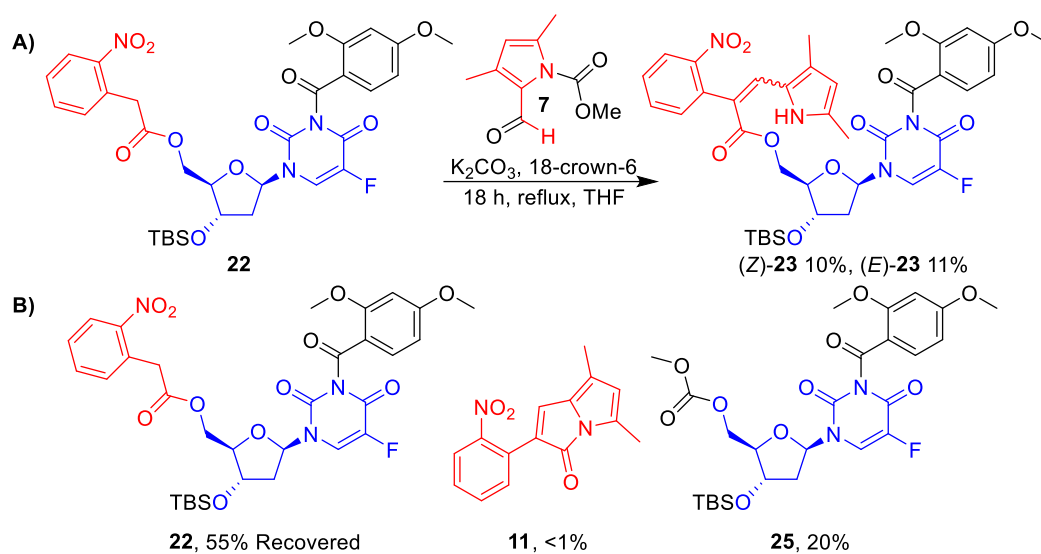


Figure 3.6 Steglich esterification produced diagnostic aromatic signals in the 500 MHz $^1\text{H-NMR}$ spectrum (CDCl_3) of **22**.

3.6 Knoevenagel Condensation of **22**

The key step in the synthesis of **2** was the Knoevenagel condensation of **22** with pyrrole aldehyde **7**. Previous attempts at the Knoevenagel condensation between **17** and **7** during my Honours year (Scheme 3.1) produced only low yields of (*Z*)-**18** (4%) and (*E*)-**18** (6%). This was partially attributed to the unstable benzoyl protecting group, which would deprotect during the reaction. With the more stable 2,4-dimethoxybenzoyl protecting group newly installed on **22**, disappointingly, only a minor improvement was seen using the standard Knoevenagel conditions ((*Z*)-**23**, 10% and (*E*)-**23**, (11%), Scheme 3.10). Substantial quantities of the starting material (55% recovery of **22**) remained unreacted and could be resubmitted to the reaction. Despite this, the yield of the reaction was still very low thus significant effort was invested into identifying reaction side-products to understand what was limiting formation of the desired product.

The first side product identified was the pyrrolizinone **11**, as observed previously in the Knoevenagel condensation with **6** in section 2.5.2. However, **11** appeared to form only in small quantities (<1% yield) so this did not explain the low reaction yield (Scheme 3.10, B). The major side-product of the reaction was identified as the methyl carbonate ester of the protected floxuridine **25** (20%, Scheme 3.10, B).

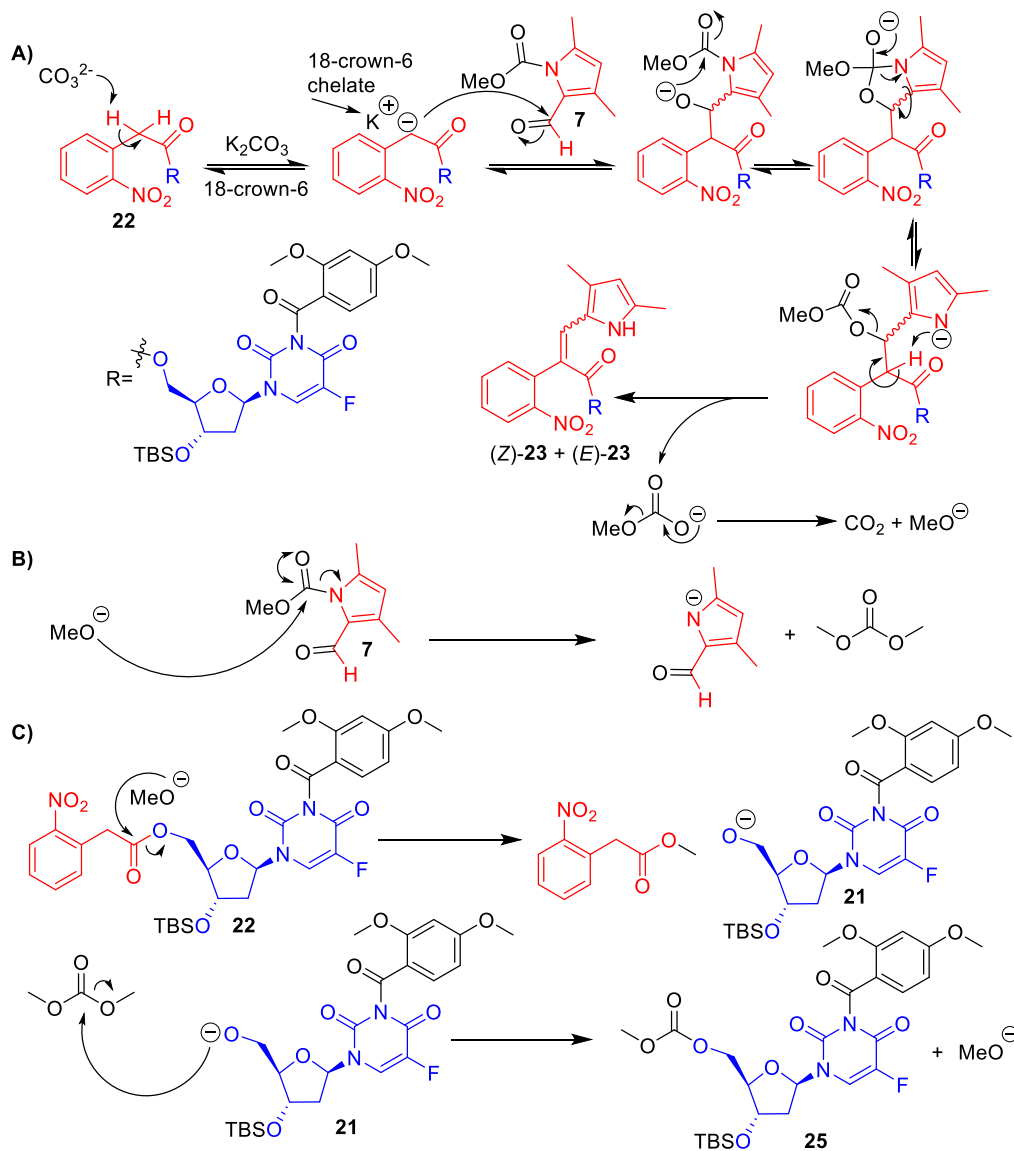


Scheme 3.10 A) Knoevenagel condensation of **22** with pyrrole aldehyde **7** gave (Z)-**23** and (E)-**23** in modest yields. B) Starting material **22** and side products **11** and **25** were also isolated from the reaction.

3.6.1 Proposed Mechanism for the Formation of **25**

To explain the formation of side product **25**, a mechanism was proposed involving the formation of methoxide after loss of the *N*-methylcarbamoyl protecting group of pyrrole aldehyde **7** (Scheme 3.11, A). During the Knoevenagel reaction, the methyl carbamate protecting group is probably lost as methyl carbonate, as explained in section 2.5.1. The methyl carbonate group could decompose into carbon dioxide and methoxide. The methoxide formed could then deprotect unreacted pyrrole aldehyde **7**, releasing dimethyl carbonate (Scheme 3.11, B). The ability of methoxide to deprotect the pyrrole aldehyde **7** was chemically confirmed by stirring a small amount of the pyrrole aldehyde **7** in THF with sodium methoxide, which led to quantitative deprotection. An equivalent of methoxide could also cleave the ester bond in the starting material **22** by transesterification (Scheme 3.11, C), releasing methyl 2-(2-nitrophenyl)acetate and protected floxuridine derivative **21**. However, methyl 2-(2-nitrophenyl)acetate was not observed in the complex mixture of products and was only inferred from the proposed mechanism. The 1° alcohol group of **21** could then react with the newly formed dimethyl carbonate, regenerating methoxide and producing the methyl carbonate side product **25**. One piece of evidence that supports this mechanism is the ratio of products to the side product **25**. In the mechanism proposed, only one molecule of **25** could form from each

molecule of (*Z*)-**23** or (*E*)-**23**. This would explain why the yield of **25** is the same as the total yield of *cis*- and *trans*-**23**.



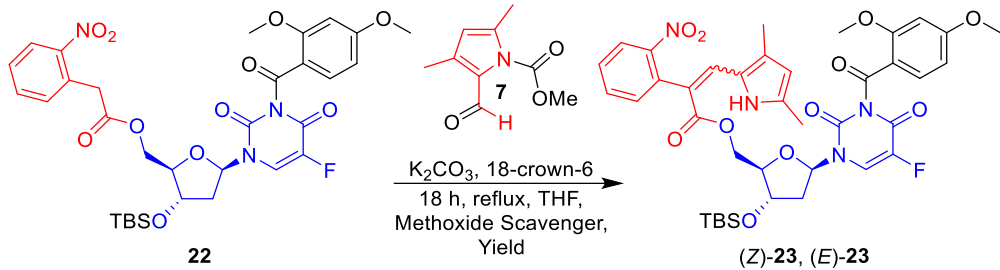
Scheme 3.11 Proposed mechanism for the formation of methoxide during the Knoevenagel reaction and subsequent formation of the major side-product **25**.

3.6.2 Attempts to Optimise the Knoevenagel Reaction

The hypothesis that methoxide was being formed in the reaction was tested by adding methoxide scavengers (Table 3.2). The first scavenger trialled was *tert*-Butyl(chloro)diphenylsilane (TBDPSCI) a silylating reagent that is very reactive towards oxygen nucleophiles like methoxide. However, no improvement was seen in the reaction yield. The next idea was to add different sized molecular sieves (3-5 Å) capable

of sequestering methoxide (and water). Of these reactions, only the 3 Å molecular sieves produced any product but no improvement in the reaction yield was seen.

Table 3.2 Knoevenagel reactions performed in the presence of methoxide scavengers.

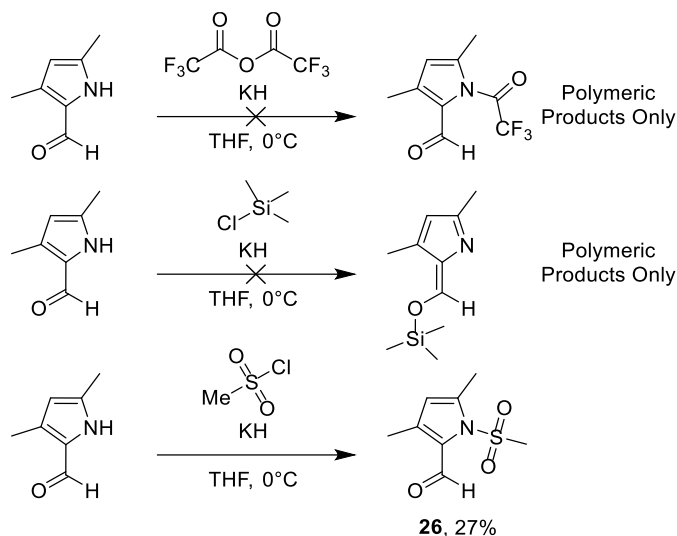


Entry	Methoxide Scavenger	(Z)-23 (%)	(E)-23 (%)
1	TBDPSCI	~10	~10
2	3 Å Ground Molecular Sieves	~10	~10
3	4 Å Ground Molecular Sieves	No Reaction	No Reaction
4	5 Å Ground Molecular Sieves	No Reaction	No Reaction

In addition to exploring methoxide scavengers, a series of alternative *N*-protecting groups for the pyrrole-2-aldehyde were considered as a means of improving the reaction yield. These protecting groups considered were trifluoroacetyl, trimethylsilyl and mesyl groups (Scheme 3.12).

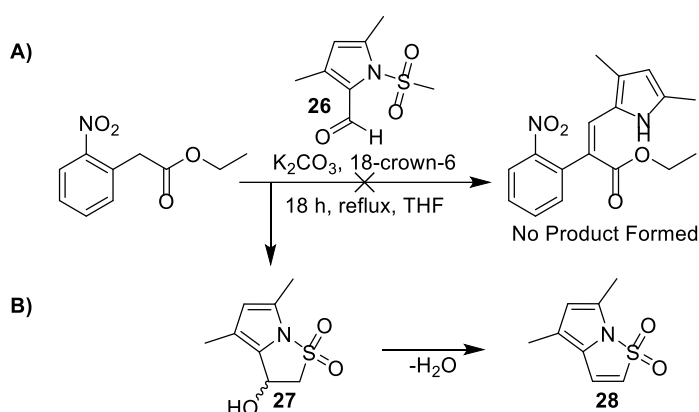
Multiple attempts at generating the *N*-trifluoroacetyl pyrrole using trifluoroacetic anhydride led only to formation of polymeric products. It was thought that the trimethylsilyl protecting group might add to the aldehyde to form the silyl enol ether due to silicon's high affinity for oxygen. However, this did not occur and once again only polymeric by-products were formed.

Mesylation of the pyrrole-2-aldehyde with mesyl chloride/KH gave a low yield of **26** (27%) but it provided sufficient material to trial some Knoevenagel reactions. The mechanism of mesylation proceeds in a similar fashion to carbamoylation with methyl chloroformate to form **7**. First, potassium hydride abstracts the pyrrole N-H to form the potassium pyrrolate salt, which then acts as a nucleophile to attack the mesyl chloride sulphur atom and displace chloride as the leaving group.



Scheme 3.12 Attempts to synthesise alternative *N*-protected pyrrole-2-aldehydes for use in the Knoevenagel reaction.

The mesyl-protected pyrrole aldehyde **26** was submitted to model Knoevenagel reactions with ethyl 2-(2-nitrophenyl)acetate as a simple surrogate for **22** (Scheme 3.13, A). No desired product was formed under the usual conditions, with **26** instead undergoing *S*-methyl deprotonation followed by intramolecular cyclisation onto the neighbouring aldehyde, yielding **27** (Scheme 3.13, B). Once formed, **27** was unstable and could only be briefly characterised by ^1H and ^{13}C NMR as the nascent alcohol eliminated water to give the stable novel *N*-heteroaryl fused vinyl sultam **28** (Scheme 3.13, B).



Scheme 3.13 *N*-Mesyl pyrrole aldehyde **26** did not undergo the desired Knoevenagel reaction but instead formed a *N*-heteroaryl fused vinyl sultam, the first example of a compound from this class.

At the time of synthesis (March 2016), **27** and **28** were both novel structures, with the fused pyrrole sulfone being a unique heterocyclic ring system. At the end of 2017, however, the group of Laha *et al* published three articles describing the same bicyclic ring system.¹⁵⁸⁻¹⁶⁰ In their work, a series of *N*-heteroaryl fused vinyl sultams were synthesised and their chemistry explored (Figure 3.7).

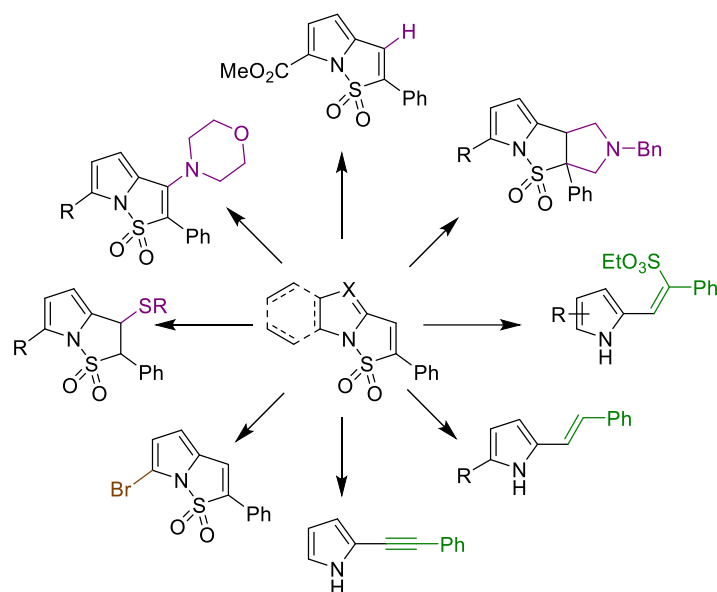


Figure 3.7 Published series of pyrrole *N*-heteroaryl fused vinyl sultams related to compound **28** and their versatile chemistry.¹⁵⁹

Although low yielding, the original Knoevenagel conditions were able to deliver sufficient quantities of (*Z*)-**23** to allow completion of the synthesis. The ability to resubmit recovered starting material **22** to repeat reactions allowed enough prodrug **2** to be synthesised for all chemical and biological studies (Chapter 4). The reaction was completed six times on increasing scale (0.1 g, 1.0 g, 1.5 g, 3.4g, 4.9g, 5.0g of **22**) with consistent (albeit low) yields. A total of 1.0 g of (*Z*)-**23** was synthesised during my PhD work.

The *trans* product (*E*)-**23**, was substantially more difficult to obtain pure than (*Z*)-**23**, due to its increased polarity. This gave it a R_f very close to the starting material **22** and the *N*-methylcarbamoyl deprotected derivative of **7**. Isomerisation of a small quantity (~30 mg) (*E*)-**23** using catalytic H_2SO_4 in THF gave similarly poor results as (*E*)-**8**, observed by TLC. It was instead found to be practically more convenient to focus on recovery of unreacted starting material **22** and performing multiple reactions to obtain (*Z*)-**23**.

3.6.3 Spectroscopic Evidence for the Formation of (*Z*)-**23**

Addition of the pyrrole fragment led to several new signals appearing in the aromatic region of the ^1H NMR spectrum of (*Z*)-**23** relative to **22** (Figure 3.8). A broad singlet appeared at 11.73 ppm, corresponding to the pyrrole N-H hydrogen bonded to the nearby carbonyl oxygen of the ester group (see Section 2.5.3). This observation confirmed that the *cis* isomer had been isolated as the same peak in (*E*)-**23** appeared at 6.71 ppm, consistent with our previous findings. The intramolecular H-bond in (*Z*)-**23** made the compound significantly less polar than (*E*)-**23** making the two isomers easily separable by silica gel column chromatography. A singlet was observed at 6.85 ppm corresponding to the newly introduced alkene hydrogen. A tight doublet at 5.94 ppm with very fine splitting corresponded to the aromatic proton on the pyrrole (H13''), which showed $^4J_{\text{H,H}}$ coupling (1.5 Hz) to the pyrrole N-H (H11'').

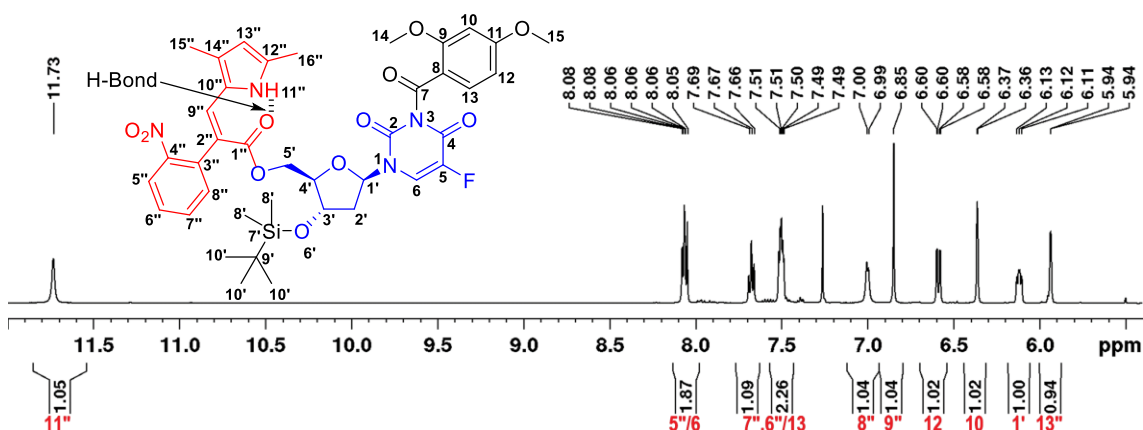
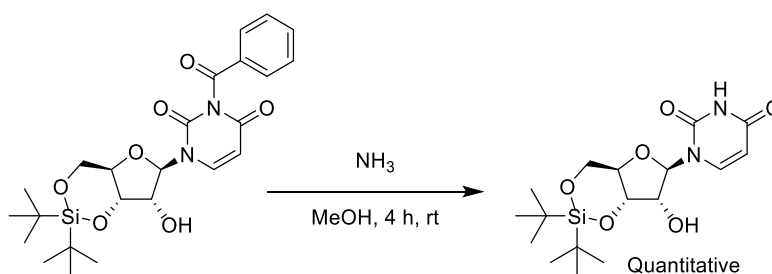


Figure 3.8 Downfield region of the 500 MHz ^1H -NMR (CDCl_3) spectrum of (*Z*)-**23** showing all of the expected signals, including the highly deshielded pyrrole N-H signal indicating the presence of an H-bond to the ester carbonyl oxygen.

The CH_2 signal of the 2-nitrophenylacetyl fragment of **22** had disappeared in (*Z*)-**23** and two new singlets at 2.36 and 2.18 ppm had appeared, each showing an integration of 3H. These singlets corresponded to the two methyl groups on the newly introduced pyrrole moiety. In the ^{13}C NMR spectrum, seven new carbon peaks were observed, consistent with introduction of the pyrrole. Finally, observation of the expected $\text{M}+\text{H}^+$ ion at m/z 793.2916 by high resolution mass spectrometry confirmed formation of (*Z*)-**23**.

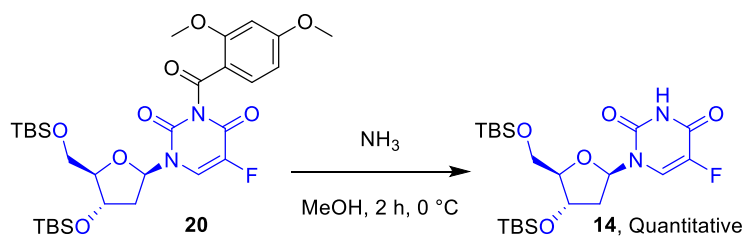
3.7 2,4-Dimethoxybenzoyl Deprotection of (Z)-**23**

With the core structure of **2** in place, the final two steps in the synthesis involved removing the 2,4-dimethoxybenzoyl and TBS protecting groups of (Z)-**23**. It was postulated that in deprotecting the 2,4-dimethoxybenzoyl protecting group first, the TBS protecting group would sterically shield the potentially liable ester of (Z)-**23** from ammonolysis, leading to a higher yield over these two final steps. The closest literature precedent for the reaction reported the quantitative benzoyl deprotection of N³-benzoyl-3',5'-O-(di-*tert*-butylsilyl)-2'-O-methyluridine using methanolic ammonia (Scheme 3.14).¹⁶¹



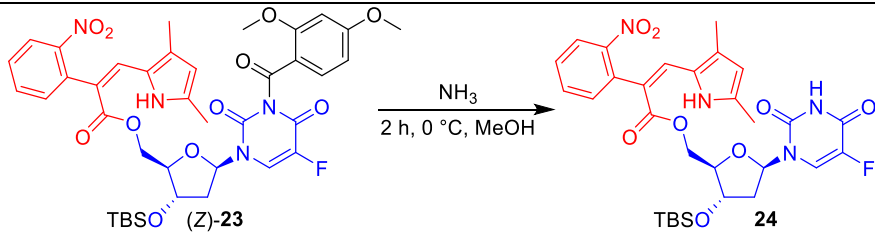
Scheme 3.14 Literature precedent for benzoyl deprotection of a structurally related uridine derivative.¹⁶¹

Before committing any of the advanced intermediate (Z)-**23** to the debenzoylation reaction, a model reaction was investigated using the more freely available precursor **20** (Scheme 3.15). The reaction was found to proceed in quantitative yield after two hours.



Scheme 3.15 Model 2,4-dimethoxybenzoyl deprotection reaction with **20** delivered **14** in quantitative yield.

Encouraged by this finding, deprotection the (Z)-**23** was attempted on 100 mg scale using 2 mL of 7 N methanolic ammonia, which delivered the desired **24** in 82% yield (Table 3.3, Entry 1).

Table 3.3 2,4-Dimethoxybenzoyl deprotection of (Z)-**23**.


Entry	(Z)- 23 (mg)	7N NH ₃ /MeOH (mL)	24 , % Yield
1	104	2	82
2	204	4	79
3	300	6	75

The reaction was repeated two more times on 200 mg and 300 mg scales, with both reactions providing over 75% yields. A total of 374 mg of **24** was produced from the three reactions.

3.7.1 Spectroscopic Evidence for the Formation of **24**

Successful deprotection of the 2,4-dimethoxybenzoyl group was evident in the ¹H NMR spectrum of **24**, with all signals arising from this group disappearing (Figure 3.9). Within the aromatic region, in (Z)-**23** disappearance of the two doublets and one doublet of doublets from the 2,4-dimethoxybenzoyl was accompanied by the appearance of a broad singlet at 8.43 ppm integrating for 1H, corresponding to the newly formed 5-fluorouracil N-H. Within the aliphatic region, two singlets at 3.85 and 3.71 ppm integrating for 3H in the spectrum of **23** were absent in **24**, consistent with loss of the two methoxy groups. The disappearance of nine peaks in the ¹³C NMR spectrum supported successful deprotection. Finally, observation of the expected M+H⁺ ion at *m/z* 629.2443 by high resolution mass spectrometry confirmed formation of **24**.

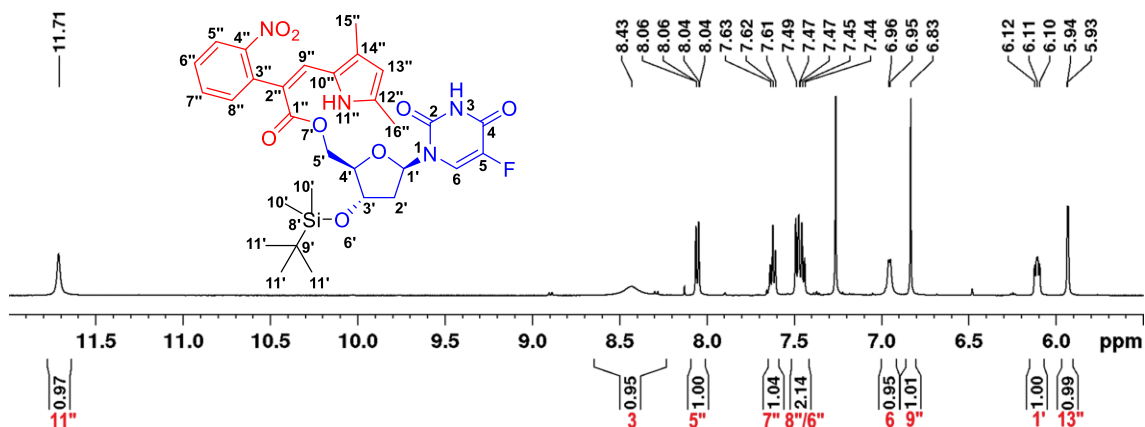
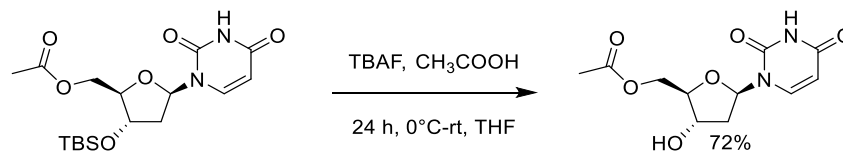


Figure 3.9 Downfield region of the 500 MHz $^1\text{H-NMR}$ (CDCl_3) spectrum of **24**.

3.8 TBS Deprotection of **24** to Mutual Prodrug **2**

The final reaction in the synthesis of **2** was removal of the TBS protecting group from the secondary alcohol. The closest literature precedent for this reaction involved a high yielding (72%) TBS-deprotection of the secondary alcohol of a deoxyuridine derivative (Scheme 3.16).¹⁶²



Scheme 3.16 Literature precedent showing TBS-deprotection of a deoxyuridine derivative.¹⁶²

Using the same conditions as in the literature precedent, the first attempted deprotection with 65 mg of **24** delivered 24 mg of **2** (Table 3.4, 49% yield). The reaction appeared to proceed well by TLC analysis, but the impurities were difficult to separate from **2** by standard column chromatography on silica gel. The reaction was repeated two more times using 128 mg and 177 mg of **24**. Different chromatography solvents were trialed in attempts to simplify isolation of **2**. Eventually it was discovered that **2** could be obtained in pure form (69% yield) using silica gel column chromatography with a gradient of 0-50% acetone in pet. spirit. A total of 301.6 mg of **2** was produced from these reactions.

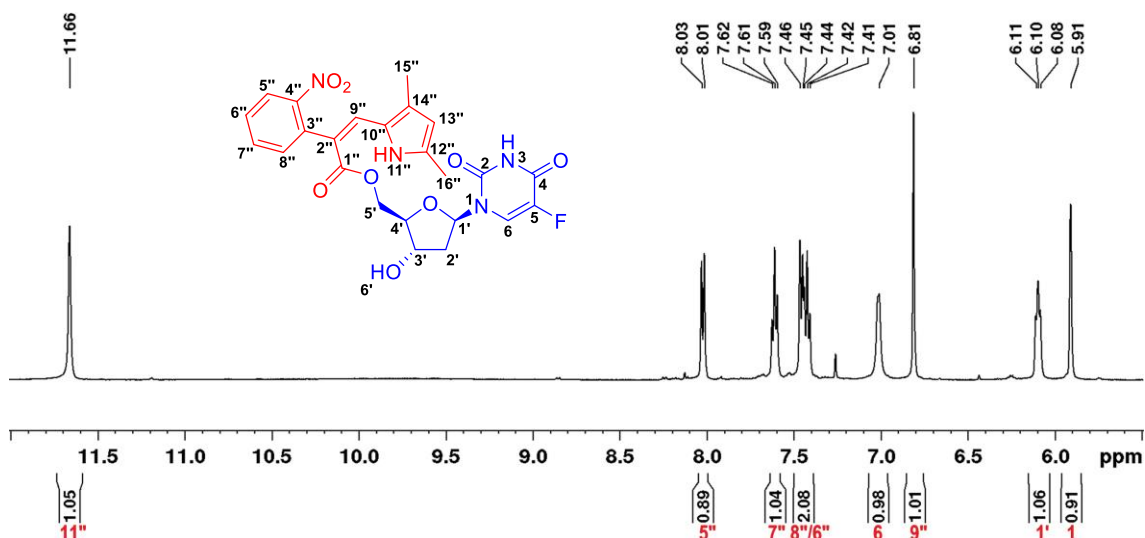
Table 3.4 Optimisation of Purification of TBAF deprotection of **24**.

Cc1c(C(=O)OC2C(C(C(CO2)OC3C=CC(=O)N3)C(=O)N4C=CC(=O)N4C(F)=C4)C=C1[NH]2)OC5(C)C=CC=C5[N+](=O)[O-]
 $\xrightarrow[24\text{ h, }0^{\circ}\text{C-rt, THF}]{\text{TBAF, CH}_3\text{COOH}}$
Cc1c(C(=O)OC2C(C(C(CO2)O)C(=O)N3C=CC(=O)N3C(F)=C3)C=C1[NH]2)O)OC4(C)C=CC=C4[N+](=O)[O-]

Entry	24 (mg)	1M TBAF (mL)	Chromatography Solvent	2 , % yield
1	65	0.5	Ethyl acetate/Pet. Spirit	49
2	128	1.0	MeOH/CH ₂ Cl ₂	66
3	177	1.5	Acetone/Pet. Spirit	69

3.9 2D Spectroscopic Analysis of **2**

Full 2D NMR characterisation of **2** was undertaken after completion of the synthesis. Within the aromatic region of the ¹H-NMR, all protons were successfully accounted for (Figure 3.10). The prodrug was confirmed as the correct *cis* isomer by the presence of the heavily deshielded pyrrole N-H signal (H-11'', δ 11.66 ppm) arising from its intramolecular hydrogen bond to the nearby ester carbonyl oxygen (C-1''). In CDCl₃, both the imide N-H (H-3) and the deprotected 2° alcohol proton (H-6') exchanged with solvent deuterium and did not appear in the spectrum.

**Figure 3.10** Aromatic region of the 500 MHz ¹H-NMR spectrum of **2** recorded in CDCl₃.

Removal of the TBS group saw loss of its characteristic singlet at 0.87 ppm and associated apparent doublet at 0.06 ppm (Figure 3.11). The ribose CH₂ signal (H2') was obscured by

the CH₃ methyl signal (H15''). The presence of this signal was confirmed from the 5H integration of the peak at 2.15 ppm, and from the gHSQC spectrum.

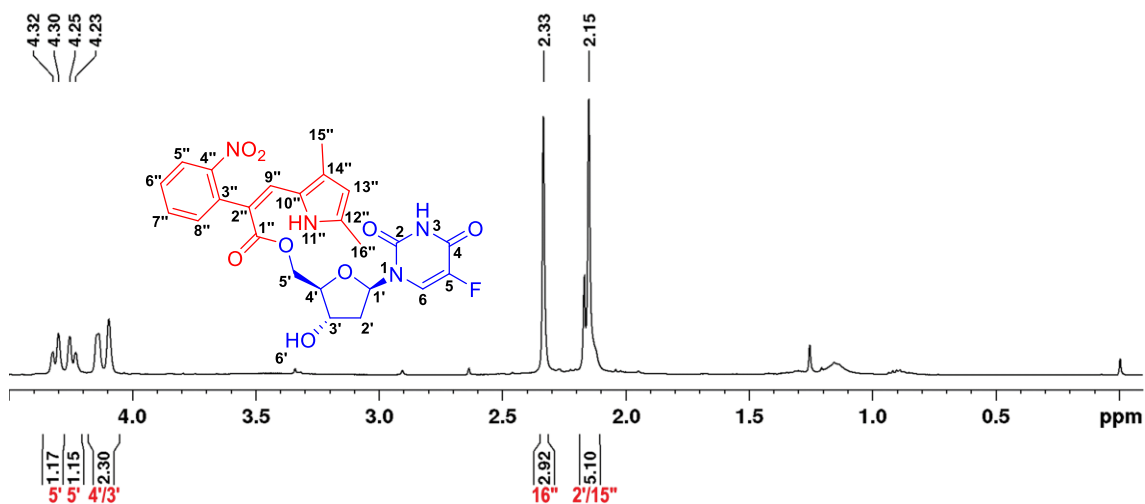


Figure 3.11 Aliphatic region of the 500 MHz ¹H-NMR spectrum of **2** recorded in CDCl₃.

3.9.1 ¹³C APT Analysis of **2**

The ¹³C APT spectrum of **2** was complex due both to the large number of unique chemical environments of the carbons within the molecule and also the splitting of peaks that occurs due to the presence of the fluorine atom at C5 (Figure 3.12). The fluorine atom causes the peak for C5 measured (140.4 ppm) to split into a doublet with a coupling constant of $J = 236.7$ Hz. This falls within the literature range for a typical C-F coupling constant (162 – 280 Hz).¹⁶³ The adjacent carbons C4 (157.2 ppm) and C6 (123.7 ppm) were also split into doublets with coupling constants $J = 27.0$ Hz and $J = 33.3$ Hz, respectively.

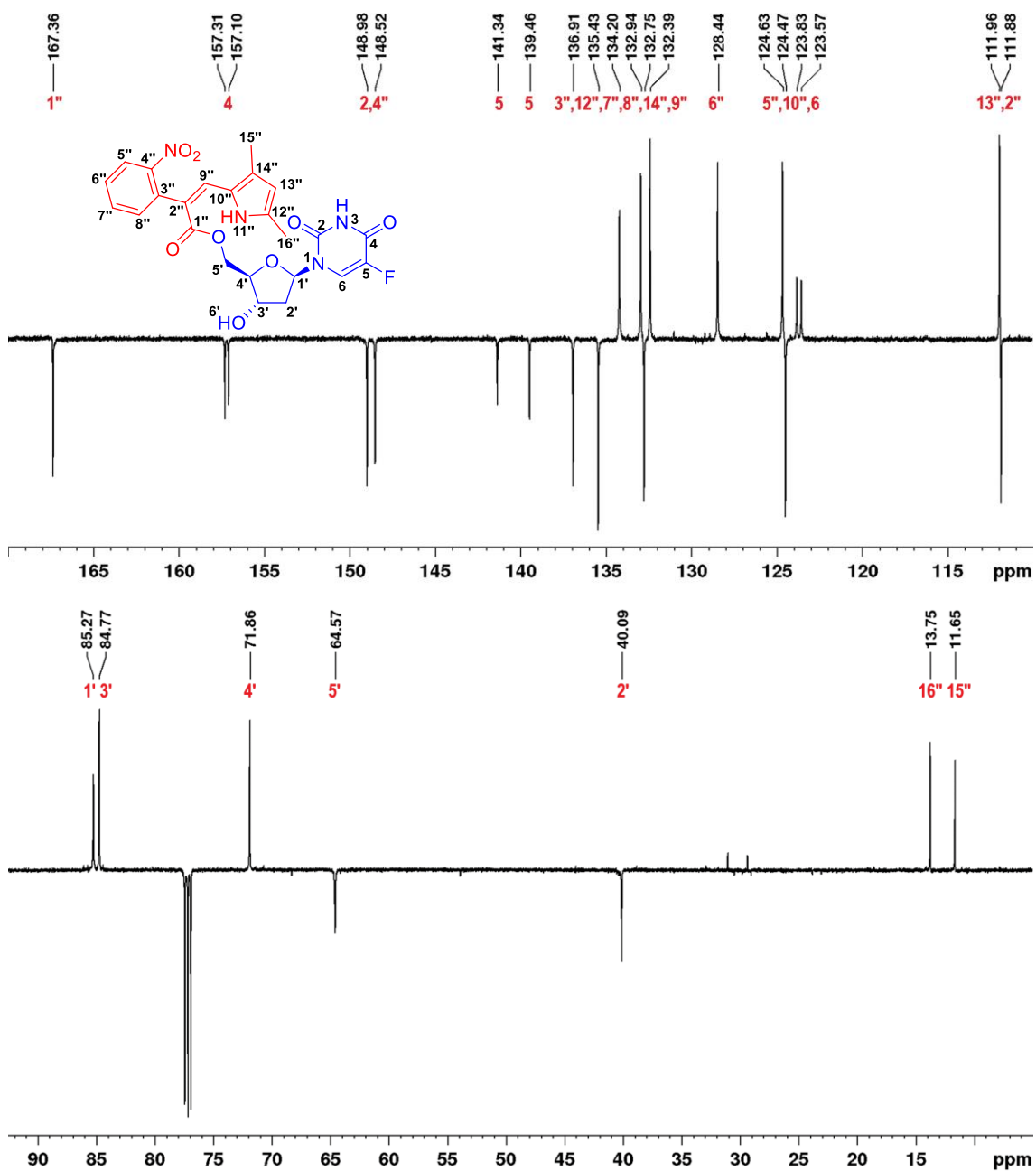


Figure 3.12 Aromatic and Aliphatic regions of the 500 MHz ^{13}C -NMR spectrum of **2** recorded in CDCl_3 .

3.9.2 *g*COSY Analysis of **2**

The *g*COSY spectrum of **2** showed the expected correlations around the nitroaromatic ring (Figure 3.13). These correlations helped to assign H6'' and H7'' starting from the diagnostic H5'' doublet, which is deshielded due to its location *ortho* to the electron withdrawing nitro group.

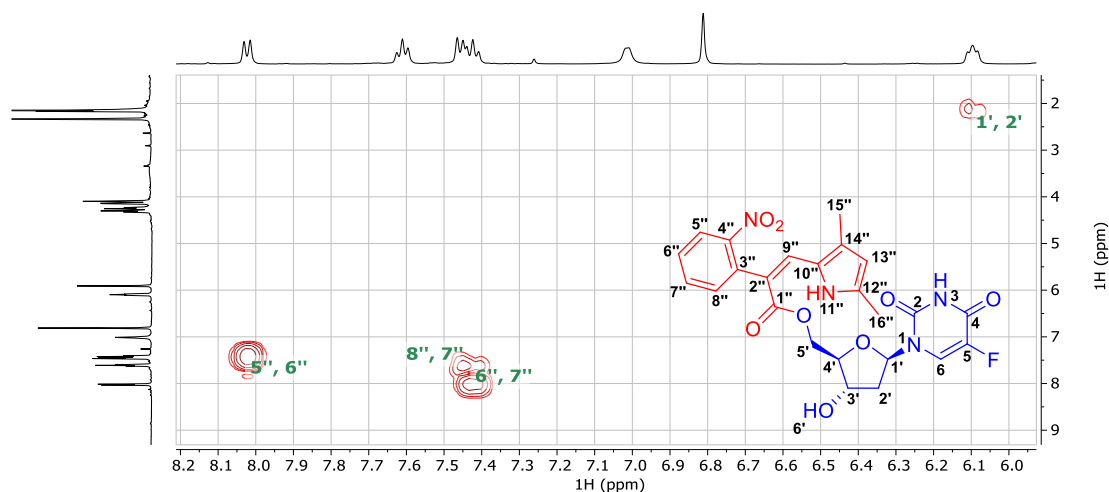


Figure 3.13 Selected correlations observed in the 500 MHz gCOSY spectrum of **2** (with diagonal suppression) recorded in CDCl₃.

3.9.3 gHSQC Analysis of **2**

Correlations for each proton-attached carbon were observed in the aromatic (Figure 3.14) and aliphatic (Figure 3.15) regions of the gHSQC spectrum of **2**. The gHSQC revealed the location of the ‘hidden peak’ for H1', which was obscured by the pyrrole methyl H15'' peak at 2.15 ppm. The gHSQC also allowed for assignment of each of the non-quaternary carbons within **2**.

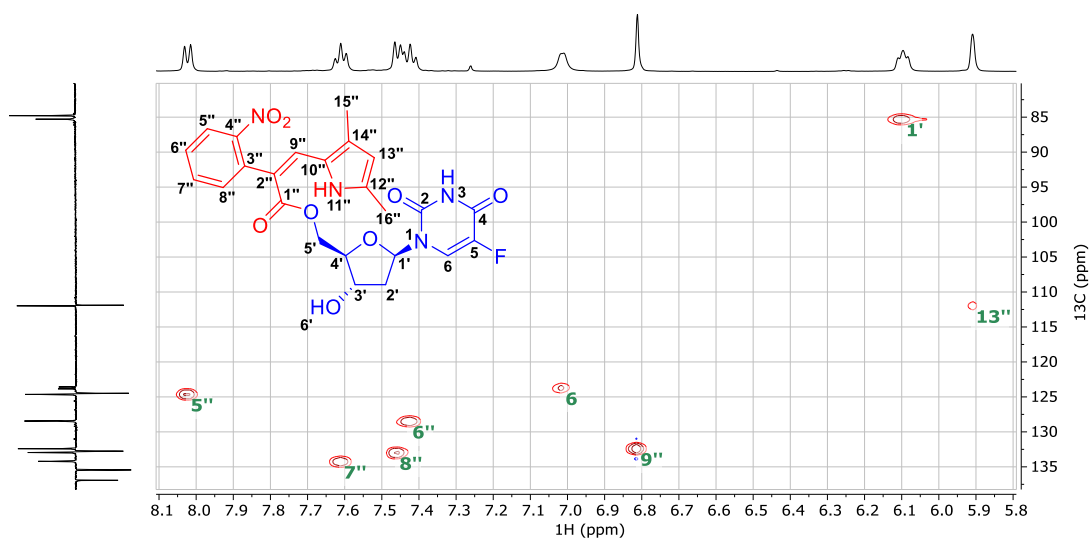


Figure 3.14 Aromatic region of the 500 MHz gHSQC spectrum of **2** recorded in CDCl₃.

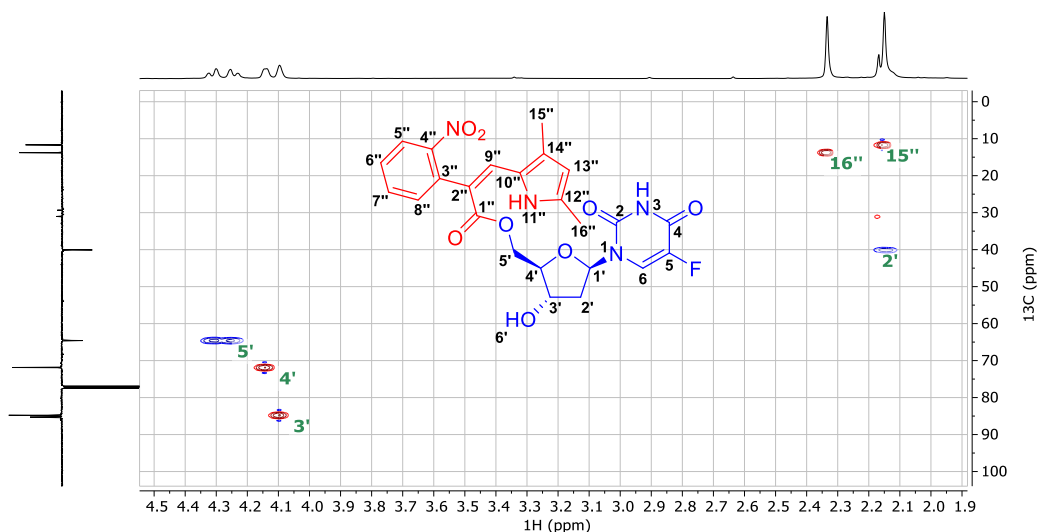


Figure 3.15 Aliphatic region of the 500 MHz gHSQC spectrum of **2** recorded in CDCl₃.

3.9.4 gHMBC Analysis of **2**

The gHMBC of **2** showed many correlations within **2** due to the large number of individual carbon environment in the molecule. Of key interest in the aromatic region (Figure 3.16) was the C-H correlations between C3'' and H5'', 7'' and 9'' and C14'' and H9'', which allowed the overlapping peaks of C3'' and C14'' to be differentiated.

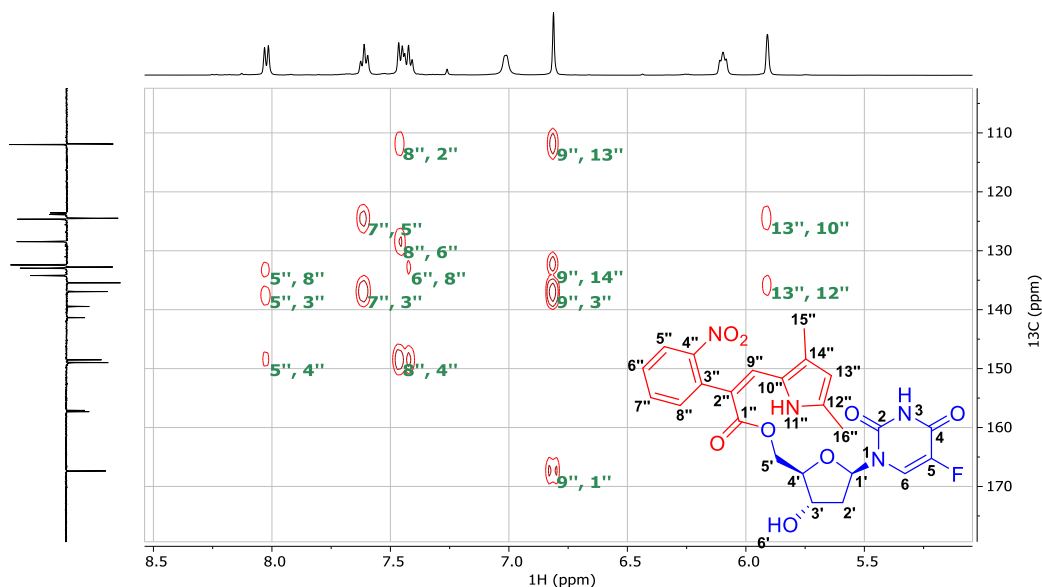


Figure 3.16 Aromatic region of the 500 MHz gHMBC spectrum of **2** recorded in CDCl₃.

The Aliphatic region of the gHMBC spectrum of **2** (Figure 3.17) was useful for assigning the methyl signals for H15'' and H16'', which could not be distinguished by ¹H-NMR alone. Assignment was evident from the correlations that H15'' made to C9'' and

C10'', beyond the range expected for correlations from H16''. In comparison, H16'' only made the correlations to C12'' and C13''.

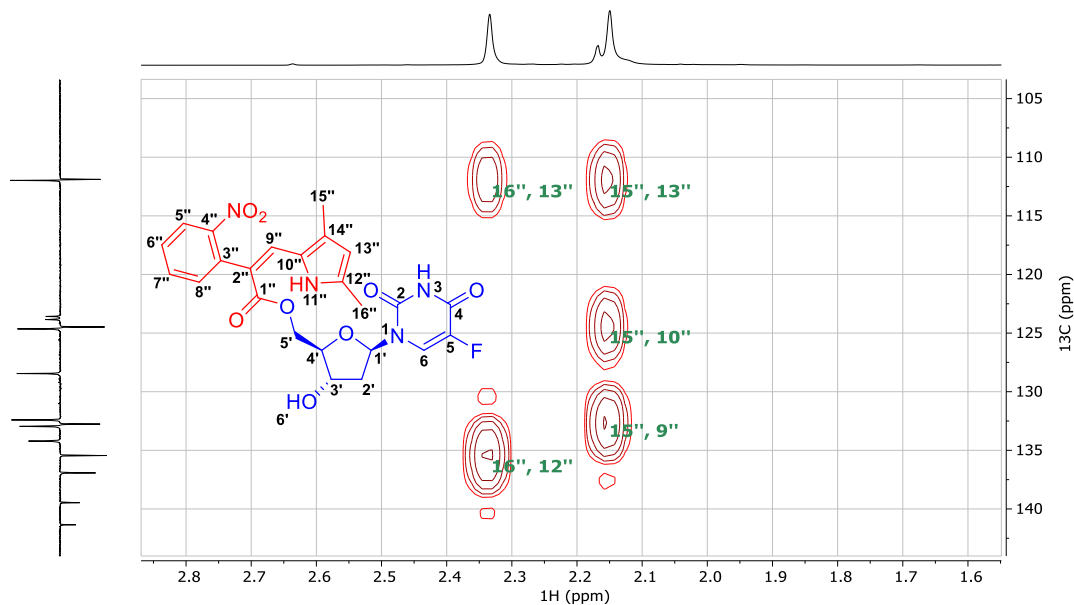
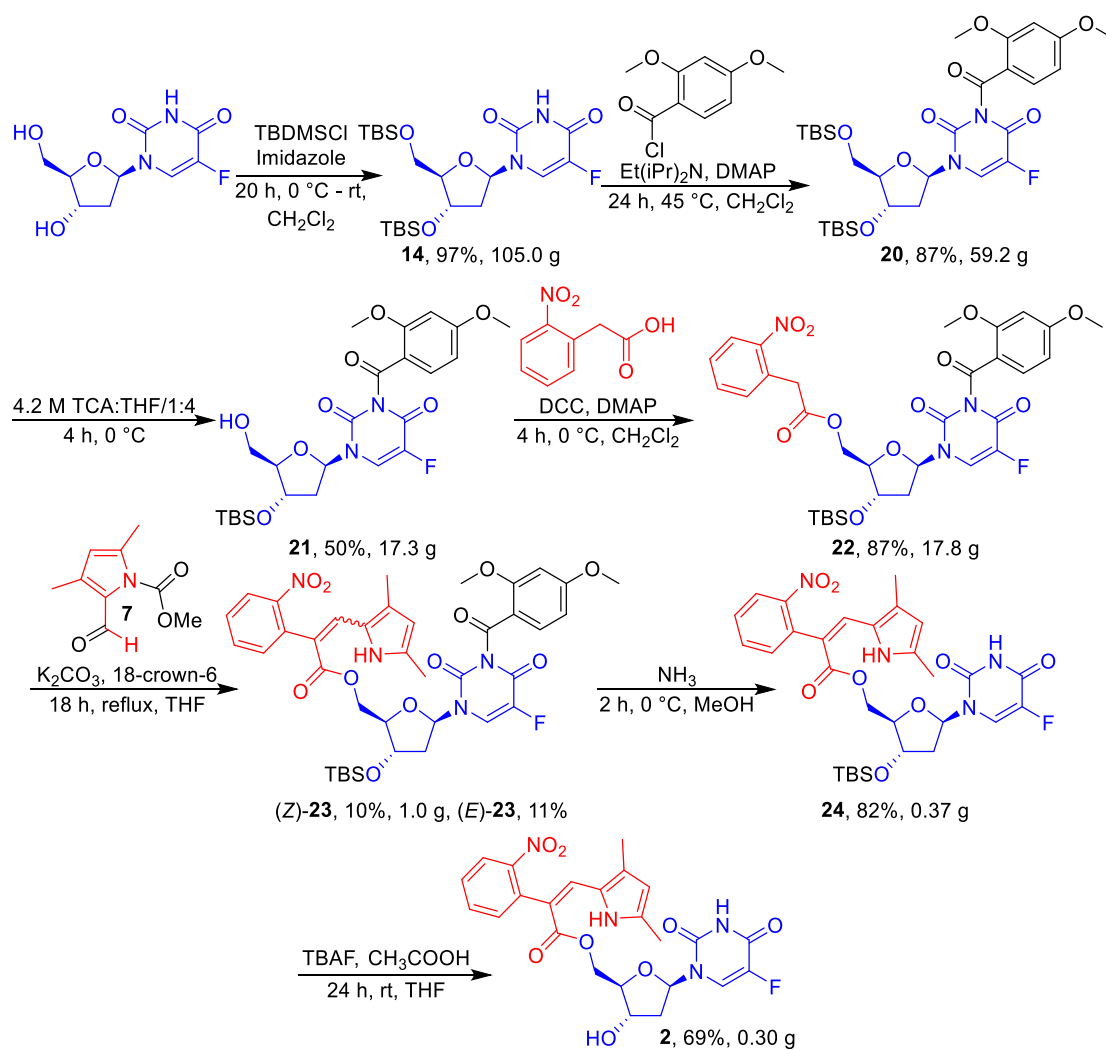


Figure 3.17 Aliphatic region of the 500 MHz gHMBC spectrum of **2** recorded in CDCl₃.

3.10 Summary of the Synthesis of **2**

The total synthesis of **2**, having been originally attempted on small scale during my Honours year, was improved and successfully scaled up to provide sufficient semaxanib|floxuridine mutual prodrug **2** for chemical and biological testing (Chapter 4). The synthesis was completed in 7 steps in an overall yield of 2.1% (Scheme 3.17) to produce a total of 301.6 mg of pure mutual prodrug **2**. The synthesis still poses challenges that should be addressed in the future, especially the problematic Knoevenagel condensation where a maximum yield of only 10% (21% combined *cis/trans*) was obtained after considerable optimisation attempts. To improve both this synthesis and the previously discussed synthesis of the mutual prodrug **1**, work carried out in Chapter 5 showed that moving the Knoevenagel reaction to earlier in the synthesis is a promising alternative route.



Scheme 3.17 Summary of the completed synthesis of **2**. Total quantities of each compound produced over the course of my PhD are shown.

Chapter 4: Proof-of-Concept Chemical Reductions and *in vitro* Biological Evaluation

4.1 Proof-of-Concept Chemical Reductions

Chemical reactions were performed on **1** and **2** to establish whether spontaneous intramolecular cyclisation occurred following reduction of the aryl nitro group, leading to release of semaxanib (SU5416) **3** and the respective cytotoxins; floxuridine and 4-aminoaniline mustard, from the prodrugs. It was anticipated that partial reduction of the nitro group and spontaneous cyclisation of the intermediate hydroxylamine might also occur, resulting to formation of the *N*-hydroxyindolin-2-one **29** (Figure 4.1). To probe these processes, reduction of the two mutual prodrugs was investigated using three standard nitroaromatic reduction conditions: (a) Fe(0) in CH₃COOH:EtOH:H₂O (1:1:1) with sonication,¹⁶⁴ (b) FeCl₃.6H₂O/Zn in DMF:H₂O (1:1)¹⁶⁵ and (c) NaBH₄/Pd-C in MeOH:H₂O (2:1).¹⁶⁶

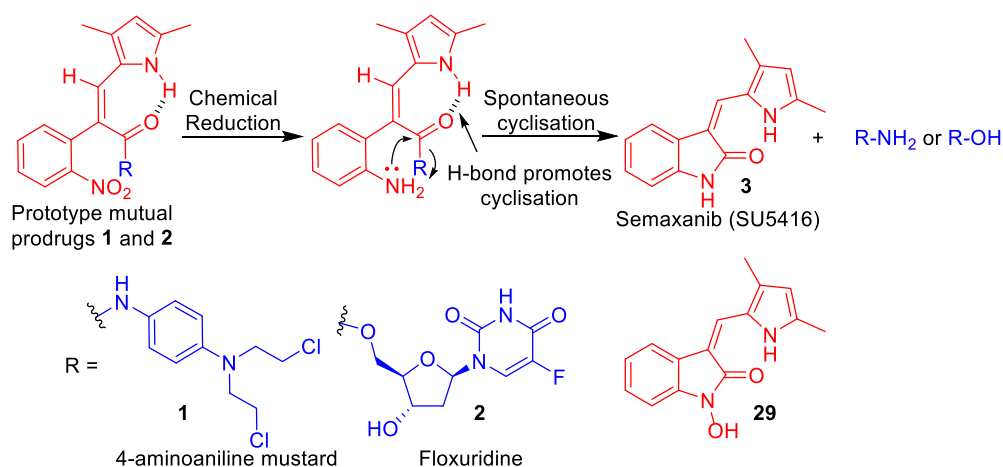
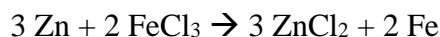


Figure 4.1 Proof-of-concept chemical reduction reactions performed with mutual prodrugs **1** and **2**.

4.1.1 Mechanism of Chemical Nitroaromatic Reductions

The mechanism of aryl nitro group reduction involves a series of electron transfers, proton transfers and dehydration steps to achieve the 6-electron reduction. The exact sequence of these events has been the subject of many detailed electrochemical studies. In the first example with Fe(0), nitro reduction may be initiated by electron transfer to form an anion radical¹⁶⁷ or by protonation to form a cation capable of accepting an electron.¹⁶⁸ The reduction proceeds via in stepwise fashion, first to the nitrosobenzene (which is not

commonly isolatable),¹⁶⁹ followed by reduction to the more stable hydroxylamine and finally the desired amine. The FeCl₃.6H₂O/Zn reaction proceeds in a similar fashion, although the Fe(III) needs to initially be reduced by Zn(0) to Fe(0) and the zinc oxidised to Zn(II) via the reaction:



The Fe(0) species is then capable of reducing the nitrobenzene in an analogous process to the above reaction. The NaBH₄/Pd-C reduction doesn't invoke radical processes, instead reducing the aryl nitro group by addition of hydride ions from a palladium on activated carbon catalyst.

4.1.2 Arylnitro Chemical Reduction Measurements

The chemical reductions were monitored by TLC analysis. The reactions were quenched after complete consumption of the starting material by filtering through celite. Reactions were all conducted on a 30 mg scale and the isolated yields of **3** and **29** were determined after purification by preparative TLC (Table 4.1). Isolation and quantitation of the yields of the 4-aminoaniline mustard and floxuridine cytotoxins was not performed as these are inferred from formation of indoline-2-ones **3** and **29**. In the case of the 4-aminoaniline mustard, isolation was not possible anyway as the compound is highly unstable and rapidly decomposes (personal observation).

Table 4.1 Chemical reduction reactions performed on mutual prodrugs **1** and **2**

Prodrug	Reduction Conditions	Solvent	t (h)	Yield 3 (%)	Yield 29 (%)	Yield 3+29 (%)
1	Fe/CH ₃ COOH	EtOH/H ₂ O	1	80	14	94
	FeCl ₃ .6H ₂ O/Zn	DMF/H ₂ O	3	53	32	85
	NaBH ₄ /Pd-C	MeOH/H ₂ O	0.5	43	37	80
2	Fe/CH ₃ COOH	EtOH/H ₂ O	1	84	11	95
	FeCl ₃ .6H ₂ O/Zn	DMF/H ₂ O	3	40	51	91
	NaBH ₄ /Pd-C	MeOH/H ₂ O	0.5	37	45	82

Semaxanib **3** was isolated from all reactions within 0.5-3 h in yields ranging from 37–84%. *N*-hydroxy semaxanib **29** was also isolated in 11-51% yield. The combined yields of indoline-2-ones **3** and **29** were thus invariably high (80-94%), indicating that

cyclisation after reduction within the scaffold is highly favoured. Downfield-shifting of the pyrrole-NH signals in the ^1H NMR spectrum of **1** (δ 12.04 ppm) and **2** (δ 11.66 ppm) had confirmed the presence of an intramolecular hydrogen bond between the pyrrole-NH and carbonyl oxygen atoms in these prodrugs (Section 1.13).¹³⁸ It seems likely therefore that this H-bond in **1** and **2** is acting as a pseudo-acid catalyst to promote spontaneous indolin-2-one cyclisation after reduction.

The success of these reduction reactions provided chemical proof-of-concept that these compounds could potentially do the same *in vivo*, thus justifying cell-based evaluation of their biological activity as a hypoxia-activated anti-tumour mutual prodrugs (Section 4.2). Formation of *N*-hydroxy semaxanib **29** in the reactions, while not ideal, was not considered a major concern as this compound is also a potent inhibitor of VEGFR-2.¹⁷⁰ Therefore, if the prodrugs were to be used *in vivo*, ejection of **29** directly into a tumour in addition to **3** after hypoxia activation would also be expected to contribute to anti-tumour effects.

4.2 *In Vitro* Biological Evaluation of **1** and **2**

Preliminary biological testing of **1** and **2** was carried out at the University of Auckland by A/Prof. Adam V. Patterson, Dr. Jeffery B. Smaill and Dr. Christopher P. Guise using MDA-MB-468 triple-negative breast cancer cells and SW620 colon cancer cells.¹²⁸ For prodrug **1**, melphalan was selected as the clinically relevant nitrogen mustard control¹⁷¹ and for prodrug **2** the comparator was Floxuridine. Melphalan is commonly used in the treatment of multiple myeloma, ovarian cancer, neuroblastoma, rhabdomyosarcoma and breast cancer. The breast cancer cell line MDA-MB-468 was chosen for use in this study as it has previously been shown to be sensitive to nitrogen mustards.¹⁷²⁻¹⁷³ Floxuridine is used to treat advanced colon, kidney and stomach cancers. Colon cancer cell line SW620 was selected for use as it has been shown to be sensitive to both floxuridine and 5-FU.¹⁷⁴⁻¹⁷⁵ Tirapazamine (Section 1.10.2) and TH-302 (Section 1.12.2) were chosen as hypoxia-activated cytotoxin positive controls for the assay. Tirapazamine has previously been demonstrated to show excellent hypoxia selectivity (100-200 fold) in cell suspension cultures.¹⁰⁷ TH-302 has shown up to 300-fold hypoxia-selective activity in HNE-1 cells.¹²¹ The compounds sent for preliminary biological testing were all determined to be >90% pure by ^1H NMR analysis.

The prodrugs were assessed first for their degree of deactivation relative to their cytotoxin control compounds under aerobic conditions (Table 4.2). The degree of prodrug deactivation was determined using the deactivation ratio (DR = aerobic IC₅₀_{prodrug}/aerobic IC₅₀_{control}). The degree of hypoxia-selective cytotoxic activation was determined as the hypoxic cytotoxicity ratio (HCR), which shows whether the cells are more sensitive to the prodrugs and effectors under anoxic conditions (HCR = aerobic IC₅₀_{prodrug}/anoxic IC₅₀_{prodrug}).

Table 4.2 *In vitro* evaluation of the hypoxia-selective cytotoxicity of drug treatments.

Cell line	Drug	Aero IC ₅₀ (μM)	Anox IC ₅₀ (μM)	DR ^a	HCR ^b
MDA-MB-468	Melphalan	1.00 ± 0.11	0.81 ± 0.16	-	1.2-fold
	Floxuridine	27.42 ± 12.52	45.53 ± 6.10	-	<1-fold
	1	8.31 ± 0.95	7.38 ± 0.88	8.3-fold	1.1-fold
	2	83.88 ± 40.93	247.96 ± 80.56	3.1-fold	<1-fold
	Tirapazamine	105.2	1.304	-	81-fold
	TH-302	4.403	0.0062	-	710-fold
SW620	Melphalan	1.81 ± 0.25	1.22 ± 0.10	-	1.5-fold
	Floxuridine	0.96 ± 0.40	1.48 ± 0.53	-	<1-fold
	1	11.48 ± 6.57	12.67 ± 4.93	6.3-fold	<1-fold
	2	18.70 ± 14.81	13.96 ± 5.39	19.4-fold	1.3-fold
	Tirapazamine	91.03	1.2	-	76-fold
	TH-302	20.6	0.052	-	396-fold

Sensitivity of MDA-MB-468 and SW620 cells to hypoxia-activated mutual prodrugs **1** and **2** and their parent cytotoxins under aerobic (Aero) and anoxic (Anox) conditions. Antiproliferative IC₅₀ values are shown (mean ± std dev, n = 3). The activity of two positive control hypoxia-activated cytotoxins Tirapazamine⁹⁶ and TH-302¹²¹ are included for comparison (n = 1). ^aThe deactivation ratio (DR) indicates the degree of deactivation of the prodrug relative to the effector under aerobic conditions (i.e. DR = Aero prodrug IC₅₀/Aero control cytotoxin IC₅₀). ^bThe hypoxic cytotoxicity ratio (HCR) indicates whether cells are more sensitive to the prodrugs or effectors under anoxic conditions (HCR = aerobic IC₅₀/anoxic IC₅₀).

For prodrug **1**, 8.3-fold and 6.3-fold deactivation was observed in the two cell-lines, while 3.1-fold and 19.4-fold deactivation was seen with **2**. It is proposed that for **1**, the amide bond pulls electron density away from the mustard nitrogen, leading to decreased DNA reactivity (and hence cytotoxicity) in the prodrug. In the case of **2**, Floxuridine is an antimetabolite that would be inactivated by the ester linkage to the bulky 2-(2-nitrophenyl)acetate moiety. The deactivation observed with prodrug **2** relative to floxuridine suggests that the ester bond remained intact under the assay conditions.

The ability of the prodrugs to undergo nitroaromatic bio-reduction and cyclisation to release the respective cytotoxins was determined using the hypoxic cytotoxicity ratio (HCR = Aerobic IC₅₀/Anoxic IC₅₀). Under the assay conditions used here, unfortunately neither prodrug showed evidence for activation under anoxia.

The two positive controls Tirapazamine and TH-302 both showed substantial activation under hypoxic conditions, with Tirapazamine displaying 76-fold and 81-fold activation in the cell lines and TH-302 showing 710-fold and 396-fold activation under anoxic versus aerobic conditions. These positive control results confirmed that the assays were able to detect hypoxic activation, and were in agreement with the reportedly high hypoxic selectivity of Tirapazamine (100-200 fold in cell suspension cultures).¹⁰⁷ Similarly, the results generated for TH-302 matched quite well with previous reports showing 300-fold hypoxic activation in HNE-1 cells.¹²¹

Both parent control drugs melphalan and floxuridine didn't show any increased activation under hypoxia. This was expected as both cytotoxins that act via reaction with/misincorporation into DNA rather than through hypoxia-driven processes. An explanation for why mutual prodrugs **1** and **2** were unable to be activated and show enhanced cytotoxicity under hypoxic conditions was explored next.

4.3 Pulse Radiolysis One-Electron Reduction Potential Measurements

To examine one possible reason for why **1** and **2** did not show enhanced cytotoxicity under anoxia, one-electron reduction potentials ($E[1]$) for the aryl nitro groups in the prodrugs were explored. It is accepted that nitroaromatic prodrugs show greatest hypoxia-selective activation when $E[1]$ falls within the range -330 to -450 mV.¹⁷⁶ Nitroaromatics that fall below this range typically are unable to be effectively reduced by cellular reductases. Tirapazamine, which performed well in the above assay, contains an aromatic

di-*N*-oxide with a one-electron reduction potential at the bottom of this desired range ($E[1] = -450$).¹⁷⁷ The positive control compound TH-302, which contains a nitroimidazole, also displays a one electron reduction potential within the desired range ($E[1] = -407$ mV).¹⁷⁸

Pulse radiolysis was the technique used to measure the 1-electron reduction potential of the **1** and **2**. This technique characterises the electron affinity of nitroaromatic compounds and, by inference, their willingness to accept an electron from human oxidoreductases. Fast reaction chemistry experiments were performed on the University of Auckland's 4 MeV DYNARAY linear accelerator using a PC-controlled, custom-built optical absorption detection system. These experiments were performed by A/Prof. Robert F. Anderson. Background on the experiments is provided below.

Pulse radiolysis is a fast-kinetic method of initiating and studying reactions occurring on a timescale faster than approximately one hundred microseconds. The technique involves exposing a sample of material to a beam of accelerated electrons (2-10 MeV) generated by a linear accelerator (Figure 4.2). The pulse duration is usually 2-200 ns long and directed towards a sample contained in a quartz or glass cell. The resulting chemical reactions are monitored using UV-visible absorption spectroscopy. A UV-visible source of light is directed into the sample perpendicular to the electron beam. After passing through the sample, the light is diffracted by a monochromator, the signal is enhanced by a photomultiplier and then recorded by an oscilloscope/computer.

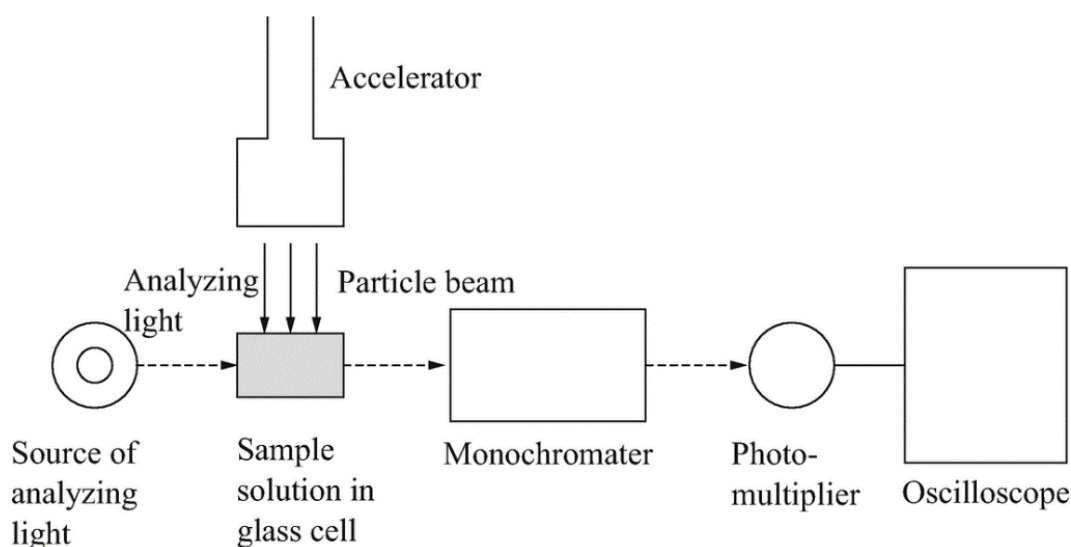


Figure 4.2 Schematic of pulse radiolysis experiments.¹⁷⁹

The data contained within the absorption spectra allows identification of free radicals and the kinetics of their formation and decay. This process has been used routinely to study nitroaromatic compounds and their one-electron nitro radical anion reduction products.¹⁸⁰⁻¹⁸¹

4.3.1 Reduction Potential Measurements with **2**

A stock solution of prodrug **2** was prepared in 0.42 M *tert*-butanol, 5 mM phosphate buffer (pH 7). A UV-visible spectrum was recorded to obtain the extinction coefficient, which was used to determine the concentration of the compound in test solutions. One-electron reduction of the compound (**2**, 50 μ M) by the e^-_{aq} was carried out by pulse radiolysis (3 Gy in 200 ns) of deaerated phosphate buffered solutions (2.5 mM, pH 7) containing *tert*-butanol (0.1 M to scavenge the \cdot OH and \cdot H radicals). Bleaching of the ground state at 400 nm (-5.55 mAbs Gy $^{-1}$) and absorbance increases at 350 nm ($+2.71$ Gy $^{-1}$) gave relatively stable transients over 10 ms (Figure 4.3).

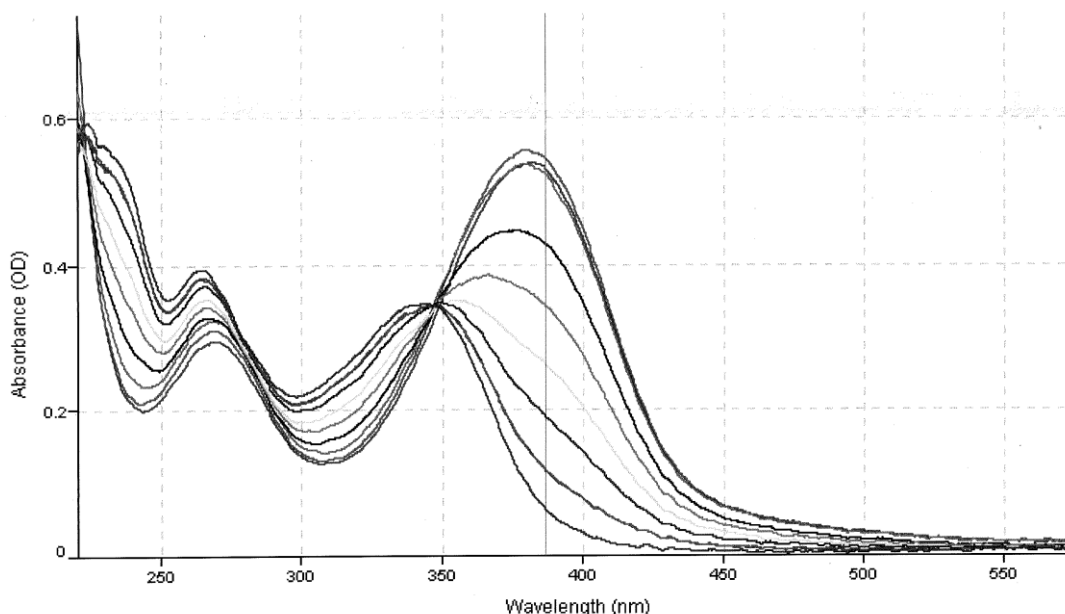
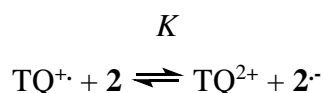


Figure 4.3 Changes in UV-vis absorption with sequential doses of γ -irradiation of **2** in an evacuated solution containing formate ions (25 mM) at pH 7 (after initial removal of a small contaminant concentration of O₂).

Redox equilibrium was established against triquat (TQ²⁺, Figure 4.4) ($E(1) = -548 \pm 7$ mV) for three mixtures of **2** / TQ²⁺: 100-400 μ M / 50 μ M and controls (at 385 nm).



$$K_{\text{av.}} = 4.69 \pm 0.69 \quad \Delta E = -(RT/F)(\ln K) = 40 \pm 4 \text{ mV} \quad E_{\text{cor}} = -11 \text{ mV (ionic strength)}$$

$$\underline{E(2/2\cdot) = -509 \pm 8 \text{ mV}}$$

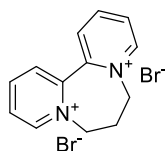
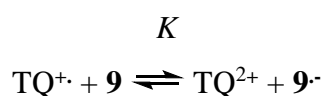


Figure 4.4 Chemical structure of viologen triquat (TQ^{2+}) used to establish redox equilibrium.

4.3.2 Reduction Potential Measurements with **9**

Reduction potential measurements for **1** were hampered by poor aqueous solubility so the measurements were instead obtained with its *bis*-alcohol precursor **9** as a proxy. It was rationalised that the remoteness of the alcohols from the aryl nitro group should limit their influence on the reduction potential, whilst increasing aqueous solubility. A stock solution of **9** was prepared in 0.42 M *tert*-butanol, 5 mM phosphate buffer (pH 7). A UV-vis spectrum was recorded to obtain the extinction coefficient, which was used to determine the concentration of the compound in test solutions. One-electron reduction of **9** (85 μM) was carried out by pulse radiolysis (3 Gy in 200 ns) of deaerated phosphate buffered (2.5 mM, pH 7) solutions containing *tert*-butanol. Initial fast bleaching of the ground state absorbance at 400 nm was followed by further bleaching at 400 nm and absorbance increases at 350 nm over 35 μs (Figure 4.5). The rate of the secondary change in absorbance was dependent on the concentration of **9**, implying that the e_{aq}^- adds to two sections of **9** (nitro group and elsewhere) followed by intermolecular electron transfer to fully form the nitro radical anion.

Redox equilibrium was established against triquat (TQ^{2+}) ($E(1) = -548 \pm 7 \text{ mV}$) for 3 mixtures of **9** / TQ^{2+} : 50-75 μM / 75-200 μM and controls (at 385 nm).



$$K_{\text{av.}} = 1.26 \pm 0.21 \quad \Delta E = -(RT/F)(\ln K) = 6 \pm 1 \text{ mV} \quad E_{\text{cor}} = -8 \text{ mV (ionic strength)}$$

$$\underline{E(\mathbf{9}/\mathbf{9}\cdot) = -550 \pm 8 \text{ mV}}$$

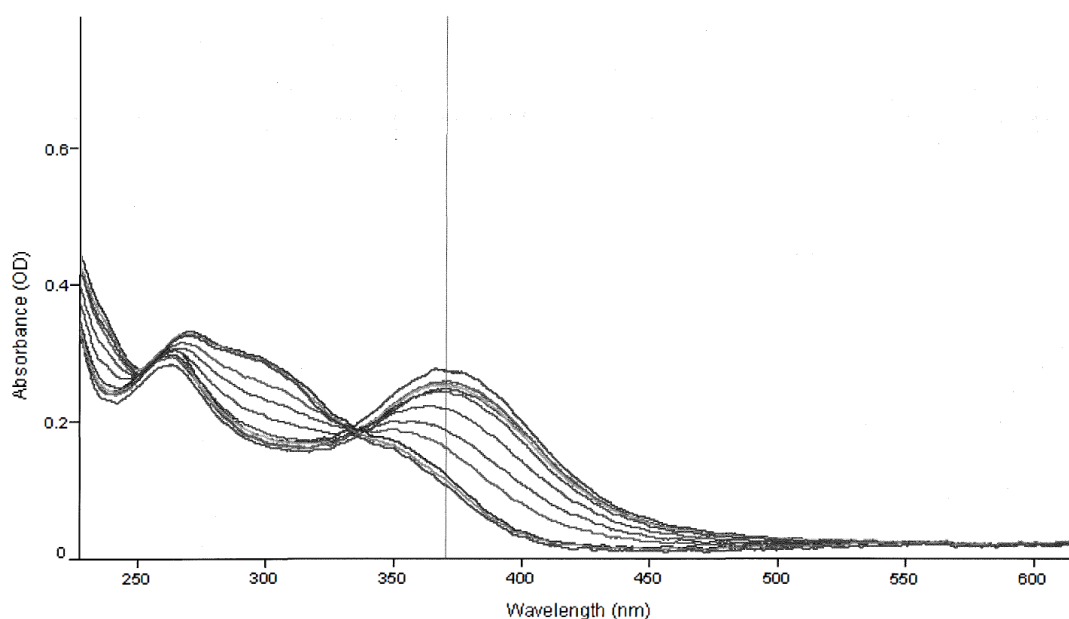


Figure 4.5 Changes in UV-visible absorption with sequential doses of γ -irradiation of **9** in an evacuated solution containing formate ions (25 mM) at pH 7.

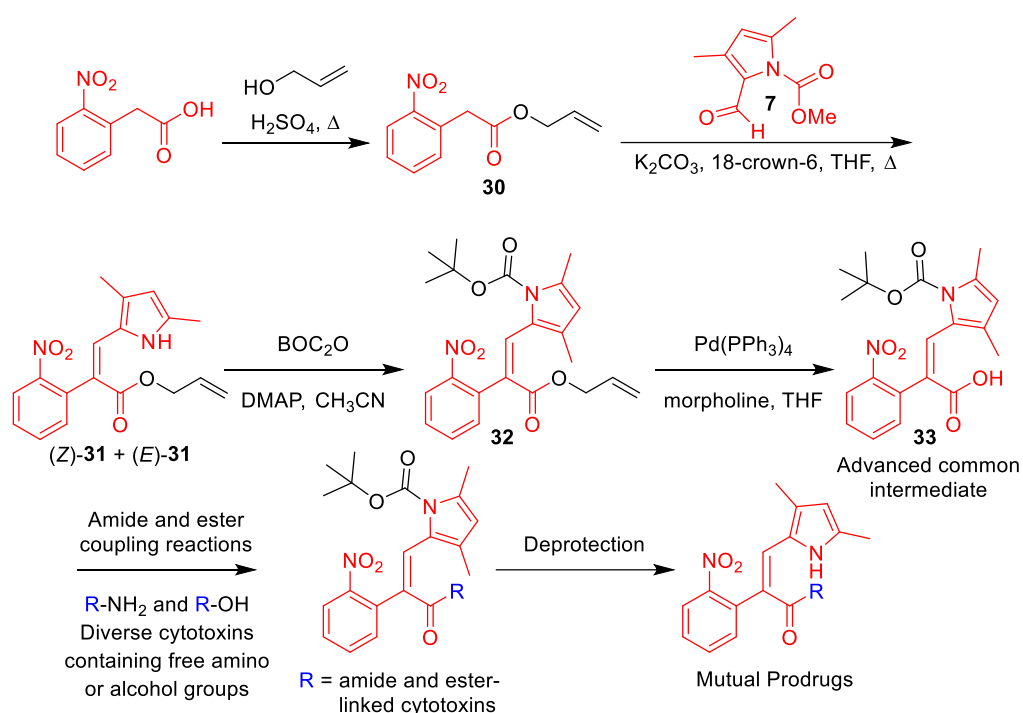
4.3.3 Conclusions

Based on the above measurements, it was concluded that the lack of bioreductive activation observed with the prodrugs under anoxia in the cellular assays was due to their low nitroaromatic one-electron reduction potentials. As described above, it is accepted that nitroaromatic prodrugs show greatest hypoxia-selectivity when $E[1]$ falls within the range -330 to -450 mV.¹⁷⁶ With $E[1]$ for **9** (-550 ± 8 mV, representative of **1**) and **2** (-509 ± 8 mV) falling well below this, the prodrugs are unable to accept electrons from one-electron reductases at appreciable rates and are therefore incapable of undergoing bioreduction in cells under anoxia. An approach for increasing the prodrug reduction potentials was the focus of Chapter 6.

Chapter 5: Development of a New Divergent Route Towards Mutual Prodrugs

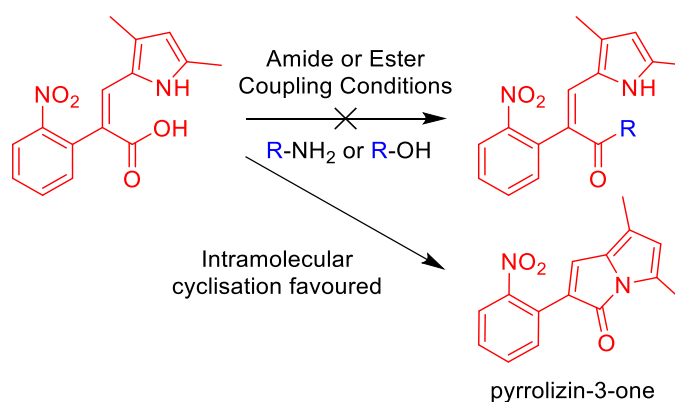
5.1 Synthetic Strategy

While waiting for mutual prodrugs **1** and **2** to undergo biological and reduction potential testing at the University of Auckland, an alternative and more divergent synthesis was scoped that could potentially deliver many mutual prodrugs bearing a diverse range of different cytotoxins. The syntheses of **1** and **2** (Chapters 2 and 3), whilst successful, were long, multi-step linear sequences that suffered from low yields in the key Knoevenagel step i.e. 21% and 10%, respectively, for the *cis* alkene intermediates (*Z*)-**8** and (*Z*)-**23**. In the new divergent strategy, the Knoevenagel reaction would be completed earlier in the synthesis on a simpler, less functionalised ester substrate (Scheme 5.1). The *cis*-alkene product (expected to be obtained in higher yield) could then be pyrrole *N*-protected (**32**) and converted to carboxylic acid **33** by de-esterification. This advanced common intermediate **33** could then be directly coupled to diverse cytotoxins containing free amino or alcohol groups, delivering a variety of amide and ester-linked mutual prodrugs (after *N*-BOC deprotection of the pyrrole).



Scheme 5.1 Proposed divergent strategy that could allow rapid access to a diverse range of amide and ester-linked mutual prodrugs.

The allyl ester **30** was selected for the Knoevenagel reaction with **7** because earlier work by other PhD students in the Kelso Lab (Nicholas Kirk and Pichit Sudta) had shown that this substrate produces the highest yields of alkene products ((*Z*)-**31** 41% and (*E*)-**31** 33%, respectively) under the optimised reaction conditions. Kirk and Sudta also demonstrated that allyl ester (*Z*)-**31** could be deprotected using tetrakis(triphenylphosphine) palladium(0) and morpholine to give the free carboxylic acid in good yield (84%). However, when their acid lacking a pyrrole *N*-protecting group was subjected to standard amide and ester coupling conditions an alternative reaction took place, where the pyrrole nitrogen cyclised onto the activated carboxylic acid to form a pyrrolizin-3-one (Scheme 5.2). Whilst frustrating for this work, this accidental discovery spurred off-shoot investigations that led to publications describing new angiogenesis inhibitors and antimalarials.^{145, 182} Nevertheless, for the new divergent route to be viable, this observation meant that the pyrrole nitrogen must be protected prior to deallylation and subsequent amide/ester coupling to cytotoxins. It was expected that the BOC protecting group would be a suitable pyrrole *N*-protecting group.

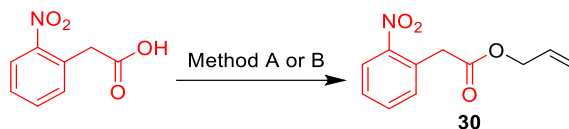


Scheme 5.2 Intramolecular cyclisation to a pyrrolizin-3-one occurs upon activation of the carboxylic acid when attempting amide or ester coupling reactions with the pyrrole nitrogen unprotected.

5.2 Esterification of 2-(2-nitrophenyl)acetic acid with Allyl Alcohol

Esterification of 2-(2-nitrophenyl)acetic acid with allyl alcohol had previously been explored in the Kelso Lab using two different approaches (Scheme 5.3). Basic conditions with allyl bromide and potassium carbonate in acetone provided a 74% yield of the desired allyl ester **30**. Acidic conditions using allyl alcohol as the solvent at reflux with catalytic sulphuric acid gave a slightly higher yield (88%). For the new divergent

synthesis, the higher yielding acid-catalysed esterification method was explored and scaled up from the previous 3 g scale to 10 g.

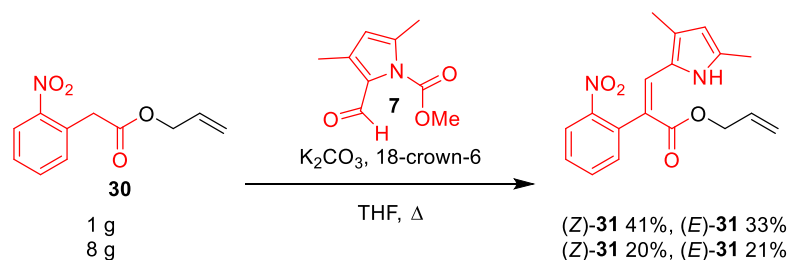


Scheme 5.3 Established methods from the Kelso Lab for the synthesis of allyl ester **30**. Method A) K₂CO₃, allyl bromide, acetone, rt, 74%. Method B) allyl alcohol, cat. H₂SO₄, reflux, 88%.

I performed the esterification reaction twice on a 10-gram scale. On the first attempt, a disappointing 64% yield was obtained. On the second attempt, the workup procedure was modified to include a sodium hydroxide washing step (instead of saturated sodium bicarbonate) to more effectively remove unreacted starting acid and simplify purification. These changes increased the isolated yield to 83% and provided a total of 18 g of pure ester **30** from the two reactions.

5.3 Knoevenagel Reaction of **30** with **7**

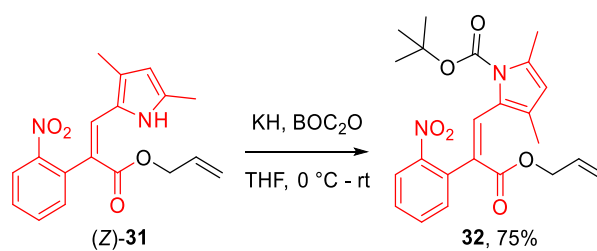
The Knoevenagel reaction of allyl ester **30** with pyrrole-2-carbaldehyde **7** had previously been explored in the Kelso Lab by PhD candidate Pichit Sudta on a 1 g scale. Sudta's reaction produced (*Z*)-**31** and (*E*)-**31** in 41% and 33% yields, respectively (Scheme 5.4).¹³⁸ To access larger quantities of the desired acid **33**, this key reaction needed to be scaled up. When I attempted the reaction with 8 g of **30** it appeared to proceed well by TLC analysis, however, purification at this larger scale proved to be challenging. Crude (*Z*)-**31** and (*E*)-**31** fractions had to first be fractionated using silica gel column chromatography with ethyl acetate/petroleum spirit as the eluent and then subjected to further purification using column chromatography with acetone/petroleum spirit as eluent. This tedious process yielded only 20% of the *cis*-alkene (*Z*)-**31** and 21% of the *trans*-alkene (*E*)-**31**. While these yields were lower than had been observed at smaller scale, sufficient quantities of (*Z*)-**31** (2.25 g) were nonetheless obtained from this single reaction to advance the synthesis, so further optimisation was not explored.



Scheme 5.4 Knoevenagel reactions of **30** with **7** afforded (*Z*)-**31** 41% and (*E*)-**31** 33% when performed on a 1 g scale (Kelso Lab PhD student Pichit Sudta). When I performed the reaction (once) under the same conditions at 8 g scale, lower yields ((*Z*)-**31** 20%, (*E*)-**31** 21%) were obtained.

5.4 *N*-BOC Protection of (*Z*)-**31**

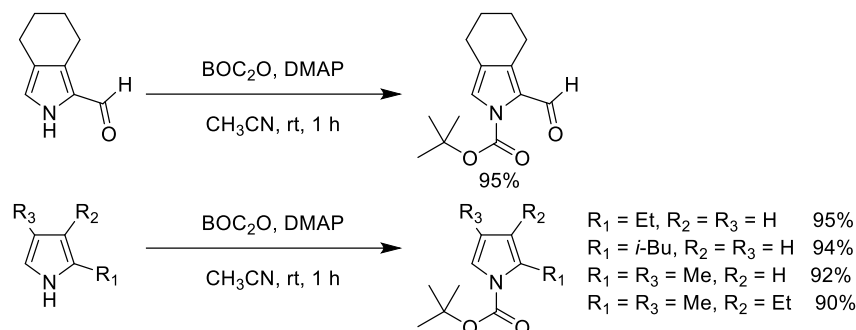
As discussed above, when the carboxylic acid (*Z*)-**31** bearing an unprotected pyrrole nitrogen was subjected to coupling conditions, an intramolecular cyclisation to the pyrrolizin-2-one occurred instead of forming the desired amide or ester. The BOC protecting group was chosen to address this issue due to its ease of protection/deprotection and stability under typical coupling reaction conditions. Pyrrole *N*-BOC protection had been scoped by Pichit Sudta using potassium hydride (to deprotonate the pyrrole nitrogen) and BOC anhydride (BOC₂O) in THF, which gave **32** in 75% yield (Scheme 5.5). Although the yield for the reaction was high, its use of pyrophoric KH carried significant risks, especially if performed on a larger scale, so I consulted the literature for possible alternatives.



Scheme 5.5 *N*-BOC protection of (*Z*)-**31** using potassium hydride affords **32** in 75% yield when performed on a small scale (Pichit Sudta).

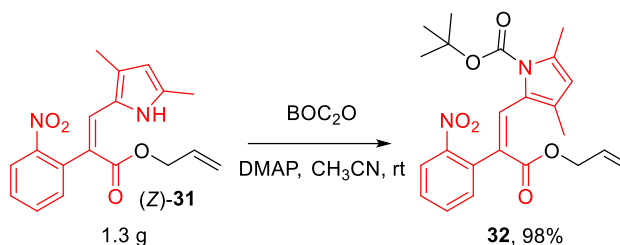
A suitable precedent was identified for a series of related pyrroles that used BOC₂O in the presence of DMAP in acetonitrile to carbamoylate pyrrole nitrogens (Scheme 5.6).¹⁸³ With yields above 90% obtained in the absence of any strong base for these closely related

analogues, including pyrroles bearing aldehyde groups at the 2-position, this reaction looked to provide an excellent alternative.



Scheme 5.6 Literature precedent for the *N*-BOC protection of diverse pyrroles using BOC_2O and DMAP in the absence of strong base.¹⁸³

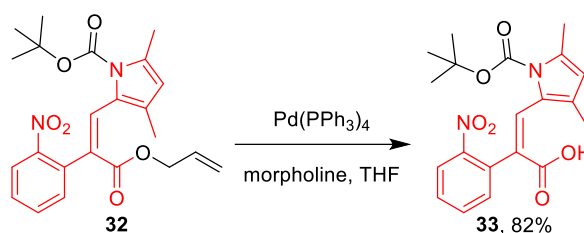
The first reaction attempted on a pilot 200 mg-scale resulted in a high yield of **32** (78%) after 3 hours of stirring at room temperature. It was noted, however, that some yield was lost during isolation due to not completely removing all of the acetonitrile before attempting a dichloromethane/water extraction, and that the presence of DMAP complicated purification by column chromatography because it smeared throughout the column. The reaction was next scaled up to 1.3 g. In this second attempt, acetonitrile was completely removed by evaporation prior to extraction and a 1 M HCl washing step was added to the workup to more effectively remove DMAP before column chromatography. These changes raised the isolated yield of **32** to 98%, affording ample quantities of **32** (~1.7 g) to continue with the synthesis (Scheme 5.7).



Scheme 5.7 Optimised *N*-BOC protection of **(Z)-31** using BOC_2O and DMAP in acetonitrile.

5.5 Deallylation of **32** to Acid **33**

Pichit Sudta had previously explored deallylation of BOC-protected **32** using 10 mole percent (relative to **32**) tetrakis(triphenylphosphine)palladium(0) and morpholine in THF at room temperature on a 200 mg-scale, achieving a yield of 79%. In my first attempt at this reaction performed on 100 mg, a yield of 74% was obtained. When I scaled the reaction up to 1.2 g the yield was improved to 82% (Scheme 5.8).



Scheme 5.8 Deallylation of **32** with Pd(PPh₃)₄ and morpholine provided acid **33**.

5.5.1 Mechanism of Palladium-Catalysed Deallylation of **32**

The allyl group has long been used as an effective protecting group for carboxylic acids and alcohols due to its ease of installation, stability and facile removal under mild conditions using a palladium(0) catalyst (Tsuji–Trost reaction).¹⁸⁴ The catalytic mechanism involves a palladium redox cycle, where Pd(0) is first oxidised and later returned to Pd(0) after reduction (Figure 5.1). The reaction is initiated by formation of π -interactions between the alkene π -electrons and the palladium atom, leading to oxidative addition of the palladium to the allyl group. Ensuing loss of carboxylate as a leaving group results in formation of a π -allyl cation. A nucleophile (in this case morpholine) then regenerates the palladium(0) species by trapping the allyl cation and forming 4-allylmorpholine. As the process is catalytic in palladium, 10 mole percent is sufficient to effect transformation of **32** to **33**, with an excess of morpholine used to drive product formation.

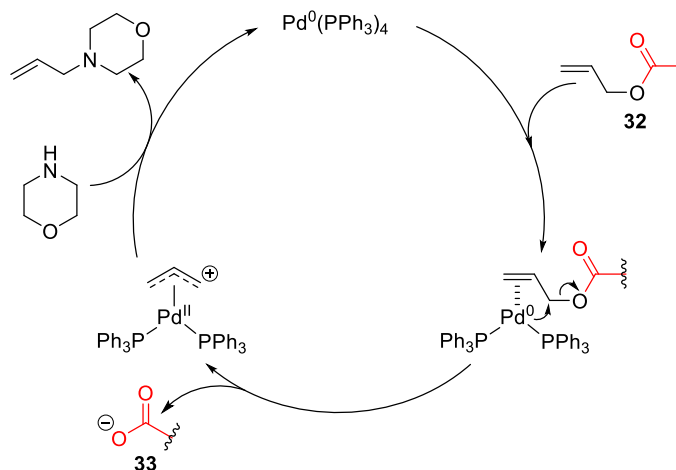


Figure 5.1 Mechanism of deallylation of **32** using a palladium(0) catalyst and morpholine.

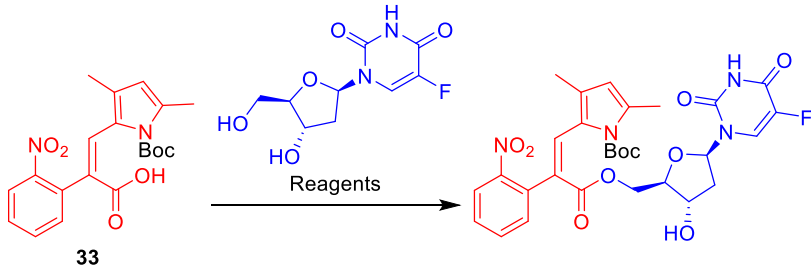
5.6 Esterification of **33** with Floxuridine

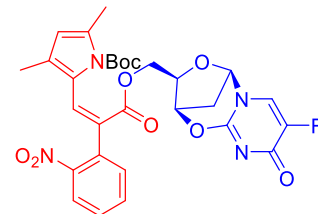
With approximately 750 mg of *N*-BOC-carboxylic acid **33** in hand, a series of esterification reactions were attempted using unprotected floxuridine. It was expected that the more reactive primary alcohol of floxuridine would esterify in preference to its hindered secondary alcohol (Table 5.1). The first attempt trialed the same conditions (DCC, DMAP in dichloromethane) that were used to prepare ester **22** from **21** during the synthesis of **2** (Section 3.5). However, this led only to a mix of the symmetrical anhydride of **33** and another common side product observed with DCC ester couplings,¹⁸⁵ the *N*-acyl urea of **33**. The related carbodiimide coupling reagent *N,N'*-diisopropylcarbodiimide (DIC) gave similar results, producing a mix of the *N*-acyl urea and anhydride of **33**. It was speculated that the electrophilic character of the activated 2-(2-nitrophenyl)acetic moiety had been substantially reduced upon introduction of the conjugated alkene, while the large pyrrole *N*-BOC protecting group also added considerable steric hindrance around the carboxylic acid that could hamper approach of the incoming alcohol nucleophile.

Other coupling reagents were trialed next, including EDCI with hydroxybenzotriazole (HOBt), HBTU, hexafluorophosphate azabenzotriazole tetramethyl uronium (HATU) and (benzotriazol-1-yloxytris(dimethylamino)phosphonium hexafluorophosphate) (BOP), but in all cases only the unreacted HOBt/HOAt activated esters were isolated. The next attempt involved converting the carboxylic acid **33** to the highly reactive acid fluoride using tetramethylfluoroformamidinium hexafluorophosphate (TFFH). In

addition to the high electrophilicity of acid fluorides, it was rationalised that the very small fluorine atom would reduce steric bulk around the activated carbonyl group, allowing easier access by the sterically bulky floxuridine nucleophile. Although the acid fluoride appeared to form after reacting **33** with TFFH (by TLC analysis), addition of floxuridine produced multiple products that could not be isolated and identified.

Table 5.1 Attempted esterification reactions with **33** and floxuridine.



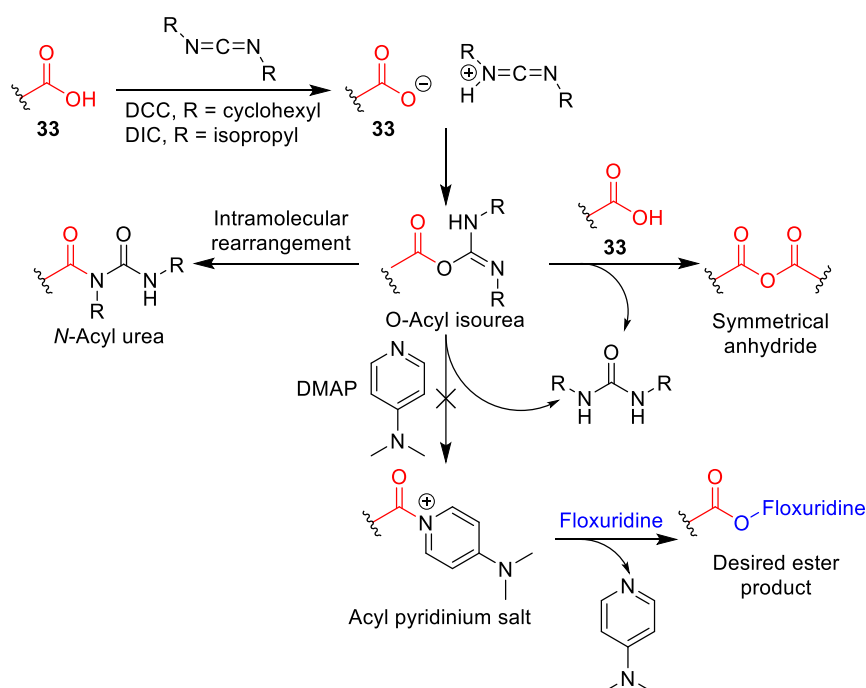
Floxuridine (eq.)	Reagents (eq.)	Additives/Base (eq.)	Solvent	Product Yields ^a
1.2	1.2 DCC	0.1 DMAP	CH ₂ Cl ₂	21% <i>N</i> -Acyl Urea 36% Anhydride
1.2	1.2 DIC	0.1 DMAP	CH ₂ Cl ₂	<i>N</i> -Acyl Urea and Anhydride mixture
2.0	1.1 EDCI	1.1 HOBt, 4.0 DMAP	CHCl ₃	HOBt Ester
2.0	1.5 HBTU	4.0 DMAP	DMF	HOBt Ester
2.0	1.5 HATU	4.0 DMAP	DMF	HOAt Ester
1.1	1.0 BOP	1.5 DIPEA	CH ₂ Cl ₂	HOBt Ester
1.1	1.0 TFFH	0.1 DMAP, 5.0 Et ₃ N	CH ₂ Cl ₂	Decomposition trace product,
1.2	1.2 DEAD, 1.2 PPh ₃	-	THF	 11%

^aProducts with no listed yields were identified by MS and ¹H NMR spectroscopy only. They were not isolated and characterised.

Speculating that the pyrrole nitrogen might be donating electron density via conjugation into the activated carboxylic acid group and thus reducing its electrophilic reactivity, a Mitsunobu-type esterification was investigated next using the reagent diethyl azodicarboxylate (DEAD). Esterification using the Mitsunobu reaction inverts the reactivity, whereby the alcohol is transformed into an electrophile and the carboxylate acts as the nucleophile. When the reaction was attempted, some trace of the desired product appeared to form (MS analysis), however, a competing intramolecular side reaction appeared to predominate. The cyclised 2,3'-anhydrofloxuridine product (Table 5.1) arises from reaction of the secondary alcohol of floxuridine, which upon being activated by DEAD after successful esterification of the primary alcohol was displaced by one of the 5-fluorouridine carbonyl groups via intramolecular cyclisation.

5.6.1 Mechanism of *N*-Acyl Urea and Anhydride Formation

Coupling reactions with carbodiimides like DIC and DCC can lead to isolation of *N*-acyl ureas and/or anhydrides when the activated carboxylic acid is not sufficiently electrophilic or the reacting alcohol has low nucleophilicity.¹⁸⁶ The mechanism of their formation starts as intended, with the carboxylate reacting with the carbodiimide to form an *O*-acyl isourea (Scheme 5.9).

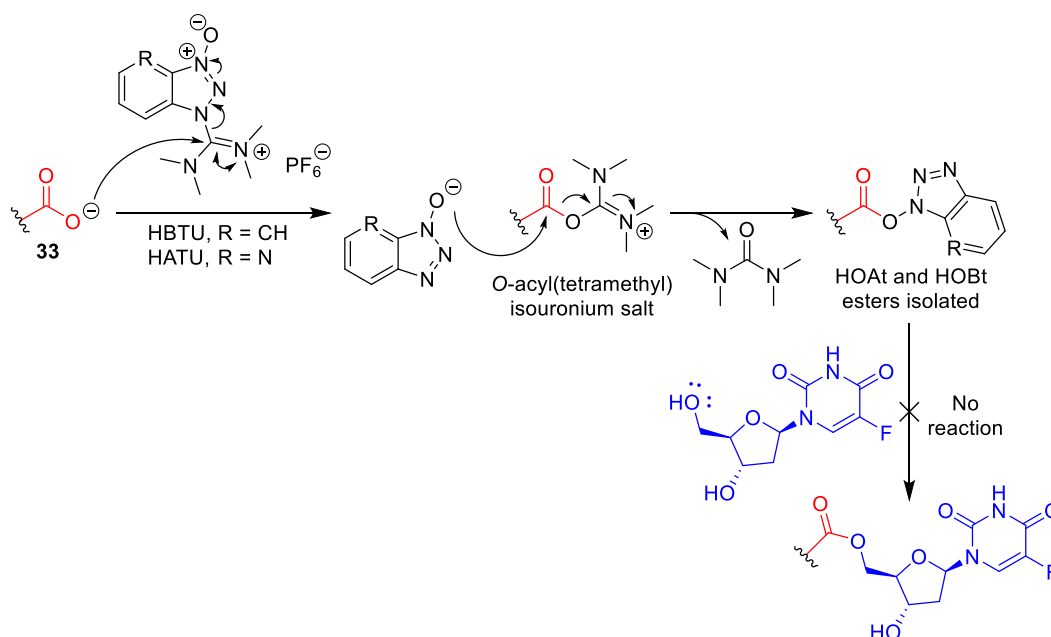


Scheme 5.9 Mechanism of *N*-acyl urea and symmetrical anhydride formation during carbodiimide-mediated ester coupling reactions with **33**.

This intermediate can then be displaced by catalytic DMAP to form a highly reactive acyl pyridinium salt, which then reacts with the alcohol to give the desired ester. If, however, the final reaction with the alcohol is slow, one of two side reactions can occur. The first occurs after intramolecular rearrangement of the *O*-acyl isourea to the more stable, unreactive *N*-acyl urea. If the carboxylate is nucleophilic enough, the second side reaction occurs, where a second molecule of the acid reacts with the *O*-acyl isourea (or acyl pyridinium salt) to form the symmetrical anhydride.

5.6.2 Mechanism of HOBt/HOAt Ester Formation

The coupling reagents HBTU and HATU are commonly used in peptide synthesis to form amides due to their mild activating properties, resistance to racemisation and high yields.¹⁸⁷ They can also be used in esterification reactions via their activation of carboxylic acids to HOBt or HOAt esters. To form these activated esters, the carboxylate anion attacks the HATU or HBTU to form an unstable *O*-acyl(tetramethyl)isouronium salt (Scheme 5.10). This salt is then displaced by the newly formed HOBt or HOAt anion, affording the activated ester and tetramethylurea. Typically, this ester would then be displaced by the alcohol nucleophile, in our case floxuridine. This displacement did not occur, however, and the unreacted HOAt and HOBt ester intermediates were isolated instead of the desired ester.

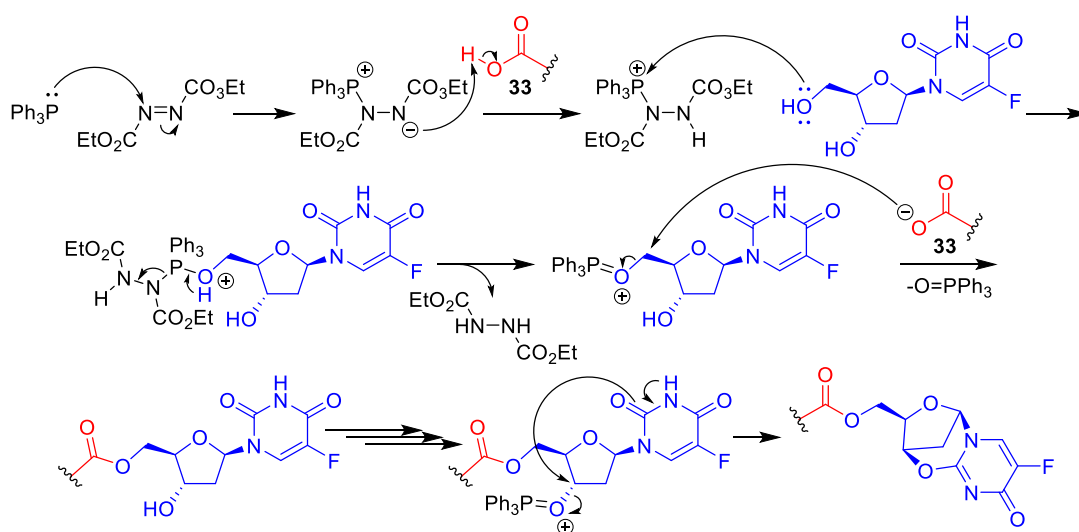


Scheme 5.10 Explanation for why HOAt/HOBt esters of **33** were isolated from attempted HATU/HBTU-mediated ester couplings with floxuridine.

5.6.3 Mechanism for the Formation of 2,3'-Anhydrofloxuridine Derivative

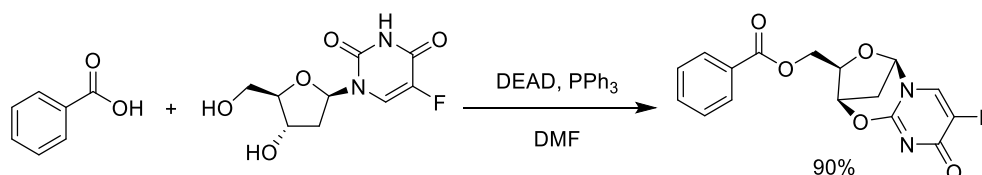
The attempted coupling reactions suggested that the activated derivatives of carboxylic acid **33** are electrophilic but the floxuridine primary alcohol is a relatively poor partner nucleophile. Steric hindrance around the activated carboxylic acid due to the spatially close and bulky BOC-group, along with the large activating groups, were probably contributing to low reactivity with the bulky floxuridine. The Mitsunobu reaction was therefore trialled as a way of inverting reactivity, where the alcohol is activated to become an electrophile and the carboxylate acts as the nucleophile.¹⁸⁸

The mechanism of the Mitsunobu reaction commences with nucleophilic addition of triphenylphosphine to DEAD, producing a basic betaine that deprotonates carboxylic acid **33** (Scheme 5.11). The primary alcohol of floxuridine then attacks the triphenylphosphonium phosphorous atom, leading to formation of an oxyphosphonium cation following loss of diethyl hydrazine-1,2-dicarboxylate. The carboxylate anion then reacts with the electrophilic oxyphosphonium cation, generating the desired product after loss of triphenylphosphine oxide. Due to the presence of the unprotected secondary alcohol, rather than stopping at the desired product a second Mitsunobu reaction ensues. Here, the secondary alcohol is similarly activated to an oxyphosphonium cation that undergoes an intramolecular cyclisation reaction with the adjacent carbonyl oxygen of the fluorouridine, leading to formation of the bridged-bicyclic side product.



Scheme 5.11 Mechanism of the Mitsunobu reaction of **33** with floxuridine and subsequent intramolecular cyclisation leading to a bridge-bicyclic side product.

In hindsight, this side-reaction should have been expected as related substrates in the literature were found to undergo the same intramolecular cyclisation when subjected to Mitsunobu conditions. For example, when benzoic acid and unprotected floxuridine were subjected to the Mitsunobu reaction, the bridged-bicyclic 2,3'-anhydrofloxuridine benzoyl ester was formed in 90% yield (Scheme 5.12).¹⁸⁹

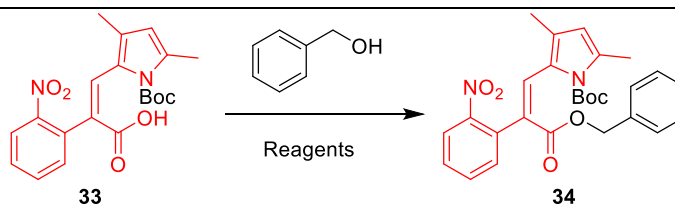


Scheme 5.12 Literature example of a Mitsunobu reaction that resulted in formation of a bridged-bicyclic floxuridine derivative.¹⁸⁹

5.7 Trial Esterification Reactions with **33** and Benzyl Alcohol

To better understand the reactivity of carboxylic acid **33**, floxuridine was replaced with the simpler benzyl alcohol in further esterification trial reactions (Table 5.2). Interestingly, benzyl alcohol showed similar results to floxuridine, whereby using BOP as the coupling reagent yielded only the HOBt ester, whereas the Mitsunobu reaction gave the desired benzyl ester **34** in quantitative yield. These findings lent evidence to the above suggestion that electrophilic activated derivatives of **33** show low reactivity, probably because of steric hinderance from the neighbouring pyrrole *N*-BOC group. On the other hand, the oxyphosphonium cation generated from the alcohol in the Mitsunobu reaction could easily undergo reaction with the carboxylate anion of **33**.

Table 5.2 Trial esterification reactions with **33** and benzyl alcohol.



Benzyl Alcohol (eq.)	Reagents (eq.)	Solvent	Yield ^a
1.1	1.0 BOP, 1.5 DIPEA	CH ₂ Cl ₂	Quantitative HOBt Ester
2.0	2.0 DEAD, 2.0 PPh ₃	THF	Quantitative 34

^aThe HOBt ester was not stable and only identified by MS and ¹H NMR spectroscopy. The desired **34** was isolated by preparative TLC and fully characterised.

5.8 Trial Amide Couplings with **33** and Benzylamine

With a promising Mitsunobu procedure now established to form esters of **33**, attention was turned to trialling amide couplings of **33** with the simple model amine benzylamine (Table 5.3). Activation of **33** to the acid fluoride with TFFH once again led to a degradation of the starting material and no observable product formation. Reaction with the coupling reagent BOP provided trace amounts of the desired amide but the major isolable product was the HOBt ester of **33**. Encouragingly, reaction of **33** with 4 equivalents of benzylamine and HBTU gave a high yield of the benzyl amide **35** (>80%). Use of the more reactive HATU gave a quantitative yield of **35** on a small scale (26 mg of **33**).

Table 5.3 Trial amide coupling reactions with **33** and benzylamine.

Benzylamine (eq.)	Coupling Reagent (eq.)	Additive/Base (eq.)	Solvent	Yield ^a
1.1	1.0 TFFH	5.0 Et ₃ N, 0.1 DMAP	CH ₂ Cl ₂	Starting Material Degraded
1.1	1.0 BOP	1.5 DIPEA	CH ₂ Cl ₂	Trace Product, Mainly HOBt Ester
4.0	1.5 HBTU	2.5 DIPEA	THF	>80% yield 35
4.0	1.5 HATU	2.5 DIPEA	THF	Quantitative 35

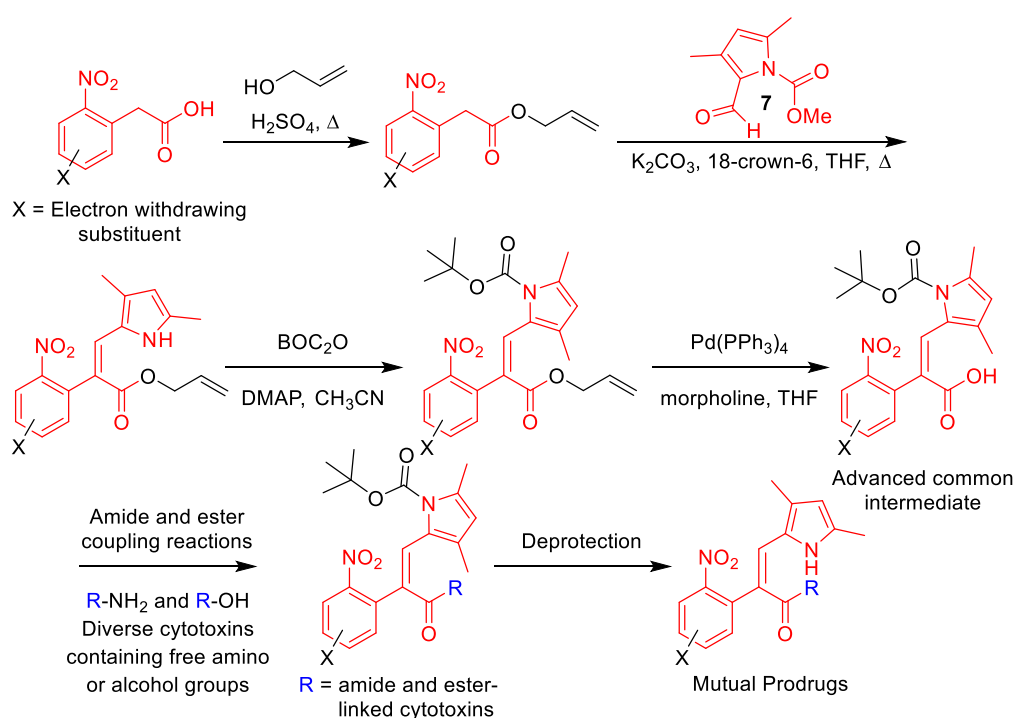
^aThe HOBt ester was not stable and only identified by MS and ¹H NMR spectroscopy. The desired **35** was isolated by preparative TLC and fully characterised.

5.9 Conclusions and Future Directions

At this point in the project, results were received back from the University of Auckland showing that the reduction potentials of **1** and **2** were too low to support hypoxia-selective activation of the prodrugs (Chapter 4.3). To address this issue, new derivatives were designed that contained additional electron withdrawing groups on the nitroaryl triggering moiety in an attempt to raise the reduction potentials. Further work on the divergent

synthesis described above was thus put on hold and the focus switched to using the original synthesis to create the target analogues (Chapter 6).

Although it potentially allows diverse cytotoxins to be appended in a single step to the prodrug scaffold, the new divergent synthesis offers no advantages in terms of accessing analogues carrying substituents in the nitroaryl ring, as these groups need to be pre-installed prior to the Knoevenagel reaction. Nevertheless, the insights gained in this chapter could be applied if/when the optimal electron withdrawing substituents are identified. For instance, the Knoevenagel reaction could be implemented with the allyl ester of the substituted 2-(2-nitrophenyl)acetate that is eventually identified (Scheme 5.13), and then the rest of the divergent route could be deployed to access mutual prodrugs containing multiple different cytotoxins, linked via esters or amides using the Mitsunobu and HATU chemistry developed here.



Scheme 5.13 Proposed future strategy allowing practical access to diverse amide and ester-linked mutual prodrugs containing addition electron withdrawing substituents on the nitroaryl ring to increase the reduction potential.

Chapter 6: Optimisation of Prodrug Nitroaromatic Reduction Potentials

6.1 Overview and Synthetic Strategy

To address the issue of poor bioreductive activation that was observed with mutual prodrugs **1** and **2** under anoxia (Section 4.2), which was attributed to their low nitroaromatic one-electron reduction potentials (Section 4.3.3), a new series of model compounds were designed to explore ways of increasing the reduction potentials towards the target minimum of -450 mV.

The effects of electron withdrawing substituents on the nitroaromatic one-electron reduction potential has been extensively studied. As part of the development of new trinitrobenzene-based explosives, a series of simple substituted mono- and dinitrobenzene analogues were synthesised and their one-electron reduction potentials measured (Figure 6.1).¹⁹⁰ In this example, it was observed that appending strong electron withdrawing substituents, such as additional nitro groups, onto the nitrobenzene substantially increases one-electron reduction potentials (~ 200 mV).

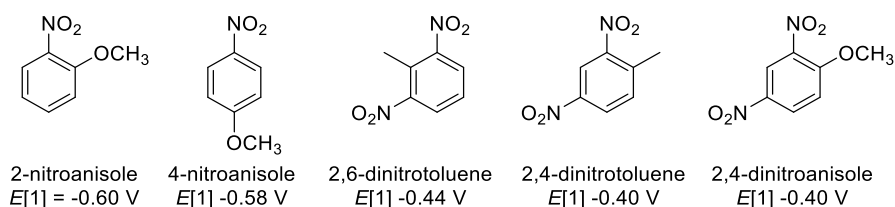


Figure 6.1 Nitroaromatic one-electron reduction potentials of a series of substituted mono- and dinitrobenzene derivatives from the literature.¹⁹⁰

The changes in reduction potentials through addition of electron withdrawing substituents can be described by the Hammett equation, a linear free-energy relationship between benzoic acid derivatives with *meta*- and *para*-substituents, described as follows:

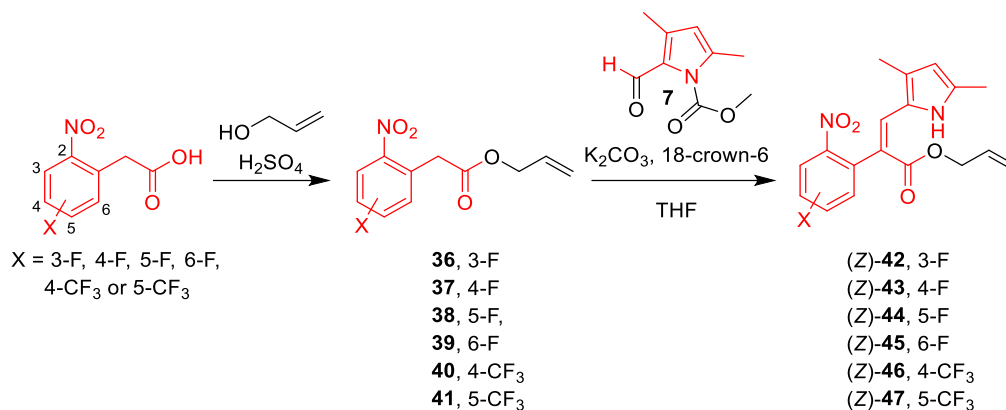
$$\log \frac{K}{K_0} = \sigma \rho$$

The equation describes the log ratio of the equilibrium constant, K , for a given reaction with substituent R with the equilibrium constant, K_0 , of the unsubstituted derivative. The right side of the equation is described by the reaction constant ρ (dependant on the type of reaction) and the substituent constant σ (dependant on the R substituent). In this

equation, an electron donating group like a *para*-methoxy substituent would have a negative substituent constant ($\sigma = -0.268$), whilst an electron withdrawing group would have a positive substituent constant (e.g. *para*-fluoro $\sigma = +0.062$, *para*-trifluoromethyl $\sigma = +0.54$ and *para*-nitro $\sigma = +0.778$).¹⁹¹

Based on the above, we hypothesised that addition of electron withdrawing substituents onto the nitroaryl ring of **1** and **2** would likely increase their reduction potentials. Conveniently, attaching electron withdrawing groups to the indoline-2-one of Semaxanib produces only minor changes in kinase inhibition.¹⁹² Thus, introduction of these groups should not diminish the kinase/angiogenesis inhibitory properties of the indolin-2-one portion of prodrugs after hypoxia-triggered release into tumours. Additionally, Denny *et al* showed that electron withdrawing groups do not affect the cyclisation rates of 2-(2-aminophenyl)acetamides formed upon reduction of 2-(2-nitrophenyl)acetamide prodrugs.¹²⁵ Cyclisation of the modified mutual prodrugs should therefore not be impaired.

To simplify testing of the hypothesis that installation of electron withdrawing groups increases the reduction potential of the prodrug scaffold, model compounds were designed that included a simple allyl ester in place of the cytotoxin. This change meant that the reliable allyl ester Knoevenagel chemistry described in Chapter 5 could be deployed in the synthesis. It was envisioned that addition of simple, unreactive electron withdrawing groups such as fluorine and trifluoromethyl to the nitroaryl ring would facilitate testing of the hypothesis while maintaining compatibility with our established chemistry. To this end, six target compounds were proposed, four containing fluorine atoms at the 3, 4, 5 and 6-positions (compounds (Z)-**42-45**, respectively, Scheme 6.1) and two containing trifluoromethyl groups at the 3 and 4-positions (compounds (Z)-**46** and (Z)-**47**). All of the required F/CF₃-substituted 2-(2-nitrophenyl)acetic acids for these targets were commercially available.



Scheme 6.1 Proposed synthesis of allyl ester model prodrugs (Z)-**42-45** containing electron withdrawing fluorine and trifluoromethyl groups on the nitroaryl ring.

Synthesis of the model prodrugs first required generating the allyl esters and then performing the Knoevenagel condensation. The reduction potentials of each *cis*-product could be measured and compared to the unaltered parent (Z)-**31**, as well as prodrugs **1** (and **9**). The new compounds could also be submitted to chemical reduction reactions to establish whether the presence of the F/CF₃ groups affects the subsequent indolin-2-one cyclisation. An undergraduate research project (CHEM341) student (Jessica Semken) joined the project in Semester 1, 2019 to assist with synthesis of the 4-F (and 5-F analogues (Z)-**43** and (Z)-**44**, respectively).

6.2 Synthesis of Ally Esters 36-41

The synthesis of allyl esters **36-41** from the commercial fluorinated and trifluoromethylated 2-(2-nitrophenyl)acetic acid precursors used the method described in Section 5.2 (Table 6.1). The reactions all proceeded well with > 80% yields obtained for the fluorinated analogues **36-39** and > 70% for the trifluoromethyl derivatives **40** and **41**. Approximately one gram of each ester was synthesised, providing ample quantities for the Knoevenagel reaction and subsequent chemical testing of the targets.

Table 6.1 Synthesis of allyl esters **36-41**.

2-(2-nitrophenyl)acetic acid	Ester	Yield (%)
3-F	36	86
4-F	37	80
5-F	38	84
6-F	39	80
4-CF ₃	40	71
5-CF ₃	41	70

6.3 Discovery of a Nucleophilic Aromatic Substitution Route to Novel Pyrroloquinoline Fluorophores

The first attempt at the Knoevenagel reaction (performed by Jessica Semken) with allyl ester **37** and pyrrole-2-aldehyde **7** under the standard conditions (Section 5.3) produced none of the desired product (*Z*)-**43**. Instead, a crystalline yellow solid was isolated as the major product, which fluorescence bright blue when held in solutions under UV light or sunlight (Figure 6.2).

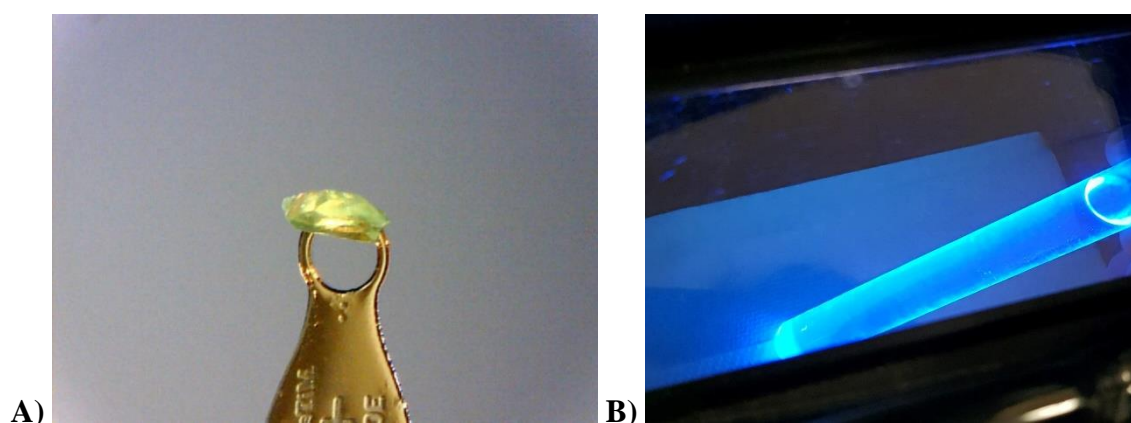
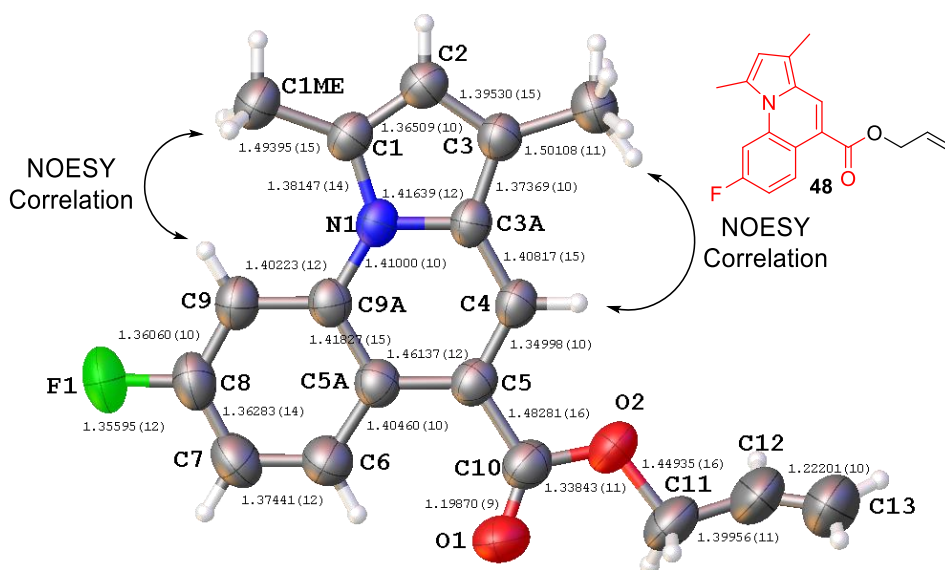


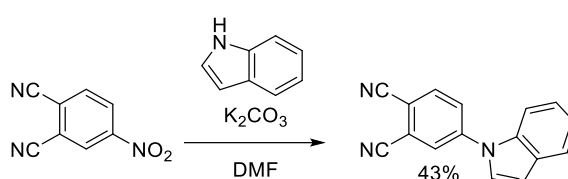
Figure 6.2 Unexpected side product formed in the attempted Knoevenagel reaction of **7** with 4-F allyl ester **37**. A) Crystal used to obtain the X-ray structure. B) Crystals dissolved in pet. spirit displayed bright blue fluorescence under 365 nm UV light.

Analysis of the NMR spectrum of the new compound revealed that although the characteristic pyrrole methyl groups were clearly still present, the pyrrole NH signal had disappeared and the ^1H and ^{13}C chemical shifts of the nitroaryl ring signals had all shifted considerably. It was proposed that after initial formation of the Knoevenagel product(s), the pyrrole N-H had cyclised via intramolecular nucleophilic aromatic substitution onto the nitroaryl group (with loss of HNO_2), forming the pyrroloquinoline **48** (Figure 6.3). The 2D NOESY spectrum revealed two key NOE correlations that supported this structure, the first being between one of the pyrrole methyl groups and the *ortho* CH on the phenyl ring. The second was a NOE between the newly formed alkene proton and the other pyrrole methyl group.

While the NMR data supported the proposed structure, further evidence was sought from X-ray crystallography. Small samples of the compound were dissolved in hexane, Et_2O , CH_2Cl_2 , EtOH and 2- PrOH in separate vials containing a needle outlet to allow slow evaporation of the solvent over a three-week period. Hexane yielded large needle-like crystals that were found to be suitable for X-ray structure determination (Dr. Christopher Richardson, UOW). The X-ray diffraction data confirmed that the structure was indeed **48** (Figure 6.3). With the structure of the compound now confirmed, its isolated yield was calculated at 38%.

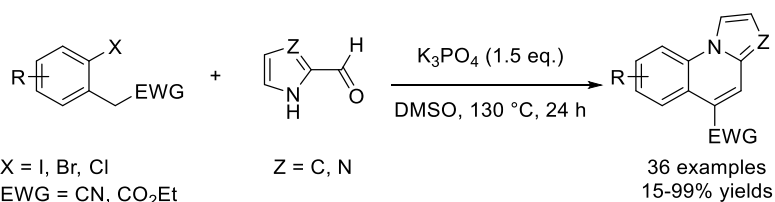


Nucleophilic aromatic substitution of the pyrrole nitrogen onto the nitroaryl ring (with loss of HNO_2) was an intriguing finding. Upon delving into the literature, examples could be found of indoles undergoing related intermolecular reactions with highly electron deficient nitroaromatics. One such example involved nucleophilic substitution of 4-nitrophthalonitrile with indole in the presence K_2CO_3 in DMF (Scheme 6.2).¹⁹³ Our new reaction, however, represents the first example of a pyrrole undergoing an intramolecular nucleophilic aromatic substitution-based cyclisation with a aryl nitro group.



Scheme 6.2 Literature report of intermolecular nucleophilic aromatic substitution of indole onto 4-nitrophthalonitrile.¹⁹³

Further searching of the literature identified a series of azole (pyrrole or imidazole)-fused quinoline ring systems structurally related to **48**.¹⁹⁴ The compounds were synthesised in a related way, where an unprotected azole-NH reacted with an *ortho*-halo substituted ethyl phenylacetate or phenyl acetonitrile in the presence of K_3PO_4 (Scheme 6.3). The reaction was initiated by a similar Knoevenagel condensation to ours, where the azole-NH of the Knoevenagel alkene product subsequently undergoes nucleophilic aromatic substitution with the *ortho*-halogen atom. Most of these analogues are reportedly fluorescent yellow solids, although their fluorescent properties, (e.g. absorption/emission maxima, extinction coefficients, quantum yields etc.) were not detailed.

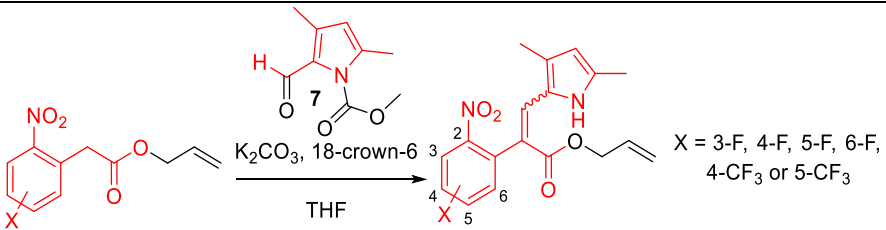


Scheme 6.3 Literature report on the synthesis of azole (pyrrole or imidazole)-fused quinolones related to **48**.¹⁹⁴

6.4 Optimisation of Knoevenagel Reaction Conditions

As the first Knoevenagel reaction with **37** produced only **48**, the reaction was modified in an attempt to reduce formation of this side product. It was hypothesised that heating the reaction was driving the nucleophilic aromatic substitution after initial formation of the desired *cis*-alkene (*Z*)-**43**. We postulated that the presence of the additional electron withdrawing fluorine atom might be allowing the Knoevenagel reaction to proceed at room temperature, despite all previous studies from the Kelso Lab showing that unsubstituted 2-(2-nitrophenyl)acetic esters required heat for the Knoevenagel reaction to proceed. Attempting Knoevenagel reactions with **7** and allyl esters **36** and **37** at room temperature delivered the desired products after 18 hours, yielding the typical mixtures of *cis* and *trans* isomers (*Z*)-**42** 28%, (*E*)-**42** 26% (Table 6.2, Entry 1) and (*Z*)-**43** 13%, (*E*)-**43** 19% (Table 6.2, Entry 2). None of the fluorescent side product analogous to **48** was observed in the reactions. The room temperature Knoevenagel reaction conditions were next trialled with allyl ester **38**, however, after 20 hours only trace amounts of the *cis/trans*-alkene products were detected by TLC analysis. However, increasing the temperature for this substrate to 45 °C and heating for an additional 24 hours generated the desired alkenes (*Z*)-**44** 22% and (*E*)-**44** 21% (Table 6.2, Entry 3).

Table 6.2 Knoevenagel reactions with allyl esters **36-38**.



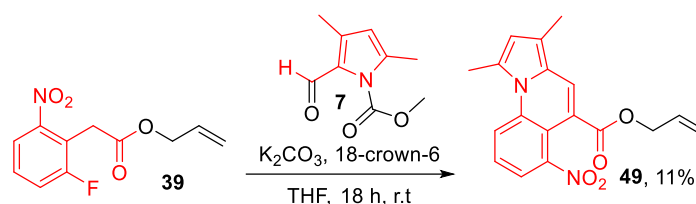
X = 3-F, 4-F, 5-F, 6-F, 4-CF₃ or 5-CF₃

Entry	Allyl Ester	Temperature	Time (h)	Product
1	36 , X = 3-F	r.t.	18	(<i>Z</i>)- 42 28%, (<i>E</i>)- 42 26%
2	37 , X = 4-F	r.t.	18	(<i>Z</i>)- 43 13%, (<i>E</i>)- 43 19%
3	38 , X = 5-F	45 °C	44	(<i>Z</i>)- 44 22%, (<i>E</i>)- 44 21%

6.4.1 Knoevenagel Reaction with Allyl Ester **39**

Surprisingly, when the 6-allyl ester **39** was subjected to room temperature Knoevenagel conditions, the nucleophilic aromatic substitution cyclisation occurred, forming pyrroloquinoline **49** (Scheme 6.4, 11%). However, in this reaction the fluorine atom

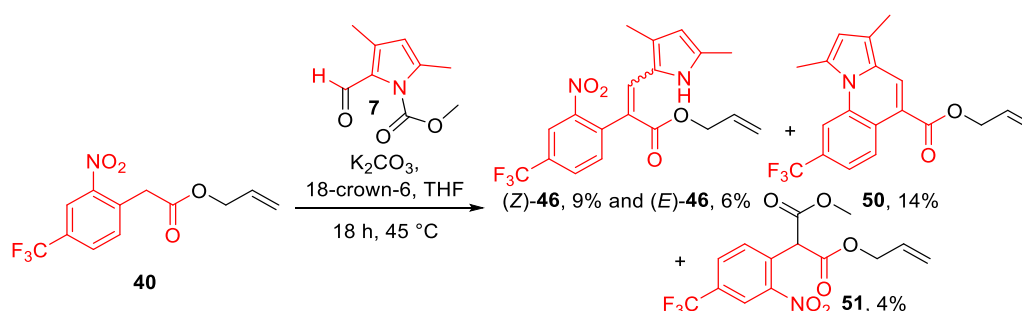
served as a much better activator and leaving group, undergoing the reaction in preference to the nitro group. The higher reactivity of the fluorine allowed the reaction to proceed at room temperature. In contrast to **48**, compound **49** was a bright red solid that did not fluoresce under UV light. As compound **49** was the major reaction product at room temperature and none of the desired alkene products were observed in this Knoevenagel reaction, efforts to produce the 6-fluoro model prodrug target (*Z*)-**45** were abandoned.



Scheme 6.4 Knoevenagel reaction of **39** with **7** at room temperature produced intramolecular nucleophilic aromatic substitution product **49**.

6.4.2 Knoevenagel Reaction with Allyl Ester **40**

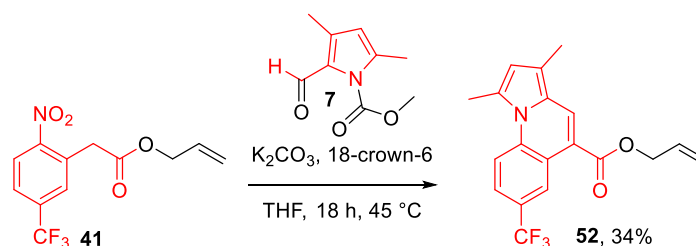
When allyl ester **40** was subjected to the room temperature Knoevenagel reaction for 18 hours only small amounts of the desired alkene products were visible by TLC analysis, and heating the reaction at 45 °C for 24 hours led to a complex mixture of products (Scheme 6.5). Nevertheless, the desired *cis/trans* alkenes (*Z*)-**46** and (*E*)-**46** were able to be isolated in 9% and 6% yields, respectively. The intramolecular nucleophilic aromatic substitution product **50** was also isolated in 14% yield. When dissolved in pet. Spirit, **50** displayed the same bright blue fluorescence as **48** under 280 nm UV light. An additional side product corresponding to the methylallyl malonate diester **51** was also isolated in 4% yield from the reaction. Compound **51** presumably forms when the carbanion of **40** attacks the methyl carbamate protecting group of **7** rather than the aldehyde.



Scheme 6.5 Knoevenagel reaction of **40** with **7** produced a mixture of the desired alkenes (*Z*)-**46** and (*E*)-**46**, along with side products **50** and **51**.

6.4.3 Knoevenagel Reaction with Allyl Ester **41**

When allyl ester **41** was subjected to the room temperature Knoevenagel conditions for 18 hours none of the desired alkenes were formed and only trace amounts of nucleophilic aromatic substitution product **52** were detected by TLC analysis. Heating the reaction at 45 °C for 24 hours gave none of the desired alkenes but increased the isolated yield of **52** to 34% (Scheme 6.6). The side product, **52**, displayed similar fluorescent properties to the other novel pyrroloquinolones **48** and **50**, fluorescing blue under 280 nm UV light. It appears that the highly electron withdrawing trifluoromethyl substituent located *para* to the nitro group was activating the compound and strongly driving nucleophilic aromatic substitution after formation of the Knoevenagel products. Attempts to synthesise the *cis*-alkene (*Z*)-**47** were abandoned.



Scheme 6.6 Knoevenagel reaction of **41** produced nucleophilic aromatic substitution product **52** as the major product.

6.5 Pulse Radiolysis One-Electron Reduction Potential Measurements

The *cis*-alkenes (*Z*)-**42**, (*Z*)-**43**, (*Z*)-**44** and (*Z*)-**46** and the parent unsubstituted alkene (*Z*)-**31** were sent to the University of Auckland for pulse radiolysis nitroaryl one-electron reduction potential measurements (as previously described in Section 4.3). The compounds were found to be considerably less soluble in aqueous solution compared to the prodrug structures **2** and **9**. While (*Z*)-**31** was soluble in 2 M aqueous *tert*-butanol, the other new compounds required 4 M *tert*-butanol to achieve sufficient concentrations for radiolysis measurements.

6.5.1 Reduction Potential of Unsubstituted Parent (*Z*)-**31**

A stock solution of the parent compound (*Z*)-**31** was prepared in 2 M *tert*-butanol containing 5 mM phosphate buffer pH 7. A UV-vis spectrum was recorded to obtain the extinction coefficient, which was used to determine the concentration of the compound in test solutions. One-electron reduction of (*Z*)-**31** (50 μ M) by the e^-_{aq} was carried out

upon pulse radiolysis (3 Gy in 200 ns) in deaerated phosphate buffer (5 mM, pH 7). Spectral changes following one-electron reduction (relative to unreduced compound) over a limited wavelength region were obtained (Figure 6.4). The initial radical anion underwent a spectral change at *ca.* $0.5\text{--}1 \times 10^4 \text{ s}^{-1}$ to another intermediate. The absorption spectrum of the unreduced compound, measured after the experiments, was taken to obtain the corrected spectra of the radical intermediates. This observation pointed to slow decomposition of solutions of (Z)-**31**.

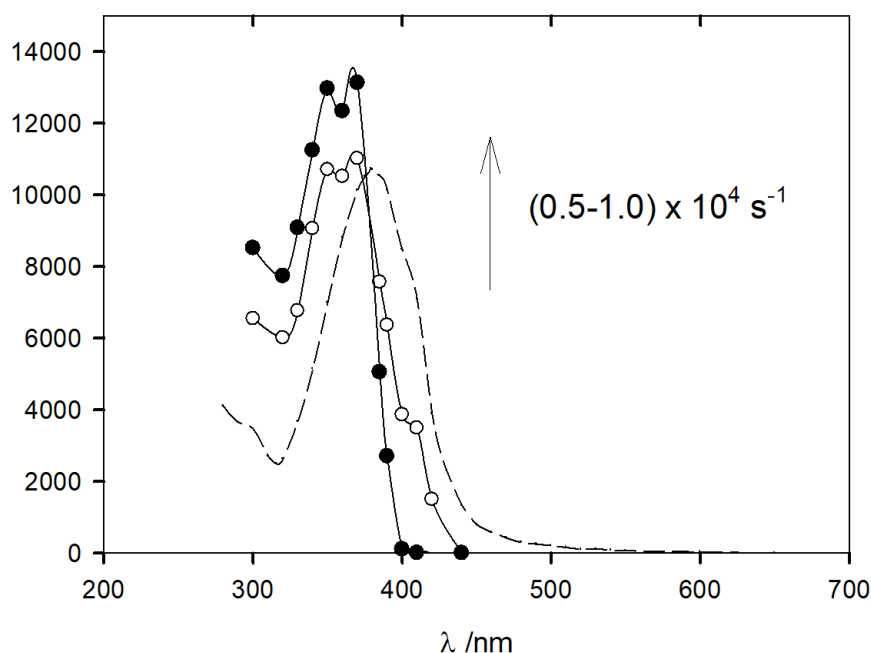
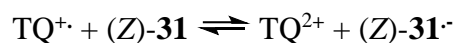


Figure 6.4 Spectral changes following pulse radiolysis (3 Gy in 200 ns) of (Z)-**31**, 75 μM in deaerated aqueous solution containing *tert*-butanol (2 M) and phosphate buffer (5 mM, pH 7), 5 μs and 200 μs after the pulse. Spectra corrected for the absorption of the pre-pulsed spectrum, dashed line.

Redox equilibrium was established against triquat (TQ^{2+}) ($E(1) = -548 \pm 7 \text{ mV}$) for 3 mixtures of (Z)-**31** / TQ^{2+} : 50-127 μM / 50-100 μM , maintaining 2 M *tert*-butanol / 5 mM phosphate pH 7.

$$K$$


$K_{\text{av.}} = 0.068 \pm 0.006$ $\Delta E = -(RT/F)(\ln K) = -69 \pm 3 \text{ mV}$ $E_{\text{cor}} = -8 \text{ mV}$ (ionic strength)

$$\underline{\underline{E((\text{Z})\text{-}\mathbf{31}/(\text{Z})\text{-}\mathbf{31}^{\cdot-}) = -625 \pm 8 \text{ mV}}}$$

At -625 mV, the reduction potential of (*Z*)-**31** was considerably lower than the values obtained previously with prodrugs **2** (-509 ± 8 mV) and **9** (-550 ± 8 mV). It was not expected that changing the distal cytotoxin group to a vinyl ester would have such a dramatic effect; i.e. lowering the reduction potential by ~ 120 mV. To confirm this result, a second sample of (*Z*)-**31** was sent for testing and the electron transfer standard tetraquat (TeQ^{2+} , Figure 6.5) was used in place of triquat.

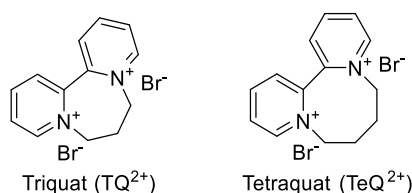
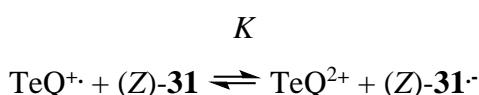


Figure 6.5 Chemical structures of triquat (TQ^{2+}) and tetraquat (TeQ^{2+}) standards used to establish redox equilibria for one-electron pulse radiolysis reduction potential measurements.

Redox equilibria were established against tetraquat (TeQ^{2+}) ($E(1) = -635 \pm 5$ mV) for 2 mixtures of (*Z*)-**31** / TeQ^{2+} : 75-84.5 μM / 100-300 μM , maintaining 2 M *tert*-butanol / 5 mM phosphate pH 7.



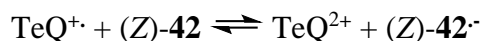
$$K_{\text{av.}} = 2.45 \pm 0.21 \quad \Delta E = -(RT/F)(\ln K) = 23 \pm 2 \text{ mV} \quad E_{\text{cor}} = -10 \text{ mV (ionic strength)}$$

$$\underline{\underline{E((\text{Z})\text{-}\mathbf{31}/(\text{Z})\text{-}\mathbf{31}^{\cdot-}) = -622 \pm 6 \text{ mV}}}$$

The new value was found to be in very close agreement with the earlier measurement. It was speculated that there could be a structural difference in the alignment of the conjugated systems in (*Z*)-**31** and **2** that give rise to this change. Whilst this observation meant that the reduction potentials of the new series of allyl ester model compounds could not be directly compared to the values obtained earlier for **2** and **9**, they could still be compared to each other and to the parent unsubstituted compound (*Z*)-**31** since they were all allyl esters. Comparing the new substituted derivatives to the parent (*Z*)-**31** thus provided a direct readout of how adding the fluorine and trifluoromethyl groups affects the one-electron reduction potential of the scaffold.

6.5.2 Reduction Potential (Z)-42

Redox equilibrium was established against tetraquat (TeQ^{2+}) ($E(1) = -635 \pm 7 \text{ mV}$) for 3 mixtures of (Z)-42 / TeQ^{2+} : 50 μM / 300 μM , in 2 M *tert*-butanol / 5 mM phosphate pH 7.

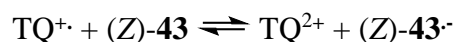
$$K$$


$$K_{\text{av.}} = 3.03 \Delta E = -(RT/F)(\ln K) = 30 \text{ mV } E_{\text{cor}} = -10 \text{ mV (ionic strength)}$$

$$\underline{E((\text{Z})\text{-42}/(\text{Z})\text{-42}^{\cdot-}) = -615 \pm 10 \text{ mV}}$$

6.5.3 Reduction Potential of (Z)-43

It was observed that (Z)-43 was less soluble in aqueous solution so the *tert*-butanol concentration was increased from 2 M to 4 M. Redox equilibrium was established against triquat (TQ^{2+}) ($E(1) = -548 \pm 7 \text{ mV}$) for a mixture of (Z)-43 / TQ^{2+} : 96 μM / 100 μM , in 4 M *tert*-butanol / 5 mM phosphate pH 7.

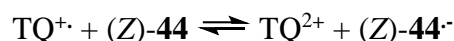
$$K$$


$$K_{\text{av.}} = 0.119 \Delta E = -(RT/F)(\ln K) = -55 \text{ mV } E_{\text{cor}} = -9 \text{ mV (ionic strength)}$$

$$\underline{E((\text{Z})\text{-43}/(\text{Z})\text{-43}^{\cdot-}) = -612 \pm 7 \text{ mV}}$$

6.5.4 Reduction Potential of (Z)-44

Once again, (Z)-44 was not as soluble in aqueous solution so the *tert*-butanol concentration was increased from 2 M to 4 M. Redox equilibrium was established against triquat (TQ^{2+}) ($E(1) = -548 \pm 7 \text{ mV}$) for a mixture of (Z)-44 / TQ^{2+} : 131 μM / 100 μM , in 4 M *tert*-butanol / 5 mM phosphate pH 7.

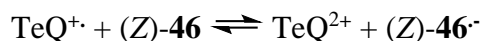
$$K$$


$$K_{\text{av.}} = 0.202 \Delta E = -(RT/F)(\ln K) = -41 \text{ mV } E_{\text{cor}} = -9 \text{ mV (ionic strength)}$$

$$\underline{E((\text{Z})\text{-44}/(\text{Z})\text{-44}^{\cdot-}) = -598 \pm 7 \text{ mV}}$$

6.5.5 Reduction Potential Measurement of (Z)-46

Redox equilibrium was established against tetraquat (TeQ^{2+}) ($E(1) = -635 \pm 7$ mV) for 3 mixtures of (Z)-46 / TeQ^{2+} : 50-124 μM / 300-800 μM , in 2 M *tert*-butanol / 5 mM phosphate pH 7.

$$K$$


$K_{\text{av.}} = 16.7 \pm 2.28$ $\Delta E = -(RT/F)(\ln K) = 72 \pm 4$ mV $E_{\text{cor}} = -12$ mV (ionic strength)

$$\underline{E((\text{Z})\text{-46}/(\text{Z})\text{-46}^-) = -575 \pm 10 \text{ mV}}$$

6.5.6 Summary of One-Electron Reduction Potential Measurements

The measured nitroaromatic one-electron reduction potentials of (Z)-31, (Z)-42, (Z)-43, (Z)-44 and (Z)-46 are summarised in Table 6.3. Whilst all measured values were far off the desired -450 mV threshold required for bioreductive activation, it seems this can partly be attributed to the allyl ester. Nevertheless, comparing potentials within the series to the unsubstituted parent (Z)-31 revealed some key insights. A fluorine atom at either the *ortho*- or *meta*-position (relative to the nitro) produced small increases in the reduction potential (~ 10 mV), whereas fluorine at the *para*-position produced a greater increase (~ 25 mV). As predicted, the stronger electron withdrawing trifluoromethyl substituent provided a larger boost of ~ 50 mV. Compared to (Z)-43, which contains a fluorine atom at the same position (*meta* to the nitro group), the 4- CF_3 derivative (Z)-46 displayed a reduction potential that was ~ 40 mV higher. From these data, it would appear that the greatest increases in reduction potential within this series would come from a *para*-trifluoromethyl substituent, but this molecule (i.e. (Z)-47) was unable to be synthesised using our current chemistry. New chemistry would need to be developed to synthesise (Z)-47 and confirm this assertion.

Table 6.3 Summary of pulse radiolysis one-electron reduction potential measurements.

Allyl Ester	<i>Tert</i> -Butanol Concentration	Electron Transfer Reagent	One-Electron Reduction Potential
(<i>Z</i>)- 31 , X = H	2 M	Triquat (TQ ²⁺)	-625 ± 8 mV
(<i>Z</i>)- 31 , X = H	2 M	Tetraquat (TeQ ²⁺)	-622 ± 6 mV
(<i>Z</i>)- 42 , X = 3-F	2 M	Tetraquat (TeQ ²⁺)	-615 ± 10 mV
(<i>Z</i>)- 43 , X = 4-F	4 M	Triquat (TQ ²⁺)	-612 ± 7 mV
(<i>Z</i>)- 44 , X = 5-F	4 M	Triquat (TQ ²⁺)	-598 ± 7 mV
(<i>Z</i>)- 46 , X = 4-CF ₃	2 M	Tetraquat (TeQ ²⁺)	-575 ± 10 mV

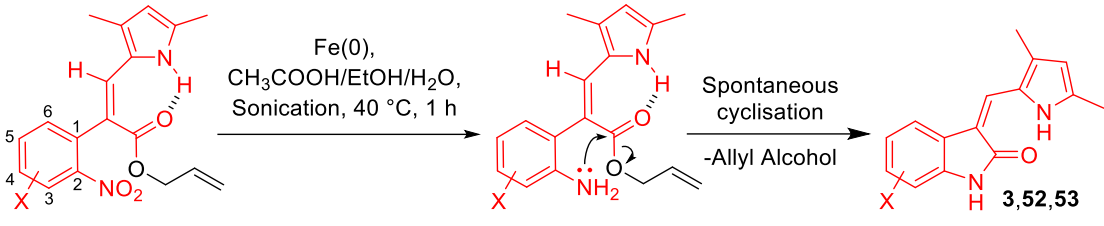
Even though none of the synthesised molecules reached the target reduction potential range of -330 to -450 mV, it was postulated that a 50 mV or more increase in the nitroaromatic one-reduction potential of the mutual prodrugs **2** (-509 ± 8 mV) and **9** (-550 ± 8 mV), such as might be expected with introduction of a CF₃ group at the 5-position, could bring the compounds close to the range for useful bioreductive activation. Extensive structure activity relationship assays performed by Sugen, inc. in the development of semaxanib and sunitinib has already shown some tolerability for substitution at the 5- position. Whilst the 5-CF₃ substituted is novel, the 5-CH₃ derivative showed comparable tyrosine kinase inhibition (IC₅₀) in assays with platelet-derived growth factor (25.5 μM, relative to semaxanib 20.26 μM) and the VEGF receptor Flk-1 (0.3 μM, relative to semaxanib 1.04 μM).¹⁹² In the same assays, the 4-F analogue of semaxanib gave a slightly improved profile relative to semaxanib for platelet-derived growth factor (18.2 μM) and the VEGF receptor Flk-1 (<0.78 μM).¹⁹²

6.6 Chemical Reductions with Fe/CH₃COOH

Introduction of the electron withdrawing substituents onto the nitroaromatic ring could affect the ability of the scaffold to undergo spontaneous cyclisation following reduction. It was therefore important to establish whether cyclisation still occurred after chemical

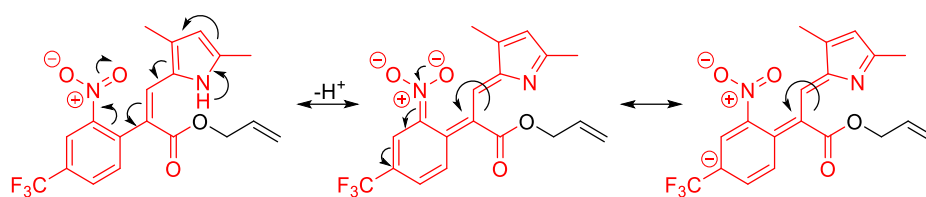
reduction. To investigate this, one of the chemical reductions explored earlier (Section 4.1), namely Fe(0) in CH₃COOH:EtOH:H₂O (1:1:1),¹⁶⁴ was applied to the new *cis* allyl esters (Table 6.4).

Table 6.4 Summary of chemical reductions of allyl ester *cis* derivatives.



<i>Cis</i> Allyl Ester	Product	Yield (%)
(<i>Z</i>)- 31 , X = H	3	78
(<i>Z</i>)- 42 , X = 3-F	N.A.	Trace product mixed with isomerised (<i>E</i>)- 42
(<i>Z</i>)- 43 , X = 4-F	53	75
(<i>Z</i>)- 44 , X = 5-F	54	80
(<i>Z</i>)- 46 , X = 4-CF ₃	N.A.	Trace product mixed with isomerised (<i>E</i>)- 46

Reduction of the unsubstituted parent (*Z*)-**31** gave semaxanib **3** in 78% yield, which was comparable to the yield obtained from the unsubstituted ethyl ester (Nicholas Kirk, 81%).¹³⁹ Both (*Z*)-**43** and (*Z*)-**44** gave good yields of their fluorinated semaxanib derivatives (**53** 75%, **54** 80%, respectively). When the same conditions were applied to (*Z*)-**42** and (*Z*)-**46**, both allyl esters gave complicated mixtures of isomerised starting material and unidentifiable side products. This was an unexpected result, possibly arising from the greater electron withdrawing properties leading to ease of donation of electrons from the pyrrole nitrogen into the nitroaromatic system, and subsequent isomerisation (Scheme 6.7). This was postulated to occur due to the resonance stabilisation afforded by the *para*-trifluoromethyl (relative to alkene) substituent in the case of (*Z*)-**46**, and increased electron withdrawing effects of the nitroaryl group with an *ortho*-fluorine atom in the case of (*Z*)-**42**. When the pyrrole nitrogen donates electrons into the nitroaromatic system, the *cis*-alkene displays greater single bond character and free rotation to the *trans* product is possible.



Scheme 6.7 Resonance forms of (Z)-46 that allow free rotation around the alkene bond.

6.7 Conclusions and Future Directions

Four novel *cis*-allyl ester model compound containing electron withdrawing substituents on the nitroaryl ring were synthesised and tested for one-electron reduction potentials and spontaneous cyclisation after nitroaryl group chemical reductions. The electronic properties of the nitroaryl group were systematically explored, with the *para* position (relative to the nitro) identified as giving the greatest increase in reduction potential. The more electron withdrawing trifluoromethyl group was shown to produce greater increases in reduction potential than fluorine substituents.

6.7.1 Future Work on Hypoxia Activated Mutual Prodrugs

The chemical reductions studies on the synthesised *cis* allyl esters showed that electron donation of the pyrrole nitrogen into the nitroaromatic could present a dilemma in continued synthesis of new derivatives. One possible way to alleviate this issue would be to modify the angiogenesis inhibitor portion of the molecule from semaxanib to the more functionalised, FDA approved drug sunitinib (Section 1.3.1). Sunitinib is a superior angiogenesis inhibitor to semaxanib but also benefits from having an amide appendage attached to the pyrrole ring. The carbonyl of this amide could act as an electron sink for the pyrrole nitrogen, both addressing the problem of isomerisation whilst also increasing the nitroaryl one-electron reduction potentials further by pulling electron density away from the nitroaryl group through conjugation. This could be further enhanced by applying the lessons learnt here from the pulse radiolysis studies and incorporating a *para* (relative to the nitro) trifluoromethyl substituent (Figure 6.6).

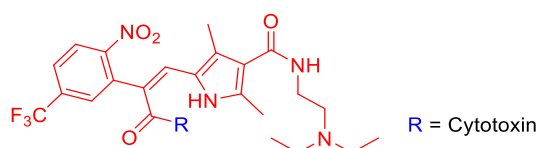
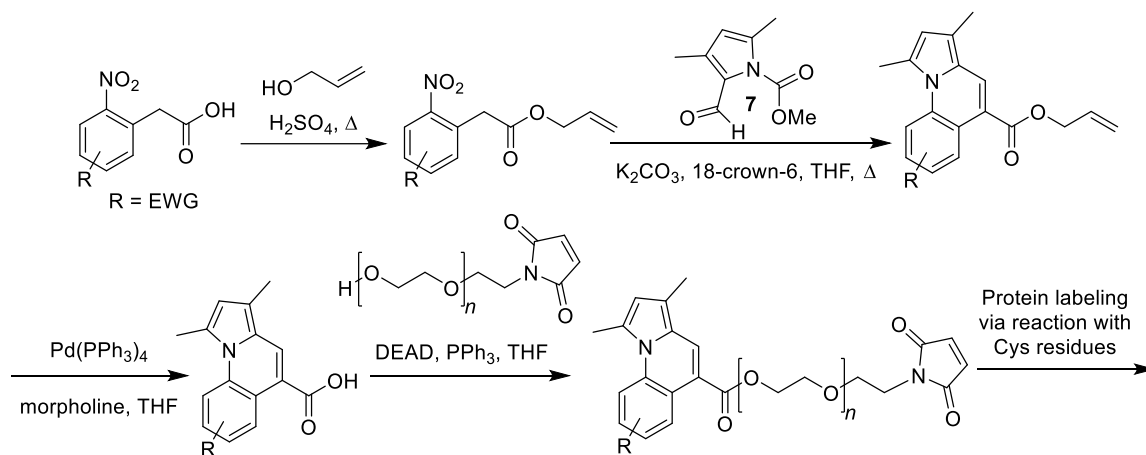


Figure 6.6 Proposed mutual prodrug based on the FDA-approved drug sunitinib, incorporating an additional *para* (relative to the nitro) trifluoromethyl substituent.

6.7.2 Future Work on Pyrroloquinoline Fluorophores

An exciting outcome from this work was the discovery of a novel intramolecular nucleophilic aromatic substitution-based cyclisation of the pyrrole nitrogen onto the nitroaryl group. In our synthesis, this produced an undesired side product, however, the pyrroloquinolines as a class have not been extensively explored and could potentially be useful probes; for example, as fluorescent tags for proteins. It was clear from this study that heating the Knoevenagel reactions to higher temperatures favours this cyclised product over the *cis/trans* alkenes and increases the yield of pyrroloquinolines (Section 6.3). Using the chemistry described in Chapter 5, the allyl group could be easily removed from pyrroloquinolines like **48**, **50** and **52** using Pd(PPh₃)₄/morpholine (Section 5.5). The Mitsunobu coupling conditions developed in Section 5.7 could then be used to attach a polyethylene glycol spacer containing a terminal maleimide, which could in turn be attached to proteins via reaction with Cys residues (Scheme 6.8). Altering the electron withdrawing substituents on the nitroaryl ring precursors and trialling a variety of appendages on the pyrrole could allow tailoring of the fluorescent properties, and potentially pharmacokinetic properties for *in vivo* imaging applications.



Scheme 6.8 Proposed synthesis of proteins labelled with pyrroloquinoline fluorescent tags using the chemistry developed in Chapters 5 and 6.

Chapter 7: Experimental

7.1 General Methods

All solvents were purchased as Analytical Reagent grade and used without further purification. The term pet. spirit refers to petroleum spirit within the boiling range 40-60 °C.

7.1.1 Chromatography

Analytical TLC was performed using aluminium-backed sheets of Merck TLC Silica Gel 60 F₂₅₄. Compounds were visualised under UV light and by staining with 4-methoxybenzaldehyde or ammonium molybdate. Preparative TLC was performed using glass-backed sheets of Whatman Partsil PK6F 60Å silica with a thickness of 1000 µm. Gradient flash column chromatography was performed using Scharlan Silica Gel 60, 0.04-0.06 mm (230-400 mesh ASTM).

7.1.2 Melting Points

Melting points (M.P.) were measured on a Reichart hot stage equipped with a eurotherm temperature controller and are uncorrected.

7.1.3 Polarimetry

Optical rotations (O.R.) were measured using a 1 mL cell in a Jasco P-2000 polarimeter. Twelve measurements were taken and the average used to calculate specific rotation.

7.1.4 Infrared Spectroscopy

Infrared spectra were obtained on a Nicolet Avatar 360 FT-IR spectrometer fitted with a Smart Omni-Sampler germanium crystal accessory.

7.1.5 Nuclear Magnetic Resonance Spectroscopy

¹H NMR spectra were recorded at 500 MHz on a Varian Unity 500 Inova spectrometer. The spectra were recorded in CDCl₃ and chemical shifts were referenced to tetramethylsilane (δ 0.00 ppm). Multiplicities are denoted as s (singlet), d (doublet), t (triplet), br (broad) or m (multiplet). ¹³C NMR and ¹³C APT spectra were recorded at 126 MHz on a Varian Inova 500 spectrometer. Compound structures were confirmed with 2D

NMR experiments, including gCOSY, NOESY, gHSQC and gHMBC spectra. ^1H and ^{13}C NMR spectra for all synthesised compounds are provided in the Appendix.

7.1.6 Mass Spectrometry

Electrospray ionization mass spectra were recorded on a micromass Platform LCZ spectrometer. ESI-high resolution mass spectra were recorded on a Waters XEVO QToF spectrometer with leucine encephalin as the internal standard.

7.2 Synthesis of *N*-(4-aminophenyl)-2-(2-nitrophenyl)acetamide **4**

2-(2-nitrophenyl)acetic acid (10.151 g, 56.0 mmol), *p*-phenylenediamine (6.690 g, 61.9 mmol) and HBTU (23.469 g, 61.9 mmol) were stirred in under argon in a round bottom flask in CH_2Cl_2 (100 mL) at 0 °C for 10 minutes. DIPEA (22.4 mL, 131.7 mmol) was then added dropwise over 10 minutes to the stirring solution and the reaction allowed to warm to room temperature and stirring for 4 hours, monitored via TLC (EtOAc). The reaction was then diluted with 250 mL CH_2Cl_2 added to a separating funnel and 300 mL 5 M HCl added and the product precipitated as a white solid in the aqueous layer. The organic layer was removed and the aqueous layer washed with a further 3 x 200 mL CH_2Cl_2 . The aqueous layer was filtered, the solid collected and neutralised with 200 mL 5 M NaOH until the precipitate changed to a pale yellow colour. Solid was filtered dried and recrystallised in hot ethanol to give **4** (12.110 g, 80%).

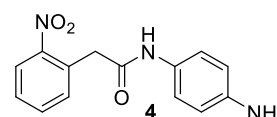
$R_f = 0.25$ (EtOAc). **M.P.** 168-170 °C. **IR:** (solid, v/cm^{-1}) 3344,

1684, 1517, 1424, 1410, 1357, 1307, 1275, 1237, 1175. **^1H NMR**

(500 MHz, d_6 -DMSO) δ 9.76 (s, 1H), 8.02 (d, $J = 8.1$ Hz, 1H),

7.69 (t, $J = 7.5$ Hz, 1H), 7.54 (t, $J = 7.1$ Hz, 3H), 7.54 (d, $J = 7.5$ Hz, 3H), 7.16 (d, $J = 8.7$ Hz, 3H), 6.48 (d, $J = 8.7$ Hz, 3H), 4.83 (s, 3H), 4.03 (s, 3H). **^{13}C NMR** (126 MHz,

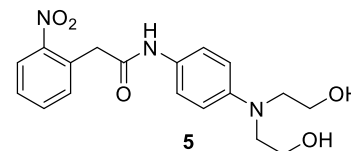
d_6 -DMSO) δ 166.9, 148.9, 144.4, 133.2, 133.0, 130.5, 127.9, 127.8, 124.1, 120.5, 113.5, 39.0. **HREI-MS:** m/z calculated for $\text{C}_{14}\text{H}_{14}\text{N}_3\text{O}_3$ $[\text{M}+\text{H}^+]$ 272.1030; observed 272.1035.



7.3 Synthesis of *N*-(4-(bis(2-hydroxyethyl)amino)phenyl)-2-(2-nitrophenyl)acetamide **5**

A mixture of **4** (4.01 g, 14.8 mmol) and anhydrous K_2CO_3 (4.09 g, 30.0 mmol) was prepared in 40 mL of 2-bromoethanol under argon. The reaction heated to 50 °C for 5 days and monitored via TLC (EtOAc). The product was precipitated with 500 mL H_2O , filtered and the aqueous layer treated with 200 mL saturated $\text{NaCl}_{(\text{aq})}$ solution causing

additional product to separate. The filtered solids combined, the impurities were crystallised at room temperature from hot ethanol and filtered off. The crude residue was recrystallised at $-20\text{ }^{\circ}\text{C}$ twice from hot ethanol to give **5** (3.31 g, 62%) as a yellow solid. $R_f = 0.65$ (EtOAc). **M.P.** 132-134 $^{\circ}\text{C}$. **IR:** (solid, v/cm^{-1}) 3276, 1653, 1559, 1539, 1517, 1507, 1340, 1261, 1180, 1074, 1049. **$^1\text{H NMR}$** (500 MHz, d_6 -DMSO) δ 9.83 (s, 1H), 8.03 (t, $J = 4.4$ Hz, 1H), 7.69 (q, $J = 5.0$ Hz, 1H), 7.55 (d, $J = 7.4$ Hz, 1H), 7.53 (t, $J = 9.6$ Hz, 1H), 7.30 (d, $J = 9.0$ Hz, 2H), 6.61 (d, $J = 9.0$ Hz, 2H), 4.70 (t, $J = 5.4$ Hz, 2H), 4.05 (s, 2H), 3.51 (q, $J = 6.0$ Hz, 4H), 3.37 (t, $J = 6.3$ Hz, 4H). **$^{13}\text{C NMR}$** (126 MHz, d_6 -DMSO) δ 166.3, 149.0, 144.2, 133.4, 133.2, 130.7, 128.1, 127.6, 124.3, 120.7, 111.1, 58.1, 53.3, 40.1. **HREI-MS:** m/z calculated for $\text{C}_{18}\text{H}_{22}\text{N}_3\text{O}_5$ [$\text{M}+\text{H}^+$] 360.1554; observed 360.1559.

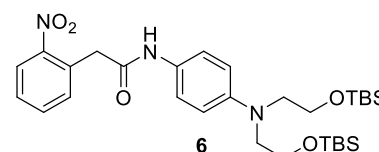


7.4 Synthesis of *N*-(4-(bis(2-((*tert*-butyldimethylsilyl)oxy)ethyl)amino)phenyl)-2-(2-nitrophenyl)acetamide **6**

To a round bottom flask, **5** (4.53 g, 12.6 mmol), TBDMSCl (5.72 g, 37.9 mmol) and imidazole (3.02 g, 44.3 mmol) were added and dissolved in 100 mL dry CH_2Cl_2 under argon. The reaction was monitored via TLC (30% EtOAc: 70% pet. spirit). After 6 hours the reaction was placed in the freezer overnight at $-20\text{ }^{\circ}\text{C}$ (to precipitate imidazole $\cdot\text{HCl}$). The imidazole $\cdot\text{HCl}$ was filtered off and the solution washed with saturated aqueous NaHCO_3 (3×100 mL) and saturated $\text{NaCl}(\text{aq})$ (1×100 mL), dried over anhydrous MgSO_4 , filtered and concentrated *in vacuo*. The crude residue was purified by recrystallisation at $-20\text{ }^{\circ}\text{C}$ from hot pet. spirit (75 mL) to give **6** (6.59 g, 89%) as a yellow solid.

$R_f = 0.76$ (30% EtOAc: 70% pet. spirit). **M.P.** 118-119 $^{\circ}\text{C}$.

IR: (solid, v/cm^{-1}) 2950, 1682, 1653, 1528, 1517, 1343, 1254, 1238, 1194, 1131, 1100, 1071, 929, 899, 836, 812.

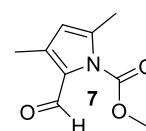


$^1\text{H NMR}$ (500 MHz, d_6 -DMSO) δ 9.83 (s, 1H), 8.02 (d, $J = 8.2$ Hz, 1H), 7.69 (t, $J = 7.5$ Hz, 1H), 7.55 (d, $J = 5.9$ Hz, 1H), 7.54 (t, $J = 5.9$ Hz, 1H), 7.30 (d, $J = 8.9$ Hz, 2H), 6.60 (d, $J = 8.9$ Hz, 2H), 4.05 (s, 2H), 3.69 (t, $J = 5.9$ Hz, 4H), 3.43 (t, $J = 5.8$ Hz, 4H), 0.85 (s, 18H), 0.00 (s, 12H). **$^{13}\text{C NMR}$** (126 MHz, CDCl_3) δ 166.9, 149.1, 145.5, 133.8, 133.5, 130.6, 128.6, 126.7, 125.3, 122.3, 111.8, 60.5, 53.9, 41.8, 26.0, 18.4, -5.2 . **HREI-MS:** m/z calculated for $\text{C}_{30}\text{H}_{50}\text{N}_3\text{O}_5\text{Si}_2$ [$\text{M}+\text{H}^+$] 588.3284; observed 588.3289.

7.5 Synthesis of methyl 2-formyl-3,5-dimethyl-1H-pyrrole-1-carboxylate 7

A solution of potassium hydride (7.45 g, 186 mmol) in 30 mL of THF under argon was cooled to 0 °C for 10 minutes. A solution 3,5-dimethyl-1H-pyrrole-2-carbaldehyde (15.3 g, 124 mmol) in 30 mL of THF was added dropwise and the solution stirred for 30 minutes at 0 °C. A solution of methyl chloroformate (23.4 g, 248 mmol) in 40 mL of THF was added slowly and the reaction allowed to warm to room temperature and monitored via TLC (20% acetone: 80% pet. spirit). After 2 hours, the reaction was quenched with 50 mL ice cold water, extracted with EtOAc (3 × 150 mL), the organic layers combined and washed with saturated NaCl_(aq) (1 × 250 mL). Organic layer was dried over anhydrous MgSO₄, filtered and concentrated *in vacuo*. The crude product was purified by silica gel column chromatography (100% pet. spirit to 10% acetone: 90% pet. spirit) and concentrated *in vacuo* to yield **7** as a yellow solid (0.32 g, 73%).

R_f = 0.53 (20% acetone: 80% pet. spirit). **M.P.** 44-45 °C; **IR:** (solid, v/cm⁻¹) 1730, 1650, 1496, 1451, 1326, 1153, 765. **¹H NMR** (500 MHz, CDCl₃) δ 9.99 (s, 1H), 5.89 (s, 1H), 3.96 (s, 3H), 2.38 (s, 3H), 2.30 (s, 3H). **¹³C NMR** (126 MHz, CDCl₃) δ 181.3, 151.6, 138.4, 135.9, 130.5, 116.1, 54.5, 15.4, 13.0. **HREI-MS:** *m/z* calculated for C₉H₁₂NO₃ [M+H⁺] 182.0812; observed 182.0817.



7.6 Synthesis of (Z)-N-(4-(bis(2-((tert)-butyldimethylsilyl)oxy)ethyl)amino)phenyl)-3-(3,5-dimethyl-1H-pyrrol-2-yl)-2-(2-nitrophenyl)acrylamide (Z)-8

Potassium carbonate (2.35 g, 17.0 mmol) and 18-crown-6 (1.14 g, 4.3 mmol) were dissolved in 50 mL dry THF and heated at 75 °C for 1 hour under nitrogen. A solution of **6** (5.01 g, 8.52 mmol) was prepared in 25 mL of dry THF, added slowly to the reaction and left to stir at 75 °C for 1 hour. A solution of **7** (1.72 g, 9.47 mmol) in 25 mL of dry THF was prepared and slowly added to the reaction. The reaction was then left for 3 hours at 75 °C and monitored via TLC (30% EtOAc: 70% pet. spirit). The solvent was reduced to less than 50 mL via rotary evaporation and transferred to a separating funnel with 100 mL of H₂O. The aqueous layer was extracted with EtOAc (3 × 50 mL). Organic layers were combined and washed with 100 mL of saturated NaCl_(aq), dried over anhydrous MgSO₄, filtered and concentrated under reduced pressure. The crude residue was purified by gradient silica gel column chromatography (100% pet. spirit to 20% EtOAc: 80% pet. spirit) to give (Z)-**8** (1.22 g, 21%) as a red solid.

R_f = 0.83 (30% EtOAc: 70% pet. spirit). **M.P.** 174-176 °C.

IR: (solid, ν/cm^{-1}) 3313, 2928, 1654, 1612, 1595, 1514,

1379, 1360, 1322, 1289, 1250, 1095, 1054, 833, 810. **¹H**

NMR (500 MHz, CDCl₃) δ 12.10 (br. s, 1H), 8.02 (dd, *J*

= 8.1, 1.2 Hz, 1H), 7.69 (td, *J* = 7.5, 1.0 Hz, 1H), 7.59 (dd, *J* = 7.6, 1.3 Hz, 1H), 7.54 (td,

J = 7.8, 1.3 Hz, 1H), 7.14 (d, *J* = 8.7 Hz, 2H), 6.68 (s, 1H), 6.63 (d, *J* = 8.8 Hz, 2H), 6.53

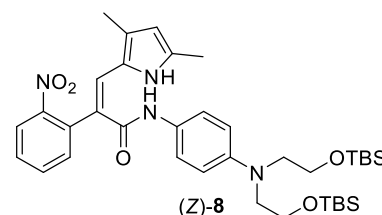
(s, 1H), 5.83 (d, *J* = 2.2 Hz, 1H), 3.73 (t, *J* = 6.4 Hz, 4H), 3.48 (t, *J* = 6.5 Hz, 4H), 2.29

(s, 3H), 2.11 (s, 3H), 0.89 (d, *J* = 0.7 Hz, 18H), 0.04 (d, *J* = 0.7 Hz, 12H). **¹³C NMR** (126

MHz, CDCl₃) δ 166.5, 149.7, 146.0, 136.4, 133.7, 133.6, 133.5, 129.5, 129.1, 128.8,

125.8, 125.0, 124.3, 124.3, 116.3, 111.7, 111.0, 60.4, 53.9, 26.0, 18.4, 13.8, 11.5, -5.2.

HREI-MS: *m/z* calculated for C₃₇H₅₇N₄O₅Si₂ [M+H⁺] 693.3862; observed 693.3861.



7.7 Synthesis of (Z)-N-(4-(bis(2-hydroxyethyl)amino)phenyl)-3-(3,5-dimethyl-1H-pyrrol-2-yl)-2-(2-nitrophenyl)acrylamide **9**

A solution of (Z)-**8** (0.50 g, 0.73 mmol) was prepared in 7 mL dry THF and cooled to 0 °C under argon. A mixture containing 3.5 mL 1 M TBAF (3.5 mmol) and 0.70 mL acetic acid (12 mmol) was added dropwise to the reaction. The reaction was monitored via TLC (EtOAc) of reaction aliquots obtained after mini-extractions (saturated NaHCO_{3(aq)}/EtOAc). After 4 hours, the reaction was diluted with 50 mL EtOAc, transferred to a separating funnel and extracted with saturated NaHCO_{3(aq)} (3 × 50 mL) and saturated NaCl_(aq) (1 × 50 mL). The organic layer was dried over anhydrous MgSO₄, filtered and concentrated under reduced pressure. The crude residue was purified by gradient silica gel column chromatography (50% EtOAc: 50% pet. spirit to 100% EtOAc) to give **9** (0.290 g, 86%) as a red solid.

R_f = 0.60 (EtOAc). **M.P.** 102-104 °C. **IR:** (solid, ν/cm^{-1})

3274, 2868, 1641, 1513, 1341, 1321, 1262, 1235, 1202,

1179, 1151, 1041, 1001. **¹H NMR** (500 MHz, CDCl₃) δ

12.02 (br. s, 1H), 8.01 (dd, *J* = 8.1, 1.2 Hz, 1H), 7.69 (td, *J*

= 7.5, 1.2 Hz, 1H), 7.59 (dd, *J* = 7.6, 1.1 Hz, 1H), 7.54 (td, *J* = 7.8, 1.4 Hz, 1H), 7.13 (d,

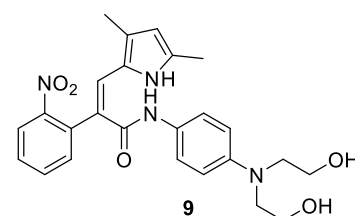
J = 8.9 Hz, 2H), 6.72 (s, 1H), 6.63 (d, *J* = 9.0 Hz, 2H), 6.54 (s, 1H), 5.83 (d, *J* = 2.6 Hz,

1H), 3.79 (t, *J* = 4.9 Hz, 4H), 3.52 (t, *J* = 4.9 Hz, 4H), 3.44 (br. s, 2H), 2.27 (s, 3H), 2.10

(s, 3H). **¹³C NMR** (126 MHz, CDCl₃) δ 166.7, 149.7, 146.0, 136.3, 133.7, 133.7, 133.6,

129.8, 129.1, 129.0, 126.8, 125.0, 124.4, 124.3, 116.2, 113.0, 111.1, 60.8, 55.4 13.7, 11.6.

HREI-MS: *m/z* calculated for C₂₅H₂₉N₄O₅ [M+H⁺] 465.2132; observed 465.2138.



7.8 Synthesis of (Z)-N-(4-(bis(2-chloroethyl)amino)phenyl)-3-(3,5-dimethyl-1H-pyrrol-2-yl)-2-(2-nitrophenyl)acrylamide **1**

A solution of **9** (0.22 g, 0.46 mmol) was prepared in 5 mL dry CH₂Cl₂ and cooled to 0 °C. Triethylamine (0.090 mL, 1.2 mmol) and methanesulfonyl chloride (0.19 mL, 1.4 mmol) were added to the reaction and stirring continued at 0 °C while monitoring via TLC (EtOAc). After 1 hour, the reaction was diluted with 20 mL CH₂Cl₂ and transferred to a separating funnel. The organic layer was extracted with saturated NaHCO_{3(aq)} (3 × 25 mL) and saturated NaCl_(aq) (1 × 25 mL), dried over anhydrous MgSO₄, filtered and concentrated under reduced pressure without heating. The crude residue was taken up in 5 mL dry DMF and lithium chloride (0.20 mg, 4.7 mmol) was added. After heating at 50 °C for 45 minutes the reaction was transferred to a separating funnel containing 25 mL H₂O and extracted with CH₂Cl₂ (3 × 25 mL). The organic layers were combined, dried over anhydrous MgSO₄, filtered and concentrated under reduced pressure. The crude residue was purified by gradient silica gel column chromatography (100% pet. spirit to 20% EtOAc: 80% pet. spirit) to give **1** (0.19 g, 80% over 2 steps) as a red solid. (Note: The bis-mesylate is highly unstable when isolated in pure form after silica gel column chromatography and is best used in crude form).

R_f = 0.81 (50% EtOAc: 50% pet. spirit). **M.P.** 180-182 °C.

IR: (solid, v/cm⁻¹) 3402, 2921, 2852, 1647, 1521, 1513,

1460, 1353, 1322, 1235, 1178, 1150, 747. **¹H NMR** (500

MHz, CDCl₃) δ 12.04 (s, 1H), 8.03 (dd, *J* = 8.1, 0.8 Hz, 1H),

7.70 (td, *J* = 7.5, 1.1 Hz, 1H), 7.60 (dd, *J* = 7.5, 0.9 Hz, 1H), 7.56 (td, *J* = 7.8, 1.2 Hz,

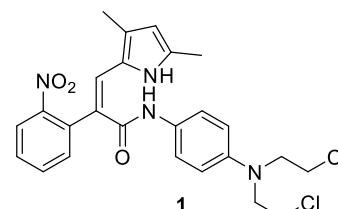
1H), 7.21 (d, *J* = 8.9 Hz, 2H), 6.68 (s, 1H), 6.64 (d, *J* = 9.0 Hz, 2H), 6.55 (s, 1H), 5.83 (d,

J = 2.0 Hz, 1H), 3.70 (t, *J* = 7.0 Hz, 4H), 3.60 (t, *J* = 6.9 Hz, 4H), 2.28 (s, 3H), 2.11 (s,

3H). **¹³C NMR** (126 MHz, CDCl₃) δ 166.9, 149.8, 144.0, 136.3, 133.8, 133.7, 133.7,

130.0, 129.2, 129.2, 127.8, 125.0, 124.6, 124.3, 115.9, 112.6, 111.1, 53.8, 40.6, 13.8,

11.6. **HREI-MS:** *m/z* calculated for C₂₅H₂₇Cl₂N₄O₃ [M+H⁺] 501.1455; observed 501.1455.



7.9 Synthesis of 1-((2R,4S,5R)-4-((tert-butyldimethylsilyl)oxy)-5-(((tert-butyldimethylsilyl)oxy)methyl)tetrahydrofuran-2-yl)-5-fluoropyrimidine-2,4(1H,3H)-dione **14**

A solution of TBDMSCl (45.91 g, 304.6 mmol) and imidazole (24.27 g, 356.6 mmol) in CH₂Cl₂ (200 mL) under argon was cooled to 0 °C for 10 minutes.

2'-Deoxy-5-fluorouridine (24.88 g, 101.1 mmol) dissolved in CH₂Cl₂ (100 mL) was added slowly, the reaction allowed to warm to room temperature and monitored by TLC (30% EtOAc: 70% pet. spirit). After 20 hours, the reaction mixture was placed in a freezer (-20 °C) for 30 minutes (to precipitate the imidazole·HCl). The imidazole·HCl was filtered off and the filtrate washed with cold CH₂Cl₂ (2 × 25 mL). The filtrate was transferred to a separating funnel and washed with saturated NaHCO_{3(aq)} (3 × 100 mL) and saturated NaCl_(aq) (1 × 100 mL), dried over anhydrous MgSO₄ and concentrated *in vacuo*. The crude residue was purified by recrystallisation from hot pet. spirit to yield **14** as a white solid (46.8 g, 97%).

R_f = 0.78 (30% EtOAc: 70% pet. spirit). **M.P.** 82-86 °C; **O.R.**

$[\alpha]_D^{25} = + 18.8$ (*c* 1.00, CHCl₃). **IR** (solid, v/cm⁻¹): 3469, 3360,

2952, 1737, 1655, 1628, 1592, 1504, 1472, 1458, 1436, 1372,

1317, 1255, 1144, 1091, 1066, 1025, 974, 884, 830, 783, 740, 676. **¹H NMR** (500 MHz,

CDCl₃) δ 9.44 (br. s, 1H), 8.05 (d, *J* = 6.2 Hz, 1H), 6.29 (td, *J* = 6.3, 1.5 Hz, 1H), 4.40

(dt, *J* = 6.0, 4.9 Hz, 1H), 3.95-3.90 (m, 2H), 3.76 (dd, *J* = 11.9, 2.2 Hz, 1H), 2.31 (ddd, *J*

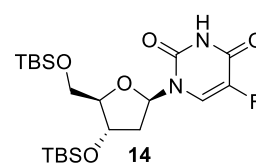
= 13.3, 6.1, 3.9 Hz, 1H), 2.05 (dt, *J* = 13.1, 6.4 Hz, 1H), 0.92 (s, 9H), 0.88 (s, 9H), 0.12

(d, *J* = 3.6 Hz, 6H), 0.07 (d, *J* = 3.0 Hz, 6H). **¹³C NMR** (126 MHz, CDCl₃) δ 157.1 (d, *J*

= 26.8 Hz), 149.0, 140.7 (d, *J* = 236.2 Hz), 124.4 (d, *J* = 34.1 Hz), 88.2, 85.7, 71.7, 62.8,

41.0, 26.0, 25.8, 18.5, 18.1, -4.5, -4.7, -5.4, -5.5. **HREI-MS**: *m/z* calculated for

C₂₁H₄₀FN₂O₅Si₂ [M+H⁺] 475.2454; observed 475.2460.



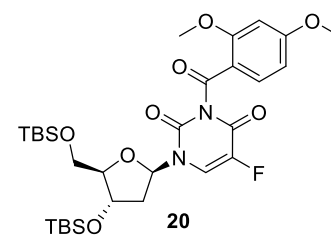
7.10 Synthesis of 1-((2*R*,4*S*,5*R*)-4-((*tert*-butyldimethylsilyl)oxy)-5-(((*tert*-butyldimethylsilyl)oxy)methyl)tetrahydrofuran-2-yl)-3-(2,4-dimethoxybenzoyl)-5-fluoropyrimidine-2,4(1*H*,3*H*)-dione **20**

2,4-Dimethoxybenzoyl chloride (79.10 g, 394.3 mmol) and DMAP (4.82 g, 39.4 mmol) were dissolved in 150 mL of CH₂Cl₂ under argon. DIPEA (68.7 mL, 394.3 mmol) was added slowly, and the reaction was heated at 45 °C for 15 minutes causing a deep red colour to develop. A solution of **14** (46.79 g, 98.6 mmol) in 100 mL of CHCl₃ was slowly added and the reaction heated at 45 °C with monitoring by TLC (0.5% MeOH: 99.5% CHCl₃). After 16 hours, the reaction was transferred to a separating funnel and washed with saturated NaHCO_{3(aq)} (3 × 250 mL), 1 M aqueous HCl (3 × 250 mL), and saturated NaCl_(aq) (1 × 250 mL). The organic layer was separated, dried over anhydrous MgSO₄

and concentrated *in vacuo*. The crude residue was purified by silica gel column chromatography (20% EtOAc: 80% pet. spirit) to yield **20** as a white solid (54.7 g, 87%).

R_f = 0.61 (30% EtOAc: 70% pet. spirit). **M.P.** 56-60 °C; **O.R.**

$[\alpha]_D^{25} = +15.3$ (*c* 1.00, CHCl₃). **IR** (solid, v/cm⁻¹): 2955, 2930, 2857, 1738, 1701, 1666, 1602, 1571, 1459, 1396, 1341, 1290, 1273, 1249, 1214, 1193, 1165, 1106, 1067, 1024, 965, 939, 913, 882, 830, 812, 778, 752, 729, 717, 706, 669, 647,



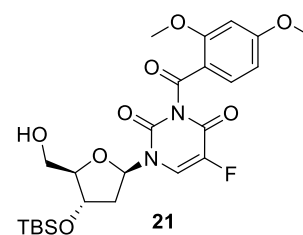
634. **¹H NMR** (500 MHz, CDCl₃) δ 8.08 (d, *J* = 6.2 Hz, 1H), 8.07 (d, *J* = 8.9 Hz, 1H), 6.59 (dd, *J* = 8.9, 2.2 Hz, 1H), 6.38 (d, *J* = 2.2 Hz, 1H), 6.29 (td, *J* = 6.3, 1.3 Hz, 1H), 4.41 (dt, *J* = 5.7, 3.3 Hz, 1H), 3.96-3.93 (m, 2H), 3.85 (s, 3H), 3.78 (dd, *J* = 12.0, 2.4 Hz, 1H), 3.76 (s, 3H), 2.31 (ddd, *J* = 13.1, 6.0, 3.7 Hz, 1H), 2.06 (dt, *J* = 13.2, 6.2 Hz, 1H), 0.94 (s, 9H), 0.87 (s, 9H), 0.15 (s, 3H), 0.14 (s, 3H), 0.07 (s, 6H). **¹³C NMR** (126 MHz, CDCl₃) δ 167.0, 163.9, 161.9, 156.2 (d, *J* = 27.8 Hz), 148.1, 140.5 (d, *J* = 237.4 Hz), 136.4, 123.3 (d, *J* = 43.5 Hz), 113.3, 106.9, 98.9, 88.3, 85.8, 71.8, 62.9, 56.4, 55.9, 41.9, 26.0, 25.8, 18.6, 18.1, -4.5, -4.7, -5.4. **HREI-MS**: *m/z* calculated for C₃₀H₄₈FN₂O₈Si₂ [M+H⁺] 639.2928; observed 639.2933.

7.11 Synthesis of 1-((2*R*,4*S*,5*R*)-4-((*tert*-butyldimethylsilyl)oxy)-5-(hydroxymethyl)tetrahydrofuran-2-yl)-3-(2,4-dimethoxybenzoyl)-5-fluoropyrimidine-2,4(1*H*,3*H*)-dione **21**

A solution of **20** (17.85 g, 27.9 mmol) in 168 mL of THF was cooled to 0 °C for 10 minutes. Trichloroacetic acid (89.05 g, 545.3 mmol) in 42 mL H₂O was added slowly and the reaction monitored by TLC (30% EtOAc: 70% pet. spirit). After 4 hours, the reaction was quenched slowly with saturated NaHCO_{3(aq)} (200 mL) and extracted with CH₂Cl₂ (3 × 200 mL). The organic fractions were combined, dried over anhydrous MgSO₄ and concentrated *in vacuo*. The crude residue was purified by silica gel column chromatography (100% pet. spirit to 60% EtOAc: 40% pet. spirit) to give **21** as a white solid (7.33 g, 50%).

R_f = 0.09 (30% EtOAc: 70% pet. spirit). **M.P.** 70-74 °C; **O.R.**

$[\alpha]_D^{25} = +10.8$ (*c* 1.00, CHCl₃). **IR**: (solid, v/cm⁻¹) 2952, 1931, 2899, 2888, 2857, 2362, 1734, 1699, 1693, 1683, 1681, 1656, 1601, 1570, 1542, 1506, 1499, 1491, 1458, 1439, 1421, 1397, 1359, 1342, 1274, 1246, 1213, 1190, 1166, 1133, 1099, 1063,



1021, 993, 943, 906, 870, 832, 779, 753, 729, 719, 684, 671, 661, 647, 631, 628, 620,

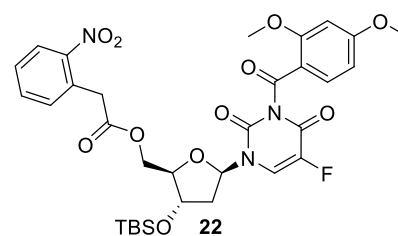
605. $^1\text{H NMR}$ (500 MHz, CDCl_3) δ 8.07 (d, $J = 8.9$ Hz, 1H), 8.06 (d, $J = 6.3$ Hz, 1H), 6.60 (dd, $J = 8.9, 2.2$ Hz, 1H), 6.38 (d, $J = 2.1$ Hz, 1H), 6.22 (t, $J = 6.4$ Hz, 1H), 4.47 (dt, $J = 5.7, 3.4$ Hz, 1H), 3.96-3.90 (m, 2H), 3.86 (s, 3H), 3.78 (dd, $J = 11.2, 1.9$ Hz, 1H), 3.76 (s, 3H), 2.28 (ddd, $J = 13.3, 6.1, 3.7$ Hz, 1H), 2.20 (dt, $J = 13.3, 6.4$ Hz, 1H), 0.87 (s, 9H), 0.07 (s, 6H). $^{13}\text{C NMR}$ (126 MHz, CDCl_3) δ 167.2, 163.8, 161.9, 156.4 (d, $J = 27.4$ Hz), 148.2, 140.5 (d, $J = 238.8$ Hz), 136.4, 124.3 (d, $J = 34.4$ Hz), 113.1, 107.0, 98.8, 88.0, 86.6, 71.9, 62.0, 56.4, 55.9, 41.5, 25.8, 18.0, -4.6, -4.8. **HREI-MS**: m/z calculated for $\text{C}_{24}\text{H}_{34}\text{FN}_2\text{O}_8\text{Si}$ [$\text{M}+\text{H}^+$] 525.2063; observed 525.2068.

7.12 Synthesis of ((2*R*,3*S*,5*R*)-3-((*tert*-butyldimethylsilyloxy)-5-(3-(2,4-dimethoxybenzoyl)-5-fluoro-2,4-dioxo-3,4-dihydropyrimidin-1(2*H*)-yl)tetrahydrofuran-2-yl)methyl 2-(2-nitrophenyl)acetate **22**

A solution of **21** (9.34 g, 17.8 mmol), 2-(2-nitrophenyl)acetic acid (3.87 g, 21.4 mmol) and DMAP (0.934 g, 7.64 mmol) in 250 mL of CH_2Cl_2 under argon was cooled to 0 °C. A solution of DCC (4.41 g, 21.4 mmol) in 50 mL of CH_2Cl_2 was added slowly and the reaction stirred at 0 °C and monitored by TLC (50% EtOAc: 50% pet. spirit). After 4 hours, the reaction was placed in a freezer (-20 °C) overnight (to precipitate the DCU by-product). The urea by-product was filtered off and the residue washed with cold CH_2Cl_2 (2 \times 50 mL). The organic layer was transferred to a separating funnel and washed with saturated $\text{NaHCO}_3(\text{aq})$ (3 \times 200 mL), 1 M aqueous HCl (3 \times 200 mL) and saturated $\text{NaCl}(\text{aq})$ solution (1 \times 200 mL). The organic layer was dried over anhydrous MgSO_4 , filtered and concentrated *in vacuo*. The crude residue was purified by gradient silica gel column chromatography (100% pet. spirit to 60% EtOAc: 40% pet. spirit) to afford **22** as a white solid (10.5 g, 87%).

$R_f = 0.57$ (50% EtOAc: 50% pet. spirit). **M.P.** 60-64 °C;

O.R. $[\alpha]_D^{25} = +15.8$ (c 1.00, CHCl_3). **IR**: (solid, v/cm^{-1}) 2958, 2930, 2903, 2856, 2361, 1735, 1700, 1693, 1684, 1665, 1639, 1601, 1570, 1562, 1541, 1526, 1507, 1499, 1489, 1468, 1457, 1439, 1420, 1397, 1373, 1344,



1274, 1255, 1212, 1194, 1166, 1132, 1101, 1087, 1019, 960, 880, 862, 832, 812, 782, 751, 718, 668, 621, 614, 608. $^1\text{H NMR}$ (500 MHz, CDCl_3) δ 8.17 (dd, $J = 8.2, 1.0$ Hz, 1H), 8.08 (d, $J = 8.9$ Hz, 1H), 7.65 (td, $J = 7.5, 1.1$ Hz, 1H), 7.62 (d, $J = 6.2$ Hz, 1H), 7.53 (td, $J = 7.8, 1.2$ Hz, 1H), 7.41 (d, $J = 7.5$ Hz, 1H), 6.60 (dd, $J = 8.9, 2.2$ Hz, 1H), 6.39 (d, $J = 2.1$ Hz, 1H), 6.20 (t, $J = 5.8$ Hz, 1H), 4.44 (dd, $J = 12.4, 3.0$ Hz, 1H), 4.34-4.29 (m,

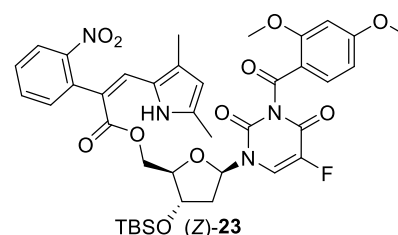
2H), 4.13-4.03 (m, 3H), 3.86 (s, 3H), 3.77 (s, 3H), 2.28 (ddd, $J = 13.5, 5.9, 3.8$ Hz, 1H), 1.85 (dt, $J = 13.1, 6.1$ Hz, 1H), 0.86 (s, 9H), 0.06 (s, 3H), 0.05 (s, 3H). $^{13}\text{C NMR}$ (126 MHz, CDCl_3) δ 169.6, 167.2, 163.7, 161.9, 156.0 (d, $J = 26.2$ Hz), 148.5, 147.9, 140.4 (d, $J = 239.1$ Hz), 136.5, 134.3, 133.7, 129.4, 129.3, 125.6, 122.9 (d, $J = 34.3$ Hz), 113.0, 106.9, 98.8, 85.7, 85.2, 71.4, 63.9, 56.5, 55.9, 41.3, 40.2, 25.7, 18.0, -4.7, -4.9. **HREI-MS**: m/z calculated for $\text{C}_{32}\text{H}_{39}\text{FN}_3\text{O}_{11}\text{Si}$ [$\text{M}+\text{H}^+$] 688.2332; observed 688.2338.

7.13 Synthesis of ((2*R*,3*S*,5*R*)-3-((*tert*-butyldimethylsilyloxy)-5-(3-(2,4-dimethoxybenzoyl)-5-fluoro-2,4-dioxo-3,4-dihydropyrimidin-1(2*H*)-yl)tetrahydrofuran-2-yl)methyl (*Z*)-3-(3,5-dimethyl-1*H*-pyrrol-2-yl)-2-(2-nitrophenyl)acrylate (*Z*)-23

A solution K_2CO_3 (2.05 g, 14.7 mmol) and 18-crown-6 (0.962 g, 3.64 mmol) in 50 mL dry THF under argon was heated at 75 °C for 1 hour. A solution of **22** (5.00 g, 7.27 mmol) in 25 mL dry THF was added slowly to the reaction and a deep blue colour appeared. After 1 hour of additional heating, a solution of **7** (1.48 g, 8.15 mmol) in 25 mL dry THF was added slowly and the reaction was continued at reflux with monitoring by TLC (30% EtOAc: 70% pet. spirit). After 18 hours, the reaction was concentrated under reduced pressure to less than 50 mL and transferred to a separating funnel containing 100 mL of H_2O . The mixture was extracted with EtOAc (3×50 mL) and the organic layers combined, washed with saturated $\text{NaHCO}_{3(\text{aq})}$ (3×100 mL), saturated $\text{NaCl}_{(\text{aq})}$ (1×100 mL), dried over anhydrous MgSO_4 and concentrated *in vacuo*. The crude residue was purified by silica gel column chromatography (100% pet. spirit to 60% EtOAc: 40% pet. spirit) to give one fraction containing (*Z*)-**23** with side product **25** and a second fraction containing (*E*)-**23**, along with recovered starting material **22**. The first fraction was further purified by silica gel column chromatography (100% CHCl_3) to yield *cis* product (*Z*)-**23** as a red solid (0.551 g, 10%) and side product **25** as a red solid (0.851 g, 20%). The second fraction was further purified by silica gel column chromatography (100% CHCl_3) to yield *trans* product (*E*)-**23** as a red solid (0.605 g, 11%) and recovered starting material **22** (2.77 g, 55%).

$R_f = 0.56$ (30% EtOAc: 70% pet. spirit). **M.P.** 96-98 °C;

O.R. $[\alpha]_D^{25} = +41.0$ (c 0.10, CHCl_3). **IR**: (solid, v/cm^{-1}) 2951, 2928, 2856, 1739, 1667, 1602, 1571, 1544, 1523, 1457, 1395, 1344, 1248, 1213, 1182, 1146, 1131, 1109, 1084, 1020, 990, 941, 921, 892, 857, 832, 781,



753, 728, 710, 666, 643, 619, 610, 608, 597, 582, 555, 535. $^1\text{H NMR}$ (500 MHz, CDCl_3)

δ 11.73 (br. s, 1H), 8.07 (dd, $J = 8.2, 0.9$ Hz, 1H), 8.06 (d, $J = 8.9$ Hz, 1H), 7.67 (t, $J = 7.4$ Hz, 1H), 7.50 (dt, $J = 7.1, 5.3$ Hz, 1H), 7.00 (d, $J = 4.5$ Hz, 1H), 6.85 (s, 1H), 6.59 (dd, $J = 8.9, 2.1$ Hz, 1H), 6.36 (d, $J = 2.0$ Hz, 1H), 6.12 (t, $J = 6.5$ Hz, 1H), 5.94 (d, $J = 1.5$ Hz, 1H), 4.37 (d, $J = 12.1$ Hz, 1H), 4.18 (d, $J = 12.1$ Hz, 1H), 4.14-4.02 (m, 2H), 3.85 (s, 3H), 3.71 (s, 3H), 2.36 (s, 3H), 2.35-2.19 (m, 1H), 2.18 (s, 3H), 1.97-1.88 (m, 1H), 0.85 (s, 9H), 0.05 (s, 3H), 0.04 (s, 3H). ^{13}C NMR (126 MHz, CDCl_3) δ 167.4, 167.2, 163.7, 161.9, 155.9 (d, $J = 25.6$ Hz), 148.8, 147.9, 140.2 (d, $J = 234.0$ Hz), 137.0, 136.5, 135.5, 134.3, 133.0, 132.9, 132.6, 128.5, 124.6, 124.6, 122.7 (d, $J = 33.6$ Hz), 113.1, 112.1, 111.8, 106.9, 98.9, 85.7, 85.4, 72.8, 64.7, 56.4, 55.9, 41.0, 25.8, 18.0, 13.8, 11.7, -4.7, -4.9. **HREI-MS**: m/z calculated for $\text{C}_{39}\text{H}_{46}\text{FN}_4\text{O}_{11}\text{Si}$ [$\text{M}+\text{H}^+$] 793.2911; observed 793.2916.

R_f = 0.34 (30% EtOAc: 70% pet. spirit). **M.P.** 76-78

$^{\circ}\text{C}$; **O.R.** $[\alpha]_D^{25} = -3.2$ (c 0.10, CHCl_3). **IR**: (solid,

v/cm^{-1}) 2953, 2926, 2854, 1737, 1698, 1665, 1601,

1569, 1557, 1525, 1504, 1489, 1457, 1424, 1397, 1379,

1344, 1274, 1248, 1219, 1170, 1147, 1132, 1111, 1085,

1021, 940, 896, 880, 856, 832, 813, 780, 752, 719, 700, 667, 646, 616, 609, 604. ^1H NMR

(500 MHz, CDCl_3) δ 8.20 (dd, $J = 8.1, 1.2$ Hz, 1H), 8.06 (d, $J = 8.9$ Hz, 1H), 7.84 (s, 1H),

7.75 (td, $J = 7.5, 0.9$ Hz, 1H), 7.67 (td, $J = 7.9, 1.5$ Hz, 1H), 7.56 (dd, $J = 7.5, 1.3$ Hz,

1H), 7.04 (d, $J = 6.0$ Hz, 1H), 6.71 (br. s, 1H), 6.59 (dd, $J = 8.9, 2.2$ Hz, 1H), 6.37 (d, $J =$

2.3 Hz, 1H), 6.11 (t, $J = 7.0$ Hz, 1H), 5.77 (d, $J = 2.1$ Hz, 1H), 4.40 (dd, $J = 12.6, 2.1$ Hz,

1H), 4.22 (dd, $J = 12.6, 2.4$ Hz, 1H), 4.18-4.15 (m, 1H), 4.09-4.07 (m, 1H), 3.86 (s, 3H),

3.73 (s, 3H), 2.33-2.27 (m, 1H), 2.21 (s, 3H), 1.97 (s, 3H), 1.85-1.77 (m, 1H), 0.85 (s,

9H), 0.06 (s, 3H), 0.05 (s, 3H). ^{13}C NMR (126 MHz, CDCl_3) δ 167.2, 166.6, 163.7, 161.9,

156.0 (d, $J = 27.8$ Hz), 149.3, 147.8, 140.2 (d, $J = 237.8$ Hz), 136.4, 135.3, 134.4, 133.3,

132.3, 132.2, 130.1, 129.5, 125.4, 123.6, 122.7 (d, $J = 33.6$ Hz), 113.8, 112.9, 111.4,

106.9, 98.8, 86.0, 85.6, 72.8, 64.9, 56.4, 55.9, 41.3, 25.8, 18.0, 13.5, 11.6, -4.8, -4.9.

HREI-MS: m/z calculated for $\text{C}_{39}\text{H}_{46}\text{FN}_4\text{O}_{11}\text{Si}$ [$\text{M}+\text{H}^+$] 793.2911; observed 793. 2916.

R_f = 0.34 (30% EtOAc: 70% pet. spirit). **M.P.** 55-57 $^{\circ}\text{C}$;

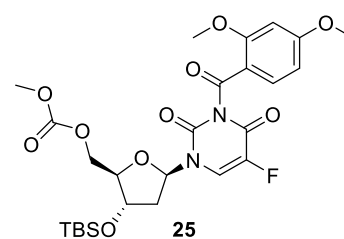
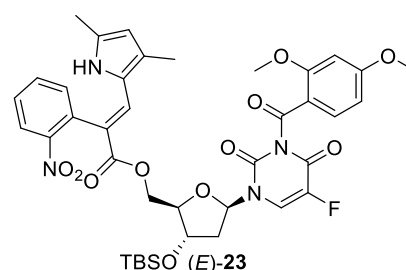
O.R. $[\alpha]_D^{25} = +13.6$ (c 1.00, CHCl_3). **IR**: (solid, v/cm^{-1})

2955, 2927, 2856, 1738, 1665, 1601, 1570, 1504, 1457,

1397, 1355, 1277, 1248, 1213, 1166, 1131, 1078, 1020, 965,

938, 865, 832, 780, 751, 670, 646. ^1H NMR (500 MHz,

CDCl_3) δ 8.08 (d, $J = 8.8$ Hz, 1H), 7.69 (d, $J = 5.9$ Hz, 1H), 6.60 (d, $J = 8.8$ Hz, 1H), 6.38



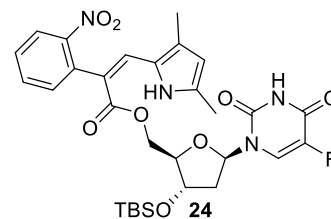
(s, 1H), 6.30 (t, $J = 5.9$ Hz, 1H), 4.43 (d, $J = 11.9$ Hz, 1H), 4.40-4.36 (m, 1H), 4.30 (d, $J = 11.9$ Hz, 1H), 4.09-4.06 (m, 1H), 3.86 (s, 3H), 3.85 (s, 3H), 3.76 (s, 3H), 2.37-2.29 (m, 1H), 2.14-2.06 (m, 1H), 0.87 (s, 9H), 0.07 (s, 6H). ^{13}C NMR (126 MHz, CDCl_3) δ 167.1, 163.7, 161.9, 156.0 (d, $J = 27.7$ Hz), 155.5, 148.1, 140.7 (d, $J = 238.6$ Hz), 136.5, 122.9 (d, $J = 34.4$ Hz), 113.2, 106.9, 98.9, 85.7, 85.1, 71.9, 66.6, 56.4, 55.9, 55.4, 41.2, 25.8, 18.0, -4.6, -4.8. **HREI-MS**: m/z calculated for $\text{C}_{26}\text{H}_{35}\text{FN}_2\text{O}_{10}\text{SiNa}$ [$\text{M}+\text{Na}^+$] 605.1937; observed 605.1943.

7.14 Synthesis of ((2*R*,3*S*,5*R*)-3-((*tert*-butyldimethylsilyloxy)-5-(5-fluoro-2,4-dioxo-3,4-dihydropyrimidin-1(2*H*)-yl)tetrahydrofuran-2-yl)methyl (*Z*)-3-(3,5-dimethyl-1*H*-pyrrol-2-yl)-2-(2-nitrophenyl)acrylate **24**

A solution of (*Z*)-**23** (0.300 g, 0.378 mmol) in 6 mL ammonia solution (7 N in methanol) at 0 °C was prepared and the reaction monitored by TLC (30% EtOAc: 70% pet. spirit). After 2 hours, the reaction was concentrated *in vacuo* and the crude residue was purified by gradient silica gel column chromatography (100% pet. spirit to 40% EtOAc: 60% pet. spirit) to yield **24** as a red solid (0.179 g, 75%).

$R_f = 0.32$ (30% EtOAc: 70% pet. spirit). **M.P.** 86-88 °C; **O.R.**

$[\alpha]_D^{25} = +8.0$ (c 0.10, CHCl_3). **IR**: (solid, v/cm^{-1}) 2953, 2928, 2857, 1751, 1702, 1606, 1573, 1560, 1543, 1523, 1464, 1441, 1401, 1391, 1349, 1315, 1266, 1249, 1182, 1148, 1129, 1104, 1081, 1049, 1024, 1006, 970, 940, 883, 858, 831, 913, 778,

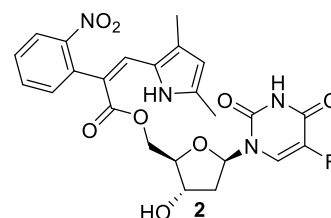


754, 711, 688, 670, 637, 617, 610. ^1H NMR (500 MHz, CDCl_3) δ 11.71 (br s, 1H), 8.43 (s, 1H), 8.05 (dd, $J = 8.1, 0.7$ Hz, 1H), 7.62 (t, $J = 7.2$ Hz, 1H), 7.48 (d, $J = 8.3$ Hz, 1H), 7.45 (t, $J = 7.6$ Hz, 1H), 6.95 (d, $J = 4.9$ Hz, 1H), 6.83 (s, 1H), 6.11 (t, $J = 7.0$ Hz, 1H), 5.93 (d, $J = 1.9$ Hz, 1H), 4.35 (d, $J = 11.1$ Hz, 1H), 4.18 (d, $J = 12.2$ Hz, 1H), 4.13-4.09 (m, 1H), 4.05-4.03 (m, 1H), 2.36 (s, 3H), 2.34-2.24 (m, 1H), 2.17 (s, 3H), 1.97-1.89 (m, 1H), 0.87 (s, 9H), 0.07 (s, 3H), 0.06 (s, 3H). ^{13}C NMR (126 MHz, CDCl_3) δ 167.3, 156.5 (d, $J = 28.2$ Hz), 148.8, 148.4, 140.3 (d, $J = 237.2$ Hz), 137.1, 135.5, 134.1, 133.0, 132.9, 132.6, 128.4, 124.6, 124.6, 123.7 (d, $J = 33.5$ Hz), 112.1, 111.7, 85.7, 85.2, 72.7, 64.6, 40.9, 25.8, 18.1, 13.9, 11.7, -4.7, -4.8. **HREI-MS**: m/z calculated for $\text{C}_{30}\text{H}_{38}\text{FN}_4\text{O}_8\text{Si}$ [$\text{M}+\text{H}^+$] 629.2437; observed 629.2443.

7.15 Synthesis of ((2*R*,3*S*,5*R*)-5-(5-fluoro-2,4-dioxo-3,4-dihydropyrimidin-1(2*H*)-yl)-3-hydroxytetrahydrofuran-2-yl)methyl (*Z*)-3-(3,5-dimethyl-1*H*-pyrrol-2-yl)-2-(2-nitrophenyl)acrylate **2**

A solution of **24** (0.177 g, 0.28 mmol) in 10 mL dry THF was prepared and cooled to 0 °C. A mixture of 1 M TBAF in THF (1.50 mL, 1.50 mmol) and glacial acetic acid (0.300 mL, 5.25 mmol) was prepared and slowly added to the reaction. The reaction was monitored via mini-extractions (H₂O/EtOAc) followed by TLC (50% EtOAc: 50% pet. spirit). After 24 hours, the reaction was transferred to a separating funnel and 50 mL of EtOAc was added. The organic layer was washed with H₂O (3 × 50 mL) and saturated NaCl_(aq) (1 × 50 mL), dried over anhydrous MgSO₄ and concentrated *in vacuo*. The crude residue was purified by gradient silica gel column chromatography (100% pet. spirit to 50% acetone:50% pet. spirit) to yield **2** as a red solid (0.099 g, 69%).

R_f = 0.69 (EtOAc). **M.P.** 89-91 °C; **O.R.** $[\alpha]_D^{25} = +54.3$ (*c* 0.10, CHCl₃). **IR:** (solid, v/cm⁻¹) 2954, 2929, 2856, 1692, 1607, 1572, 1560, 1543, 1522, 1502, 1471, 1441, 1393, 1341, 1315, 1265, 1180, 1149, 1129, 1101, 1080, 1047, 1025, 1006,

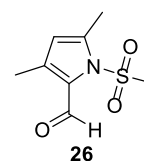


983, 970, 939, 922, 881, 858, 830, 810, 788, 779, 753, 711, 667, 650, 637, 617, 610. **¹H NMR** (500 MHz, CDCl₃) δ 11.66 (br s, 1H), 8.02 (d, *J* = 8.1 Hz, 1H), 7.61 (t, *J* = 7.4 Hz, 1H), 7.46 (d, *J* = 7.6 Hz, 1H), 7.42 (t, *J* = 7.8 Hz, 1H), 7.01 (s, 1H), 6.81 (s, 1H), 6.10 (t, *J* = 6.5 Hz, 1H), 5.91 (s, 1H), 4.31 (d, *J* = 11.3 Hz, 1H), 4.24 (d, *J* = 11.5 Hz, 1H), 4.16-4.07 (m, 2H), 2.33 (s, 3H), 4.18-4.13 (m, 5H). **¹³C NMR** (126 MHz, CDCl₃) δ 167.4, 157.2 (d, *J* = 27.0 Hz), 149.0, 148.5, 140.4 (d, *J* = 236.7 Hz), 136.9, 135.4, 134.2, 132.9, 132.8, 132.4, 128.4, 124.6, 124.5, 123.7 (d, *J* = 33.3 Hz), 112.0, 111.9, 85.3, 84.8, 71.9, 64.6, 40.1, 13.8, 11.6. **HREI-MS:** *m/z* calculated for C₂₄H₂₄FN₄O₈ [M+H⁺] 515.1573; observed 515.1578.

7.16 Characterisation of Side Product 3,5-dimethyl-1-(methylsulfonyl)-1*H*-pyrrole-2-carbaldehyde **26**

R_f = 0.29 (20% EtOAc: 80% pet. spirit). **M.P.** 58-61 °C; **IR** (solid, v/cm⁻¹):

3009, 2959, 2927, 2871, 2859, 1724, 1651, 1573, 1481, 1439, 1424, 1379, 1357, 1337, 1289, 1230, 1175, 1154, 1073, 1048, 1004, 969, 891, 871, 858, 853, 826, 784, 766, 746, 708, 674, 662, 647, 625, 611, 608, 606. **¹H NMR**

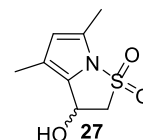


(500 MHz, CDCl₃) δ 9.91 (s, 1H), 5.97 (s, 1H), 3.42 (s, 3H), 2.46 (s, 3H), 2.33 (s, 3H).

^{13}C NMR (126 MHz, CDCl_3) δ 179.0, 140.9, 138.8, 130.7, 117.1, 43.5, 15.6, 12.6. **HREI-MS**: m/z calculated for $\text{C}_8\text{H}_{12}\text{NO}_3\text{S}$ [$\text{M}+\text{H}^+$] 202.0532; observed 202.0534.

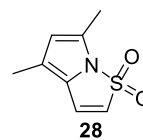
7.17 Characterisation of Side Product 4,6-dimethylpyrrolo[1,2-*b*]isothiazole 1,1-dioxide **27**

R_f = 0.20 (20% EtOAc: 80% pet. spirit). ^1H NMR (400 MHz, CDCl_3) δ 5.89 (s, 1H), 5.31 (d, J = 6.1 Hz, 1H), 4.04 (dd, J = 13.7, 6.3 Hz, 1H), 3.74 (dd, J = 13.7, 1.2 Hz, 1H), 2.88 (br s, 1H), 2.35 (s, 3H), 2.03 (s, 3H). ^{13}C NMR (126 MHz, CDCl_3) δ 128.6, 126.1, 117.7, 117.2, 63.1, 61.5, 11.3, 10.1.



7.18 Characterisation of Side Product 4,6-dimethylpyrrolo[1,2-*b*]isothiazole 1,1-dioxide **28**

R_f = 0.69 (20% EtOAc: 80% pet. spirit). **M.P.** 68-70 °C; **IR** (solid, v/cm^{-1}): 3096, 2925, 1605, 1526, 1516, 1512, 1394, 1371, 1337, 1310, 1298, 1264, 1158, 1143, 1094, 1073, 1038, 996, 901, 800, 792, 694, 680, 628, 613. ^1H NMR (500 MHz, CDCl_3) δ 7.04 (d, J = 6.6 Hz, 1H), 6.24 (d, J = 6.6 Hz, 1H), 5.80 (s, 1H), 2.46 (s, 3H), 2.03 (s, 3H). ^{13}C NMR (126 MHz, CDCl_3) δ 134.5, 126.3, 126.2, 122.4, 122.1, 116.8, 11.7, 10.5. **HREI-MS**: m/z calculated for $\text{C}_8\text{H}_{10}\text{NO}_2\text{S}$ [$\text{M}+\text{H}^+$] 184.0427; observed 184.0428.



7.19 Proof of Concept Chemical Reductions with Fe(0) in CH_3COOH

A mixture of **2** (0.030 g, 0.058 mmol) and Fe(0) (0.033 g, 0.584 mmol) was dissolved in 6 mL $\text{CH}_3\text{COOH}:\text{EtOH}:\text{H}_2\text{O}$ (1:1:1) and sonicated for 1 hour at room temperature. After consumption of starting material (TLC analysis), the reaction was filtered through celite and washed with EtOH (30 mL). The mixture was concentrated under vacuum and redissolved in Et_2O (30 mL). The organic layer was extracted with 1 M $\text{NaOH}_{(\text{aq})}$ (3×30 mL). The organic and aqueous layers were separated. The organic layer was dried over anhydrous MgSO_4 , filtered and concentrated *in vacuo* to give crude **3**. The aqueous layer was acidified with 1 M $\text{HCl}_{(\text{aq})}$ (100 mL) and extracted with Et_2O (2×30 mL). The organic layers were combined, dried over anhydrous MgSO_4 , filtered and concentrated *in vacuo* to give crude **29**. The crude products were purified by preparative TLC (20% acetone: 80% pet. spirit) to yield **3** as a yellow solid (11.6 mg, 84%) and **29** as a yellow solid (1.6 mg, 11%). The same procedure with **1** yielded **3** (11.4 mg, 80%) and **29** (2.1 mg, 14%).

7.20 Proof of Concept Chemical Reductions with FeCl₃·6H₂O/Zn

A mixture of **2** (0.030 g, 0.058 mmol), FeCl₃·6H₂O (0.076 g, 0.281 mmol) and Zn(0) dust (0.078 g, 1.198 mmol) was dissolved in 3 mL DMF:H₂O (1:1) and stirred for 3 hours at room temperature. After consumption of starting material (TLC analysis), the reaction was filtered through celite and washed with Et₂O (30 mL). The organic layer was extracted with 1 M NaOH_(aq) (3 × 30 mL) and the organic and aqueous layers collected separately. The organic layer was dried over anhydrous MgSO₄, filtered and concentrated *in vacuo* to give crude **3**. The aqueous layer was acidified with 1 M HCl_(aq) (100 mL) and extracted with Et₂O (2 × 30 mL). The organic layers were combined, dried over anhydrous MgSO₄, filtered and concentrated *in vacuo* to give crude **29**. The crude products were purified by preparative TLC (20% acetone: 80% pet. spirit) to yield **3** as a yellow solid (5.9 mg, 40%) and **29** as a yellow solid (7.1 mg, 51%). The same procedure with **1** yielded **3** (7.6 mg, 53%) and **29** (4.8 mg, 32%).

7.21 Proof of Concept Chemical Reductions with NaBH₄/Pd-C

A mixture of **2** (0.030 g, 0.058 mmol), NaBH₄ (0.022 g, 0.582 mmol) and Pd-C (0.020 g) was dissolved in 6 mL MeOH:H₂O (2:1) and stirred for 30 minutes at room temperature. After consumption of starting material (TLC analysis), the reaction was filtered through celite and washed with Et₂O (30 mL). The organic layer was extracted with 1 M NaOH_(aq) (3 × 30 mL) and the organic and aqueous layers collected separately. The organic layer was dried over anhydrous MgSO₄, filtered and concentrated *in vacuo* to give crude **3**. The aqueous layer was acidified with 1 M HCl_(aq) (100 mL) and extracted with Et₂O (2 × 30 mL). The organic layers were combined, dried over anhydrous MgSO₄, filtered and concentrated *in vacuo* to give crude **29**. The crude products were purified by preparative TLC (20% acetone: 80% pet. spirit) to yield **3** as a yellow solid (5.1 mg, 37%) and **29** as a yellow solid (6.7 mg, 45%). The same procedure with **1** yielded **3** (6.1 mg, 43%) and **29** (5.6 mg, 37%).

7.22 *In Vitro* Biological Evaluation of **1** and **2**

The methods used by our collaborators for the cell-based cytotoxicity assays are briefly described here. MDA-MB-468 and SW620 cells were harvested and counted to identify the required number of cells to obtain 1,000 cells per well in a 96-well plate. The cells were centrifuged, excess supernatant was aspirated off and the cells either re-suspended in aerobic media or taken into the anoxic chamber and re-suspended in anoxia-

equilibrated media. The cells were then transferred to 96-well plates and incubated for 2 hours to allow attachment to the plate (100 μL per well) (Figure 7.1) Test compounds were prepared from DMSO stocks to a final concentration of 300 μM . Media was removed from the end well of the plate and replaced with 150 μL of media containing drug. A multi-channel pipette was used to perform 3-fold dilutions down the plate (50 μL at a time). Drug-free rows and cell-free rows were included as controls. After 4 hours of drug exposure, the cells were removed from the two anoxic or normoxic chambers and the wells washed 3 times to remove excess drug. Cells were then incubated in drug-free media for 5 days before fixing with trichloroacetic acid, staining with sulforhodamine B (to measure total protein) and measurements were obtained from a plate reader.¹⁹⁵ The sulforhodamine B dye binds to basic amino acids of cellular proteins, giving an indication of total protein mass that can in turn be correlated to the number of cells. Based on the original cell count, this number is used to determine the IC_{50} of each drug under the relevant conditions.

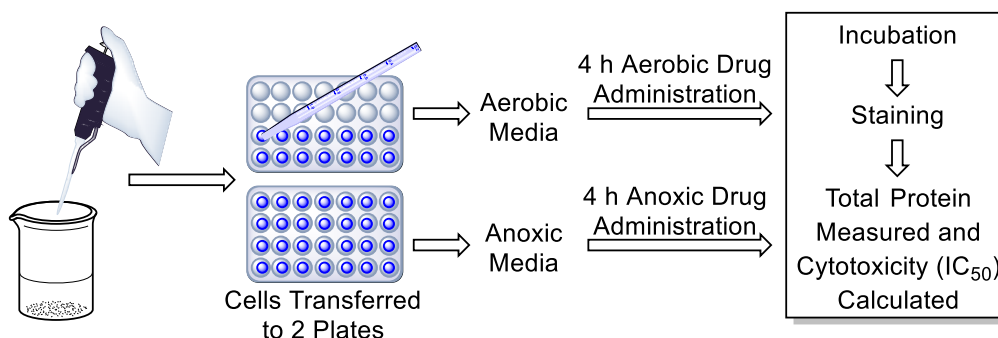


Figure 7.1 Summary of the protocol used for *in vitro* testing of hypoxia-activated cytotoxicity of mutual prodrugs **1** and **2**.

7.23 Synthesis of allyl 2-(2-nitrophenyl)acetate **30**

To a solution of 2-(2-nitrophenyl)acetic acid (10.021 g, 55.318 mmol) in neat distilled allyl alcohol (50 mL, 735.19 mmol) 3 drops of conc. H_2SO_4 was added and the reaction was refluxed under argon. The reaction was monitored by TLC (10% EtOAc: 90% pet. spirit). After 20 hours and complete consumption of the starting material, the allyl alcohol was removed under vacuum and the crude product was redissolved in EtOAc (100 mL). The solution was extracted with 1M NaOH (3 \times 100 mL), the organic layer collected, dried over anhydrous MgSO_4 , filtered and concentrated *in vacuo*. The crude product was

purified by isocratic silica gel column chromatography (20% EtOAc: 80% pet. spirit) to yield **30** as a colourless oil (10.213 g, 83%).

R_f = 0.73 (10% EtOAc: 90% pet. spirit). **IR:** (oil, ν/cm^{-1}): 3073, 2942,

2870, 1734, 1613, 1580, 1523, 1413, 1344, 1211, 1159, 986, 929, 862,

822, 788, 752, 713, 669, 485. **¹H NMR** (400 MHz, CDCl₃) δ 8.12 (dd,

$J = 8.2, 1.3$ Hz, 1H), 7.60 (td, $J = 7.5, 1.4$ Hz, 1H), 7.48 (td, $J = 7.8, 1.5$ Hz, 1H), 7.37

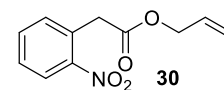
(dd, $J = 7.6, 1.1$ Hz, 1H), 5.90 (ddt, $J = 17.2, 10.4, 8.6$ Hz, 1H), 5.30 (dq, $J = 17.2, 1.5$

Hz, 1H), 5.23 (dq, $J = 10.4, 1.3$ Hz, 1H), 4.62 (dt, $J = 5.8, 1.4$ Hz, 2H), 4.06 (s, 2H). **¹³C**

NMR (101 MHz, CDCl₃) δ 169.8, 149.0, 133.7, 133.5, 131.9, 129.8, 128.8, 125.4, 118.7,

66.0, 39.9. **HREI-MS:** m/z calculated for C₁₁H₁₂NO₄ [M+H⁺] 222.0761; observed

222.0733.



7.24 Synthesis of allyl (Z)-3-(3,5-dimethyl-1H-pyrrol-2-yl)-2-(2-nitrophenyl)acrylate (Z)-31

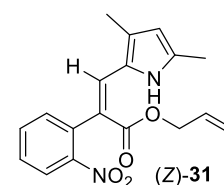
A mixture of **30** (7.754 g, 35.051 mmol), K₂CO₃ (9.730 g, 70.401 mmol) and 18-crown-6 (4.662 g, 17.650 mmol) was dissolved in dry THF (50 mL) and refluxed for 1 hour under argon. A solution of **7** (7.227 g, 39.888 mmol) in dry THF (50 mL) was added dropwise to the reaction mixture and the reaction monitored via TLC (20% EtOAc:80% pet. spirit). After 17 hours, the reaction volume was reduced under vacuum and redissolved in EtOAc (100 mL). The organic layer was extracted with saturated NaHCO_{3(aq)} (100 mL), the aqueous layer collected, washed with EtOAc (2 × 100 mL) and the organic layers combined. The organic layer was then further extracted with saturated NaCl_(aq) (1 × 100 mL), dried over anhydrous MgSO₄, filtered and concentrated *in vacuo*. The crude product was purified by gradient silica gel column chromatography (100% pet. spirit to 45% EtOAc:55% pet. spirit) to give one fraction containing crude (Z)-**31** and a second fraction containing crude (E)-**31** and unreacted **30**. The first fraction was further purified by gradient silica gel column chromatography (100% pet. spirit to 5% acetone: 95% pet. spirit) to yield (Z)-**31** as a red solid (2.248 g, 20%). The second fraction was also further purified by gradient silica gel column chromatography (100% pet. spirit to 30% acetone: 70% pet. spirit) to yield (E)-**31** as a red solid (2.352 g, 21%).

R_f = 0.78 (20% EtOAc: 80% pet. spirit). **M.P.** 70-72 °C; **IR** (solid,

ν/cm^{-1}): 3300, 2360, 1685, 1577, 1570, 1542, 1517, 1507, 1364, 1312,

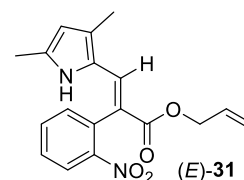
1182, 1144, 966, 932, 858, 790. **¹H NMR** (500 MHz, CDCl₃) δ 11.83

(br s, 1H), 8.04 (d, $J = 8.1$ Hz, 1H), 7.62 (t, $J = 7.5$ Hz, 1H), 7.45 (d,



$J = 8.8$ Hz, 1H), 7.43 (d, $J = 7.8$ Hz, 1H), 6.82 (s, 1H), 5.91 (s, 1H), 5.80 (ddt, $J = 16.8$, 11.1, 8.4 Hz, 1H), 5.15-5.08 (m, 2H), 4.56 (d, $J = 5.4$ Hz, 2H), 2.35 (s, 3H), 2.17 (s, 3H). ^{13}C NMR (126 MHz, CDCl_3) δ 167.3, 148.8, 137.3, 134.4, 133.5, 132.8, 131.9, 131.5, 131.4, 127.9, 124.6, 124.5, 118.1, 114.1, 111.5, 65.6, 13.8, 11.7. **HREI-MS**: m/z calculated for $\text{C}_{18}\text{H}_{19}\text{N}_2\text{O}_4$ [$\text{M}+\text{H}^+$] 327.1339; observed 327.1342.

$R_f = 0.49$ (20% EtOAc: 80% pet. spirit). **M.P.** 102-105 °C; **IR** (solid, v/cm^{-1}): 3455, 1687, 1610, 1557, 1524, 1343, 1257, 1232, 1068, 869, 733. ^1H NMR (500 MHz, CDCl_3) δ 8.20 (dd, $J = 8.0$, 1.1 Hz, 1H), 7.78 (s, 1H), 7.69 (td, $J = 7.5$, 1.2 Hz, 1H), 7.61 (td, $J = 7.8$,

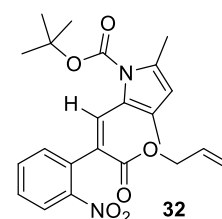


1.4 Hz, 1H), 7.51 (dd, $J = 7.5$, 1.1 Hz, 1H), 6.76 (br s, 1H), 5.87 (ddt, $J = 16.9$, 11.1, 5.6 Hz, 1H), 5.74- (d, $J = 1.6$ Hz, 1H), 5.22-5.14 (m, 2H), 4.68-4.58 (m, 2H), 2.20 (s, 3H), 1.96 (s, 3H). ^{13}C NMR (126 MHz, CDCl_3) δ 166.5, 149.4, 134.1, 133.7, 133.3, 132.6, 132.5, 130.6, 129.5, 127.6, 125.4, 123.6, 117.7, 116.3, 110.9. **HREI-MS**: m/z calculated for $\text{C}_{18}\text{H}_{19}\text{N}_2\text{O}_4$ [$\text{M}+\text{H}^+$] 327.1339; observed 327.1342.

7.25 Synthesis of *tert*-butyl (*Z*)-2-(3-(allyloxy)-2-(2-nitrophenyl)-3-oxoprop-1-en-1-yl)-3,5-dimethyl-1*H*-pyrrole-1-carboxylate **32**

A mixture of (*Z*)-**31** (1.293 g, 3.961 mmol), BOC anhydride (1.2246 g, 5.611 mmol) and DMAP (0.052 g, 0.427 mmol) was dissolved in dry acetonitrile (50 mL), under argon at r.t. and monitored via TLC (10% EtOAc: 90% pet. spirit). After 3 hours and complete consumption of starting material, the solvent was removed under reduced pressure and the reaction redissolved in CH_2Cl_2 (50 mL). The solution was then extracted with 1M $\text{HCl}_{(\text{aq})}$ (1 \times 50 mL) and saturated $\text{NaCl}_{(\text{aq})}$ (1 \times 50 mL), organic layer collected, dried over anhydrous Na_2SO_4 , filtered and concentrated *in vacuo*. The crude product was purified by gradient silica gel column chromatography (100% pet. spirit to 5% EtOAc: 95% pet. spirit) to yield **32** as a red solid (1.661 g, 98%).

$R_f = 0.61$ (20% EtOAc: 80% pet. spirit). **M.P.** 99-101 °C; **IR** (solid, v/cm^{-1}): 2980, 2930, 1749, 1704, 1627, 1570, 1516, 1473, 1437, 1388, 1367, 1335, 1303, 1272, 1245, 1188, 1139, 1084, 1028, 1010, 987, 924, 879, 855, 794, 771, 750, 710, 668, 651, 620, 595, 552, 476, 447.



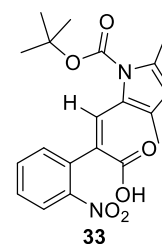
^1H NMR (500 MHz, CDCl_3) δ 8.12 (d, $J = 8.0$ Hz, 1H), 7.94 (s, 1H), 7.45 (t, $J = 7.4$ Hz, 1H), 7.40 (t, $J = 7.7$ Hz, 1H), 7.25 (d, $J = 7.5$ Hz, 1H), 5.87 (ddt, $J = 16.7$, 10.9, 5.7 Hz, 1H), 5.62 (s, 1H), 5.24 (d, $J = 17.3$ Hz, 1H), 5.19 (d, $J = 10.3$ Hz, 1H), 4.62 (d, $J = 5.1$ Hz, 2H), 2.39 (s, 3H), 1.62 (s, 9H), 1.28 (s, 3H). ^{13}C NMR (126 MHz, CDCl_3) δ 165.6,

150.0, 148.6, 134.8, 134.8, 133.4, 133.3, 133.1, 132.1, 128.5, 127.3, 125.4, 124.9, 124.8, 118.5, 115.3, 84.5, 66.1, 28.2, 16.2, 11.6. **HREI-MS:** m/z calculated for $C_{23}H_{27}N_2O_6$ $[M+H^+]$ 427.1864; observed 427.1879.

7.26 Synthesis of (Z)-3-(1-(tert-butoxycarbonyl)-3,5-dimethyl-1H-pyrrol-2-yl)-2-(2-nitrophenyl)acrylic acid **33**

To a stirring solution of **32** (1.213 g, 2.845 mmol) and $Pd(PPh_3)_4$ (0.352 g, 0.305 mmol) in dry THF (40 mL) under argon, morpholine (2.7 mL, 30 mmol) was added dropwise. The reaction was monitored via TLC (30% acetone: 70% pet. spirit) and after complete consumption of starting material, the solvent was removed under reduced pressure and the reaction mixture redissolved in EtOAc (100 mL). The organic layer was extracted with 1M $HCl_{(aq)}$ (3×100 mL) and saturated $NaCl_{(aq)}$ (1×100 mL), organic layer collected, dried over anhydrous Na_2SO_4 , filtered and concentrated *in vacuo*. The crude product was purified by gradient silica gel column chromatography (100% pet. spirit to 40% acetone: 60% pet. spirit) to yield **33** as a red solid (0.749 g, 82%).

$R_f = 0.56$ (30% EtOAc: 70% pet. spirit). **M.P.** 83-84 °C; **IR** (solid, v/cm^{-1}): 2968, 1745, 1727, 1673, 1601, 1519, 1480, 1437, 1421, 1370, 1351, 1330, 1306, 1280, 1254, 1141, 1119, 1091, 1013, 997, 934, 883, 854, 804, 788, 761, 747, 720, 709, 694, 667, 620, 582, 542, 492, 456. **1H NMR** (500 MHz, $CDCl_3$) δ 8.13 (d, $J = 8.1$ Hz, 1H), 8.01 (s, 1H), 7.46 (t, $J = 7.5$ Hz, 1H), 7.40 (t, $J = 7.6$ Hz, 1H), 7.25 (d, $J = 8.5$ Hz, 1H), 5.62 (s, 1H), 2.39 (s, 3H), 1.63 (s, 9H), 1.27 (s, 3H). **^{13}C NMR** (126 MHz, $CDCl_3$) δ 171.3, 150.0, 148.5, 136.4, 135.4, 133.5, 133.4, 132.7, 128.8, 126.5, 125.5, 125.4, 125.0, 115.5, 84.9, 28.3, 16.3, 11.6. **HREI-MS:** m/z calculated for $C_{20}H_{23}N_2O_6$ $[M+H^+]$ 387.1551; observed 387.1563.

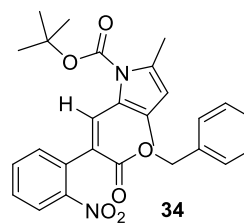


7.27 Synthesis of tert-butyl (Z)-2-(3-(benzyloxy)-2-(2-nitrophenyl)-3-oxoprop-1-en-1-yl)-3,5-dimethyl-1H-pyrrole-1-carboxylate **34**

A solution of **33** (0.018 g, 0.046 mmol) and PPh_3 (0.025 g, 0.095 mmol) in dry THF (0.2 mL) was sonicated until fully dissolved. Benzyl alcohol (10 μ L, 0.098 mmol) was added dropwise to the reaction followed by diethyl azodicarboxylate (15 μ L, 0.097 mmol). The reaction was then sonicated for 60 minutes and monitored via TLC (30% EtOAc: 70% pet. spirit). After complete consumption of starting material the reaction was diluted with EtOAc (5 mL) and extracted with 1M $HCl_{(aq)}$ (1×5 mL) and saturated $NaCl_{(aq)}$ (1×5

mL), organic layer collected and concentrated *in vacuo* yielding pure **34** as a red solid (0.022 g, quantitative yield).

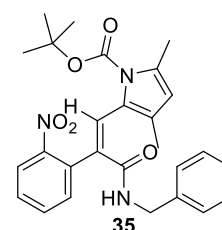
R_f = 0.69 (30% EtOAc: 70% pet. spirit). **M.P.** 74-78 °C; **IR** (solid, ν/cm^{-1}): 2926, 1707, 1608, 1523, 1455, 1369, 1344, 1324, 1307, 1270, 1222, 1174, 1139, 1089, 1018, 928, 881, 855, 790, 744, 697, 665, 618, 476. **¹H NMR** (500 MHz, CDCl₃) δ 8.13 (dd, $J = 8.1, 1.3$ Hz, 1H), 7.91 (s, 1H), 7.44 (td, $J = 7.5, 1.5$ Hz, 1H), 7.39 (td, $J = 7.7, 1.6$ Hz, 1H), 7.34-7.27 (m, 5H), 7.24 (dd, $J = 7.6, 1.5$ Hz, 1H), 5.61 (s, 1H), 5.18 (s, 2H), 2.38 (s, 3H), 1.53 (s, 9H), 1.27 (s, 3H). **¹³C NMR** (101 MHz, *d*₆-DMSO) δ 165.0, 149.0, 147.7, 135.7, 134.2, 134.1, 134.0, 132.7, 132.0, 129.3, 128.4, 128.1, 128.0, 126.6, 124.8, 124.7, 123.6, 115.0, 84.3, 66.3, 27.4, 15.5, 11.0. **HREI-MS**: m/z calculated for C₂₇H₂₈N₂O₆Na [M+Na⁺] 499.1840; observed 499.1839.



7.28 Synthesis of *tert*-butyl (*Z*)-2-(3-(benzylamino)-2-(2-nitrophenyl)-3-oxoprop-1-en-1-yl)-3,5-dimethyl-1*H*-pyrrole-1-carboxylate **35**

A solution of **33** (0.026 g, 0.068 mmol) and HATU (0.028 g, 0.075 mmol) in dry CH₂Cl₂ (5 mL) under argon was cooled to 0 °C. Benzyl amine (14 μ L, 0.130 mmol) was added dropwise to the reaction followed by DIPEA (28 μ L, 0.162 mmol). The reaction was allowed to warm to r.t. and stirred overnight. Upon consumption of the starting material, the reaction was diluted with CH₂Cl₂ (20 mL) and extracted with 1M HCl_(aq) (2 \times 25 mL) and saturated NaHCO_{3(aq)} (2 \times 25 mL). The organic layer was dried over anhydrous MgSO₄, filtered and concentrated *in vacuo* yielding pure **35** as a red solid (0.032 g, quantitative yield).

R_f = 0.51 (30% EtOAc: 70% pet. spirit). **M.P.** 110-113 °C; **IR** (solid, ν/cm^{-1}): 3422, 2977, 2854, 2926, 1725, 1644, 1601, 1513, 1452, 1400, 1383, 1367, 1328, 1259, 1216, 1143, 1094, 1031, 1002, 916, 851, 809, 786, 768, 741, 699, 670, 626, 594, 579, 548, 482, 452, 409. **¹H NMR** (400 MHz, CDCl₃) δ 8.04 (dd, $J = 8.1, 1.2$ Hz, 1H), 7.62 (td, $J = 7.5, 1.3$ Hz, 1H), 7.53 (dd, $J = 7.6, 1.4$ Hz, 1H), 7.48 (td, $J = 7.7, 1.5$ Hz, 1H), 7.30-7.24 (m, 3H), 7.15-7.13 (m, 2H), 6.90 (s, 1H), 6.31 (t, $J = 5.4$ Hz, 1H), 5.80 (s, 1H), 4.41 (d, $J = 5.8$ Hz, 2H), 2.38 (s, 3H), 1.89 (s, 3H), 1.48 (s, 9H). **¹³C NMR** (101 MHz, CDCl₃) δ 166.6, 149.9, 148.5, 138.2, 135.2, 134.7, 133.7, 133.3, 133.2, 128.9, 128.7, 128.0, 127.7, 127.4, 124.9, 124.6, 124.2, 115.0, 84.6, 44.1, 28.2, 16.3, 12.0. **HREI-MS**: m/z calculated for C₂₇H₂₉N₃O₅Na [M+Na⁺] 498.1999; observed 498.2001.



7.29 Allyl Esterification General Method 1

The appropriate fluorinated 2-(2-nitrophenyl)acetic acid was dissolved in 10 mL of freshly distilled allyl alcohol, 2 drops of conc. H₂SO₄ (98%) was added and the reaction refluxed under argon overnight. Upon complete consumption of the starting material, the allyl alcohol was reduced under vacuum and the reaction redissolved in ethyl acetate (100 mL). The organic layer was then extracted with NaHCO₃(aq) (3 × 100 mL) and saturated NaCl(aq) (1 × 100 mL), dried over anhydrous MgSO₄, filtered and reduced under vacuum. Crude products were purified by gradient column chromatography (0-10% acetone/pet. spirit).

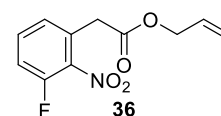
7.30 Synthesis of Allyl 2-(3-fluoro-2-nitrophenyl)acetate 36

Compound **36** was synthesised using General Method 1 with 2-(3-fluoro-2-nitrophenyl)acetic acid (1.021 g, 5.129 mmol) to afford **36** (1.059 g, 86%) as a colourless oil.

R_f = 0.75 (20% EtOAc: 80% pet. spirit). **IR** (oil, v/cm⁻¹): 3087, 3947,

2885, 1735, 1617, 1591, 1532, 1459, 1358, 1273, 1174, 982, 932, 854,

802, 771, 724, 555, 468, 417. **¹H NMR** (500 MHz, CDCl₃) δ 7.49 (td,



J = 8.1, 5.2 Hz, 1H), 7.22 (ddd, *J* = 9.6, 8.5, 1.1 Hz, 1H), 7.17 (d, *J* = 7.7 Hz, 1H), 5.89 (ddt, *J* = 17.2, 10.5, 5.8 Hz, 1H), 5.30 (dq, *J* = 17.2, 1.4 Hz, 1H), 5.24 (dq, *J* = 10.4, 1.2 Hz, 1H), 4.61 (dt, *J* = 5.8, 1.3 Hz, 2H), 3.86 (s, 2H). **¹³C NMR** (126 MHz, CDCl₃) δ 169.0, 154.8 (d, *J* = 260.8 Hz), 139.6 (d, *J* = 11.1 Hz), 132.7 (d, *J* = 8.2 Hz), 131.6, 129.8 (d, *J* = 1.4 Hz), 127.6 (d, *J* = 3.7 Hz), 119.0, 116.9 (d, *J* = 19.2 Hz), 66.3, 37.6 (d, *J* = 1.8 Hz). **HREI-MS**: *m/z* calculated for C₁₁H₁₁FNO₄ [M+H⁺] 240.0667; observed 240.0672.

7.31 Synthesis of Allyl 2-(4-fluoro-2-nitrophenyl)acetate 37

Compound **37** was synthesised using General Method 1 with 2-(4-fluoro-2-nitrophenyl)acetic acid (0.999 g, 5.017 mmol) to afford **37** (0.964 g, 80%) as a colourless oil.

R_f = 0.86 (20% EtOAc: 80% Pet. Spirit). **IR**: (oil, v/cm⁻¹) 3084 ,

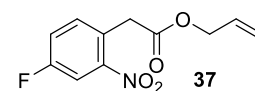
2945 , 2882 , 1734 , 1532 , 1499, 1423 , 1342 , 1238 , 1192 , 1159

, 986 , 928 , 878 , 817 , 800 , 722 , 684 , 543 , 506 , 361 . **¹H NMR** (500 MHz, CDCl₃) δ

7.86 (dd, *J* = 8.4, 2.5 Hz, 1H), 7.38-7.31 (m, 2H), 5.90 (ddt, *J* = 17.2, 10.4, 5.8 Hz, 1H),

5.30 (dq, *J* = 17.2, 1.5 Hz, 1H), 5.24 (dq, *J* = 10.4, 1.2 Hz, 1H), 4.61 (dt, *J* = 5.8, 1.4 Hz,

2H), 4.03 (s, 2H). **¹³C NMR** (126 MHz, CDCl₃) δ 169.6, 161.6 (d, *J* = 251.0 Hz), 149.2

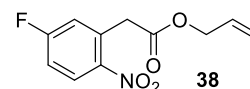


(d, $J = 8.3$ Hz), 134.9 (d, $J = 8.3$ Hz), 131.8, 125.86 (d, $J = 4.1$ Hz), 121.0 (d, $J = 21.0$ Hz), 118.9, 113.2 (d, $J = 26.5$ Hz), 66.1, 39.3. **HREI-MS**: m/z calculated for $C_{11}H_{11}FNO_4$ $[M+H^+]$ 240.0667; observed 240.0672.

7.32 Synthesis of Allyl 2-(5-fluoro-2-nitrophenyl)acetate **38**

Compound **38** was synthesised using General Method 1 with 2-(5-fluoro-2-nitrophenyl)acetic acid (0.996 g, 5.003 mmol) to afford **38** (1.003 g, 84%) as a colourless oil.

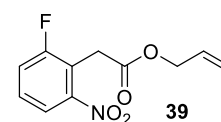
$R_f = 0.81$ (20% EtOAc: 80% Pet. Spirit). **IR**: (oil, ν/cm^{-1}) 3086, 2944, 2865, 1734, 1624, 1590, 1525, 1484, 1410, 1343s, 1276, 1251, 1175, 1154, 1077, 990, 934, 875, 838, 750, 719, 615, 432, 356. **1H NMR** (400 MHz, $CDCl_3$) δ 8.19 (dd, $J = 9.1, 5.2$ Hz, 1H), 7.15 (ddd, $J = 9.1, 7.2, 2.7$ Hz, 1H), 7.07 (dd, $J = 8.6, 2.7$ Hz, 1H), 5.90 (ddt, $J = 17.2, 10.4, 5.8$ Hz, 1H), 5.30 (dq, $J = 17.2, 1.5$ Hz, 1H), 5.24 (dq, $J = 10.4, 1.2$ Hz, 1H), 4.62 (dt, $J = 5.8, 1.3$ Hz, 2H), 4.04 (s, 2H). **^{13}C NMR** (101 MHz, $CDCl_3$) δ 169.2, 164.9 (d, $J = 257.6$ Hz), 145.0, 133.3 (d, $J = 9.3$ Hz), 131.8, 128.3 (d, $J = 10.2$ Hz), 120.4 (d, $J = 23.8$ Hz), 118.9, 115.7 (d, $J = 23.1$ Hz), 66.2, 40.0 (d, $J = 1.0$ Hz). **HREI-MS**: m/z calculated for $C_{11}H_{11}FNO_4$ $[M+H^+]$ 240.0667; observed 240.0672.



7.33 Synthesis of Allyl 2-(2-fluoro-6-nitrophenyl)acetate **39**

Compound **39** was synthesised using General Method 1 with 2-(3-fluoro-2-nitrophenyl)acetic acid (0.979 g, 4.917 mmol) to afford **39** (0.938 g, 80%) as a colourless oil.

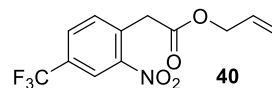
$R_f = 0.74$ (20% EtOAc: 80% pet. spirit). **IR** (oil, ν/cm^{-1}): 3098, 2948, 2882, 1737, 1530, 1469, 1417, 1342, 1252, 1208, 1170, 983, 931, 842, 796, 733, 681, 530, 366. **1H NMR** (400 MHz, $CDCl_3$) δ 7.91 (dt, $J = 8.1, 1.3$ Hz, 1H), 7.46 (td, $J = 8.2, 5.7$ Hz, 1H), 7.40 (td, $J = 8.6, 1.4$ Hz, 1H), 5.90 (ddt, $J = 17.2, 10.5, 5.7$ Hz, 1H), 5.30 (dq, $J = 17.2, 1.5$ Hz, 1H), 5.23 (dq, $J = 10.4, 1.3$ Hz, 1H), 4.63 (dt, $J = 5.7, 1.4$ Hz, 2H), 4.09 (d, $J = 1.2$ Hz, 2H). **^{13}C NMR** (101 MHz, $CDCl_3$) δ 168.9 (d, $J = 1.0$ Hz), 161.3 (d, $J = 250.0$ Hz), 149.8 (d, $J = 3.8$ Hz), 131.8, 129.1 (d, $J = 9.5$ Hz), 121.0 (d, $J = 3.4$ Hz), 120.8 (d, $J = 24.0$ Hz), 118.7, 118.4 (d, $J = 19.1$ Hz), 66.1, 30.9 (d, $J = 5.0$ Hz). **HREI-MS**: m/z calculated for $C_{11}H_{11}FNO_4$ $[M+H^+]$ 240.0667; observed 240.0672.



7.34 Synthesis of Allyl 2-(2-nitro-4-(trifluoromethyl)phenyl)acetate **40**

Compound **40** was synthesised using General Method 1 with 2-(3-fluoro-2-nitrophenyl)acetic acid (1.011 g, 4.059 mmol) to afford **40** (0.835 g, 71%) as a colourless oil.

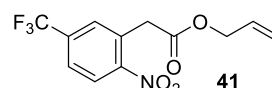
R_f = 0.55 (20% acetone: 80% pet. spirit). **IR** (oil, ν/cm^{-1}): 3087, 2947, 1736, 1633, 1540, 1506, 1425, 1407, 1352, 1323, 1217, 1130, 1088, 986, 906, 848, 821, 786, 732, 693. **$^1\text{H NMR}$** (500 MHz, CDCl_3) δ 8.38 (d, J = 1.2 Hz, 1H), 7.85 (dd, J = 8.0, 1.3 Hz, 1H), 7.54 (d, J = 8.0 Hz, 1H), 5.90 (ddt, J = 17.2, 10.4, 5.8 Hz, 1H), 5.31 (dq, J = 17.2, 1.5 Hz, 1H), 5.25 (dq, J = 10.4, 1.2 Hz, 1H), 4.63 (dt, J = 5.8, 1.3 Hz, 2H), 4.13 (s, 2H). **$^{13}\text{C NMR}$** (126 MHz, CDCl_3) δ 169.0, 149.0, 134.4, 133.7, 131.7, 131.6 (q, J = 34.3 Hz), 130.1 (q, J = 3.5 Hz), 122.9 (q, J = 272.7 Hz), 122.8 (q, J = 3.8 Hz), 119.1, 66.3, 39.7. **HREI-MS**: m/z calculated for $\text{C}_{12}\text{H}_{19}\text{F}_3\text{NO}_4$ [$\text{M}-\text{H}^+$] 288.0489; observed 288.0490.



7.35 Synthesis of Allyl 2-(2-nitro-5-(trifluoromethyl)phenyl)acetate **41**

Compound **41** was synthesised using General Method 1 with 2-(3-fluoro-2-nitrophenyl)acetic acid (1.037 g, 4.163 mmol) to afford **41** (0.841 g, 70%) as a colourless oil.

R_f = 0.65 (20% acetone: 80% pet. spirit). **IR** (oil, ν/cm^{-1}): 3089, 2948, 1736, 1532, 1429, 1325, 1170, 1129, 1096, 1070, 987, 896, 836, 754, 702, 510, 419. **$^1\text{H NMR}$** (400 MHz, CDCl_3) δ 8.20 (d, J = 8.5 Hz, 1H), 7.75 (dd, J = 8.5, 1.6 Hz, 1H), 7.65 (d, J = 1.3 Hz, 1H), 5.90 (ddt, J = 17.2, 10.4, 5.8 Hz, 1H), 5.31 (dq, J = 17.2, 1.5 Hz, 1H), 5.25 (dq, J = 10.4, 1.2 Hz, 1H), 4.63 (dt, J = 5.8, 1.3 Hz, 2H), 4.11 (s, 2H). **$^{13}\text{C NMR}$** (101 MHz, CDCl_3) δ 168.9, 150.9, 135.0 (q, J = 33.5 Hz), 131.6, 130.7, 130.5 (q, J = 3.7 Hz), 125.9, 125.9 (q, J = 3.6 Hz), 122.8 (q, J = 273.1 Hz), 119.0, 66.2, 39.5. **HREI-MS**: m/z calculated for $\text{C}_{12}\text{H}_{19}\text{F}_3\text{NO}_4$ [$\text{M}-\text{H}^+$] 288.0489; observed 288.0490.



7.36 Knoevenagel Condensation General Method 2

A mixture of K_2CO_3 and 18-Crown-6 were dissolved in dry THF (5 mL) under argon. A solution of the appropriate allyl alcohol **36-41** in dry THF (5 mL) was added dropwise and the reaction allowed to stir at room temperature. After 1 hour a solution of **7** in dry THF (5 mL) was added dropwise to the reaction mixture and the reaction monitored via TLC (20% acetone: 80% pet. spirit). After 18 hours if the reaction had not proceeded, the

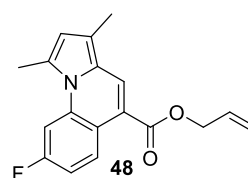
reaction was heated to 45 °C for a further 24 hours. Upon consumption of starting material, the solvent was reduced under vacuum and the reaction mixture redissolved in EtOAc (50 mL). The organic layer was extracted with saturated NaHCO_{3(aq)} (2 × 50 mL). The combined aqueous layers were further extracted with ethyl acetate (2 × 50 mL) and the organic layers combined. The combined organic layers were extracted with saturated NaCl_(aq) (1 × 50 mL), dried over anhydrous MgSO₄ and concentrated *in vacuo*. The crude products and side products were then purified by gradient silica gel column chromatography (100% pet. spirit to 30% EtOAc: 70% pet. spirit). Impure compounds were then further purified by preparative TLC for characterisation and chemical testing.

7.37 Synthesis of Allyl 8-fluoro-1,3-dimethylpyrrolo[1,2-*a*]quinoline-5-carboxylate **48**

Compound **48** was inadvertently synthesised using General Method 2 with allyl ester **37** (0.509 g, 2.128 mmol), **7** (0.418 g, 2.307 mmol), K₂CO₃ (0.585 g, 4.233 mmol) and 18-crown-6 (0.279 g, 1.056 mmol) reacted at 66 °C for 18 hours affording **48** (0.240 g, 38%) as a yellow highly fluorescent solid (blue in hexane under 365 nm UV light), (*Z*)-**43** (0.049 g, 7%) as an orange solid and (*E*)-**43** (0.075 g, 10%) as a red solid.

R_f = 0.81 (20% Acetone: 80% Pet. Spirit). **M.P.** 79-81 °C. **IR:**

(solid, v/cm⁻¹) 2922, 2854, 2853, 1691, 1609, 1567, 1538, 1501, 1428, 1369, 1332, 1214, 1194, 1161, 1131, 1027, 993, 927, 906, 844, 827, 811, 768, 736, 715, 645, 598, 482, 442, 405, 367. **¹H**



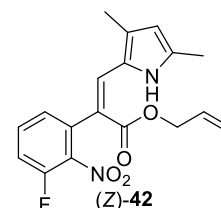
NMR (400 MHz, CDCl₃) δ 8.98 (dd, *J* = 9.2, 6.9 Hz, 1H), 8.12 (s, 1H), 7.91 (dd, *J* = 11.6, 2.6 Hz, 1H), 7.06 (ddd, *J* = 9.7, 7.2, 2.1 Hz, 1H), 6.43 (s, 1H), 6.10 (ddt, *J* = 17.2, 10.5, 5.7 Hz, 1H), 5.45 (dq, *J* = 17.2, 1.5 Hz, 1H), 5.32 (dq, *J* = 10.4, 1.3 Hz, 1H), 4.85 (dt, *J* = 5.7, 1.4 Hz, 2H), 2.88 (s, 3H), 2.37 (s, 3H). **¹³C NMR** (101 MHz, CDCl₃) δ 166.1, 160.9 (d, *J* = 245.0 Hz), 136.2 (d, *J* = 9.8 Hz), 132.7, 128.9 (d, *J* = 9.2 Hz), 128.6, 127.6, 123.4 (d, *J* = 2.0 Hz), 119.1 (d, *J* = 2.6 Hz), 118.2, 118.2, 117.7, 112.8 (d, *J* = 1.3 Hz), 111.1 (d, *J* = 21.5 Hz), 102.8 (d, *J* = 27.3 Hz), 65.3, 18.2, 10.7. **HREI-MS:** Adduct could not be detected by high resolution mass spectrometry.

7.38 Synthesis of Allyl (*Z*)-3-(3,5-dimethyl-1H-pyrrol-2-yl)-2-(3-fluoro-2-nitrophenyl)acrylate (*Z*)-**42**

Compound (*Z*)-**42** was synthesised using General Method 2 with allyl ester **36** (0.369 g, 1.541 mmol), **7** (0.297 g, 1.639 mmol), K₂CO₃ (0.422 g, 3.056 mmol) and 18-crown-6

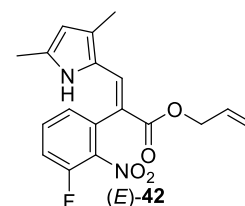
(0.200 g, 0.757 mmol) reacted at room temperature for 18 hours affording (*Z*)-**42** (0.147 g, 28%) as a red solid and (*E*)-**42** (0.137 g, 26%) as a red solid.

R_f = 0.78 (20% EtOAc: 80% pet. spirit). **M.P.** 64-68 °C; **IR** (solid, ν/cm^{-1}): 3276, 2918, 2869, 1686, 1650, 1604, 1570, 1526, 1463, 1395, 1351, 1317, 1256, 1240, 1188, 1153, 1071, 974, 929, 907, 854, 823, 805, 791, 769, 725, 708, 662, 615, 554, 472, 427. **¹H NMR** (500 MHz, CDCl_3) δ 11.82 (br s, 1H), 7.47 (td, $J = 8.1, 5.4$ Hz, 1H), 7.21-7.17 (m, 2H), 6.81 (s, 1H), 5.91 (d, $J = 2.0$ Hz, 1H), 5.85 (ddt, $J = 16.7, 11.1, 5.6$ Hz, 1H), 5.19-5.15 (m, 2H), 4.60 (dt, $J = 5.5, 1.3$ Hz, 2H), 2.33 (s, 3H), 2.15 (s, 3H).



¹³C NMR (126 MHz, CDCl_3) δ 166.8, 154.1 (d, $J = 259.0$ Hz), 139.4 (d, $J = 11.7$ Hz), 137.7, 135.3, 133.2, 132.7, 131.9 (d, $J = 2.7$ Hz), 131.8, 127.6 (d, $J = 3.7$ Hz), 124.3, 118.0, 115.7 (d, $J = 19.9$ Hz), 111.8, 110.0 (d, $J = 1.8$ Hz), 65.6, 13.7, 11.5. **HREI-MS**: m/z calculated for $\text{C}_{18}\text{H}_{18}\text{FN}_2\text{O}_4$ [$\text{M}+\text{H}^+$] 345.1245; observed 345.1246.

R_f = 0.55 (20% EtOAc: 80% pet. spirit). **M.P.** 80-84 °C; **IR** (solid, ν/cm^{-1}): 3460, 3381, 3082, 2923, 2881, 1689, 1599, 1554, 1531, 1472, 1446, 1356, 1262, 1230, 1198, 1150, 1065, 973, 923, 853, 804, 762, 733, 703, 671, 637, 541. **¹H NMR** (500 MHz, CDCl_3) δ



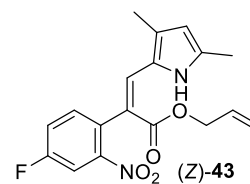
7.81 (s, 1H), 7.58 (td, $J = 8.1, 5.2$ Hz, 1H), 7.35 (t, $J = 8.9$ Hz, 1H), 7.25 (d, $J = 7.7$ Hz, 1H), 6.93 (s, 1H), 5.89 (ddt, $J = 16.8, 11.1, 5.7$ Hz, 1H), 5.78 (d, $J = 1.7$ Hz, 1H), 5.22 (dq, $J = 17.2, 1.4$ Hz, 1H), 5.18 (dq, $J = 10.5, 1.2$ Hz, 1H), 4.63 (dt, $J = 5.5, 1.3$ Hz, 2H), 2.19 (s, 3H), 2.02 (s, 3H). **¹³C NMR** (126 MHz, CDCl_3) δ 166.0, 154.5 (d, $J = 260.9$ Hz), 139.9 (d, $J = 11.9$ Hz), 135.2, 133.4, 132.7 (d, $J = 8.5$ Hz), 132.3, 131.7, 129.8, 127.8 (d, $J = 3.3$ Hz), 123.3, 117.7, 117.3 (d, $J = 19.5$ Hz), 112.5 (d, $J = 1.7$ Hz), 111.2, 65.6, 13.4, 11.4. **HREI-MS**: m/z calculated for $\text{C}_{18}\text{H}_{18}\text{FN}_2\text{O}_4$ [$\text{M}+\text{H}^+$] 345.1245; observed 345.1246.

7.39 Synthesis of Allyl (*Z*)-3-(3,5-dimethyl-1*H*-pyrrol-2-yl)-2-(4-fluoro-2-nitrophenyl)acrylate (*Z*)-**43**

Compound (*Z*)-**43** was synthesised using General Method 2 with allyl ester **37** (0.509 g, 2.128 mmol), **7** (0.418 g, 2.307 mmol), K_2CO_3 (0.585 g, 4.233 mmol) and 18-crown-6 (0.279 g, 1.056 mmol) reacted at room temperature for 18 hours affording (*Z*)-**43** (0.098 g, 13% yield) as an orange solid and (*E*)-**43** (0.142 g, 19%) as a red solid.

R_f = 0.76 (20% Acetone: 80% Pet. Spirit). **M.P.** 88-90 °C. **IR:**

(solid, ν/cm^{-1}) 3275, 2920, 1689, 1571, 1527, 1462, 1406, 1363, 1343, 1314, 1269, 1177, 1147, 987, 969, 939, 871, 838, 818, 795, 731, 686, 672, 602, 554, 466, 420, 374. **¹H NMR** (500 MHz,

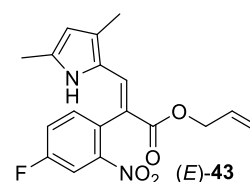


CDCl_3) δ 11.82 (br s, 1H), 7.79 (dd, $J = 8.4, 2.7$ Hz, 1H), 7.42 (dd, $J = 8.5, 5.6$ Hz, 1H), 7.36 (ddd, $J = 8.5, 7.4, 2.7$ Hz, 1H), 6.78 (s, 1H), 5.91 (d, $J = 2.6$ Hz, 1H), 5.79 (ddt, $J = 17.1, 10.5, 5.7$ Hz, 1H), 5.16-5.10 (m, 2H), 4.55 (dt, $J = 5.6, 1.4$ Hz, 2H), 2.35 (s, 3H), 2.17 (s, 3H). **¹³C NMR** (126 MHz, CDCl_3) δ 167.0, 160.9 (d, $J = 251.1$ Hz), 148.8 (d, $J = 8.2$ Hz), 134.6, 134.1 (d, $J = 7.7$ Hz), 133.3 (d, $J = 4.0$ Hz), 131.7, 131.6, 131.6, 124.3, 120.6 (d, $J = 20.6$ Hz), 118.2, 112.7, 112.1 (d, $J = 26.0$ Hz), 111.5, 65.6, 13.7, 11.6.

HREI-MS: m/z calculated $\text{C}_{18}\text{H}_{17}\text{FN}_2\text{O}_4\text{Na}$ [$\text{M}+\text{Na}^+$] 367.1065; observed 367.1070.

R_f = 0.46 (20% Acetone: 80% Pet. Spirit). **M.P.** 132-135 °C. **IR:**

(solid, ν/cm^{-1}) 3465, 3370, 3091, 2923, 2854, 1742, 1691, 1648, 1602, 1557, 1531, 1497, 1441, 1344, 1263, 1229, 1204, 1166, 1147, 1065, 1024, 992, 970, 924, 877, 838, 810, 763, 718, 675, 657, 636,

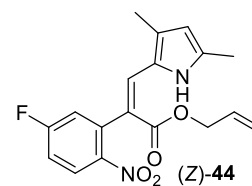


605, 583, 516, 434, 375. **¹H NMR** (400 MHz, CDCl_3) δ 7.94 (dd, $J = 8.2, 2.6$ Hz, 1H), 7.79 (s, 1H), 7.49 (dd, $J = 8.5, 5.6$ Hz, 1H), 7.41 (ddd, $J = 8.5, 7.3, 2.7$ Hz, 1H), 6.80 (br s, 1H), 5.87 (ddt, $J = 17.2, 10.5, 5.5$ Hz, 1H), 5.77 (d, $J = 2.5$ Hz, 1H), 5.23-5.16 (m, 2H), 4.67-4.57 (m, 2H), 2.20 (s, 3H), 2.01 (s, 3H). **¹³C NMR** (101 MHz, CDCl_3) δ 166.3, 161.8 (d, $J = 252.3$ Hz), 149.8 (d, $J = 8.7$ Hz), 134.8 (d, $J = 7.2$ Hz), 134.4, 132.3, 130.9, 128.5 (d, $J = 4.6$ Hz), 127.9, 123.4, 120.9 (d, $J = 21.0$ Hz), 117.8, 115.1, 113.1 (d, $J = 26.3$ Hz), 111.1, 65.6, 13.4, 11.4. **HREI-MS:** m/z calculated $\text{C}_{18}\text{H}_{17}\text{FN}_2\text{O}_4\text{Na}$ [$\text{M}+\text{Na}^+$] 367.1065; observed 367.1070.

7.40 Synthesis of Allyl (Z)-3-(3,5-dimethyl-1H-pyrrol-2-yl)-2-(5-fluoro-2-nitrophenyl)acrylate (Z)-44

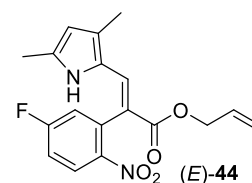
Compound (Z)-44 was synthesised using General Method 2 with allyl ester **38** (0.506 g, 2.115 mmol), **7** (0.421 g, 2.324 mmol), K_2CO_3 (0.587 g, 4.247 mmol) and 18-crown-6 (0.276 g, 1.044 mmol) reacted at room temperature for 20 hours followed by a further 24 hours of heating at 45 °C to afford (Z)-44 (0.161 g, 22%) as an orange solid and (E)-44 (0.151 g, 21%) as a red solid.

R_f = 0.62 (20% Acetone: Pet. Spirit). **M.P.** 91-93 °C. **IR:** (solid, ν/cm^{-1}) 3283, 3068, 2922, 2853, 1730, 1679, 1615, 1570, 1540, 1520, 1461, 1412, 1389, 1343, 1309, 1269, 1252, 1236, 1198, 1178, 1151, 1087, 1029, 999, 974, 940, 910, 888, 849, 834, 821, 795, 779,



762, 725, 708, 684, 670, 634, 614, 584, 551, 491, 468, 439, 419, 382, 368. **¹H NMR** (500 MHz, CDCl₃) δ 11.81 (br s, 1H), 8.12-8.09 (m, 1H), 7.12-7.08 (m, 2H), 6.80 (s, 1H), 5.91 (d, $J = 2.6$ Hz, 1H), 5.79 (ddt, $J = 17.1, 10.6, 5.7$ Hz, 1H), 5.15 (dq, $J = 6.4, 1.4$ Hz, 1H), 5.12 (dq, $J = 13.0, 1.5$ Hz, 1H), 4.56 (dt, $J = 5.7, 1.4$ Hz, 2H), 2.35 (s, 3H), 2.18 (s, 3H). **¹³C NMR** (126 MHz, CDCl₃) δ 166.8, 164.7 (d, $J = 256.8$ Hz), 144.9, 140.5 (d, $J = 9.3$ Hz), 134.9, 132.1, 131.7, 131.5, 127.2 (d, $J = 10.1$ Hz), 124.3, 119.4 (d, $J = 23.1$ Hz), 118.2, 114.5 (d, $J = 23.1$ Hz), 113.0, 111.6, 65.6, 13.7, 11.6. **HREI-MS:** m/z calculated for C₁₈H₁₇FN₂O₄ [M+H⁺] 345.1245; observed 345.1329, m/z calculated C₁₈H₁₇FN₂O₄ [M+Na⁺] 367.1065; observed 367.1148.

R_f = 0.56 (20% Acetone: Pet. Spirit). **M.P.** 138-140 °C. **IR:** (solid, ν/cm^{-1}) 3457, 3074, 2922, 2852, 1684, 1612, 1582, 1557, 1522, 1439, 1363, 1335, 1218, 1149, 1082, 1031, 983, 962, 935, 911, 889, 844, 802, 763, 748, 726, 666, 639, 622, 604, 553, 522, 452, 419,

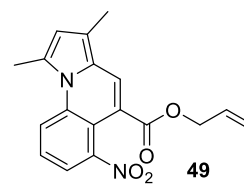


380. **¹H NMR** (400 MHz, CDCl₃) δ 8.26 (dd, $J = 9.1, 5.1$ Hz, 1H), 7.77 (s, 1H), 7.27 (ddd, $J = 9.5, 6.7, 2.4$ Hz, 1H), 7.19 (dd, $J = 8.4, 2.8$ Hz, 1H), 6.85 (br s, 1H), 5.86 (ddt, $J = 17.2, 10.5, 5.5$ Hz, 1H), 5.78 (d, $J = 2.4$ Hz, 1H), 5.23-5.16 (m, 2H), 4.68-4.57 (m, 2H), 2.20 (s, 3H), 2.02 (s, 3H). **¹³C NMR** (101 MHz, CDCl₃) δ 166.0, 164.7 (d, $J = 254.8$ Hz), 145.5 (d, $J = 3.0$ Hz), 135.8 (d, $J = 9.7$ Hz), 134.7, 132.3, 131.2, 128.1 (d, $J = 10.1$ Hz), 127.7, 123.2, 120.0 (d, $J = 22.8$ Hz), 117.8, 116.3 (d, $J = 23.3$ Hz), 115.2, 111.2, 65.6, 13.4, 11.4. **HREI-MS:** m/z calculated for C₁₈H₁₇FN₂O₄ [M+H⁺] 345.1245; observed 345.1251.

7.41 Synthesis of Allyl 1,3-dimethyl-6-nitropyrrolo[1,2-a]quinoline-5-carboxylate **49**

Compound **49** was inadvertently synthesised using General Method 2 with allyl ester **39** (0.360 g, 1.506 mmol), **7** (0.296 g, 1.634 mmol), K₂CO₃ (0.426 g, 3.082 mmol) and 18-crown-6 (0.204 g, 0.770 mmol) reacted at room temperature for 18 hours affording **49** (0.055 g, 11%) as an intensely red solid.

R_f = 0.22 (10% acetone: 90% pet. spirit). **M.P.** 70-74 °C; **IR** (solid, ν/cm^{-1}): 2960, 2923, 2855, 1701, 1650, 1620, 1592, 1541, 1514, 1475, 1441, 1420, 1387, 1362, 1345, 1322, 1290, 1261, 1234, 1179, 1096, 1008, 992, 965, 935, 918, 874, 832, 805, 772, 759, 735, 715,

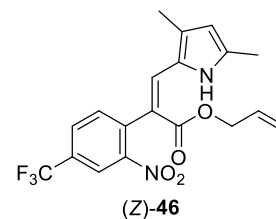


649, 622, 589, 560, 511, 467, 433. $^1\text{H NMR}$ (500 MHz, CDCl_3) δ 8.45 (dd, J = 8.6, 0.5 Hz, 1H), 8.06 (s, 1H), 7.84 (dd, J = 7.9, 0.9 Hz, 1H), 7.50 (t, J = 8.3 Hz, 1H), 6.52 (s, 1H), 6.02 (ddt, J = 17.1, 10.4, 6.0 Hz, 1H), 5.38 (dq, J = 17.2, 1.4 Hz, 1H), 5.28 (dq, J = 10.4, 1.2 Hz, 1H), 4.75 (dt, J = 6.0, 1.2 Hz, 2H), 2.91 (s, 3H), 2.39 (s, 3H). $^{13}\text{C NMR}$ (126 MHz, CDCl_3) δ 166.4, 148.4, 136.9, 132.1, 129.3, 127.5, 125.8, 125.5, 120.1, 120.1, 119.0, 118.9, 118.8, 116.2, 113.4, 65.8, 18.6, 10.7. **HREI-MS**: Adduct not detected by high resolution mass spectrometry.

7.42 Synthesis of Allyl (Z)-3-(3,5-dimethyl-1H-pyrrol-2-yl)-2-(2-nitro-4-(trifluoromethyl)phenyl)acrylate (Z)-46

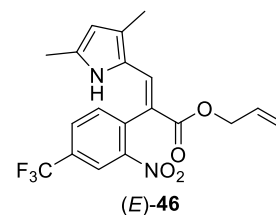
Compound (Z)-46 was synthesised using General Method 2 with allyl ester 40 (0.436 g, 1.509 mmol), 7 (0.300 g, 1.656 mmol), K_2CO_3 (0.423 g, 3.057 mmol) and 18-crown-6 (0.205 g, 0.776 mmol) reacted at room temperature for 20 hours followed by a further 24 hours of heating at 45 °C to afford (Z)-46 (0.052 g, 9%) as a red solid, (E)-46 (0.034 g, 6%) as a red solid, 50 (0.076 g, 14%) as a yellow highly fluorescent solid (blue in hexane under 365 nm UV light) and 51 (0.023 g, 4%) as a yellow tinged oil.

R_f = 0.55 (10% acetone: 90% pet. spirit). **M.P.** 90-93 °C; **IR** (solid, ν/cm^{-1}): 3531, 3395, 3286, 3089, 2922, 2878, 1692, 1650, 1626, 1572, 1535, 1500, 1431, 1391, 1320, 1264, 1244, 1223, 1175, 1114, 1087, 1028, 983, 919, 824, 803, 780, 728, 705, 666, 615,



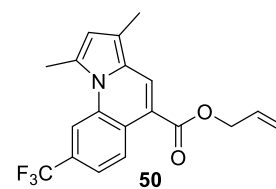
551, 453. $^1\text{H NMR}$ (500 MHz, CDCl_3) δ 11.85 (br s, 1H), 8.29 (d, J = 0.9 Hz, 1H), 7.86 (dd, J = 8.0, 1.3 Hz, 1H), 7.58 (d, J = 8.0 Hz, 1H), 6.83 (s, 1H), 5.93 (d, J = 2.4 Hz, 1H), 5.79 (ddt, J = 17.1, 10.6, 5.8 Hz, 1H), 5.16 (dq, J = 10.4, 1.2 Hz, 1H), 5.14 (dq, J = 17.1, 1.4 Hz, 1H), 4.56 (dt, J = 5.8, 1.3 Hz, 2H), 2.36 (s, 3H), 2.18 (s, 3H). $^{13}\text{C NMR}$ (126 MHz, CDCl_3) δ 166.5, 148.7, 140.7, 135.4, 133.5, 132.6, 132.1, 131.6, 130.1 (q, J = 33.9 Hz), 129.7 (q, J = 3.3 Hz), 124.5, 123.0 (q, J = 272.4 Hz), 121.8 (q, J = 3.8 Hz), 118.6, 112.2, 111.9, 65.8, 13.7, 11.6. **HREI-MS**: m/z calculated for $\text{C}_{19}\text{H}_{18}\text{F}_3\text{N}_2\text{O}_4$ [$\text{M}+\text{H}^+$] 395.1213; observed 395.1201.

R_f = 0.33 (10% acetone: 90% pet. spirit). **M.P.** 110-115 °C; **IR** (solid, ν/cm^{-1}): 3526, 3398, 2922, 2853, 1688, 1604, 1539, 1502, 1458, 1354, 1323, 1222, 1173, 1110, 1075, 970, 929, 797, 666, 601, 439. **¹H NMR** (500 MHz, CDCl₃) δ 8.45 (d, J = 1.0 Hz, 1H),



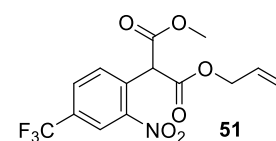
7.90 (dd, J = 7.9, 1.1 Hz, 1H), 7.83 (s, 1H), 7.67 (d, J = 7.9 Hz, 1H), 6.80 (br s, 1H), 5.87 (ddt, J = 17.1, 10.8, 8.2 Hz, 1H), 5.79 (d, J = 1.8 Hz, 1H), 5.24-5.17 (m, 2H), 4.67-4.58 (m, 2H), 2.20 (s, 3H), 2.01 (s, 3H). **¹³C NMR** (126 MHz, CDCl₃) δ 165.7, 149.5, 136.3, 135.0, 134.3, 132.1, 131.7 (q, J = 34.3 Hz), 131.7, 129.7 (q, J = 3.3 Hz), 128.3, 123.1, 122.7 (q, J = 272.9 Hz), 122.6 (q, J = 3.8 Hz), 118.1, 114.6, 111.4, 65.8, 13.4, 11.5. **HREI-MS**: m/z calculated for C₁₉H₁₈F₃N₂O₄ [M+H⁺] 395.1213; observed 395.1195.

R_f = 0.76 (10% acetone: 90% pet. spirit). **M.P.** 110-114 °C; **IR** (solid, ν/cm^{-1}): 2959, 2924, 2855, 1730, 1692, 1651, 1629, 1601, 1535, 1507, 1456, 1428, 1391, 1321, 1274, 1244, 1220, 1161, 1134, 1112, 1087, 1025, 920, 863, 824, 769, 736, 658, 648, 616,



575, 549, 437. **¹H NMR** (400 MHz, CDCl₃) δ 9.12 (d, J = 8.6 Hz, 1H), 8.47 (s, 1H), 8.27 (s, 1H), 7.56 (dd, J = 8.7, 1.1 Hz, 1H), 6.51 (s, 1H), 6.12 (ddt, J = 17.2, 10.5, 5.7 Hz, 1H), 5.46 (dq, J = 17.2, 1.5 Hz, 1H), 5.33 (dq, J = 10.4, 1.3 Hz, 1H), 4.88 (dt, J = 5.7, 1.4 Hz, 2H), 2.93 (s, 3H), 2.40 (s, 3H). **¹³C NMR** (101 MHz, CDCl₃) δ 166.0, 134.9, 132.7, 129.8, 127.9 (q, J = 32.5 Hz), 127.8, 126.1, 125.8, 125.8, 124.3 (q, J = 272.1 Hz), 120.0 (q, J = 3.5 Hz), 119.2, 118.7, 118.4, 113.1 (q, J = 4.3 Hz), 112.3, 65.5, 18.4, 10.8. **HREI-MS**: m/z calculated for C₁₉H₁₇F₃NO₂ [M+H⁺] 348.1206; observed 348.1208.

R_f = 0.31 (10% acetone: 90% pet. spirit). **IR** (oil, ν/cm^{-1}): 3089, 2958, 1737, 1632, 1580, 1541, 1507, 1438, 1413, 1354, 1325, 1274, 1225, 1131, 1088, 988, 906, 843, 787, 747, 705, 685, 643,

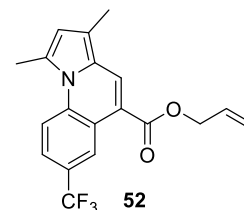


551, 511, 434. **¹H NMR** (400 MHz, CDCl₃) δ 8.33 (d, J = 1.2 Hz, 1H), 7.91 (dd, J = 8.2, 1.5 Hz, 1H), 7.73 (d, J = 8.2 Hz, 1H), 5.90 (ddt, J = 17.2, 10.5, 5.8 Hz, 1H), 5.40 (s, 1H), 5.33 (dq, J = 17.2, 1.4 Hz, 1H), 5.28 (dq, J = 10.4, 1.2 Hz, 1H), 4.71 (dt, J = 5.8, 1.3 Hz, 2H), 3.82 (s, 3H). **¹³C NMR** (101 MHz, CDCl₃) δ 167.1, 166.3, 149.0, 132.8, 132.2 (q, J = 34.6 Hz), 131.7, 131.0, 130.1 (q, J = 3.4 Hz), 122.7 (q, J = 272.9 Hz), 122.7 (q, J = 3.9 Hz), 119.6, 67.2, 54.1, 53.6. **HREI-MS**: m/z calculated for C₁₄H₁₃F₃NO₆ [M+H⁺] 348.0689; observed 348.0689.

7.43 Synthesis of Allyl 1,3-dimethyl-7-(trifluoromethyl)pyrrolo[1,2-*a*]quinoline-5-carboxylate **52**

Compound **52** was synthesised using General Method 2 with allyl ester **41** (0.438 g, 1.514 mmol), **7** (0.301 g, 1.661 mmol), K₂CO₃ (0.423 g, 3.124 mmol) and 18-crown-6 (0.201 g, 0.760 mmol) reacted at room temperature for 20 hours followed by a further 24 hours of heating at 45 °C affording **52** (0.180 g, 34%) as a yellow highly fluorescent solid (blue in hexane under 365 nm UV light).

R_f = 0.68 (20% acetone: 80% pet. spirit). **M.P.** 106-110 °C; **IR** (solid, ν/cm^{-1}): 2923, 2883, 2856, 1683, 1623, 1541, 1494, 1447, 1372, 1336, 1320, 1288, 1254, 1221, 1156, 1111, 1084, 1030, 992, 934, 919, 864, 811, 774, 747, 733, 687, 665, 617, 498, 426. **¹H NMR**



(500 MHz, CDCl₃) δ 9.38 (d, $J = 0.9$ Hz, 1H), 8.31 (d, $J = 8.9$ Hz, 1H), 8.27 (s, 1H), 7.64 (dd, $J = 8.9, 1.7$ Hz, 1H), 6.51 (s, 1H), 6.13 (ddt, $J = 17.1, 10.6, 8.5$ Hz, 1H), 5.47 (dq, $J = 17.2, 1.4$ Hz, 1H), 5.34 (dq, $J = 10.6, 1.2$ Hz, 1H), 4.88 (dt, $J = 5.6, 1.2$ Hz, 2H), 2.93 (s, 3H), 2.40 (s, 3H). **¹³C NMR** (126 MHz, CDCl₃) δ 165.9, 137.2, 132.6, 129.7, 129.5, 128.0, 125.6 (q, $J = 32.8$ Hz), 125.5, 124.7 (q, $J = 3.9$ Hz), 124.5 (q, $J = 271.6$ Hz), 123.0 (q, $J = 3.5$ Hz), 119.0, 118.9, 118.5, 116.3, 112.6, 65.6, 18.7, 10.8. **HREI-MS**: m/z calculated for C₁₉H₁₇F₃NO₂ [M+H⁺] 348.1206; observed 348.1207.

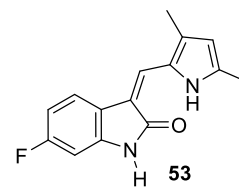
7.44 Fe/CH₃COOH Reduction General Method 3

A mixture of the appropriate *cis* allyl ester and Fe(0) were dissolved in 6 mL CH₃COOH:EtOH:H₂O (1:1:1) and sonicated for 1 hour at 40 °C. After consumption of starting material (TLC analysis), the reaction was filtered through celite and washed with Et₂O (50 mL). The organic layer was extracted with H₂O (3 × 50 mL). The organic layer was dried over anhydrous MgSO₄, filtered and concentrated *in vacuo*. The crude products were purified by preparative TLC (5% acetone: 95% pet. spirit) yielding **53**, **54** and **3**.

7.45 Synthesis of (Z)-3-((3,5-dimethyl-1H-pyrrol-2-yl)methylene)-6-fluoroindolin-2-one **53**

Compound **53** was synthesised using General Method 3 with (Z)-**43** (0.030 g, 0.088 mmol) and Fe(0) (0.049 g, 0.877 mmol) yielding **53** (0.017 g, 75%) as a yellow solid.

R_f = 0.39 (20% Acetone: 80% Pet. spirit). $^1\text{H NMR}$ (500 MHz, d_6 -Acetone) δ 13.28 (br s, 1H), 9.88 (br s, 1H), 7.64 (dd, J = 8.1, 5.2 Hz, 1H), 7.57 (s, 1H), 6.77-6.72 (m, 2H), 5.99 (d, J = 2.5 Hz, 1H), 2.34 (s, 3H), 2.31 (s, 3H). $^{13}\text{C NMR}$ (126 MHz, d_6 -Acetone) δ 170.9,

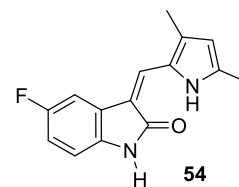


162.6 (d, J = 240.5 Hz, 1C), 140.1 (d, J = 12.3 Hz), 136.7, 132.9, 128.0, 124.1 (d, J = 1.8 Hz), 123.5 (d, J = 2.1 Hz), 119.6 (d, J = 9.6 Hz), 113.3, 112.7, 108.3 (d, J = 22.8 Hz), 98.1 (d, J = 27.1 Hz), 13.7, 11.5. **HREI-MS:** m/z calculated $\text{C}_{15}\text{H}_{13}\text{FN}_2\text{O}$ [$\text{M}+\text{Na}^+$] 279.0904; observed 279.0909.

7.46 Synthesis of (Z)-3-((3,5-dimethyl-1H-pyrrol-2-yl)methylene)-5-fluoroindolin-2-one **54**

Compound **54** was synthesised using General Method 3 with (Z)-**44** (0.030 g, 0.88 mmol) and Fe(0) (0.051 g, 0.906 mmol) yielding **54** (0.018 g, 80%) as a yellow solid.

R_f = 0.38 (20% Acetone: 80% Pet. spirit). $^1\text{H NMR}$ (400 MHz, d_6 -Acetone) δ 13.49 (br s, 1H), 9.75 (br s, 1H), 7.65 (s, 1H), 7.48 (dd, J = 9.3, 2.5 Hz, 1H), 6.91 (dd, J = 8.4, 4.6 Hz, 1H), 6.84 (ddd, J = 9.5, 8.5, 2.5 Hz, 1H), 6.02 (d, J = 2.5 Hz, 1H), 2.35 (s, 3H), 2.34 (s,



3H). $^{13}\text{C NMR}$ (101 MHz, d_6 -Acetone) δ 170.8, 159.8 (d, J = 234.6 Hz), 137.7, 135.6 (d, J = 3.5 Hz), 133.9, 131.5, 129.5, 128.1, 125.3, 113.7, 112.4 (d, J = 24.3 Hz), 110.7 (d, J = 8.7 Hz), 105.7 (d, J = 25.7 Hz), 13.8, 11.6. **HREI-MS:** m/z calculated for $\text{C}_{15}\text{H}_{13}\text{FN}_2\text{O}$ [$\text{M}+\text{H}^+$] 257.1085; observed 257.1090, m/z calculated $\text{C}_{15}\text{H}_{13}\text{FN}_2\text{O}$ [$\text{M}+\text{Na}^+$] 279.0904; observed 279.0910.

7.47 Synthesis of (Z)-3-((3,5-dimethyl-1H-pyrrol-2-yl)methylene)indolin-2-one **3**

Compound **3** was synthesised using General Method 3 with (Z)-**31** (0.030 g, 0.092 mmol) and Fe(0) (0.053 g, 0.949 mmol) yielding **3** (0.017 g, 78%) as a yellow solid (NMR data matched the literature).¹⁹²

References

1. Papac, R. J., Origins of cancer therapy. *Yale J. Biol. Med.* **2001**, *74* (6), 391-8.
2. Gilman, A., The initial clinical trial of nitrogen mustard. *Am. J. Surg.* **1963**, *105*, 574-578.
3. Lind, M. J., Principles of cytotoxic chemotherapy. *Medicine (Baltimore)* **2008**, *36* (1), 19-23.
4. Szybalski, W.; Iyer, V. N., Crosslinking of DNA by enzymatically or chemically activated mitomycins and porfiromycins, bifunctionally "alkylating" antibiotics. *Fed. Proc.* **1964**, *23*, 946-57.
5. Verweij, J.; Pinedo, H. M., Mitomycin C: mechanism of action, usefulness and limitations. *Anti-Cancer Drugs* **1990**, *1* (1), 5-13.
6. Farber, S.; Diamond, L. K.; Mercer, R. D.; Sylvester, R. F.; Wolff, J. A., Temporary remissions in acute leukemia in children produced by folic antagonist, 4-aminopteroylglutamic acid (aminopterin). *N. Engl. J. Med.* **1948**, *238*, 787-793.
7. Parker, W. B., Enzymology of purine and pyrimidine antimetabolites used in the treatment of cancer. *Chem. Rev.* **2009**, *109* (7), 2880-93.
8. McGuire, W. P.; Rowinsky, E. K.; Rosenshein, N. B.; Grumbine, F. C.; Ettinger, D. S.; Armstrong, D. K.; Donehower, R. C., Taxol: a unique antineoplastic agent with significant activity in advanced ovarian epithelial neoplasms. *Ann. Intern. Med.* **1989**, *111* (4), 273-9.
9. Saltz, L. B.; Cox, J. V.; Blanke, C.; Rosen, L. S.; Fehrenbacher, L.; Moore, M. J.; Maroun, J. A.; Ackland, S. P.; Locker, P. K.; Pirota, N.; Elfring, G. L.; Miller, L. L., Irinotecan plus fluorouracil and leucovorin for metastatic colorectal cancer. Irinotecan Study Group. *N. Engl. J. Med.* **2000**, *343* (13), 905-14.
10. Dubost, M.; Ganter, P.; Maral, R.; Ninet, L.; Pinnert, S.; Preudhomme, J.; Werner, G. H., A new antibiotic with cytostatic properties: rubidomycin. *Comptes rendus hebdomadaires des seances de l'Academie des sciences* **1963**, *257*, 1813-5.

11. Tacar, O.; Sriamornsak, P.; Dass, C. R., Doxorubicin: an update on anticancer molecular action, toxicity and novel drug delivery systems. *J. Pharm. Pharmacol.* **2013**, *65* (2), 157-170.
12. van Der Heijden, R.; Jacobs, D. I.; Snoeijer, W.; Hallard, D.; Verpoorte, R., The Catharanthus alkaloids: pharmacognosy and biotechnology. *Curr. Med. Chem.* **2004**, *11* (5), 607-28.
13. Jordan, M. A., Mechanism of Action of Antitumor Drugs that Interact with Microtubules and Tubulin. *Current Medicinal Chemistry - Anti-Cancer Agents* **2002**, *2* (1), 1-17.
14. Pnina, Y.; Aviv, G.; Chaim, G.; Alexander, L., Blocking of EGF-Dependent Cell Proliferation by EGF Receptor Kinase Inhibitors. *Science* **1988**, (4880), 933.
15. Gazit, A.; Osherov, N.; Posner, I.; Yaish, P.; Poradosu, E.; Gilon, C.; Levitzki, A., Tyrphostins. II. Heterocyclic and .alpha.-substituted benzyldenemalononitrile tyrphostins as potent inhibitors of EGF receptor and ErbB2/neu tyrosine kinases. *J. Med. Chem.* **1991**, *34* (6), 1896-1907.
16. Scott, A. M.; Wolchok, J. D.; Old, L. J., Antibody therapy of cancer. *Nature Reviews Cancer* **2012**, *12*, 278.
17. Papetti, M., Mechanisms of normal and tumor-derived angiogenesis. *Am. J. Physiol. Cell Physiol.* **2002**, *282*, C497-C970.
18. Dor, Y., Vascular endothelial growth factor and vascular adjustments to perturbations in oxygen homeostasis. *Am. J. Physiol. Cell Physiol.* **2001**, *280*, C1367-C1374.
19. Pettersson, A., Heterogeneity of the angiogenic response induced in different normal adult tissues by vascular permeability factor/vascular endothelial growth factor. *Lab. Invest.* **2000**, *80*, 99-115.
20. Rahimi, N., The ubiquitin-proteasome system meets angiogenesis. *Mol. Cancer Ther.* **2012**, *11* (3), 538-48.

21. Raza, A.; Franklin, M. J.; Dudek, A. Z., Pericytes and vessel maturation during tumor angiogenesis and metastasis. *Am. J. Hematol.* **2010**, *85* (8), 593-598.
22. Pharmacia Announces Closing of SU5416 (semaxanib) Clinical Trials. *PR Newswire* 2002 Feb 08, 2002, p 1.
23. FDA approves new treatment for gastrointestinal, kidney cancer. *US Fed News Service, Including US State News* 2006 Jan 26, 2006.
24. Raymond, E.; Dahan, L.; Raoul, J.-L.; Bang, Y.-J.; Borbath, I.; Lombard-Bohas, C.; Valle, J.; Metrakos, P.; Smith, D.; Vinik, A.; Chen, J.-S.; Hörsch, D.; Hammel, P.; Wiedenmann, B.; Van Cutsem, E.; Patyna, S.; Lu, D. R.; Blanckmeister, C.; Chao, R.; Ruzzniewski, P., Sunitinib Malate for the Treatment of Pancreatic Neuroendocrine Tumors. *New Engl. J. Med.* **2011**, *364* (6), 501-513.
25. Mendel, D. B.; Schreck, R. E.; West, D. C.; Li, G.; Strawn, L. M.; Tanciongco, S. S.; Vasile, S.; Shawver, L. K.; Cherrington, J. M., The angiogenesis inhibitor SU5416 has long-lasting effects on vascular endothelial growth factor receptor phosphorylation and function. *Clin. Cancer. Res.* **2000**, *6* (12), 4848-58.
26. Gan, H. K.; Seruga, B.; Knox, J. J., Sunitinib in solid tumors. *Expert Opin. Investig. Drugs* **2009**, *18* (6), 821-821.
27. Foye's principles of medicinal chemistry, 5th ed. *Scitech Book News* Jun 2002, 2002.
28. Mena, A. C.; Pulido, E. G.; Guillen-Ponce, C., Understanding the molecular-based mechanism of action of the tyrosine kinase inhibitor: sunitinib. *Anticancer Drugs* **2010**, *21 Suppl 1*, S3-11.
29. Geiduschek, E. P., "Reversible" DNA. *Proc. Natl. Acad. Sci. U. S. A.* **1961**, *47* (7), 950-955.
30. Brookes, P.; Lawley, P. D., The reaction of mono- and di-functional alkylating agents with nucleic acids. *Biochem. J* **1961**, *80* (3), 496-503.
31. Bhatia, U.; Danishefsky, K.; Traganos, F.; Darzynkiewicz, Z., Induction of apoptosis and cell cycle-specific change in expression of p53 in normal

- lymphocytes and MOLT-4 leukemic cells by nitrogen mustard. *Clin. Cancer. Res.* **1995**, *1* (8), 873-80.
32. Guainazzi, A.; Scharer, O. D., Using synthetic DNA interstrand crosslinks to elucidate repair pathways and identify new therapeutic targets for cancer chemotherapy. *Cell. Mol. Life Sci.* **2010**, *67* (21), 3683-97.
33. Handbook, A. M.; Australia, P. S. o., *Australian Medicines Handbook 2013*. Australian Medicines Handbook Pty. Limited: 2013.
34. Scrip, *Scrip's 1991 Cancer Chemotherapy Report*. PJB Publications: 1991.
35. Wohlhueter, R. M.; McIvor, R. S.; Plagemann, P. G. W., Facilitated transport of uracil and 5-fluorouracil, and permeation of orotic-acid into cultured mammalian-cells. *J. Cell. Physiol.* **1980**, *104* (3), 309-319.
36. Diasio, R. B.; Harris, B. E., CLINICAL-PHARMACOLOGY OF 5-FLUOROURACIL. *Clin. Pharmacokinet.* **1989**, *16* (4), 215-237.
37. Heggie, G. D.; Sommadossi, J.-P.; Cross, D. S.; Huster, W. J.; Diasio, R. B., Clinical Pharmacokinetics of 5-Fluorouracil and Its Metabolites in Plasma, Urine, and Bile. *Cancer Res.* **1987**, *47* (8), 2203-2206.
38. Kanamaru, R.; Kakuta, H.; Sato, T.; Ishioka, C.; Wakui, A., The inhibitory effects of 5-fluorouracil on the metabolism of preribosomal and ribosomal RNA in L-1210 cells in vitro. *Cancer Chemother. Pharmacol.* **1986**, *17*, 43-46.
39. Ghoshal, K.; Jacob, S. T., Specific inhibition of pre-ribosomal RNA processing in extracts from the lymphosarcoma cells treated with 5-fluorouracil. *Cancer Res.* **1994**, *54*, 632-636.
40. Santi, D. V.; Hardy, L. W., Catalytic mechanism and inhibition of tRNA (uracil-5-)methyltransferase: evidence for covalent catalysis. *Biochemistry (Mosc.)* **1987**, *26*, 8599-8606.
41. Randerath, K.; Tseng, W. C.; Harris, J. S.; Lu, L. J., Specific effects of 5-fluoropyrimidines and 5-azapyrimidines on modification of the 5 position of

- pyrimidines, in particular the synthesis of 5-methyluracil and 5-methylcytosine in nucleic acids. *Recent Results Cancer Res.* **1983**, *84*, 283-297.
42. Patton, J. R., Ribonucleoprotein particle assembly and modification of U2 small nuclear RNA containing 5-fluorouridine. *Biochemistry (Mosc.)* **1993**, *32*, 8939-8944.
 43. Doong, S. L.; Dolnick, B. J., 5-Fluorouracil substitution alters pre-mRNA splicing in vitro. *J. Biol. Chem.* **1988**, *263*, 4467-4473.
 44. Sommer, H.; Santi, D. V., Purification and amino acid analysis of an active site peptide from thymidylate synthetase containing covalently bound 5-fluoro-2'-deoxyuridylate and methylenetetrahydrofolate. *Biochem. Biophys. Res. Commun.* **1974**, *57*, 689-695.
 45. Santi, D. V.; McHenry, C. S.; Sommer, H., Mechanism of interaction of thymidylate synthetase with 5-fluorodeoxyuridylate. *Biochemistry (Mosc.)* **1974**, *13*, 471-481.
 46. Jackson, R. C.; Grindley, G. B., The Biochemical Basis for Methotrexate Cytotoxicity. 1984; pp 289-315.
 47. Houghton, J. A.; Tillman, D. M.; Harwood, F. G., Ratio of 2'-deoxyadenosine-5'-triphosphate/thymidine-5'-triphosphate influences the commitment of human colon carcinoma cells to thymineless death. *Clin. Cancer Res.* **1995**, *1*, 723-730.
 48. Yoshioka, A., Deoxyribonucleoside triphosphate imbalance. 5-Fluorodeoxyuridine-induced DNA double strand breaks in mouse FM3A cells and the mechanism of cell death. *J. Biol. Chem.* **1987**, *262*, 8235-8241.
 49. Aherne, G. W.; Hardcastle, A.; Raynaud, F.; Jackman, A. L., Immunoreactive dUMP and TTP pools as an index of thymidylate synthase inhibition; effect of tomudex (ZD1694) and a nonpolyglutamated quinazoline antifolate (CB30900) in L1210 mouse leukaemia cells. *Biochem. Pharmacol.* **1996**, *51*, 1293-1301.

50. Mitrovski, B.; Pressacco, J.; Mandelbaum, S.; Erlichman, C., Biochemical effects of folate-based inhibitors of thymidylate synthase in MGH-U1 cells. *Cancer Chemother. Pharmacol.* **1994**, *35*, 109-114.
51. Webley, S. D.; Hardcastle, A.; Ladner, R. D.; Jackman, A. L.; Aherne, G. W., Deoxyuridine triphosphatase (dUTPase) expression and sensitivity to the thymidylate synthase (TS) inhibitor ZD9331. *Br. J. Cancer* **2000**, *83*, 792-799.
52. Ladner, R. D., The role of dUTPase and uracil-DNA repair in cancer chemotherapy. *Curr. Protein Pept. Sci.* **2001**, *2*, 361-370.
53. Lindahl, T., An N-glycosidase from Escherichia coli that releases free uracil from DNA containing deaminated cytosine residues. *Proc. Natl Acad. Sci. USA* **1974**, *71*, 3649-3653.
54. Longley, D. B.; Harkin, D. P.; Johnston, P. G., 5-Fluorouracil: mechanisms of action and clinical strategies. *Nat. Rev. Cancer* **2003**, *3* (5), 330-338.
55. Kemeny, N.; Daly, J.; Reichman, B.; Geller, N.; Botet, J.; Oderman, P., Intrahepatic or systemic infusion of fluorodeoxyuridine in patients with liver metastases from colorectal carcinoma. A randomized trial. *Ann. Intern. Med.* **1987**, *107* (4), 459-465.
56. Cancer, M.-A. G. I., Reappraisal of Hepatic Arterial Infusion in the Treatment of Nonresectable Liver Metastases From Colorectal Cancer. *J. Natl. Cancer Inst.* **1996**, *88* (5), 252-258.
57. Dawson, R. M. C., *Data for biochemical research*. Clarendon Press: Oxford, 1986; p 267.
58. Tranoy-Opalinski, I.; Fernandes, A.; Thomas, M.; Gesson, J. P.; Papot, S., Design of Self-Immolative Linkers for Tumour-Activated Prodrug Therapy. *Anticancer Agents Med. Chem.* **2008**, *8* (6), 618-637.
59. Silverman, R. B., *The organic chemistry of drug design and drug action / Richard B. Silverman*. Academic Press: San Diego :, 1992.

60. Menger, F. M.; Rourk, M. J., Synthesis and Reactivity of 5-Fluorouracil/Cytarabine Mutual Prodrugs. *J. Organic Chem.* **1997**, *62* (26), 9083-8.
61. Wang, W.-S.; Tzeng, C.-H.; Chiou, T.-J.; Liu, J.-H.; Hsieh, R.-K.; Yen, C.-C.; Chen, P.-M., High-Dose Cytarabine and Mitoxantrone as Salvage Therapy for Refractory Non-Hodgkin's Lymphoma. *Jpn. J. Clin. Oncol.* **1997**, *27* (3), 154-7.
62. Parise, R. A.; Egorin, M. J.; Eiseman, J. L.; Joseph, E.; Covey, J. M.; Beumer, J. H., Quantitative determination of the cytidine deaminase inhibitor tetrahydrouridine (THU) in mouse plasma by liquid chromatography/electrospray ionization tandem mass spectrometry. *Rapid Commun. Mass Spectrom.* **2007**, *21* (13), 1991-7.
63. Bildstein, L.; Dubernet, C.; Couvreur, P., Prodrug-based intracellular delivery of anticancer agents. *Adv. Drug Deliv. Rev.* **2011**, *63* (1-2), 3-23.
64. Joubert, N.; Denevault-Sabourin, C.; Bryden, F.; Viaud-Massuard, M. C., Towards antibody-drug conjugates and prodrug strategies with extracellular stimuli-responsive drug delivery in the tumor microenvironment for cancer therapy. *Eur. J. Med. Chem.* **2017**, *142*, 393-415.
65. Trail, P. A.; King, H. D.; Dubowchik, G. M., Monoclonal antibody drug immunoconjugates for targeted treatment of cancer. *Cancer Immunology, Immunotherapy: CII* **2003**, *52* (5), 328-337.
66. Frigerio, M.; Kyle, A. F., The Chemical Design and Synthesis of Linkers Used in Antibody Drug Conjugates. *Curr. Top. Med. Chem.* **2017**, *17* (32), 3393-3424.
67. de Claro, R. A.; McGinn, K. M.; Kwitkowski, V. E.; Bullock, J.; Khandelwal, A.; Habtemariam, B. A.; Ouyang, Y.; Saber, H.; Lee, K.; Koti, K.; Rothmann, M. D.; Shapiro, M.; Borrego, F.; Clouse, K.; Chen, X. H.; Brown, J.; Akinsanya, L.; Kane, R. C.; Kaminskis, E.; Farrell, A.; Pazdur, R., U.S. Food and Drug Administration Approval Summary: Brentuximab Vedotin for the Treatment of Relapsed Hodgkin Lymphoma or Relapsed Systemic Anaplastic Large Cell Lymphoma. *Clin. Cancer. Res.* **2012**.

68. Francisco, J. A.; Cervený, C. G.; Meyer, D. L.; Mixan, B. J.; Klussman, K.; Chace, D. F.; Rejniak, S. X.; Gordon, K. A.; DeBlanc, R.; Toki, B. E.; Law, C. L.; Doronina, S. O.; Siegall, C. B.; Senter, P. D.; Wahl, A. F., cAC10-vcMMAE, an anti-CD30-monomethyl auristatin E conjugate with potent and selective antitumor activity. *Blood* **2003**, *102* (4), 1458-65.
69. Doronina, S. O.; Toki, B. E.; Torgov, M. Y.; Mendelsohn, B. A.; Cervený, C. G.; Chace, D. F.; DeBlanc, R. L.; Gearing, R. P.; Bovee, T. D.; Siegall, C. B.; Francisco, J. A.; Wahl, A. F.; Meyer, D. L.; Senter, P. D., Development of potent monoclonal antibody auristatin conjugates for cancer therapy. *Nat. Biotechnol.* **2003**, *21* (7), 778-784.
70. Alley, S. C.; Zhang, X.; Okeley, N. M.; Anderson, M.; Law, C.-L.; Senter, P. D.; Benjamin, D. R., The Pharmacologic Basis for Antibody-Auristatin Conjugate Activity. *J. Pharmacol. Exp. Ther.* **2009**, *330* (3), 932-938.
71. Amiri-Kordestani, L.; Blumenthal, G. M.; Xu, Q. C.; Zhang, L.; Tang, S. W.; Ha, L.; Weinberg, W. C.; Chi, B.; Candau-Chacon, R.; Hughes, P.; Russell, A. M.; Miksinski, S. P.; Chen, X. H.; McGuinn, W. D.; Palmby, T.; Schrieber, S. J.; Liu, Q.; Wang, J.; Song, P.; Mehrotra, N.; Skarupa, L.; Clouse, K.; Al-Hakim, A.; Sridhara, R.; Ibrahim, A.; Justice, R.; Pazdur, R.; Cortazar, P., FDA approval: ado-trastuzumab emtansine for the treatment of patients with HER2-positive metastatic breast cancer. *Clin. Cancer Res.* **2014**, *20* (17), 4436-41.
72. Le, X.-F.; Pruefer, F.; Bast, R. C., HER2-targeting Antibodies Modulate the Cyclin-dependent Kinase Inhibitor p27Kip1 via Multiple Signaling Pathways. *Cell Cycle* **2005**, *4* (1), 87-95.
73. Dean-Colomb, W.; Esteva, F. J., Her2-positive breast cancer: Herceptin and beyond. *Eur. J. Cancer* **2008**, *44* (18), 2806-2812.
74. Cho, H.-S.; Mason, K.; Ramyar, K. X.; Stanley, A. M.; Gabelli, S. B.; Denney Jr, D. W.; Leahy, D. J., Structure of the extracellular region of HER2 alone and in complex with the Herceptin Fab. *Nature* **2003**, *421*, 756.
75. Barok, M.; Joensuu, H.; Isola, J., Trastuzumab emtansine: mechanisms of action and drug resistance. *Breast Cancer Res.* **2014**, *16* (2), 209.

76. Petrova, V.; Annicchiarico-Petruzzelli, M.; Melino, G.; Amelio, I., The hypoxic tumour microenvironment. *Oncogenesis* **2018**, *7* (1), 10.
77. Siemann, D. W., The Unique Characteristics of Tumor Vasculature and Preclinical Evidence for its Selective Disruption by Tumor-Vascular Disrupting Agents. *Cancer Treat. Rev.* **2011**, *37* (1), 63-74.
78. Pérez de Heredia, F.; Wood, I. S.; Trayhurn, P., Hypoxia stimulates lactate release and modulates monocarboxylate transporter (MCT1, MCT2, and MCT4) expression in human adipocytes. *Pflügers Archiv - European Journal of Physiology* **2010**, *459* (3), 509-518.
79. Denning, C.; Pitts, J. D., Bystander effects of different enzyme-prodrug systems for cancer gene therapy depend on different pathways for intercellular transfer of toxic metabolites, a factor that will govern clinical choice of appropriate regimes. *Hum. Gene Ther.* **1997**, *8* (15), 1825-35.
80. Wilson, W. R.; Moselen, J. W.; Cliffe, S.; Denny, W. A.; Ware, D. C., Exploiting tumor hypoxia through bioreductive release of diffusible cytotoxins: The cobalt(III)-nitrogen mustard complex SN 24771. *International Journal of Radiation Oncology*Biology*Physics* **1994**, *29* (2), 323-327.
81. Lienhart, W.-D.; Gudipati, V.; Macheroux, P., The human flavoproteome. *Arch. Biochem. Biophys.* **2013**, *535* (2), 150-162.
82. Hunter, F. W.; Wouters, B. G.; Wilson, W. R., Hypoxia-activated prodrugs: paths forward in the era of personalised medicine. *Br. J. Cancer* **2016**, *114* (10), 1071-7.
83. Chen, Y.; Hu, L., Design of anticancer prodrugs for reductive activation. *Med. Res. Rev.* **2009**, *29* (1), 29-64.
84. Belcourt, M. F.; Hodnick, W. F.; Rockwell, S.; Sartorelli, A. C., Exploring the mechanistic aspects of mitomycin antibiotic bioactivation in Chinese hamster ovary cells overexpressing NADPH:cytochrome C (P-450) reductase and DT-diaphorase. *Adv. Enzyme Regul.* **1998**, *38*, 111-33.

85. Bailey, S. M.; Wyatt, M. D.; Friedlos, F.; Hartley, J. A.; Knox, R. J.; Lewis, A. D.; Workman, P., Involvement of DT-diaphorase (EC 1.6.99.2) in the DNA cross-linking and sequence selectivity of the bioreductive anti-tumour agent EO9. *Br. J. Cancer* **1997**, *76* (12), 1596-1603.
86. Phillips, R. M.; Hendriks, H. R.; Sweeney, J. B.; Reddy, G.; Peters, G. J., Efficacy, pharmacokinetic and pharmacodynamic evaluation of apaziquone in the treatment of non-muscle invasive bladder cancer. *Expert Opin. Drug Metab. Toxicol.* **2017**, *13* (7), 783-791.
87. Lajin, B.; Alachkar, A., The NQO1 polymorphism C609T (Pro187Ser) and cancer susceptibility: a comprehensive meta-analysis. *Br. J. Cancer* **2013**, *109* (5), 1325-1337.
88. Srijiwangsa, P.; Na Bangchang, K., *Roles of NAD (P) H-Quinone Oxidoreductase 1 (NQO1) On Cancer Progression and Chemoresistance*. 2017; Vol. 06.
89. Sugiura, K., Antitumor activity of purine N-oxides and effect of selected compounds on tumors induced by purine N-oxides. *Cancer Chemotherapy Reports Part 2* **1968**, *1* (2S), 383-&.
90. Hugo, C.; Mercedes, G., N-Oxides as Hypoxia Selective Cytotoxins. *Mini-Rev. Med. Chem.* **2001**, *1* (3), 219-231.
91. Raleigh, S. M.; Wanogho, E.; Burke, M. D.; McKeown, S. R.; Patterson, L. H., Involvement of human cytochromes P450 (CYP) in the reductive metabolism of AQ4N, a hypoxia activated anthraquinone di-N-oxide prodrug. *Int. J. Radiat. Oncol. Biol. Phys.* **1998**, *42* (4), 763-767.
92. Nishida, C. R.; Ortiz de Montellano, P. R., Reductive heme-dependent activation of the n-oxide prodrug AQ4N by nitric oxide synthase. *J. Med. Chem.* **2008**, *51* (16), 5118-5120.
93. Patterson, L. H.; Craven, M. R.; Fisher, G. R.; Teesdale-Spittle, P., Aliphatic amine N-oxides of DNA binding agents as bioreductive drugs. *Oncol. Res.* **1994**, *6* (10-11), 533-8.

94. Albertella, M. R.; Loadman, P. M.; Jones, P. H.; Phillips, R. M.; Rampling, R.; Burnet, N.; Alcock, C.; Anthoney, A.; Vjaters, E.; Dunk, C. R.; Harris, P. A.; Wong, A.; Lalani, A. S.; Twelves, C. J., Hypoxia-Selective Targeting by the Bioreductive Prodrug AQ4N in Patients with Solid Tumors: Results of a Phase I Study. *Clin. Cancer. Res.* **2008**, *14* (4), 1096-1104.
95. Steward, W. P.; Middleton, M.; Benghiat, A.; Loadman, P. M.; Hayward, C.; Waller, S.; Ford, S.; Halbert, G.; Patterson, L. H.; Talbot, D., The use of pharmacokinetic and pharmacodynamic end points to determine the dose of AQ4N, a novel hypoxic cell cytotoxin, given with fractionated radiotherapy in a phase I study. *Ann. Oncol.* **2007**, *18* (6), 1098-1103.
96. Zeman, E. M.; Brown, J. M.; Lemmon, M. J.; Hirst, V. K.; Lee, W. W., SR-4233: a new bioreductive agent with high selective toxicity for hypoxic mammalian cells. *Int. J. Radiat. Oncol. Biol. Phys.* **1986**, *12* (7), 1239-42.
97. Chinje, E. C.; Cowen, R. L.; Feng, J.; Sharma, S. P.; Wind, N. S.; Harris, A. L.; Stratford, I. J., Non-nuclear localized human NOSII enhances the bioactivation and toxicity of tirapazamine (SR4233) in vitro. *Mol. Pharmacol.* **2003**, *63* (6), 1248-55.
98. Patterson, A. V.; Saunders, M. P.; Chinje, E. C.; Patterson, L. H.; Stratford, I. J., Enzymology of tirapazamine metabolism: a review. *Anticancer. Drug Des.* **1998**, *13* (6), 541-73.
99. Chowdhury, G.; Junnotula, V.; Daniels, J. S.; Greenberg, M. M.; Gates, K. S., DNA Strand Damage Product Analysis Provides Evidence that the Tumor Cell-Specific Cytotoxin Tirapazamine Produces Hydroxyl Radical and Acts as a Surrogate for O(2). *J. Am. Chem. Soc.* **2007**, *129* (42), 12870.
100. Daniels, J. S.; Gates, K. S., DNA Cleavage by the Antitumor Agent 3-Amino-1,2,4-benzotriazine 1,4-Dioxide (SR4233): Evidence for Involvement of Hydroxyl Radical. *J. Am. Chem. Soc.* **1996**, *118* (14), 3380-3385.
101. DiSilvestro, P. A.; Ali, S.; Craighead, P. S.; Lucci, J. A.; Lee, Y.-C.; Cohn, D. E.; Spiertos, N. M.; Tewari, K. S.; Muller, C.; Gajewski, W. H.; Steinhoff, M. M.; Monk, B. J., Phase III Randomized Trial of Weekly Cisplatin and Irradiation

- Versus Cisplatin and Tirapazamine and Irradiation in Stages IB2, IIA, IIB, IIIB, and IVA Cervical Carcinoma Limited to the Pelvis: A Gynecologic Oncology Group Study. *J. Clin. Oncol.* **2014**, *32* (5), 458-464.
102. Rischin, D.; Hicks, R. J.; Fisher, R.; Binns, D.; Corry, J.; Porceddu, S.; Peters, L. J., Prognostic Significance of [18F]-Misonidazole Positron Emission Tomography–Detected Tumor Hypoxia in Patients With Advanced Head and Neck Cancer Randomly Assigned to Chemoradiation With or Without Tirapazamine: A Substudy of Trans-Tasman Radiation Oncology Group Study 98.02. *J. Clin. Oncol.* **2006**, *24* (13), 2098-2104.
103. Blower, P. J.; Dilworth, J. R.; Maurer, R. I.; Mullen, G. D.; Reynolds, C. A.; Zheng, Y., Towards new transition metal-based hypoxic selective agents for therapy and imaging. *J. Inorg. Biochem.* **2001**, *85* (1), 15-22.
104. Ware, D. C.; Palmer, B. D.; Wilson, W. R.; Denny, W. A., Hypoxia-selective antitumor agents. 7. Metal complexes of aliphatic mustards as a new class of hypoxia-selective cytotoxins. Synthesis and evaluation of cobalt(III) complexes of bidentate mustards. *J. Med. Chem.* **1993**, *36* (13), 1839-46.
105. Ware, D. C.; Palmer, H. R.; Pruijn, F. B.; Anderson, R. F.; Brothers, P. J.; Denny, W. A.; Wilson, W. R., Bis(dialkyl)dithiocarbamate cobalt(III) complexes of bidentate nitrogen mustards: synthesis, reduction chemistry and biological evaluation as hypoxia-selective cytotoxins. *Anticancer. Drug Des.* **1998**, *13* (2), 81-103.
106. Ware, D. C.; Wilson, W. R.; Denny, W. A.; Rickard, C. E. F., Design and synthesis of cobalt(III) nitrogen mustard complexes as hypoxia selective cytotoxins. The X-ray crystal structure of bis(3-chloropentane-2,4-dionato)(*RS-N,N'*-bis(2-chloroethyl)ethylenediamine)cobalt(III) perchlorate, [Co(Clacac)₂(bce)]ClO₄. *J. Chem. Soc., Chem. Commun.* **1991**, (17), 1171-1173.
107. Denny, W. A., Review: The role of hypoxia-activated prodrugs in cancer therapy. *Lancet Oncol.* **2000**, *1*, 25-29.
108. Chang, J. Y.-C.; Lu, G.-L.; Stevenson, R. J.; Brothers, P. J.; Clark, G. R.; Botting, K. J.; Ferry, D. M.; Tercel, M.; Wilson, W. R.; Denny, W. A.; Ware, D. C., Cross-

- Bridged Cyclen or Cyclam Co(III) Complexes Containing Cytotoxic Ligands as Hypoxia-Activated Prodrugs. *Inorg. Chem.* **2013**, *52* (13), 7688-7698.
109. Parker, L. L.; Lacy, S. M.; Farrugia, L. J.; Evans, C.; Robins, D. J.; O'Hare, C. C.; Hartley, J. A.; Jaffar, M.; Stratford, I. J., A Novel Design Strategy for Stable Metal Complexes of Nitrogen Mustards as Bioreductive Prodrugs. *J. Med. Chem.* **2004**, *47* (23), 5683-5689.
110. Palmer, B. D.; Wilson, W. R.; Pullen, S. M.; Denny, W. A., Hypoxia-selective antitumor agents. 3. Relationships between structure and cytotoxicity against cultured tumor cells for substituted *N,N*-bis(2-chloroethyl)anilines. *J. Med. Chem.* **1990**, *33* (1), 112-121.
111. Guise, C. P.; Wang, A. T.; Theil, A.; Bridewell, D. J.; Wilson, W. R.; Patterson, A. V., Identification of human reductases that activate the dinitrobenzamide mustard prodrug PR-104A: a role for NADPH:cytochrome P450 oxidoreductase under hypoxia. *Biochem. Pharmacol.* **2007**, *74* (6), 810-20.
112. Moradi Manesh, D.; El-Hoss, J.; Evans, K.; Richmond, J.; Toscan, C. E.; Bracken, L. S.; Hedrick, A.; Sutton, R.; Marshall, G. M.; Wilson, W. R.; Kurmasheva, R. T.; Billups, C.; Houghton, P. J.; Smith, M. A.; Carol, H.; Lock, R. B., AKR1C3 is a biomarker of sensitivity to PR-104 in preclinical models of T-cell acute lymphoblastic leukemia. *Blood* **2015**, *126* (10), 1193-202.
113. Benito, J.; Shi, Y.; Szymanska, B.; Carol, H.; Boehm, I.; Lu, H.; Konoplev, S.; Fang, W.; Zweidler-McKay, P. A.; Campana, D.; Borthakur, G.; Bueso-Ramos, C.; Shpall, E.; Thomas, D. A.; Jordan, C. T.; Kantarjian, H.; Wilson, W. R.; Lock, R.; Andreeff, M.; Konopleva, M., Pronounced Hypoxia in Models of Murine and Human Leukemia: High Efficacy of Hypoxia-Activated Prodrug PR-104. *PLoS ONE* **2011**, *6* (8), e23108.
114. Konopleva, M., Phase I/II study of the hypoxia-activated prodrug PR104 in refractory/relapsed acute myeloid leukemia and acute lymphoblastic leukemia. *Haematologica (Roma)* *100* (7), 927-934.
115. Gu, Y.; Tingle, M. D.; Wilson, W. R., Glucuronidation of anticancer prodrug PR-104A: species differences, identification of human UDP-

- glucuronosyltransferases, and implications for therapy. *J. Pharmacol. Exp. Ther.* **2011**, *337* (3), 692-702.
116. Zheng, L., Physiologic hypoxia and oxygen homeostasis in the healthy intestine. A Review in the Theme: Cellular Responses to Hypoxia. *Am. J. Physiol. Cell Physiol.* **309** (6), C350-C360.
117. Eliasson, P.; Jonsson, J. I., The hematopoietic stem cell niche: low in oxygen but a nice place to be. *J. Cell. Physiol.* **2010**, *222* (1), 17-22.
118. Franko, A. J., Misonidazole and other hypoxia markers: metabolism and applications. *Int. J. Radiat. Oncol. Biol. Phys.* **1986**, *12* (7), 1195-202.
119. Raleigh, J. A.; Liu, S. F., Reductive fragmentation of 2-nitroimidazoles: amines and aldehydes. *Int. J. Radiat. Oncol. Biol. Phys.* **1984**, *10* (8), 1337-40.
120. Duan, J.-X.; Jiao, H.; Kaizerman, J.; Stanton, T.; Evans, J. W.; Lan, L.; Lorente, G.; Banica, M.; Jung, D.; Wang, J.; Ma, H.; Li, X.; Yang, Z.; Hoffman, R. M.; Ammons, W. S.; Hart, C. P.; Matteucci, M., Potent and Highly Selective Hypoxia-Activated Achiral Phosphoramidate Mustards as Anticancer Drugs. *J. Med. Chem.* **2008**, *51* (8), 2412-2420.
121. Huang, Y.; Tian, Y.; Zhao, Y.; Xue, C.; Zhan, J.; Liu, L.; He, X.; Zhang, L., Efficacy of the hypoxia-activated prodrug evofosfamide (TH-302) in nasopharyngeal carcinoma in vitro and in vivo. *Cancer Commun.* **2018**, *38* (1), 15.
122. Weiss, G. J.; Infante, J. R.; Chiorean, E. G.; Borad, M. J.; Bendell, J. C.; Molina, J. R.; Tibes, R.; Ramanathan, R. K.; Lewandowski, K.; Jones, S. F.; Lacouture, M. E.; Langmuir, V. K.; Lee, H.; Kroll, S.; Burris, H. A., 3rd, Phase 1 study of the safety, tolerability, and pharmacokinetics of TH-302, a hypoxia-activated prodrug, in patients with advanced solid malignancies. *Clin. Cancer. Res.* **2011**, *17* (9), 2997-3004.
123. Borad, M. J.; Reddy, S. G.; Bahary, N.; Uronis, H. E.; Sigal, D.; Cohn, A. L.; Schelman, W. R.; Stephenson, J., Jr.; Chiorean, E. G.; Rosen, P. J.; Ulrich, B.; Dragovich, T.; Del Prete, S. A.; Rarick, M.; Eng, C.; Kroll, S.; Ryan, D. P.,

- Randomized Phase II Trial of Gemcitabine Plus TH-302 Versus Gemcitabine in Patients With Advanced Pancreatic Cancer. *J. Clin. Oncol.* **2015**, *33* (13), 1475-81.
124. Constantinidou, A.; van der Graaf, W. T. A., The fate of new fosfamides in phase III studies in advanced soft tissue sarcoma. *Eur. J. Cancer* **2017**, *84*, 257-261.
125. Atwell, G. J.; Sykes, B. M.; O'Connor, C. J.; Denny, W. A., Relationships between structure and kinetics of cyclization of 2-aminoaryl amides: potential prodrugs of cyclization-activated aromatic mustards. *J. Med. Chem.* **1994**, *37* (3), 371-380.
126. Wilson, W. R.; Hay, M. P., Targeting hypoxia in cancer therapy. *Nat. Rev. Cancer* **2011**, *11* (6), 393-410.
127. McKeown, S. R.; Cowen, R. L.; Williams, K. J., Bioreductive drugs: from concept to clinic. *Clin. Oncol. (R. Coll. Radiol.)* **2007**, *19* (6), 427-42.
128. O'Connor, L. J.; Cazares-Körner, C.; Saha, J.; Evans, C. N. G.; Stratford, M. R. L.; Hammond, E. M.; Conway, S. J., Design, synthesis and evaluation of molecularly targeted hypoxia-activated prodrugs. *Nat. Protoc.* **2016**, *11* (4), 781-794.
129. Mistry, I. N.; Thomas, M.; Calder, E. D. D.; Conway, S. J.; Hammond, E. M., Clinical Advances of Hypoxia-Activated Prodrugs in Combination With Radiation Therapy. *Int. J. Radiat. Oncol. Biol. Phys.* **2017**, *98* (5), 1183-1196.
130. Parveen, I.; Naughton, D. P.; Whish, W. J. D.; Threadgill, M. D., 2-Nitroimidazol-5-ylmethyl as a potential bioreductively activated prodrug system: reductively triggered release of the parp inhibitor 5-bromoisoquinolinone. *Bioorg. Med. Chem. Lett.* **1999**, *9* (14), 2031-2036.
131. Cazares-Korner, C.; Pires, I. M.; Swallow, I. D.; Grayer, S. C.; O'Connor, L. J.; Olcina, M. M.; Christlieb, M.; Conway, S. J.; Hammond, E. M., CH-01 is a hypoxia-activated prodrug that sensitizes cells to hypoxia/reoxygenation through inhibition of Chk1 and Aurora A. *ACS Chem. Biol.* **2013**, *8* (7), 1451-9.

132. Lindquist, K.; Cran, J.; Kordic, K.; Chua, P.; Winters, G.; Tan, J.; Lozada, J.; Kyle, A.; Evans, J.; Minchinton, A., Selective radiosensitization of hypoxic cells using BCCA621C: A novel hypoxia activated prodrug targeting DNA-dependent protein kinase. *Tumor Microenvironment and Therapy* **2013**, *1*, 46-55.
133. Patterson, A. V.; Jaswail, J.; Syddall, S. P.; Abbattista, M.; van Leeuwen, W.; Puryer, M.; Thompson, A.; Hsu, A.; Mehta, S.; Pruijn, A.; Lu, G. L.; Donate, F.; Denny, W. A.; Wilson, W. R.; Smaill, J. B., Cellular metabolism, murine pharmacokinetics and preclinical antitumor activity of SN29966, a novel hypoxia-activated irreversible pan-HER inhibitor. 2009; Vol. 8.
134. Patterson, A. V.; Jaiswal, J.; Carlin, K.; Abbattista, M. R.; Guise, C. P.; Silva, S.; Lee, H.; Lu, G.-L.; Anderson, R. F.; Melink, T. J.; Gutheil, J. C.; Smaill, J. B., PR610: A novel hypoxia-selective tyrosine kinase inhibitor in phase I clinical trial. 2013; Vol. 12.
135. Lu, G.-L.; Ashoorzadeh, A.; Anderson, R. F.; Patterson, A. V.; Smaill, J. B., Synthesis of substituted 5-bromomethyl-4-nitroimidazoles and use for the preparation of the hypoxia-selective multikinase inhibitor SN29966. *Tetrahedron* **2013**, *69* (43), 9130-9138.
136. Phillips, R. M., Targeting the hypoxic fraction of tumours using hypoxia-activated prodrugs. *Cancer Chemother. Pharmacol.* **2016**, *77* (3), 441-457.
137. Patterson, A. V.; Silva, S.; Guise, C.; Bull, M.; Abbattista, M.; Hsu, A.; Sun, J. D.; Hart, C. P.; Pearce, T. E.; Smaill, J. B., TH-4000, a hypoxia-activated EGFR/Her2 inhibitor to treat EGFR-TKI resistant T790M-negative NSCLC. *J. Clin. Oncol.* **2015**, *33* (15_suppl), e13548-e13548.
138. Sudta, P.; Kirk, N.; Bezos, A.; Gurlica, A.; Mitchell, R.; Weber, T.; Willis, A. C.; Prabpai, S.; Kongsaree, P.; Parish, C. R.; Suksamrarn, S.; Kelso, M. J., Synthesis, Structural Characterisation, and Preliminary Evaluation of Non-Indolin-2-one-based Angiogenesis Inhibitors Related to Sunitinib (Sutent®). *Aust. J. Chem.* **2013**, *66* (8), 864-873.

139. Kirk, N. Synthetic and Biological Investigations into Hypoxia-Activated Anti-Tumour Codrugs. Doctor of Philosophy, University of Wollongong, Wollongong NSW 2522, Australia, 2015.
140. Leng, X.; Yang, B.; Liu, Y.; Xie, Y.; Tong, J., Synthesis and Characterization of Three Novel Nitrogen-containing Macrolides. In *Zeitschrift für Naturforschung B*, 2011; Vol. 66, p 930.
141. Pola, M. K.; Ramakrishnam Raju, M. V.; Lin, C.-M.; Putikam, R.; Lin, M.-C.; Epperla, C. P.; Chang, H.-C.; Chen, S.-Y.; Lin, H.-C., A fully-aqueous red-fluorescent probe for selective optical sensing of Hg²⁺ and its application in living cells. *Dyes and Pigments* **2016**, *130*, 256-265.
142. Gong, W.-L.; Xiong, Z.-J.; Xin, B.; Yin, H.; Duan, J.-S.; Yan, J.; Chen, T.; Hua, Q.-X.; Hu, B.; Huang, Z.-L.; Zhu, M.-Q., Twofold photoswitching of NIR fluorescence and EPR based on the PMI-N-HABI for optical nanoimaging of electrospun polymer nanowires. *Journal of Materials Chemistry C* **2016**, *4* (13), 2498-2505.
143. Niculescu-Duvaz, D.; Scanlon, I.; Niculescu-Duvaz, I.; Springer, C. J., A higher yielding synthesis of the clinical prodrug ZD2767P using di-protected 4-[N,N-bis(2-hydroxyethyl)amino]phenyl chloroformate. *Tetrahedron Lett.* **2005**, *46* (40), 6919-6922.
144. Corey, E. J.; Venkateswarlu, A., Protection of hydroxyl groups as tert-butyldimethylsilyl derivatives. *J. Am. Chem. Soc.* **1972**, *94* (17), 6190-6191.
145. Kirk, N. S.; Bezos, A.; Willis, A. C.; Sudta, P.; Suksamrarn, S.; Parish, C. R.; Ranson, M.; Kelso, M. J., Synthesis and preliminary evaluation of 5,7-dimethyl-2-aryl-3H-pyrrolizin-3-ones as angiogenesis inhibitors. *Bioorg. Med. Chem. Lett.* **2016**, *26* (7), 1813-1816.
146. Huang, A.; Liu, F.; Zhan, C.; Liu, Y.; Ma, C., One-pot synthesis of pyrrolo[1,2-a]quinoxalines. *Org. Biomol. Chem.* **2011**, *9* (21), 7351-7357.
147. Cottrell, T. L., *The Strengths of Chemical Bonds*. Butterworths Scientific Publications: 1958.

148. Hay, M. P.; Anderson, R. F.; Ferry, D. M.; Wilson, W. R.; Denny, W. A., Synthesis and Evaluation of Nitroheterocyclic Carbamate Prodrugs for Use with Nitroreductase-Mediated Gene-Directed Enzyme Prodrug Therapy. *J. Med. Chem.* **2003**, *46* (25), 5533-5545.
149. Niculescu-Duvaz, D.; Niculescu-Duvaz, I.; Friedlos, F.; Martin, J.; Lehouritis, P.; Marais, R.; Springer, C. J., Self-Immolative Nitrogen Mustards Prodrugs Cleavable by Carboxypeptidase G2 (CPG2) Showing Large Cytotoxicity Differentials in GDEPT. *J. Med. Chem.* **2003**, *46* (9), 1690-1705.
150. Gourdie, T. A.; Valu, K. K.; Gravatt, G. L.; Boritzki, T. J.; Baguley, B. C.; Wakelin, L. P.; Wilson, W. R.; Woodgate, P. D.; Denny, W. A., DNA-directed alkylating agents. 1. Structure-activity relationships for acridine-linked aniline mustards: consequences of varying the reactivity of the mustard. *J. Med. Chem.* **1990**, *33* (4), 1177-86.
151. Zhu, X.-F.; Williams, H. J.; Ian Scott, A., Aqueous Trichloroacetic Acid: Another Useful Reagent for Highly Selective 5'-Desilylation of Multisilylated Nucleosides. *Synth. Commun.* **2003**, *33* (12), 2011-6.
152. Madhuri, V.; Kumar, V. A., Design and Synthesis of Dephosphono DNA Analogues Containing 1,2,3-Triazole Linker and Their UV-Melting Studies with DNA/RNA. *Nucleosides Nucleotides Nucleic Acids* **2012**, *31* (2), 97-111.
153. Madhuri, V.; Kumar, V. A., Design and synthesis of dephosphono DNA analogues containing 1,2,3-triazole linker and their UV-melting studies with DNA/RNA. *Nucleosides Nucleotides Nucl. Acids* **2012**, *31* (2), 97-111.
154. Wijtmans, M.; Maussang, D.; Sirci, F.; Scholten, D. J.; Canals, M.; Mujić-Delić, A.; Chong, M.; Chatalic, K. L. S.; Custers, H.; Janssen, E.; de Graaf, C.; Smit, M. J.; de Esch, I. J. P.; Leurs, R., Synthesis, modeling and functional activity of substituted styrene-amides as small-molecule CXCR7 agonists. *Eur. J. Med. Chem.* **2012**, *51*, 184-192.
155. Zhu, X.-F.; Williams, H. J.; Scott, A. I., Facile and highly selective 5'-desilylation of multisilylated nucleosides. *Perkin Trans. 1* **2000**, (15), 2305-6.

156. Hwu, J. R.; Kapoor, M.; Li, R.-Y.; Lin, Y.-C.; Horng, J.-C.; Tsay, S.-C., Synthesis of Nucleobase-Functionalized Carbon Nanotubes and Their Hybridization with Single-Stranded DNA. *Chemistry – An Asian Journal* **2014**, *9* (12), 3408-3412.
157. Bernhard, N.; Wolfgang, S., Simple Method for the Esterification of Carboxylic Acids. *Angew. Chem. Int. Ed. Engl.* **1978**, *17* (7), 522-524.
158. Laha, J. K.; Sharma, S.; Bhimpuria, R. A.; Dayal, N.; Dubey, G.; Bharatam, P. V., Integration of oxidative arylation with sulfonyl migration: one-pot tandem synthesis of densely functionalized (NH)-pyrroles. *New J. Chem.* **2017**, *41* (17), 8791-8803.
159. Laha, J. K.; Sharma, S.; Kirar, S.; Banerjee, U. C., Design, Sustainable Synthesis, and Programmed Reactions of Templated N-Heteroaryl-Fused Vinyl Sultams. *The Journal of Organic Chemistry* **2017**, *82* (18), 9350-9359.
160. Laha, J. K.; Bhimpuria, R. A.; Kumar, A. M., Post-synthetic diversification of pyrrole-fused benzosultams via trans-sulfonylations and reactions on the periphery of pyrrole. *Organic Chemistry Frontiers* **2017**, *4* (11), 2170-2174.
161. Zhu, L.; dos Santos, O.; Seeman, N. C.; Canary, J. W., Reaction of N³-benzoyl-3',5'-O-(di-tert-butylsilanediy)uridine with hindered electrophiles: intermolecular N³ to 2'-O protecting group transfer. *Nucleosides Nucleotides Nucleic Acids* **2002**, *21* (10), 723-35.
162. Nguyen, C.; Kasinathan, G.; Leal-Cortijo, I.; Musso-Buendia, A.; Kaiser, M.; Brun, R.; Ruiz-Perez, L. M.; Johansson, N. G.; Gonzalez-Pacanowska, D.; Gilbert, I. H., Deoxyuridine triphosphate nucleotidohydrolase as a potential antiparasitic drug target. *J. Med. Chem.* **2005**, *48* (19), 5942-54.
163. Dolbier, W. R., An Overview of Fluorine NMR. In *Guide to Fluorine NMR for Organic Chemists*, John Wiley & Sons: 2016; pp 9-53.
164. Gamble, A. B.; Garner, J.; Gordon, C. P.; O'Conner, S. M. J.; Keller, P. A., Aryl Nitro Reduction with Iron Powder or Stannous Chloride under Ultrasonic Irradiation. *Synth. Commun.* **2007**, *37* (16), 2777-2786.

165. Desai, D. G.; Swami, S. S.; Hapase, S. B., "Rapid and Inexpensive Method for Reduction of Nitroarenes to Anilines". *Synth. Commun.* **1999**, *29* (6), 1033-1036.
166. Pogorelić, I.; Filipan-Litvić, M.; Merkaš, S.; Ljubić, G.; Capanec, I.; Litvić, M., Rapid, efficient and selective reduction of aromatic nitro compounds with sodium borohydride and Raney nickel. *J. Mol. Catal. A: Chem.* **2007**, *274* (1), 202-207.
167. Laviron, E.; Vallat, A.; Meunier-Prest, R., The reduction mechanism of aromatic nitro compounds in aqueous medium: Part V. The reduction of nitrosobenzene between pH 0.4 and 13. *J. Electroanal. Chem.* **1994**, *379* (1), 427-435.
168. Zuman, P. F., Z; Dumanovic, D; Sužnjević, D., Polarographic and electrochemical studies of some aromatic and heterocyclic nitro compounds, part I: General mechanistic aspects. *Electroanalysis* **1992**, *4* (8), 783-794.
169. Shindo, H.; Nishihara, C., Detection of nitrosobenzene as an intermediate in the electrochemical reduction of nitrobenzene on Ag in a flow reactor. *Journal of Electroanalytical Chemistry and Interfacial Electrochemistry* **1989**, *263* (2), 415-420.
170. Bouérat, L.; Fensholdt, J.; Liang, X.; Havez, S.; Nielsen, S. F.; Hansen, J. R.; Bolvig, S.; Andersson, C., Indolin-2-ones with High in Vivo Efficacy in a Model for Multiple Sclerosis. *J. Med. Chem.* **2005**, *48* (17), 5412-5414.
171. Facon, T.; Mary, J. Y.; Hulin, C.; Benboubker, L.; Attal, M.; Pegourie, B.; Renaud, M.; Harousseau, J. L.; Guillermin, G.; Chaletteix, C.; Dib, M.; Voillat, L.; Maisonneuve, H.; Troncy, J.; Dorvaux, V.; Monconduit, M.; Martin, C.; Casassus, P.; Jaubert, J.; Jardel, H.; Doyen, C.; Kolb, B.; Anglaret, B.; Grosbois, B.; Yakoub-Agha, I.; Mathiot, C.; Avet-Loiseau, H., Melphalan and prednisone plus thalidomide versus melphalan and prednisone alone or reduced-intensity autologous stem cell transplantation in elderly patients with multiple myeloma (IFM 99-06): a randomised trial. *Lancet* **2007**, *370* (9594), 1209-18.
172. Hunter, F. W.; Hsu, H.-L.; Su, J.; Pullen, S. M.; Wilson, W. R.; Wang, J., Dual Targeting of Hypoxia and Homologous Recombination Repair Dysfunction in Triple-Negative Breast Cancer. *Mol. Cancer Ther.* **2014**, *13* (11), 2501-2514.

173. Descôteaux, C.; Brasseur, K.; Leblanc, V.; Parent, S.; Asselin, É.; Bérubé, G., Design of novel tyrosine-nitrogen mustard hybrid molecules active against uterine, ovarian and breast cancer cell lines. *Steroids* **2012**, *77* (5), 403-412.
174. Axelson, M. D.; Davis, M. A.; Ethier, S. P.; Lawrence, T. S., HPV16-E7 expression causes fluorodeoxyuridine-mediated radiosensitization in SW620 human colon cancer cells. *Neoplasia* **1999**, *1* (2), 177-82.
175. Matuo, R.; Sousa, F. G.; Escargueil, A. E.; Grivicich, I.; Garcia-Santos, D.; Chies, J. A. B.; Saffi, J.; Larsen, A. K.; Henriques, J. A. P., 5-Fluorouracil and its active metabolite FdUMP cause DNA damage in human SW620 colon adenocarcinoma cell line. *J. Appl. Toxicol.* **2009**, *29* (4), 308-316.
176. Denny, W. A., Prodrug strategies in cancer therapy. *Eur. J. Med. Chem.* **2001**, *36* (7), 577-595.
177. Priyadarsini, K. I.; Tracy, M.; Wardman, P., The one-electron reduction potential of 3-amino-1,2,4-benzotriazine 1,4-dioxide (tirapazamine): a hypoxia-selective bioreductive drug. *Free Radic. Res.* **1996**, *25* (5), 393-9.
178. Meng, F.; Evans, J. W.; Bhupathi, D.; Banica, M.; Lan, L.; Lorente, G.; Duan, J.-X.; Cai, X.; Mowday, A. M.; Guise, C. P.; Maroz, A.; Anderson, R. F.; Patterson, A. V.; Stachelek, G. C.; Glazer, P. M.; Matteucci, M. D.; Hart, C. P., Molecular and Cellular Pharmacology of the Hypoxia-Activated Prodrug TH-302. *Mol. Cancer Ther.* **2012**, *11* (3), 740.
179. Katsumura, Y.; Kudo, H., Pulse Radiolysis. In *Radiation Applications*, Kudo, H., Ed. Springer Singapore: Singapore, 2018; pp 31-36.
180. Anderson, R. F.; Denny, W. A.; Li, W.; Packer, J. E.; Tercel, M.; Wilson, W. R., Pulse Radiolysis Studies on the Fragmentation of Arylmethyl Quaternary Nitrogen Mustards by One-Electron Reduction in Aqueous Solution. *The Journal of Physical Chemistry A* **1997**, *101* (50), 9704-9709.
181. Steckhan, E.; Kuwana, T., Spectroelectrochemical Study of Mediators I. Bipyridylium Salts and Their Electron Transfer Rates to Cytochrome c. *Berichte der Bunsengesellschaft für physikalische Chemie* **1974**, *78* (3), 253-259.

182. Kirk, N. S.; Sansom, G. N.; Sudta, P.; Suksamrarn, S.; Willis, A. C.; Bremner, J. B.; Kelso, M. J., Unexpected synthesis of 3-imino-2-(pyrrol-2-yl) isatogen derivatives affords facile access to a 2-pyrrolyl isatogen. *Synth. Commun.* **2017**, *47* (1), 62-67.
183. Kancharla, P.; Kelly, J. X.; Reynolds, K. A., Synthesis and Structure–Activity Relationships of Tambjamines and B-Ring Functionalized Prodiginines as Potent Antimalarials. *J. Med. Chem.* **2015**, *58* (18), 7286-7309.
184. Guibe, F.; M'Leux, Y. S., The allyloxycarbonyl group for alcohol protection: quantitative removal or transformation into allyl protecting group via π -allyl complexes of palladium. *Tetrahedron Lett.* **1981**, *22* (37), 3591-3594.
185. Arendt, A.; M. Kołodziejczyk, A., O- and N-acylureas in peptide synthesis by DCC method. New observations. *Tetrahedron Lett.* **1978**, *19* (40), 3867-3868.
186. Montalbetti, C. A. G. N.; Falque, V., Amide bond formation and peptide coupling. *Tetrahedron* **2005**, *61* (46), 10827-10852.
187. Knorr, R.; Trzeciak, A.; Bannwarth, W.; Gillessen, D., New coupling reagents in peptide chemistry. *Tetrahedron Lett.* **1989**, *30* (15), 1927-1930.
188. Fletcher, S., The Mitsunobu reaction in the 21st century. *Organic Chemistry Frontiers* **2015**, *2* (6), 739-752.
189. Naimi, E.; Zhou, A.; Khalili, P.; Wiebe, L. I.; Balzarini, J.; De Clercq, E.; Knaus, E. E., Synthesis of 3'- and 5'-Nitrooxy Pyrimidine Nucleoside Nitrate Esters: "Nitric Oxide Donor" Agents for Evaluation as Anticancer and Antiviral Agents. *J. Med. Chem.* **2003**, *46* (6), 995-1004.
190. Uchimiya, M.; Gorb, L.; Isayev, O.; Qasim, M. M.; Leszczynski, J., One-electron standard reduction potentials of nitroaromatic and cyclic nitramine explosives. *Environ. Pollut.* **2010**, *158* (10), 3048-53.
191. Hammett, L. P., The Effect of Structure upon the Reactions of Organic Compounds. Benzene Derivatives. *J. Am. Chem. Soc.* **1937**, *59* (1), 96-103.

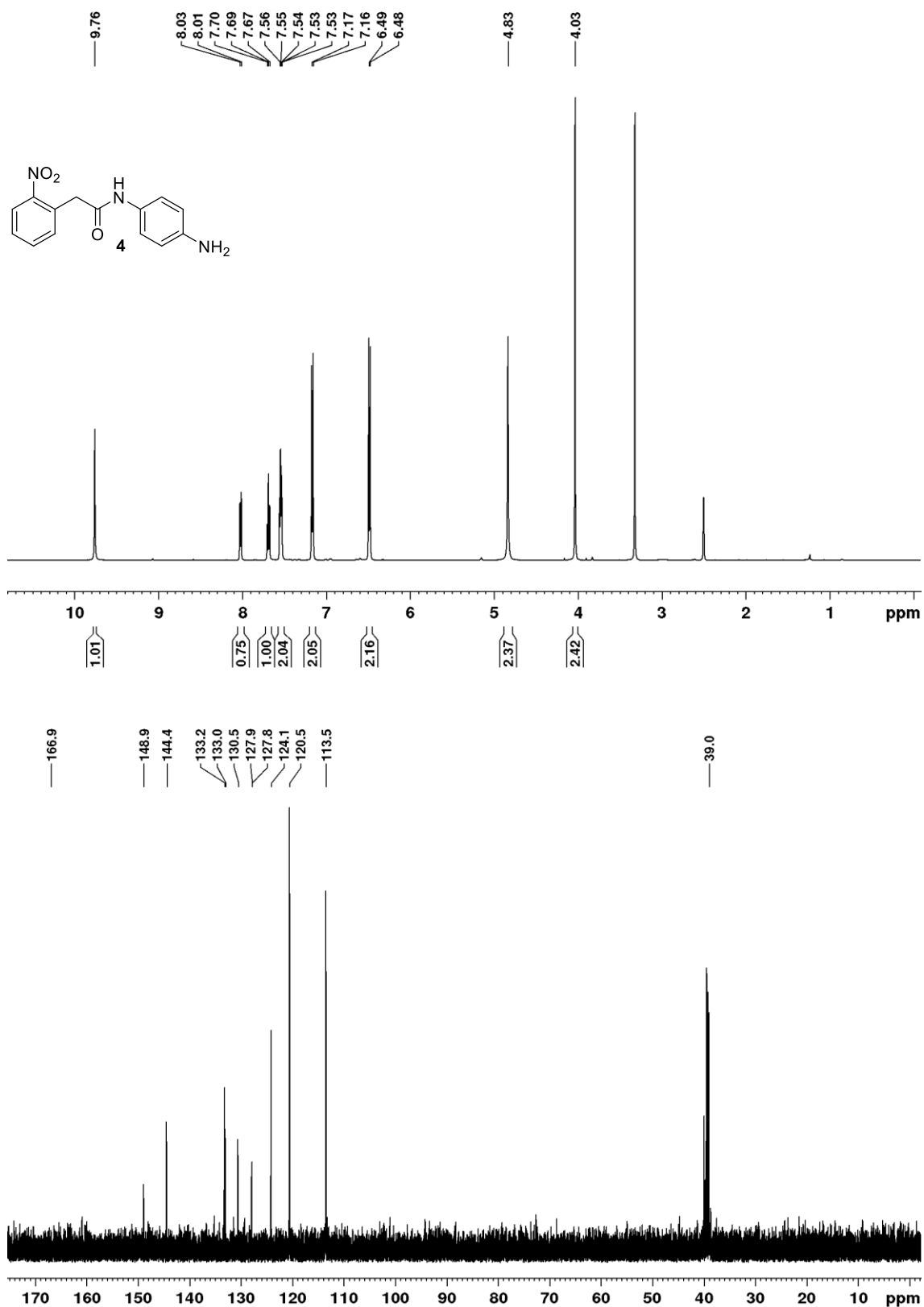
192. Sun, L.; Tran, N.; Tang, F.; App, H.; Hirth, P.; McMahon, G.; Tang, C., Synthesis and Biological Evaluations of 3-Substituted Indolin-2-ones: A Novel Class of Tyrosine Kinase Inhibitors That Exhibit Selectivity toward Particular Receptor Tyrosine Kinases. *J. Med. Chem.* **1998**, *41* (14), 2588-2603.
193. Zhang, X.-F.; Guo, W., Indole substituted zinc phthalocyanine: Improved photosensitizing ability and modified photooxidation mechanism. *J. Photochem. Photobiol. A: Chem.* **2011**, *225* (1), 117-124.
194. Jiang, Z.-q.; Miao, D.-z.; Tong, Y.; Pan, Q.; Li, X.-t.; Hu, R.-h.; Han, S.-q., One-Pot Base-Mediated Synthesis of Functionalized Aza-Fused Polycyclic Quinoline Derivatives. *Synthesis* **2015**, *47* (13), 1913-1921.
195. Vichai, V.; Kirtikara, K., Sulforhodamine B colorimetric assay for cytotoxicity screening. *Nat. Protoc.* **2006**, *1* (3), 1112-6.

Appendix 1: X-ray Crystallographic Data for 48

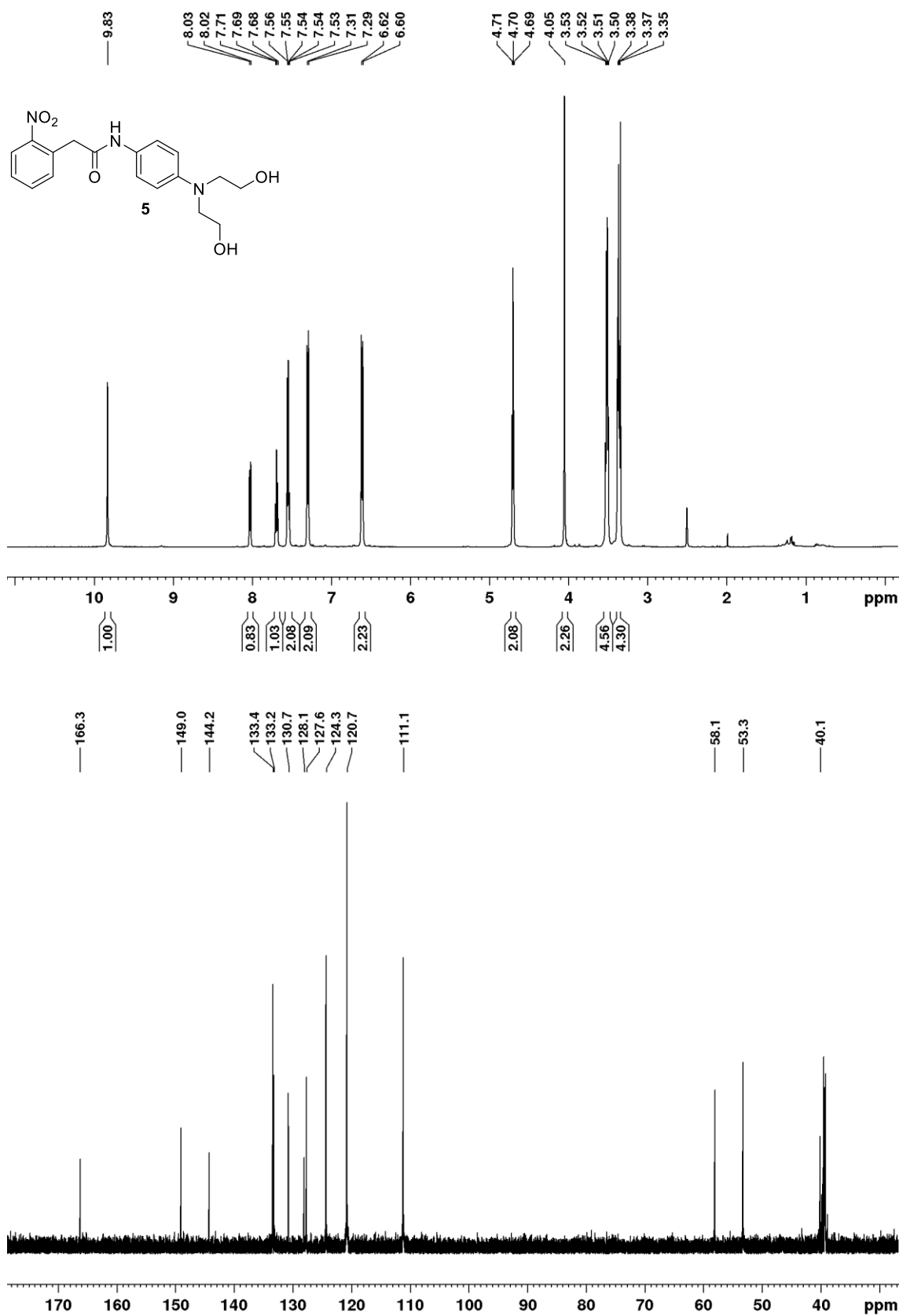
Empirical formula	C ₁₈ H ₁₆ FNO ₂
Formula weight	297.32
Temperature/K	294
Crystal system	triclinic
Space group	P-1
a/Å	8.0663(4)
b/Å	8.5923(5)
c/Å	11.8061(6)
α/°	111.046(5)
β/°	101.373(4)
γ/°	90.074(5)
Volume/Å³	746.35(8)
Z	2
ρ_{calc}/cm³	1.323
μ/mm-1	0.095
F(000)	312.0
Crystal size/mm³	0.4 × 0.16 × 0.1
Radiation	MoKα (λ = 0.71073)
2θ range for data collection/°	3.782 to 61.242
Index ranges	-11 ≤ h ≤ 11, -12 ≤ k ≤ 12, -16 ≤ l ≤ 16
Reflections collected	18232
Independent reflections	4383 [R int = 0.0293, R sigma = 0.0325]
Data/restraints/parameters	4383/2/215
Goodness-of-fit on F²	1.023
Final R indexes [I ≥ 2σ (I)]	R1 = 0.0538, wR2 = 0.1463
Final R indexes [all data]	R1 = 0.1049, wR2 = 0.1743
Largest diff. peak/hole / e Å⁻³	0.21/-0.19

Appendix 2: NMR Spectra

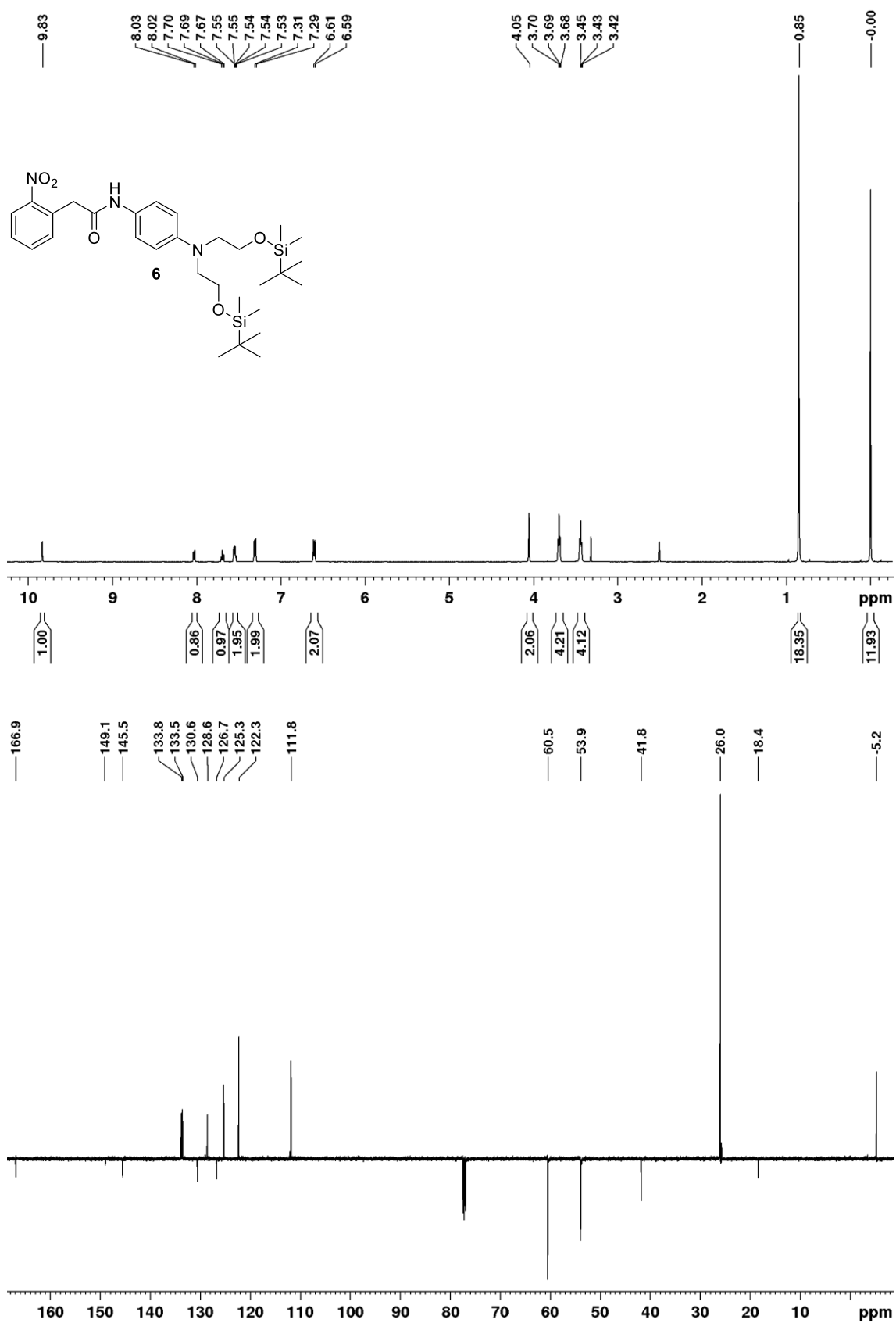
^1H (500 MHz, d_6 -DMSO) and ^{13}C Carbon (126 MHz, d_6 -DMSO) NMR spectra of **4**



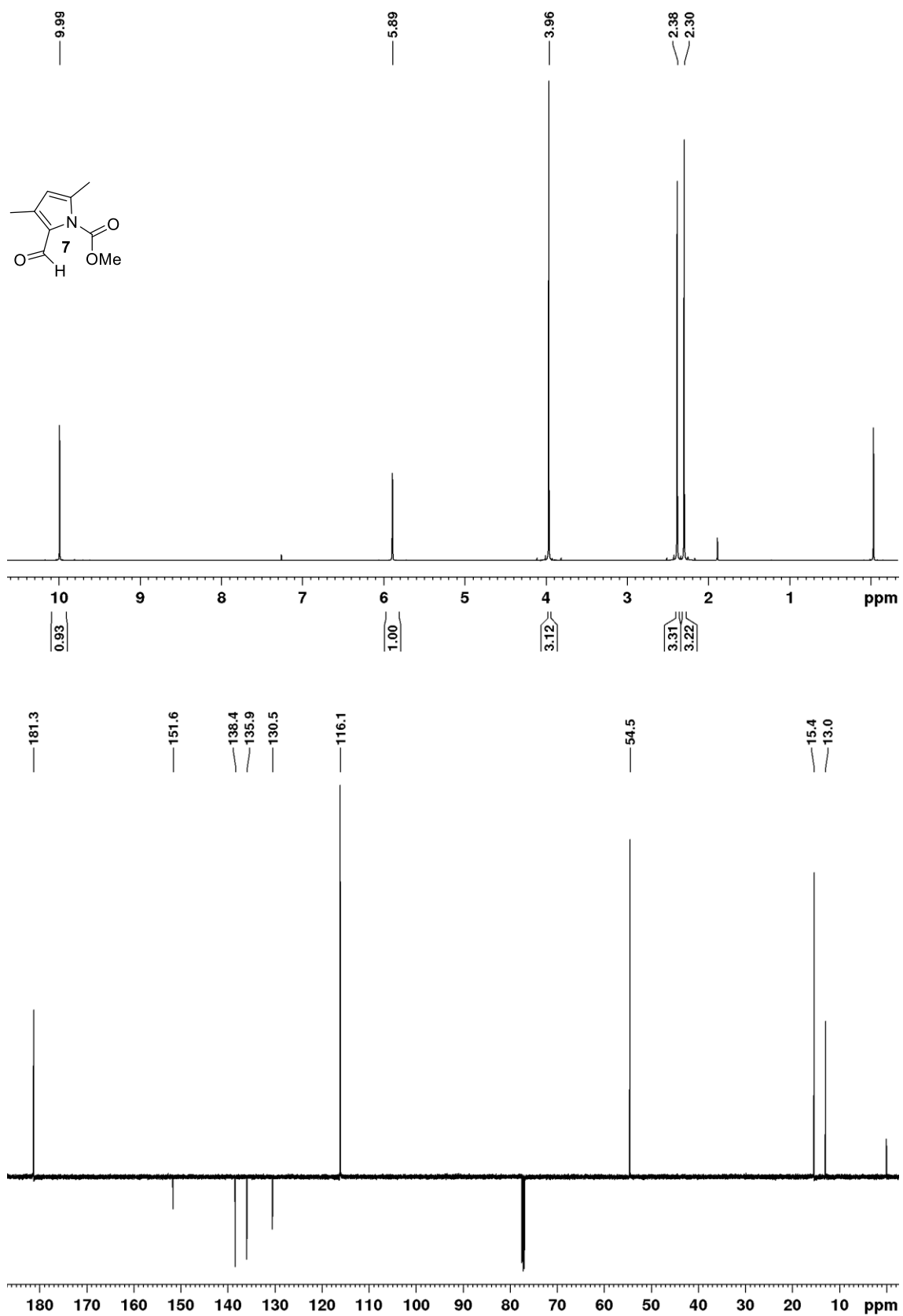
^1H (500 MHz, d_6 -DMSO) and ^{13}C Carbon (126 MHz, d_6 -DMSO) NMR spectra of **5**

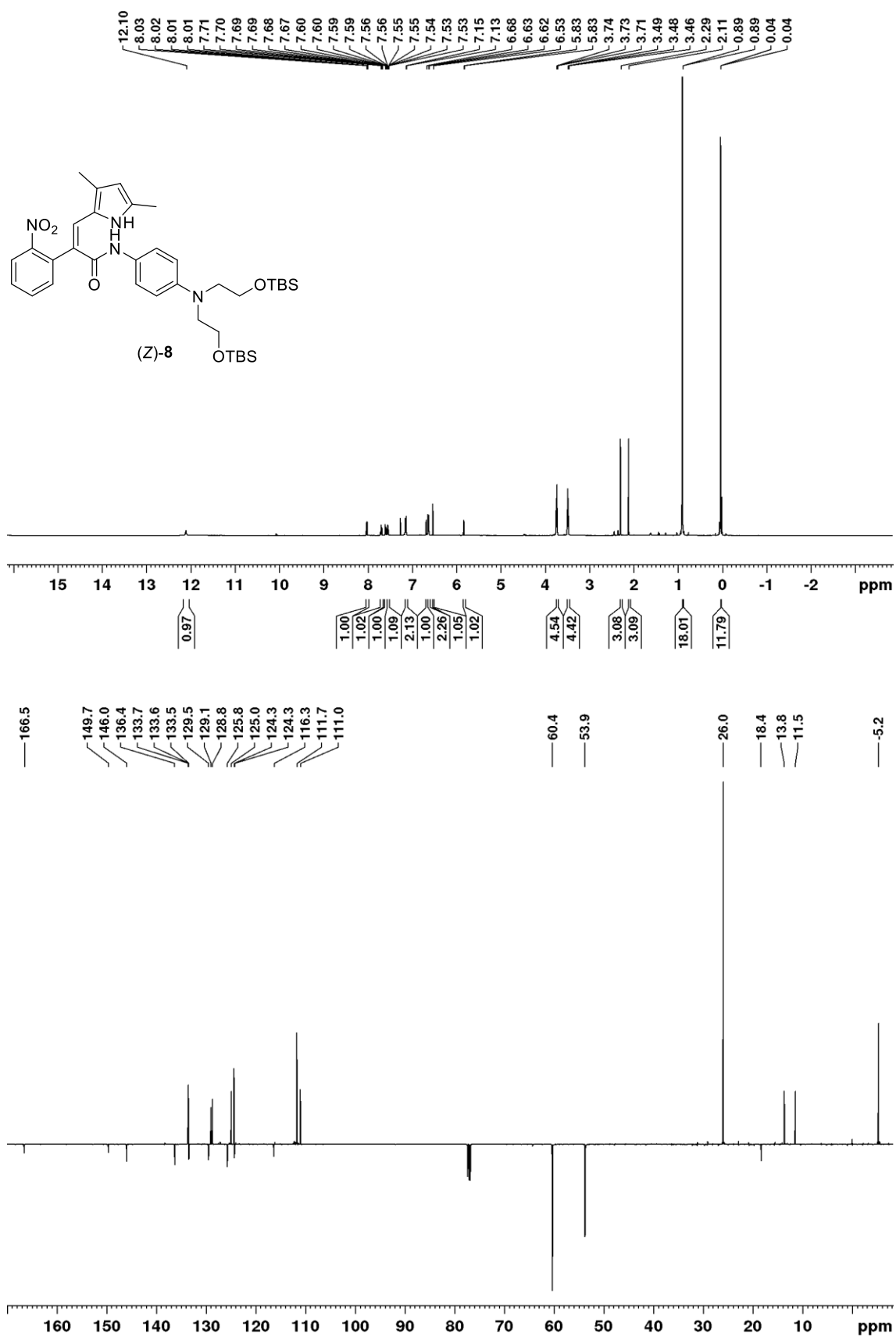


^1H (500 MHz, d_6 -DMSO) and ^{13}C APT (126 MHz, CDCl_3) NMR spectra of **6**

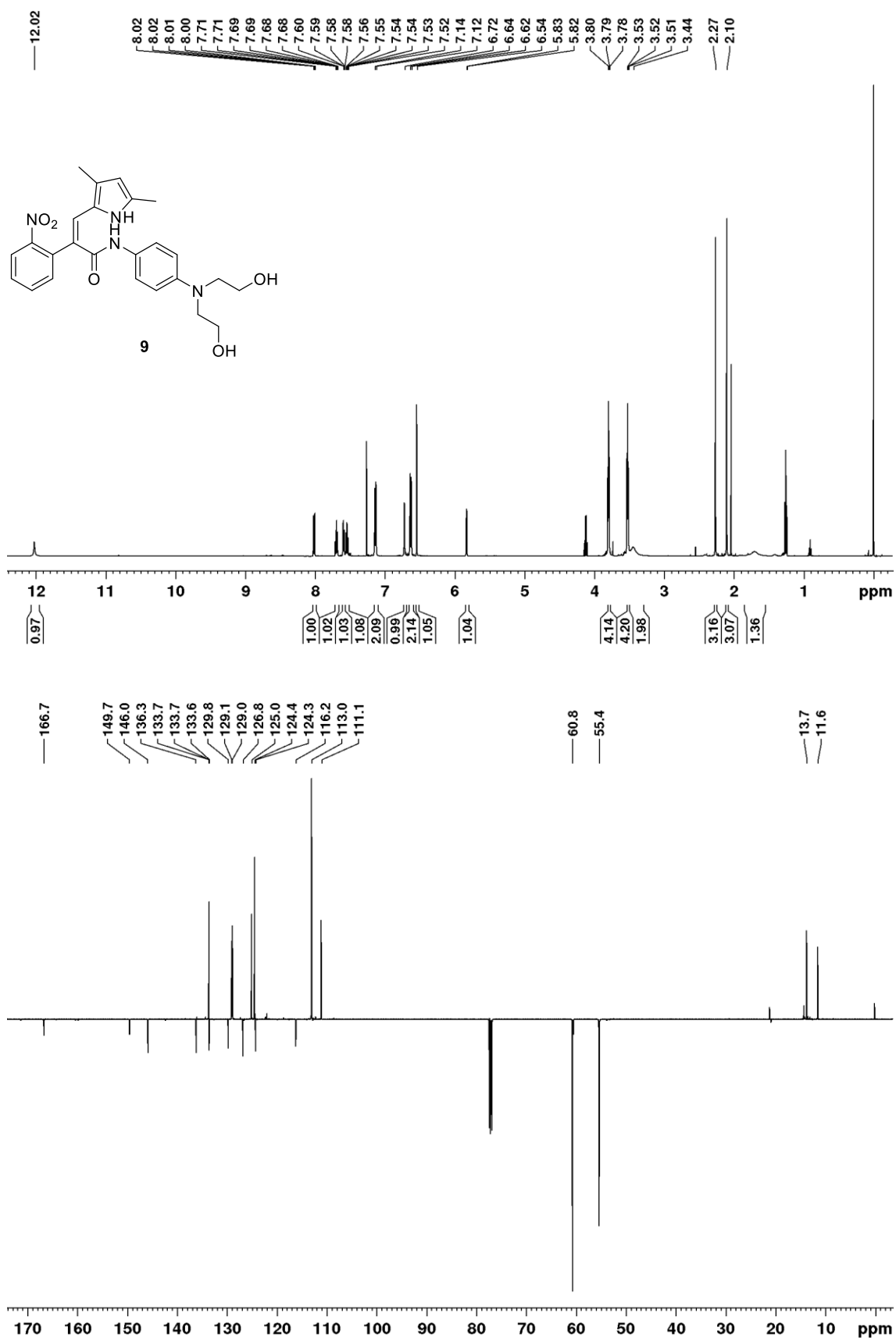


^1H (500 MHz, CDCl_3) and ^{13}C APT (126 MHz, CDCl_3) NMR spectra of **7**

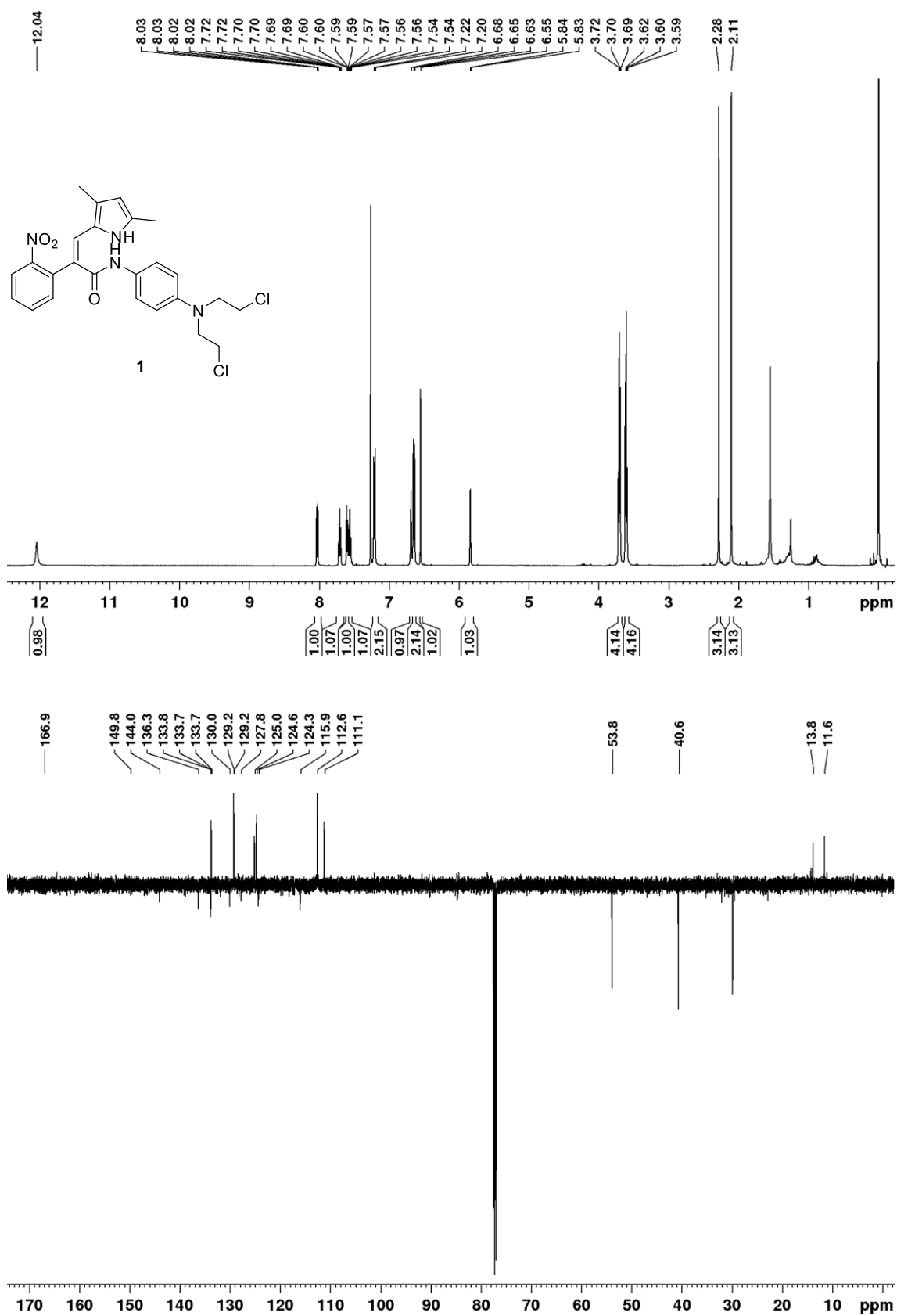


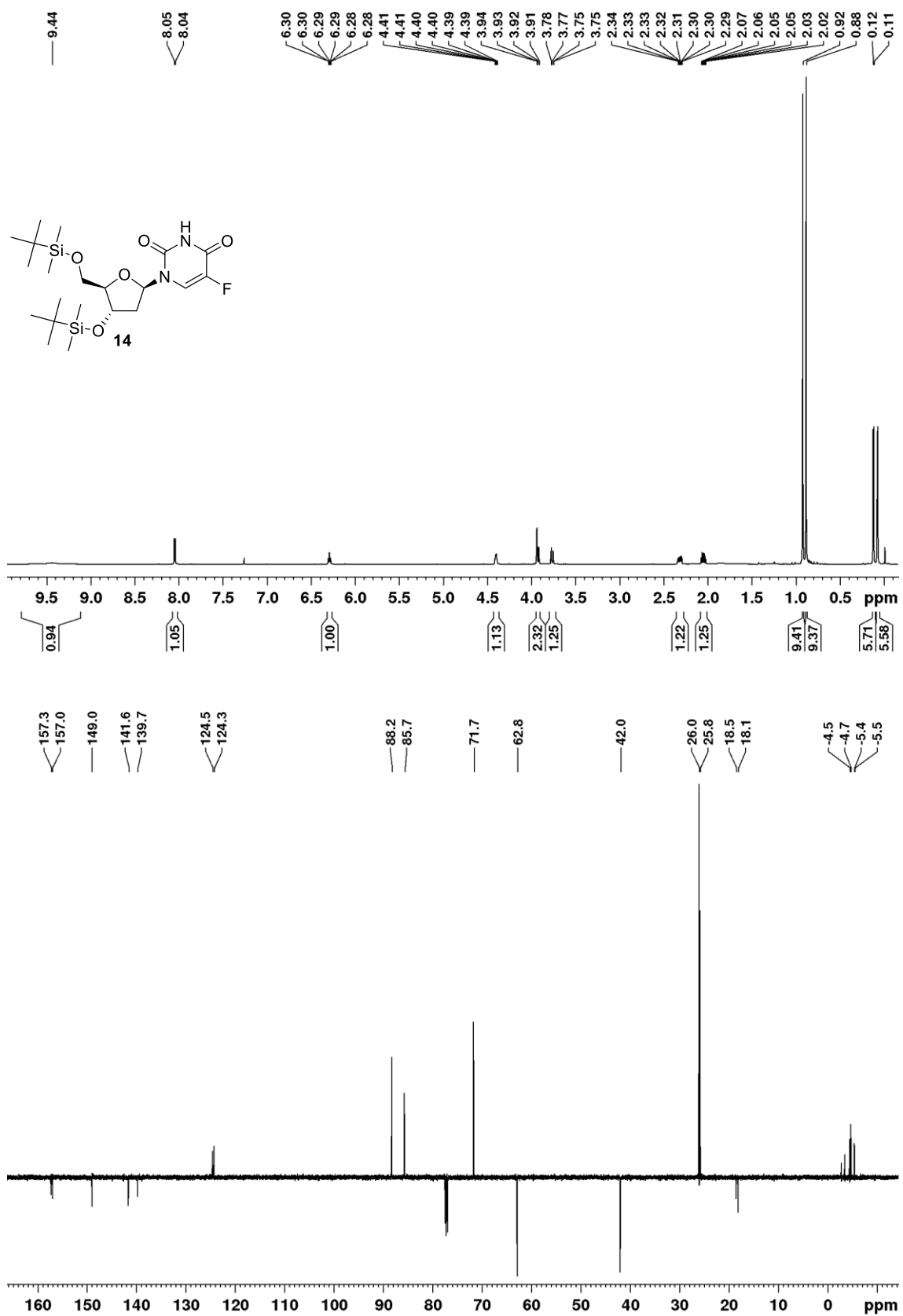
^1H (500 MHz, CDCl_3) and ^{13}C APT (126 MHz, CDCl_3) NMR spectra of (Z)-8

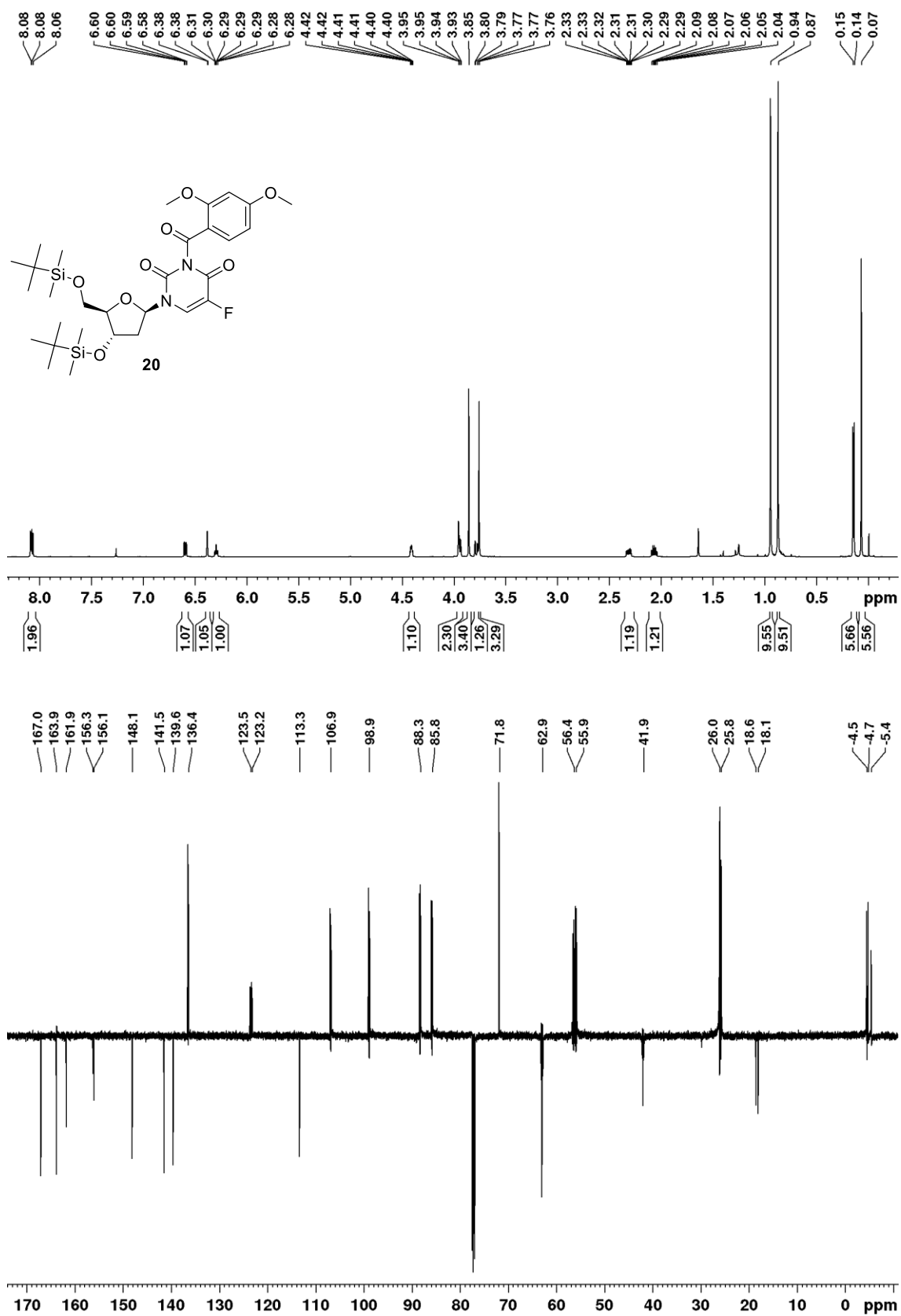
^1H (500 MHz, CDCl_3) and ^{13}C APT (126 MHz, CDCl_3) NMR spectra of **9**

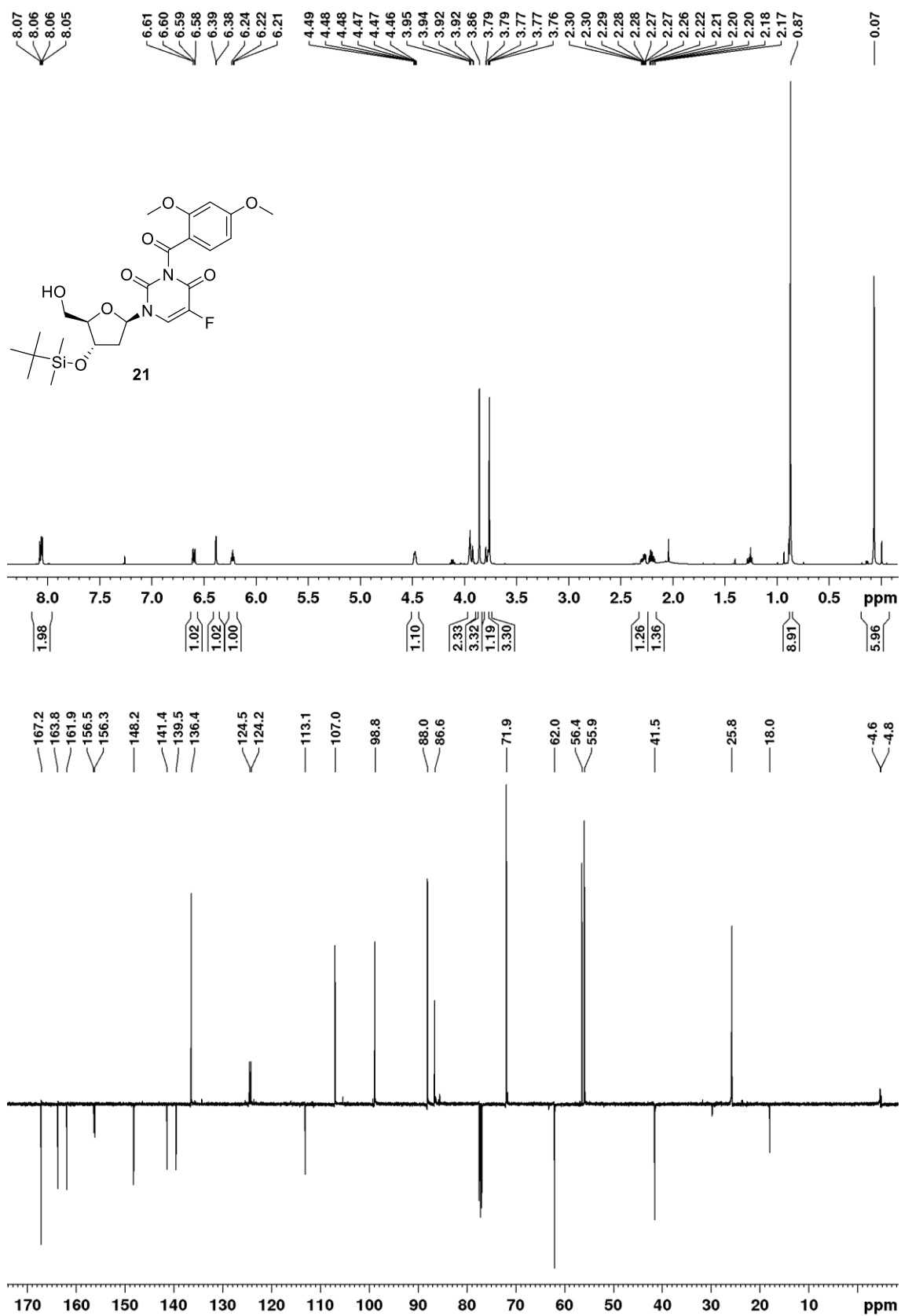


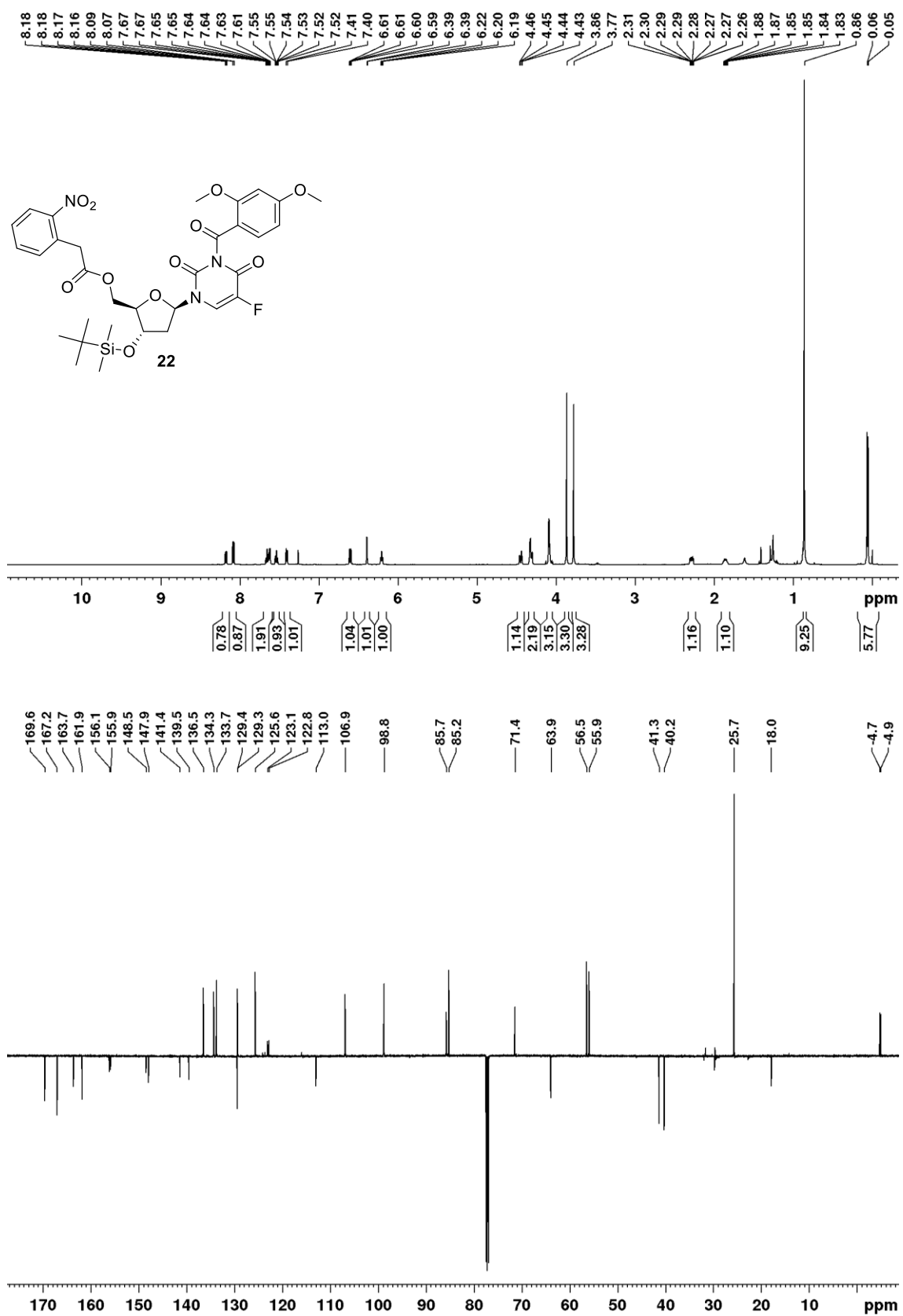
^1H (500 MHz, CDCl_3) and ^{13}C APT (126 MHz, CDCl_3) NMR spectra of **1**

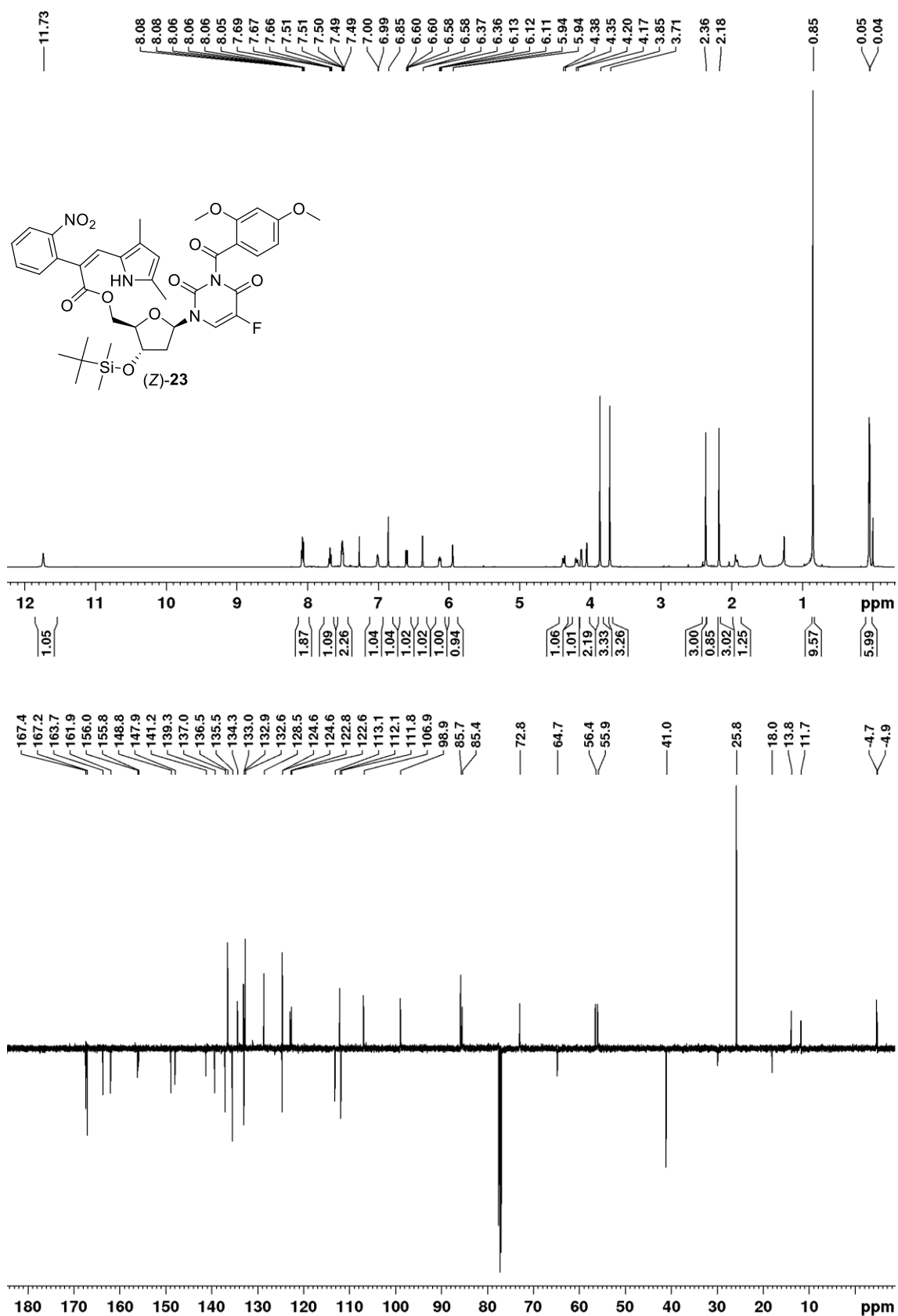


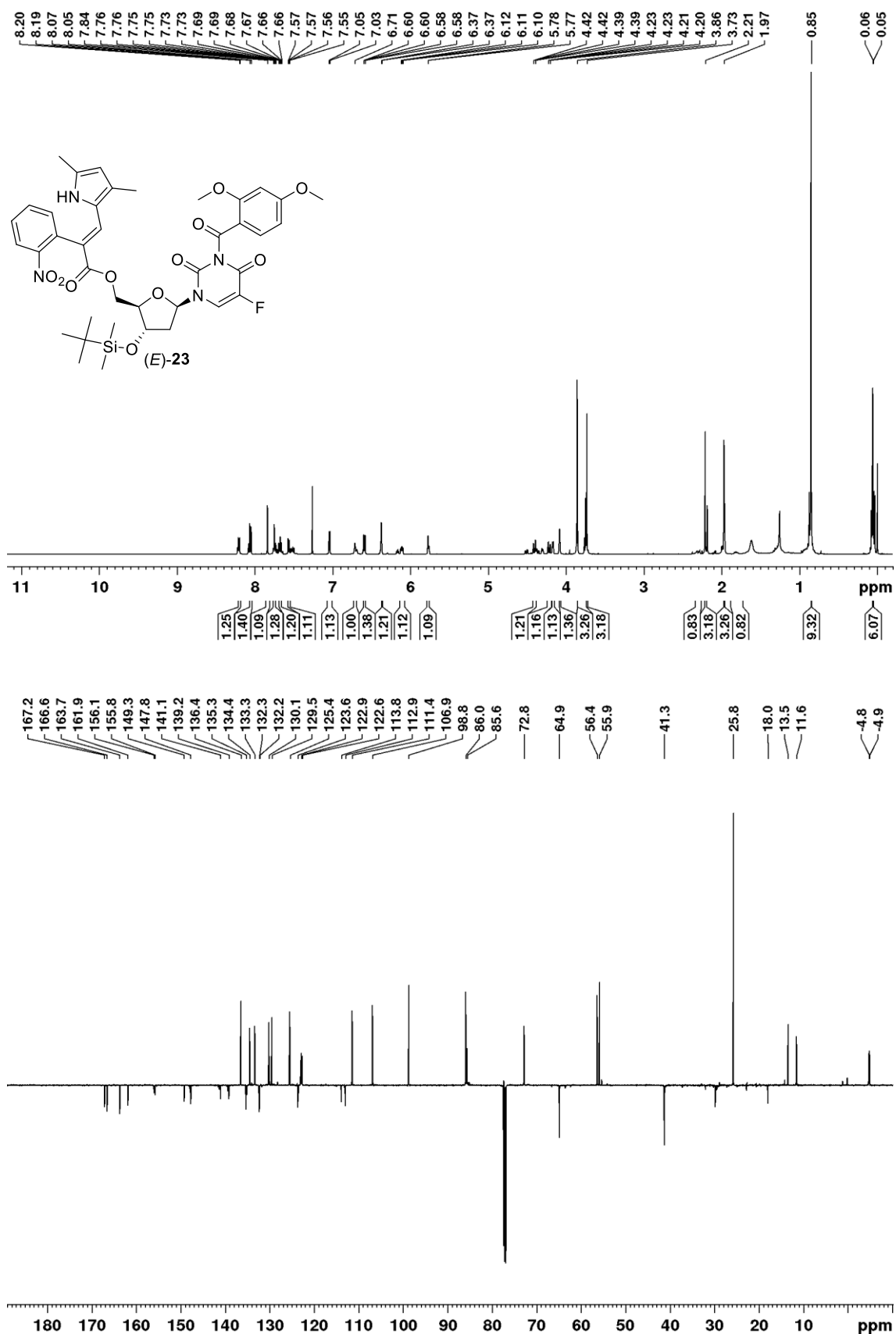
^1H (500 MHz, CDCl_3) and ^{13}C APT (126 MHz, CDCl_3) NMR spectra of **14**

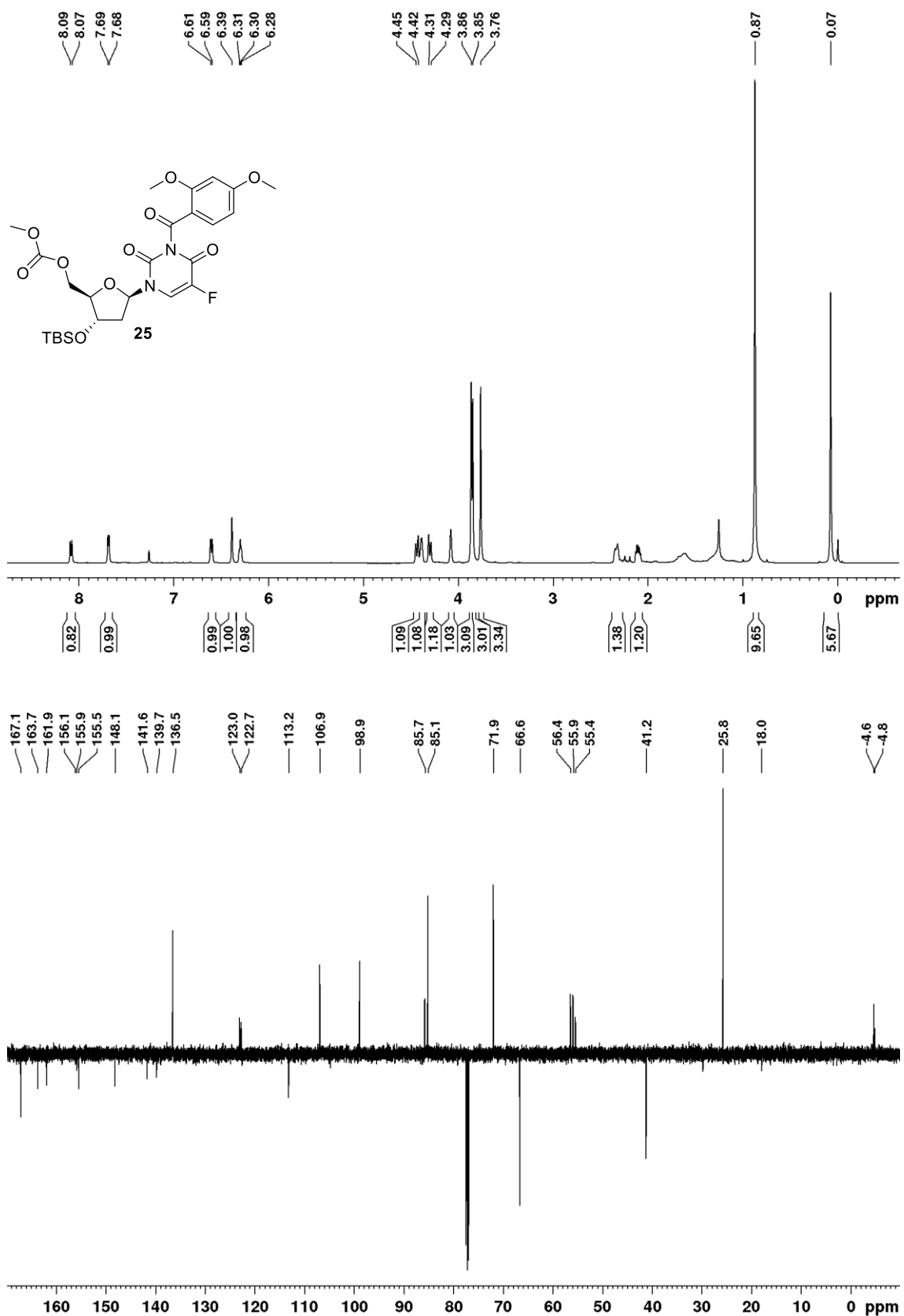
^1H (500 MHz, CDCl_3) and ^{13}C APT (126 MHz, CDCl_3) NMR spectra of **20**

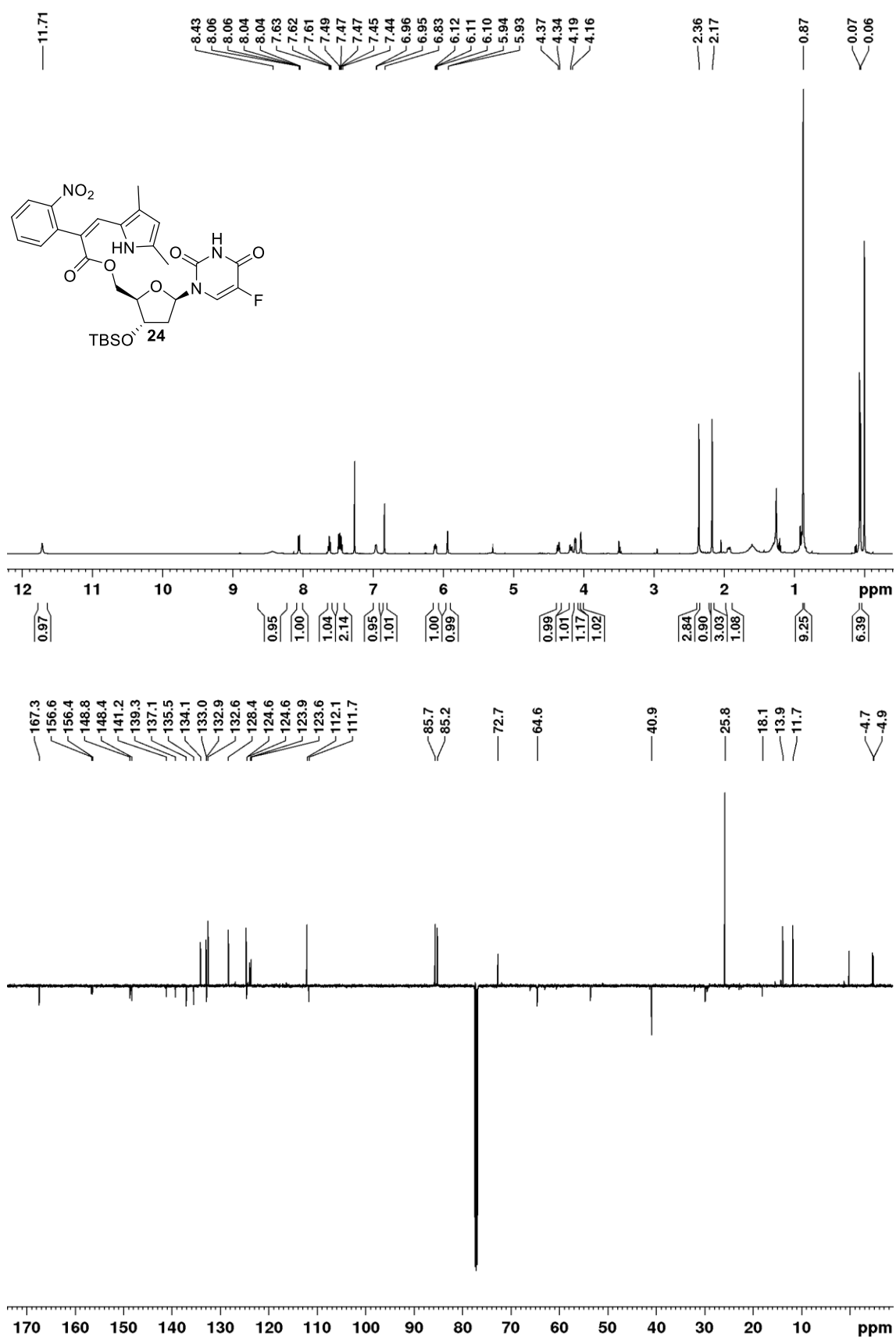
^1H (500 MHz, CDCl_3) and ^{13}C APT (126 MHz, CDCl_3) NMR spectra of **21**

^1H (500 MHz, CDCl_3) and ^{13}C APT (126 MHz, CDCl_3) NMR spectra of **22**

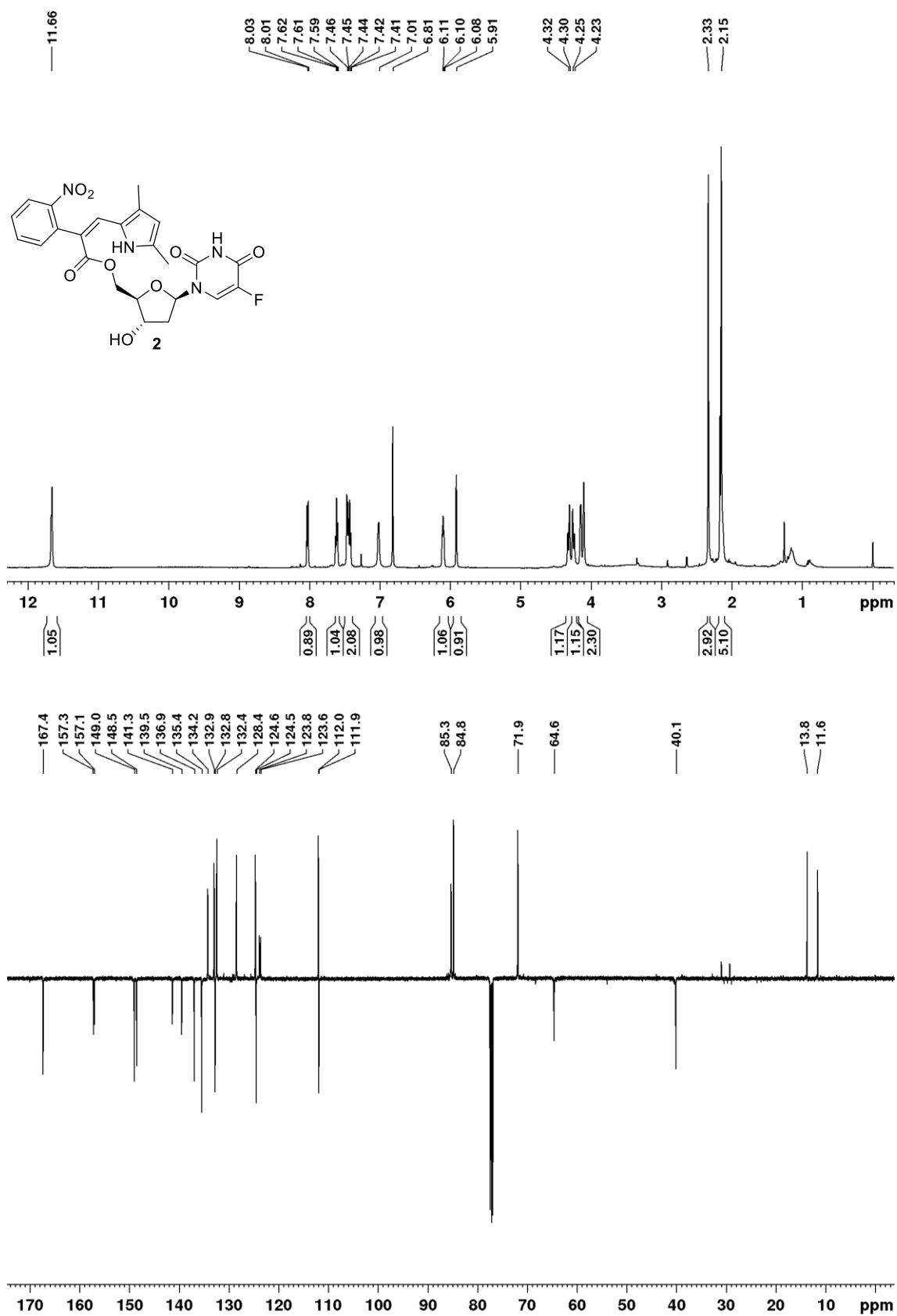
^1H (500 MHz, CDCl_3) and ^{13}C APT (126 MHz, CDCl_3) NMR spectra of (Z)-**23**

^1H (500 MHz, CDCl_3) and ^{13}C APT (126 MHz, CDCl_3) NMR spectra of (*E*)-**23**

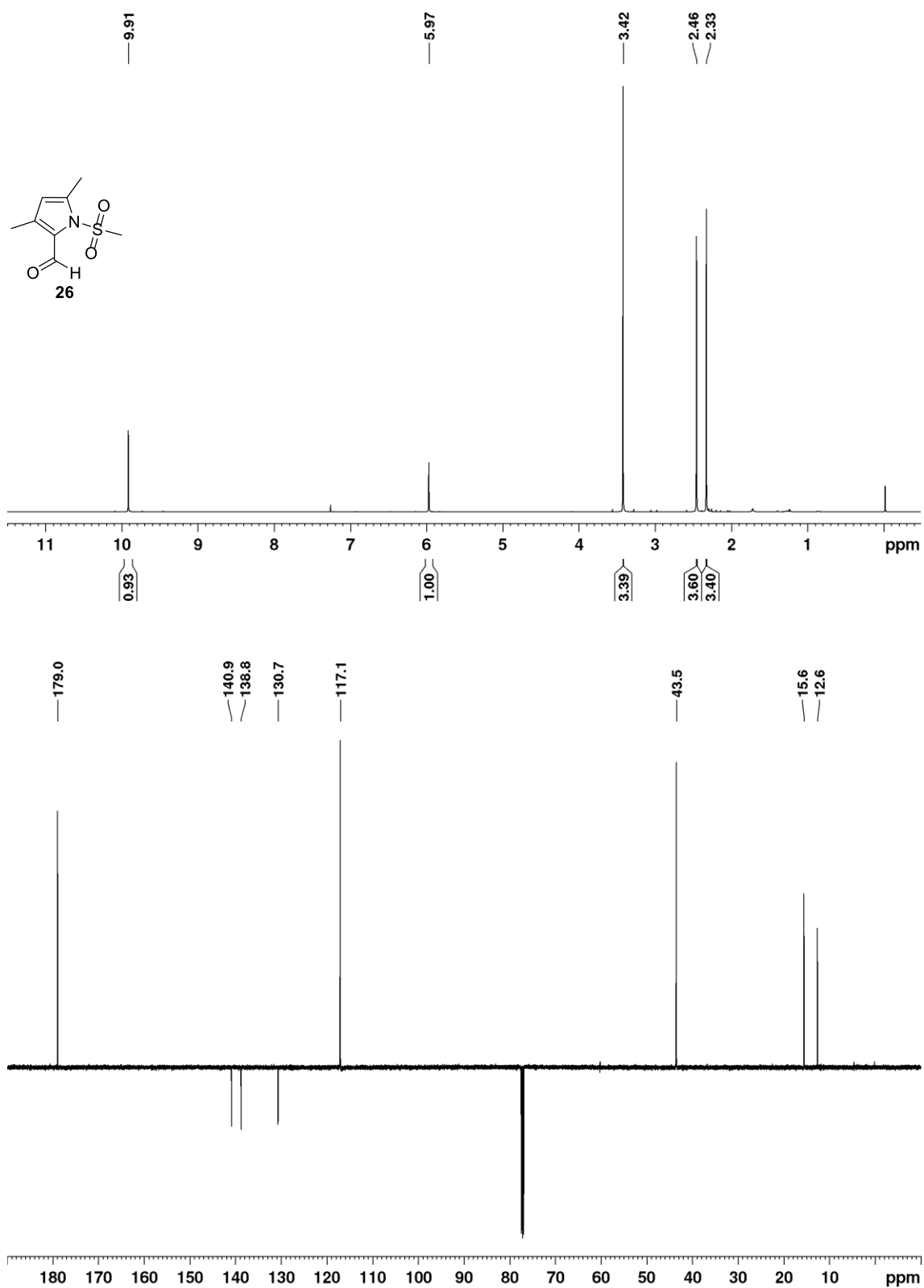
^1H (500 MHz, CDCl_3) and ^{13}C APT (126 MHz, CDCl_3) NMR spectra of **25**

^1H (500 MHz, CDCl_3) and ^{13}C APT (126 MHz, CDCl_3) NMR spectra of **24**

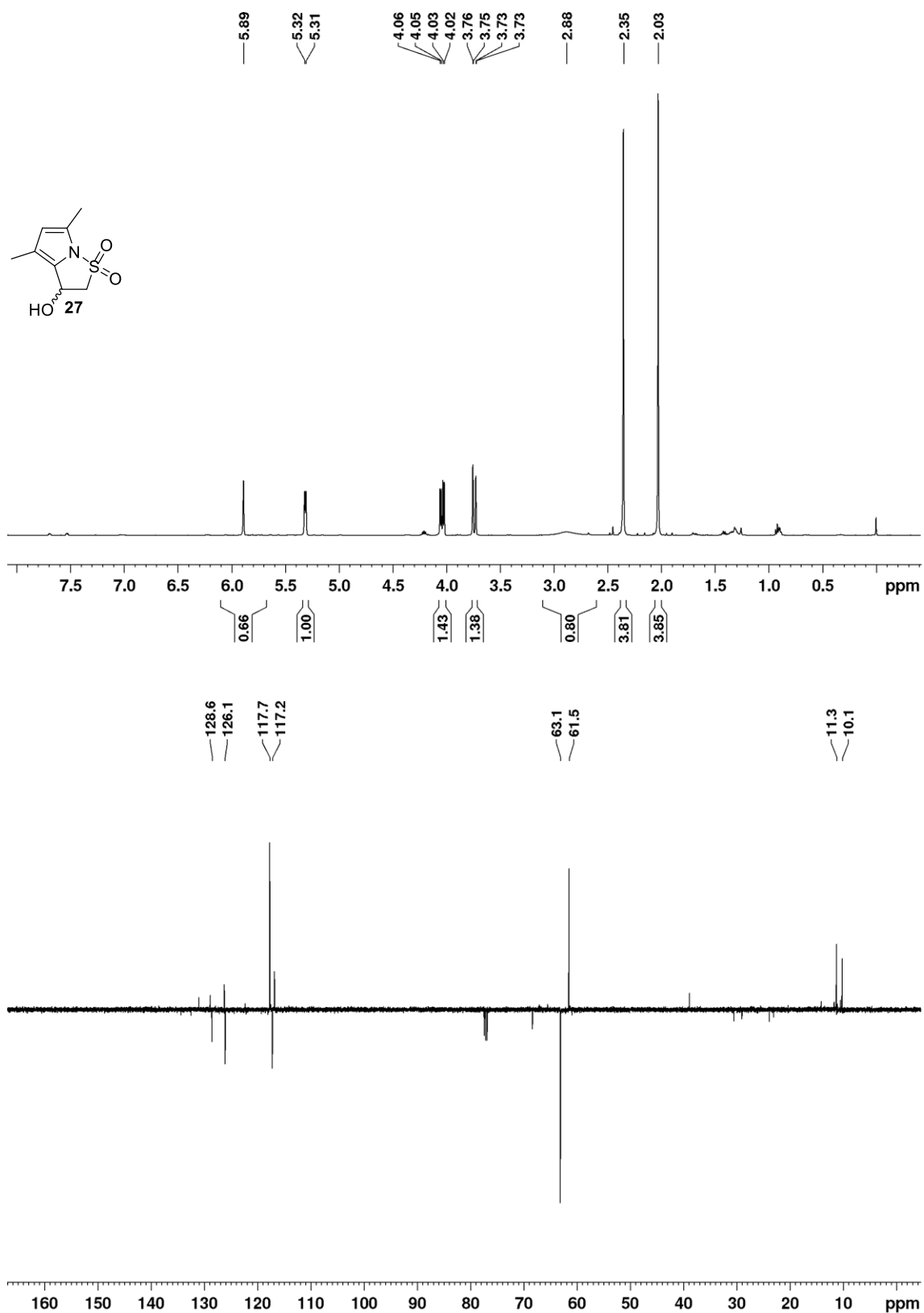
^1H (500 MHz, CDCl_3) and ^{13}C APT (126 MHz, CDCl_3) NMR spectra of **2**



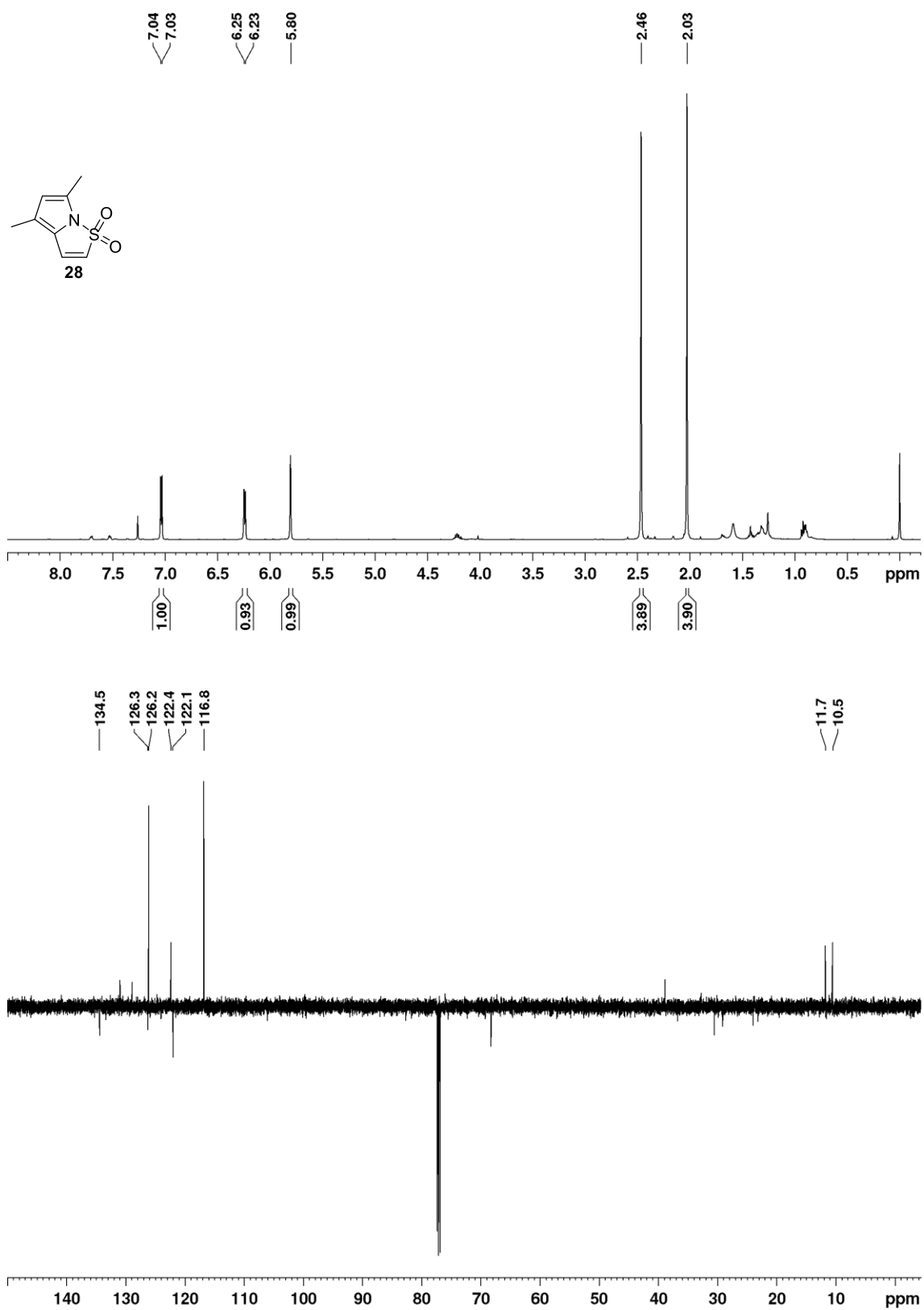
^1H (500 MHz, CDCl_3) and ^{13}C APT (126 MHz, CDCl_3) NMR spectra of **26**



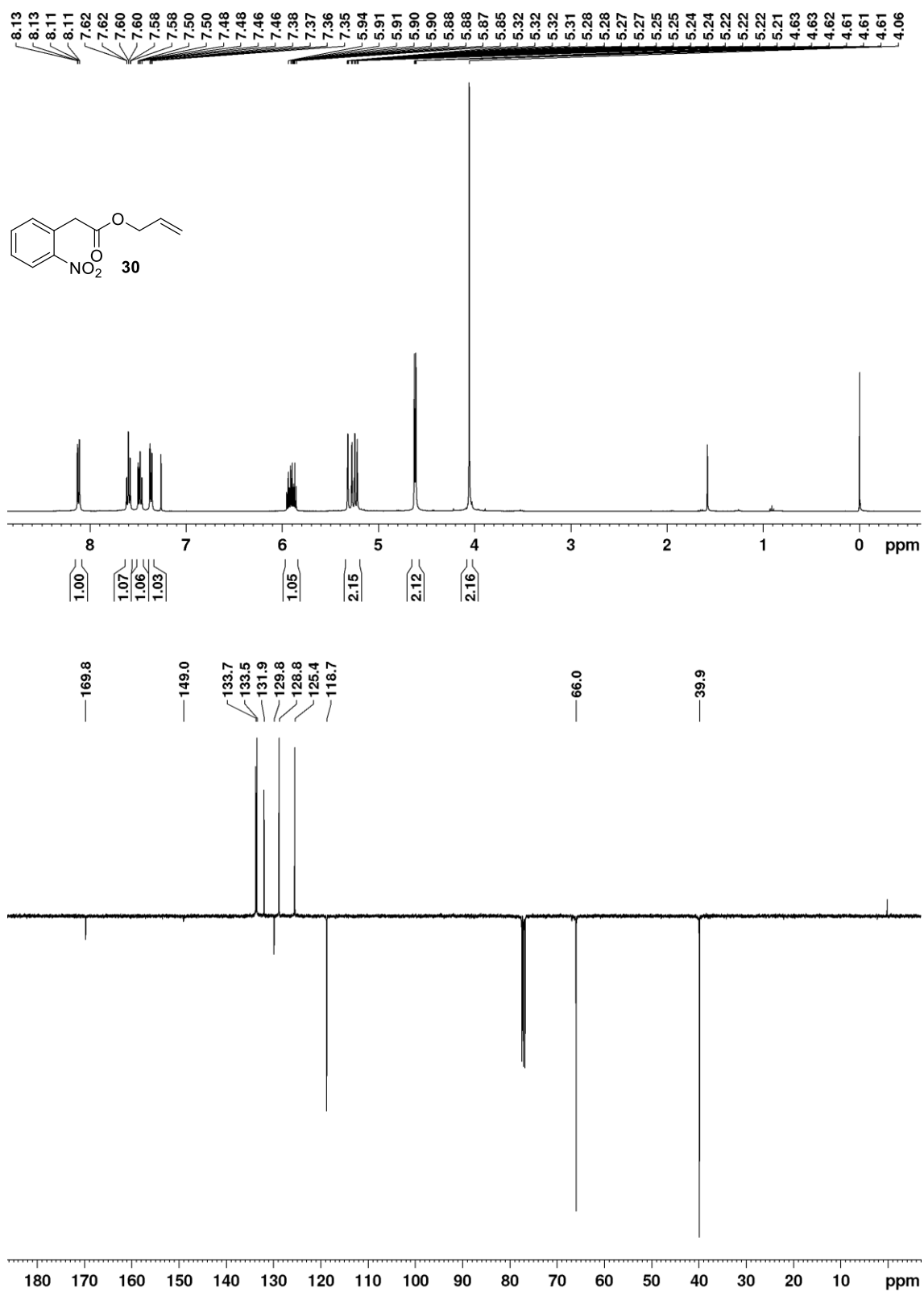
^1H (500 MHz, CDCl_3) and ^{13}C APT (126 MHz, CDCl_3) NMR spectra of **27**



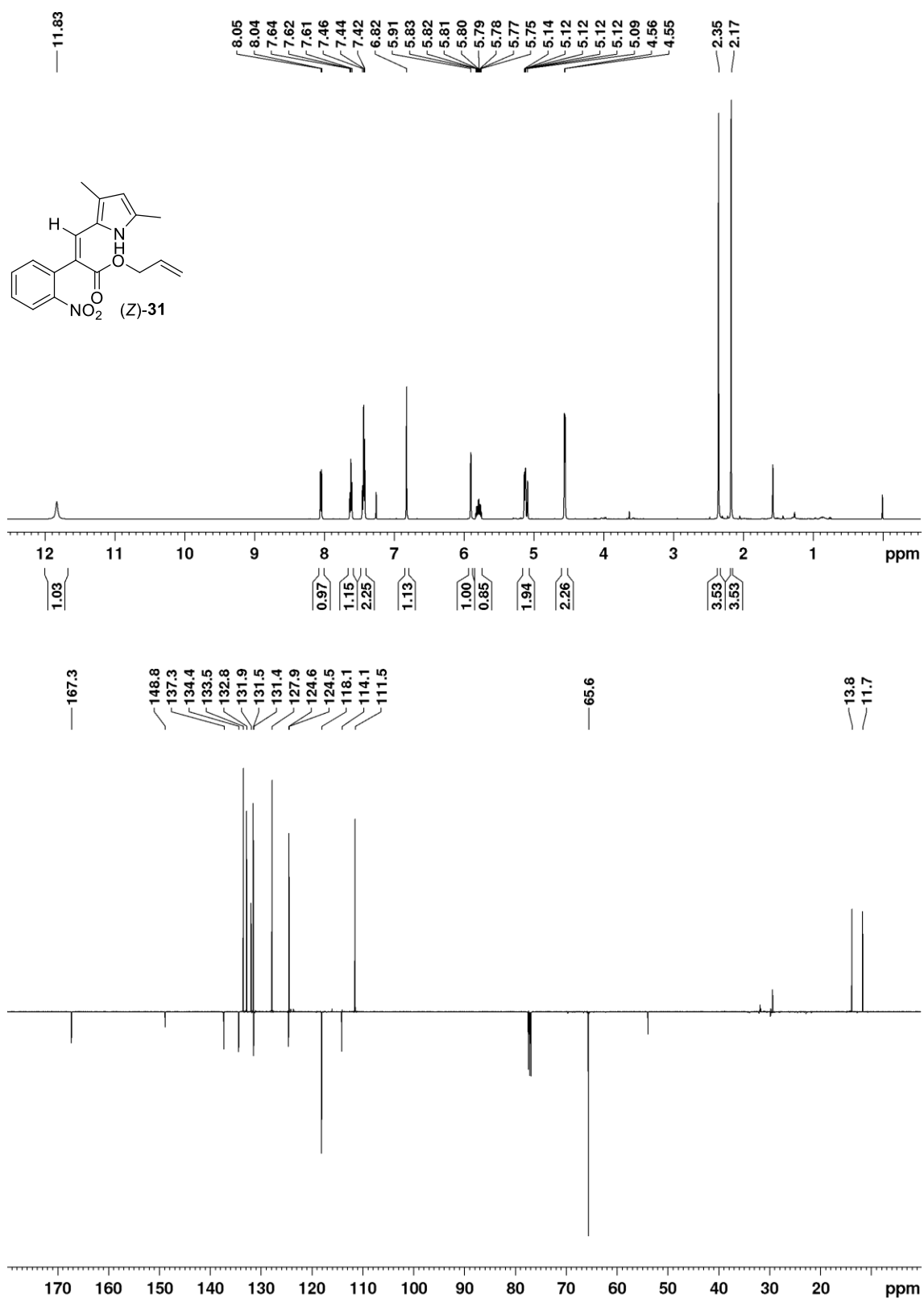
^1H (500 MHz, CDCl_3) and ^{13}C APT (126 MHz, CDCl_3) NMR spectra of **28**



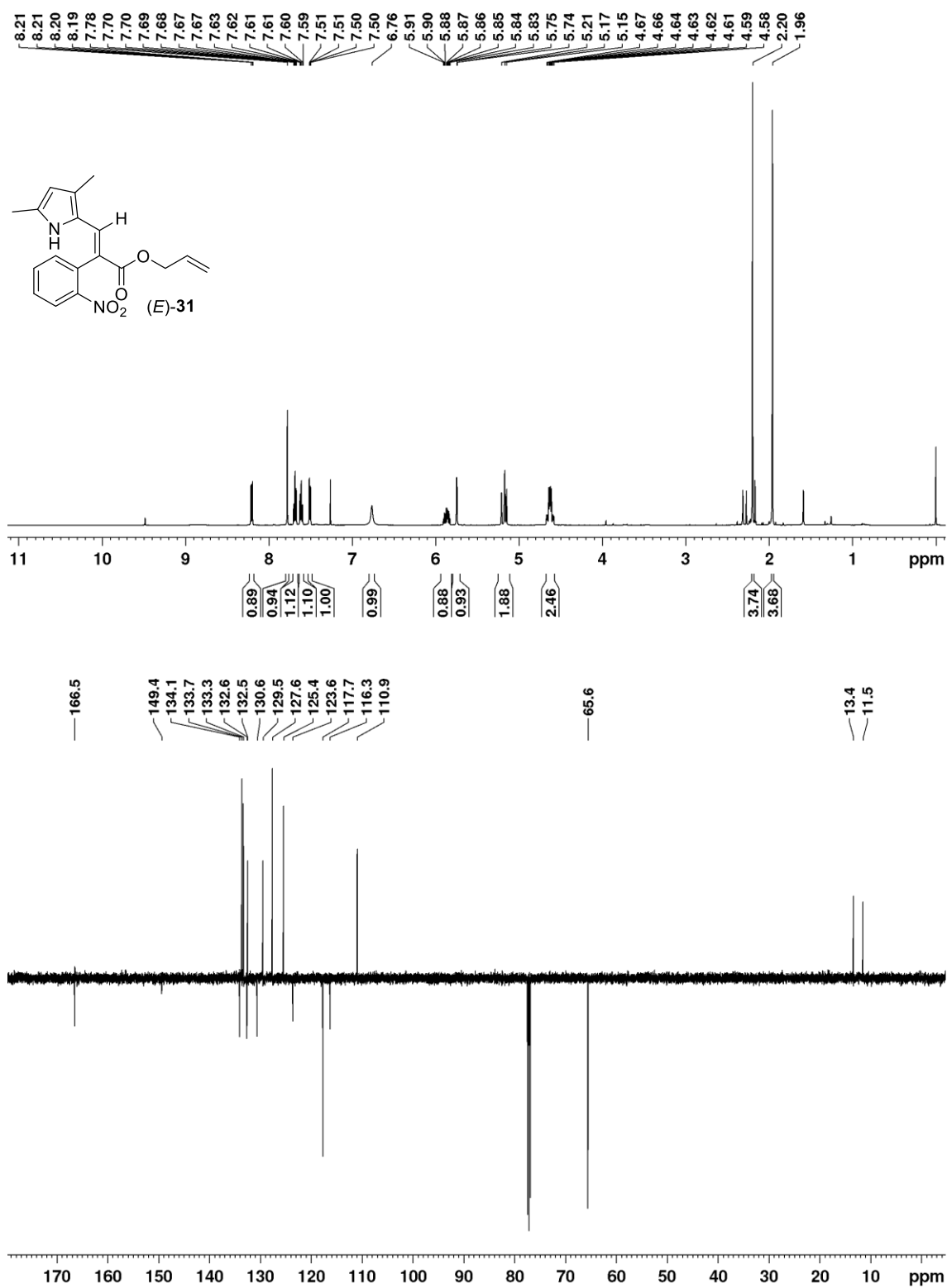
^1H (400 MHz, CDCl_3) and ^{13}C APT (101 MHz, CDCl_3) NMR spectra of **30**



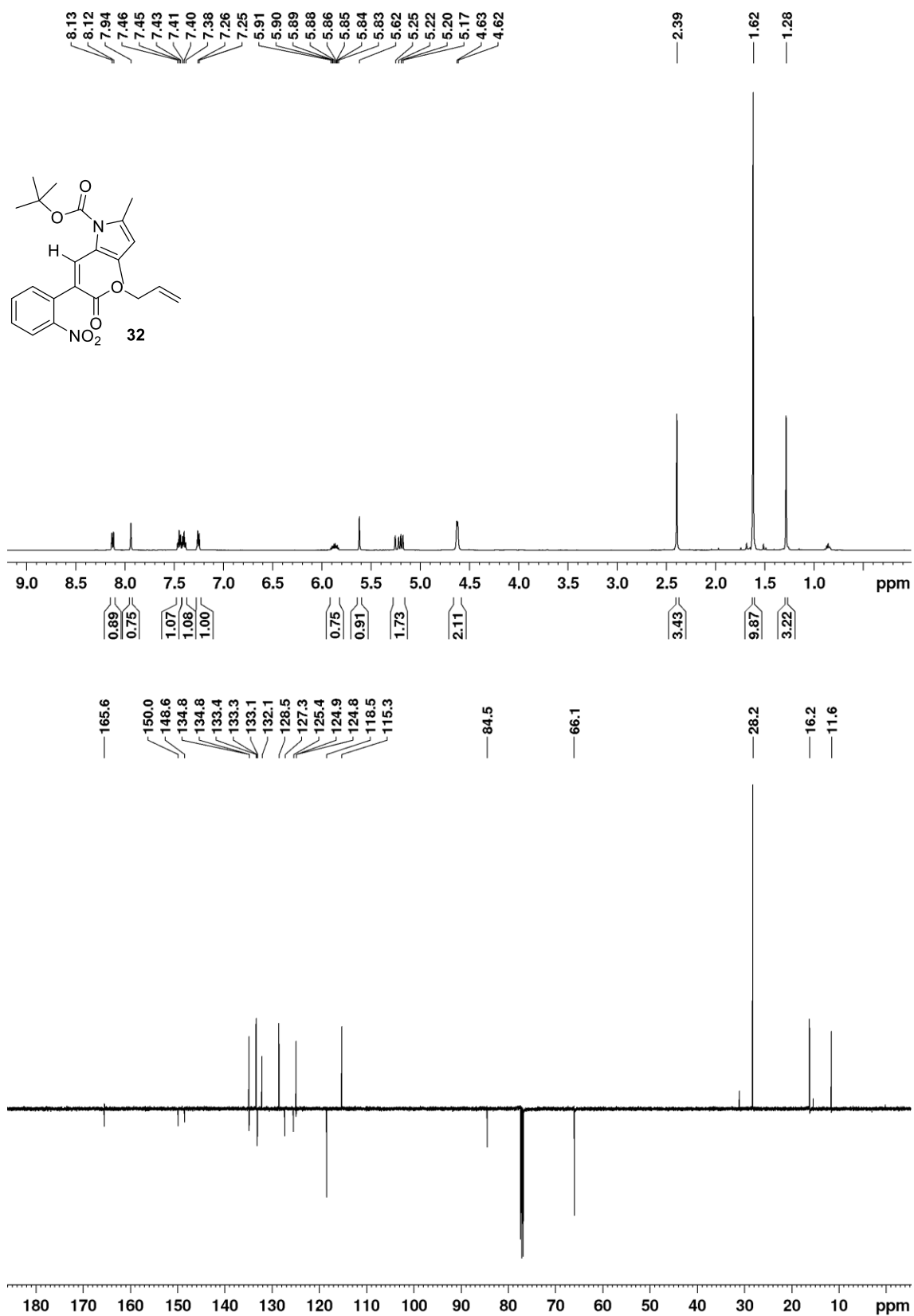
^1H (500 MHz, CDCl_3) and ^{13}C APT (126 MHz, CDCl_3) NMR spectra of (Z)-31



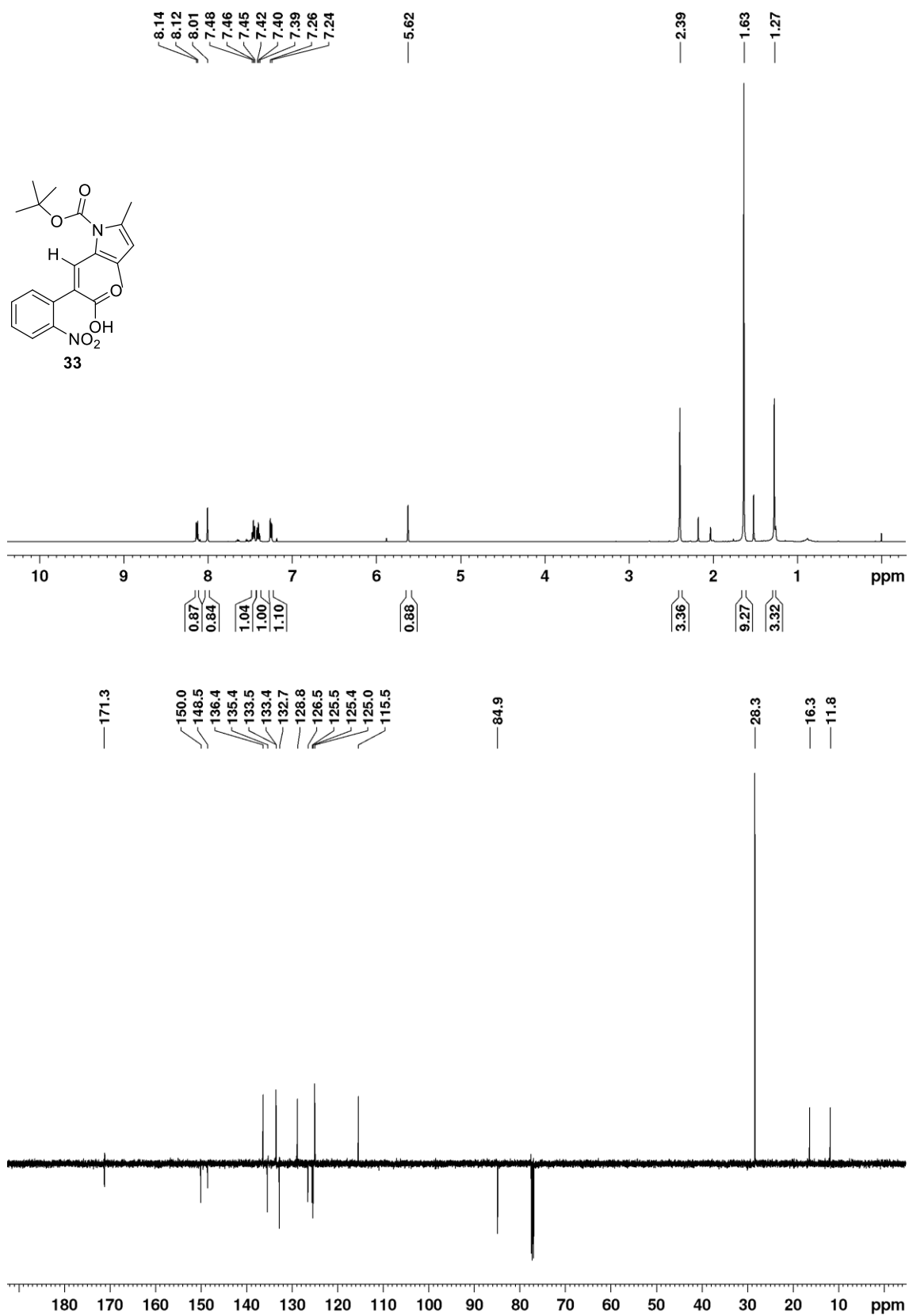
^1H (500 MHz, CDCl_3) and ^{13}C APT (126 MHz, CDCl_3) NMR spectra of (*E*)-**31**



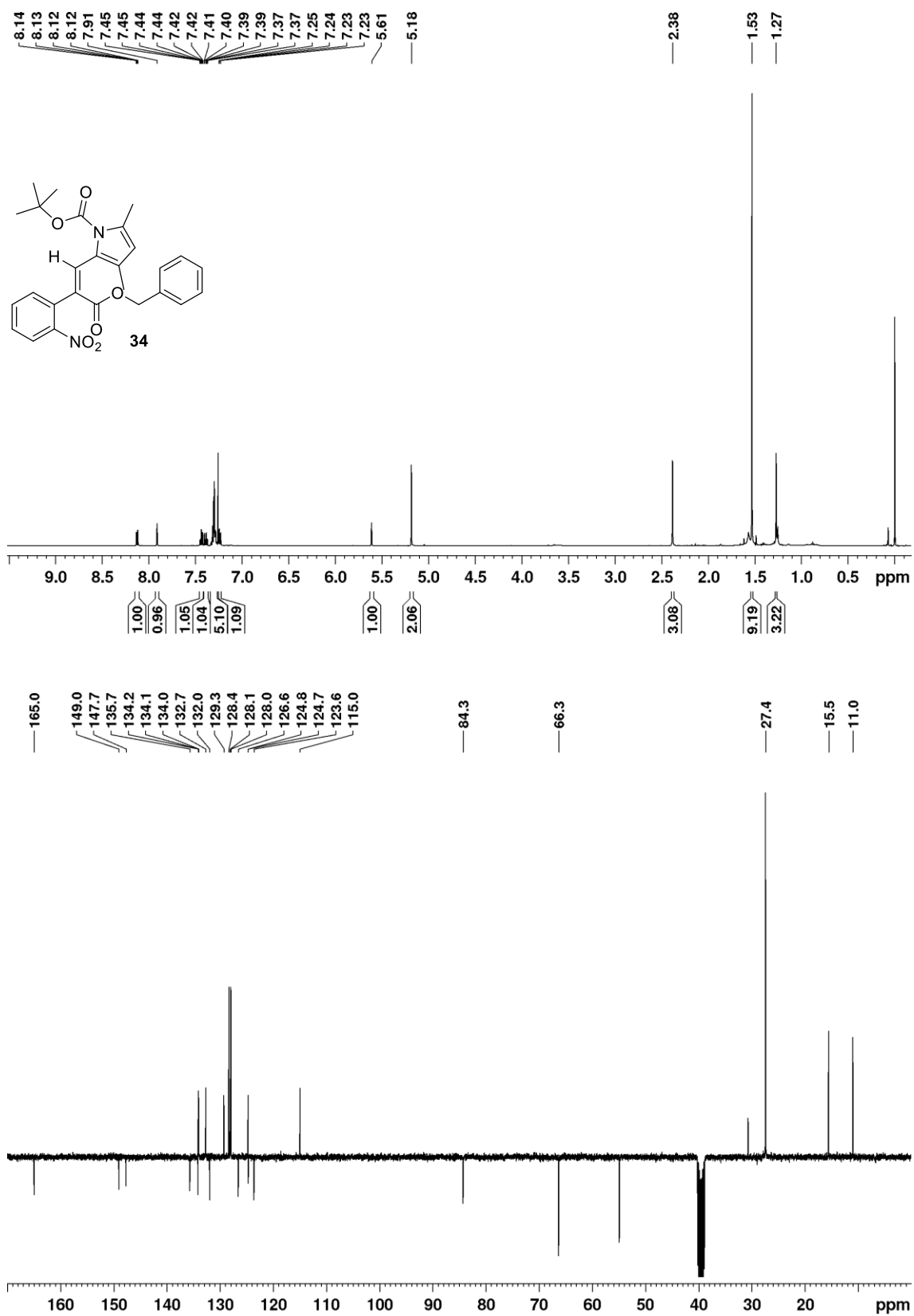
^1H (500 MHz, CDCl_3) and ^{13}C APT (126 MHz, CDCl_3) NMR spectra of **32**



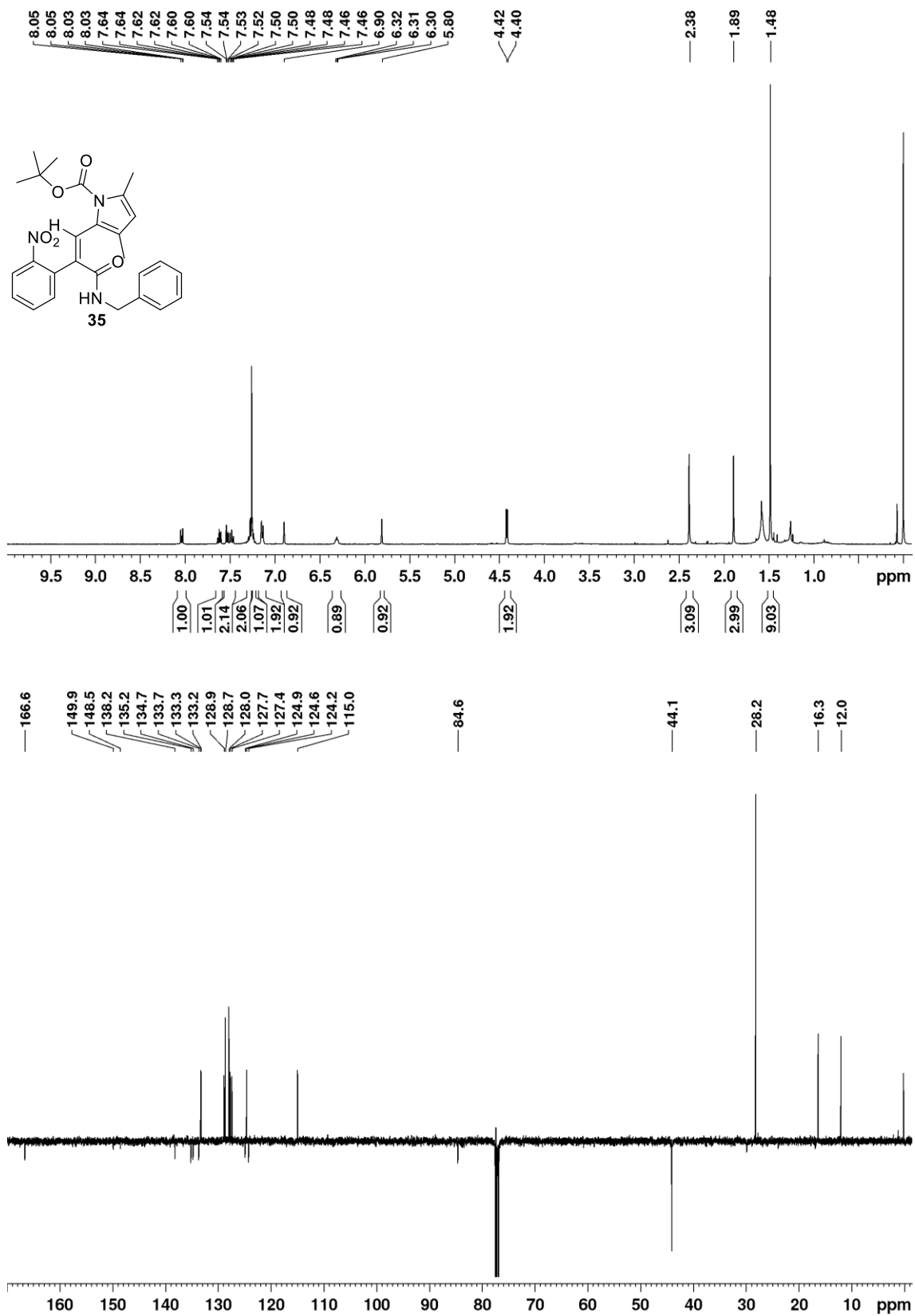
^1H (500 MHz, CDCl_3) and ^{13}C APT (126 MHz, CDCl_3) NMR spectra of **33**



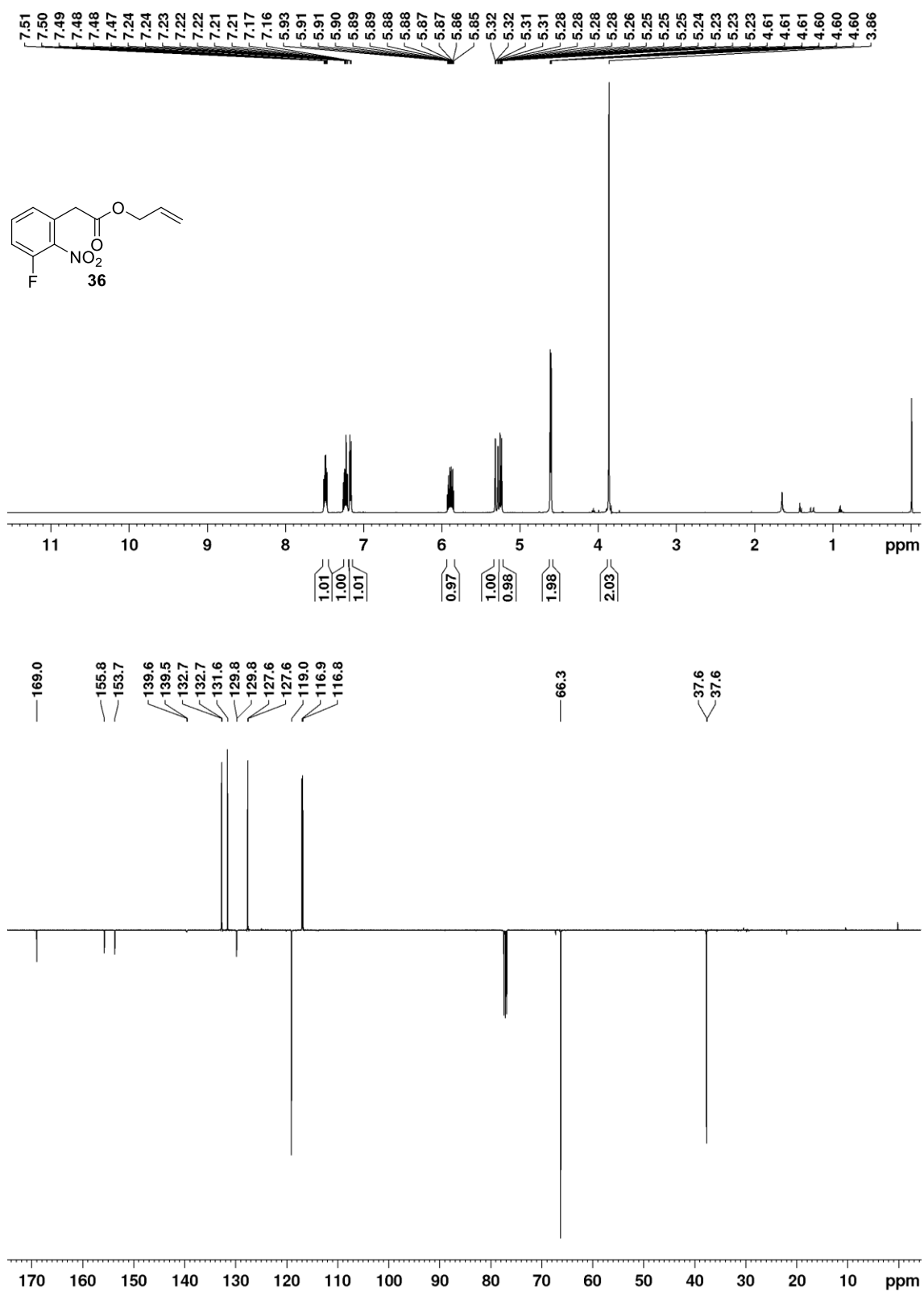
^1H (500 MHz, CDCl_3) and ^{13}C APT (101 MHz, d_6 -DMSO) NMR spectra of **34**



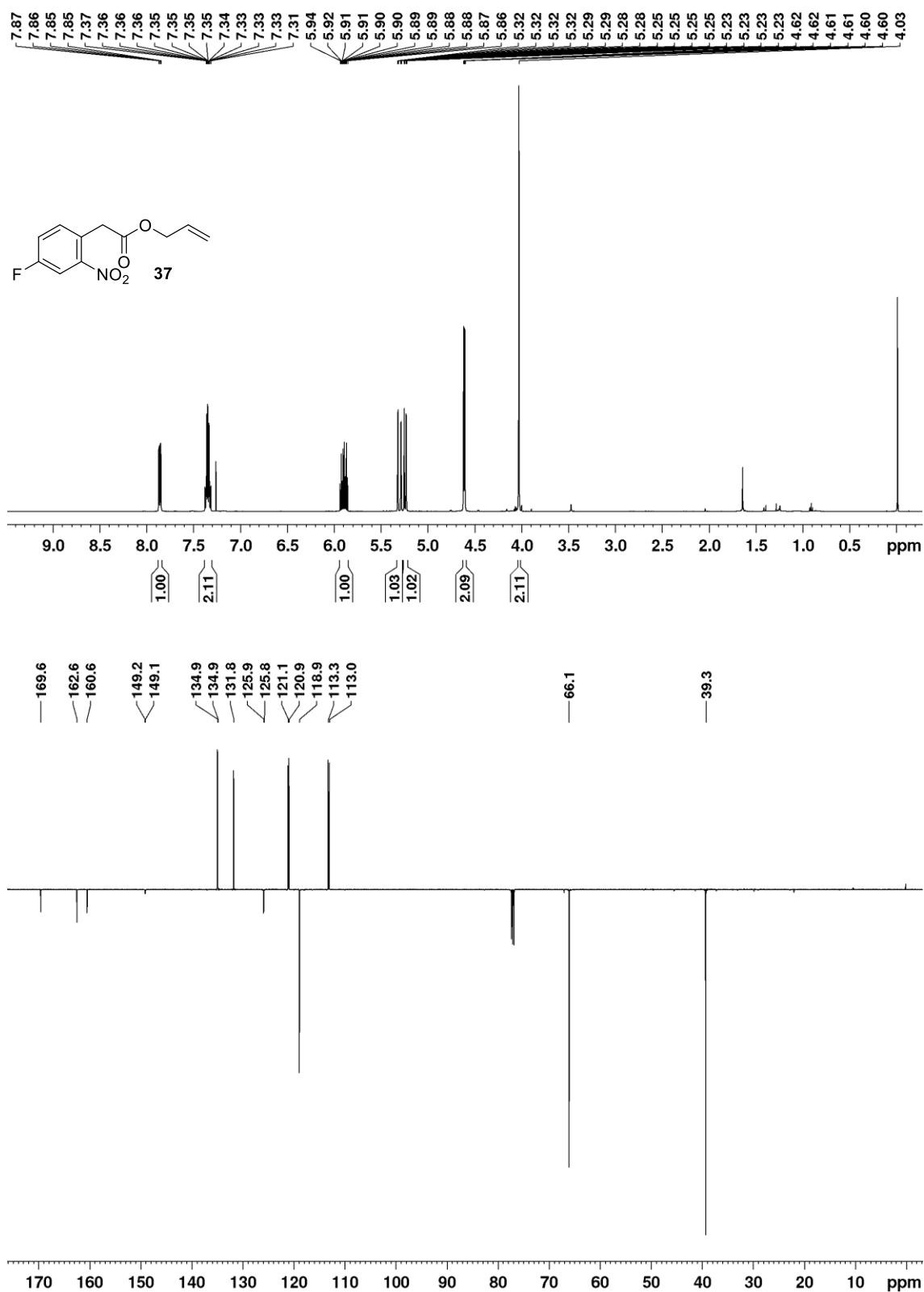
^1H (500 MHz, CDCl_3) and ^{13}C APT (CDCl_3) NMR spectra of **35**



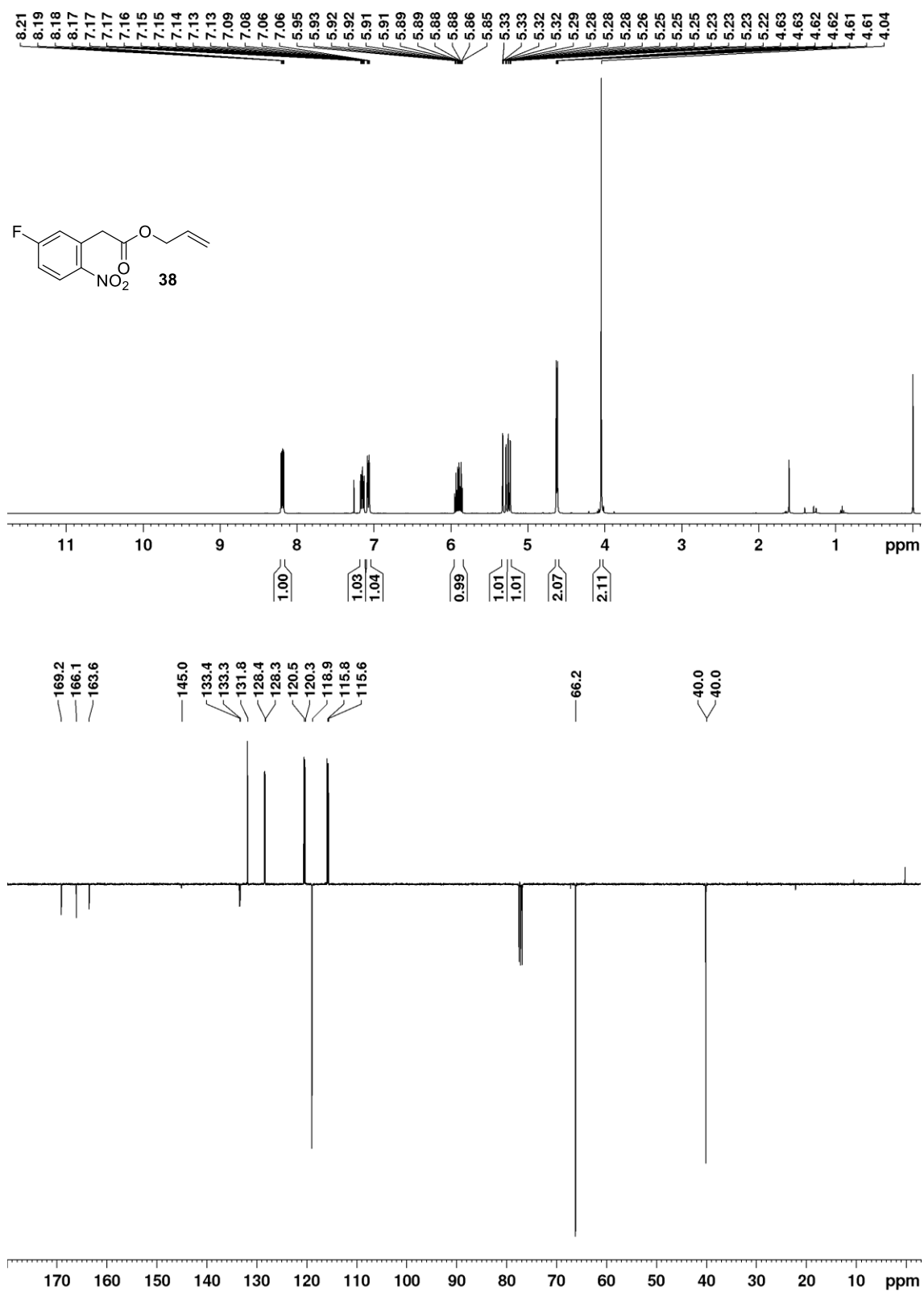
^1H (500 MHz, CDCl_3) and ^{13}C APT (126 MHz, CDCl_3) NMR spectra of **36**



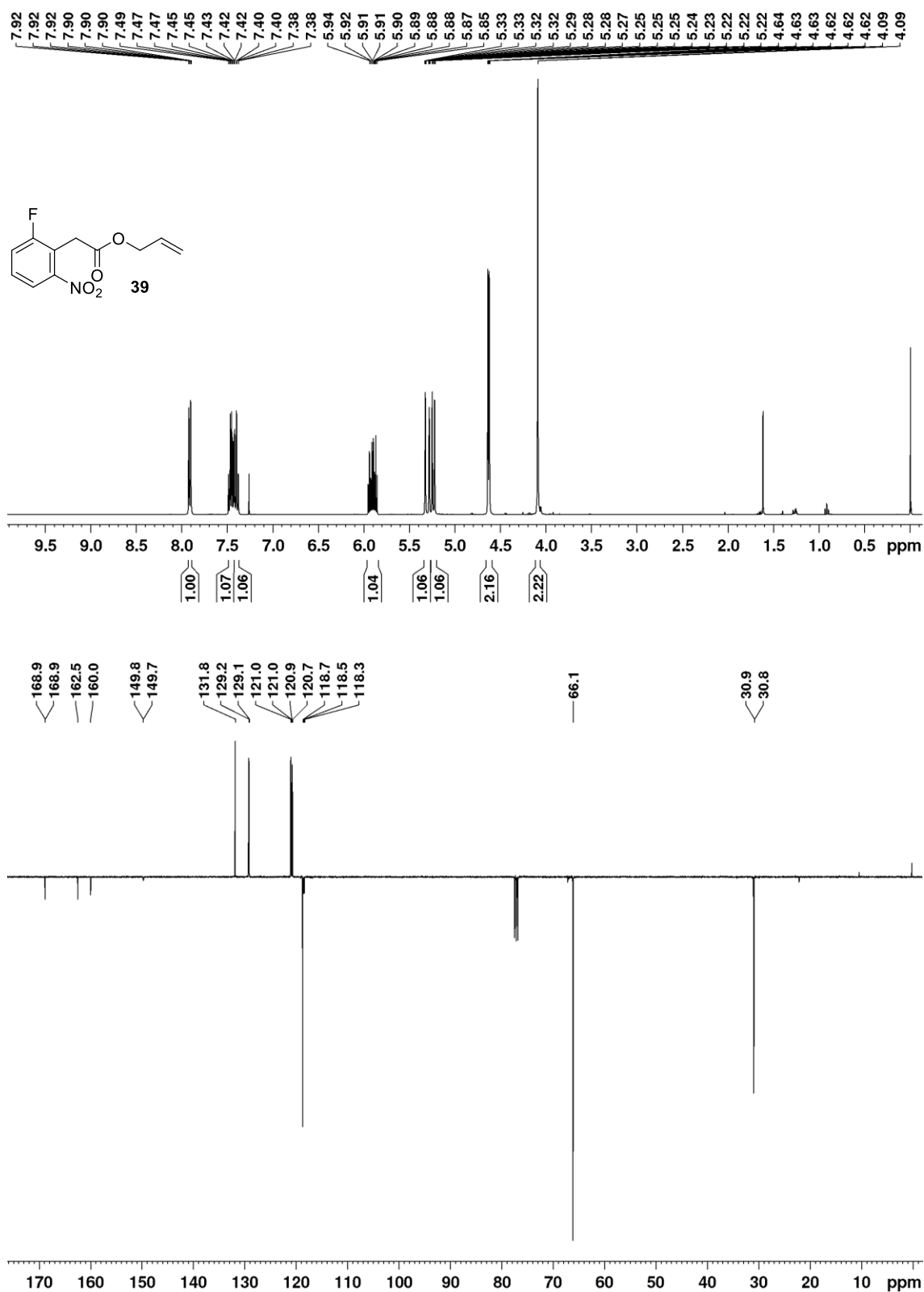
^1H (500 MHz, CDCl_3) and ^{13}C APT (126 MHz, CDCl_3) NMR spectra of **37**



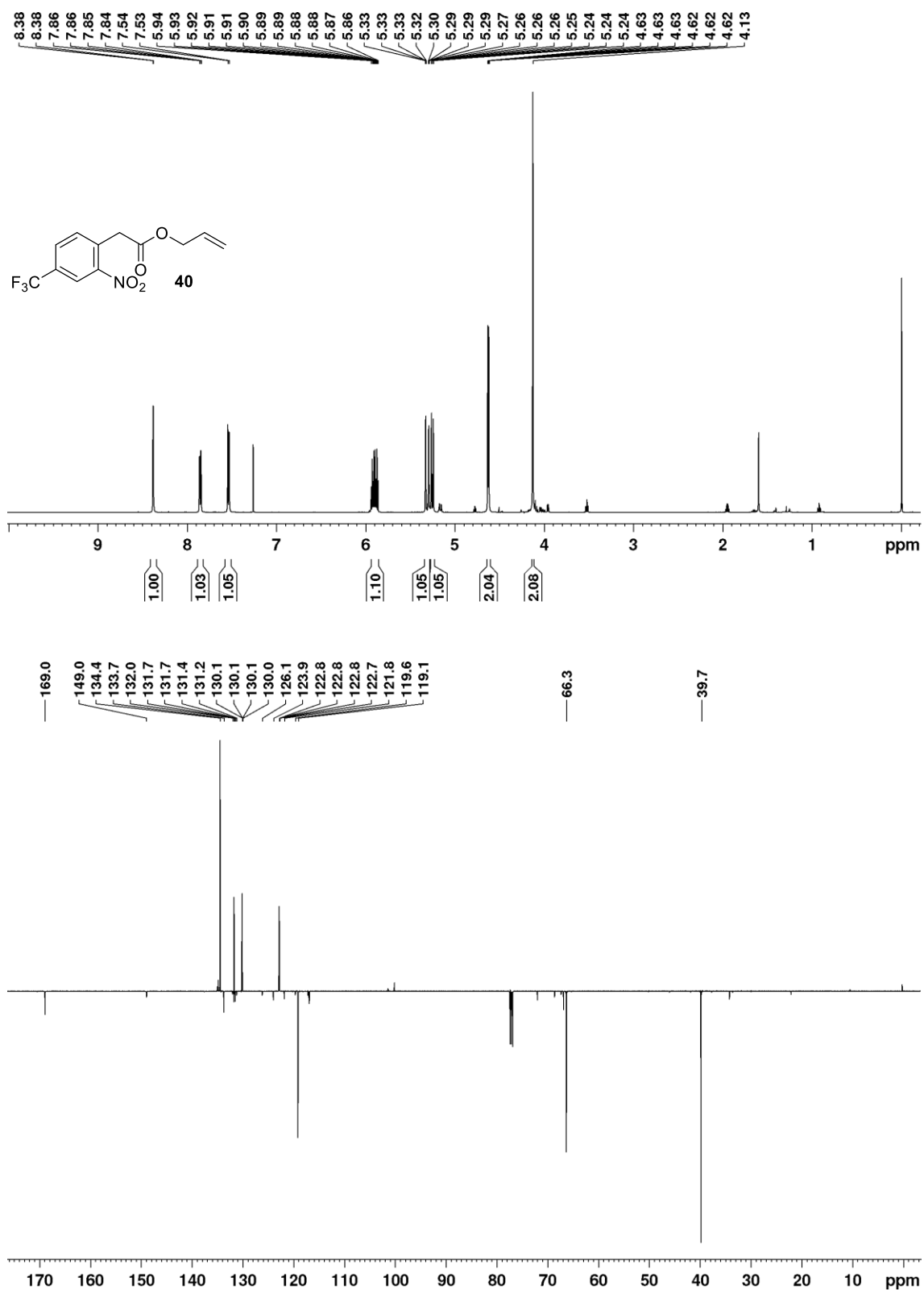
^1H (400 MHz, CDCl_3) and ^{13}C APT (101 MHz, CDCl_3) NMR spectra of **38**



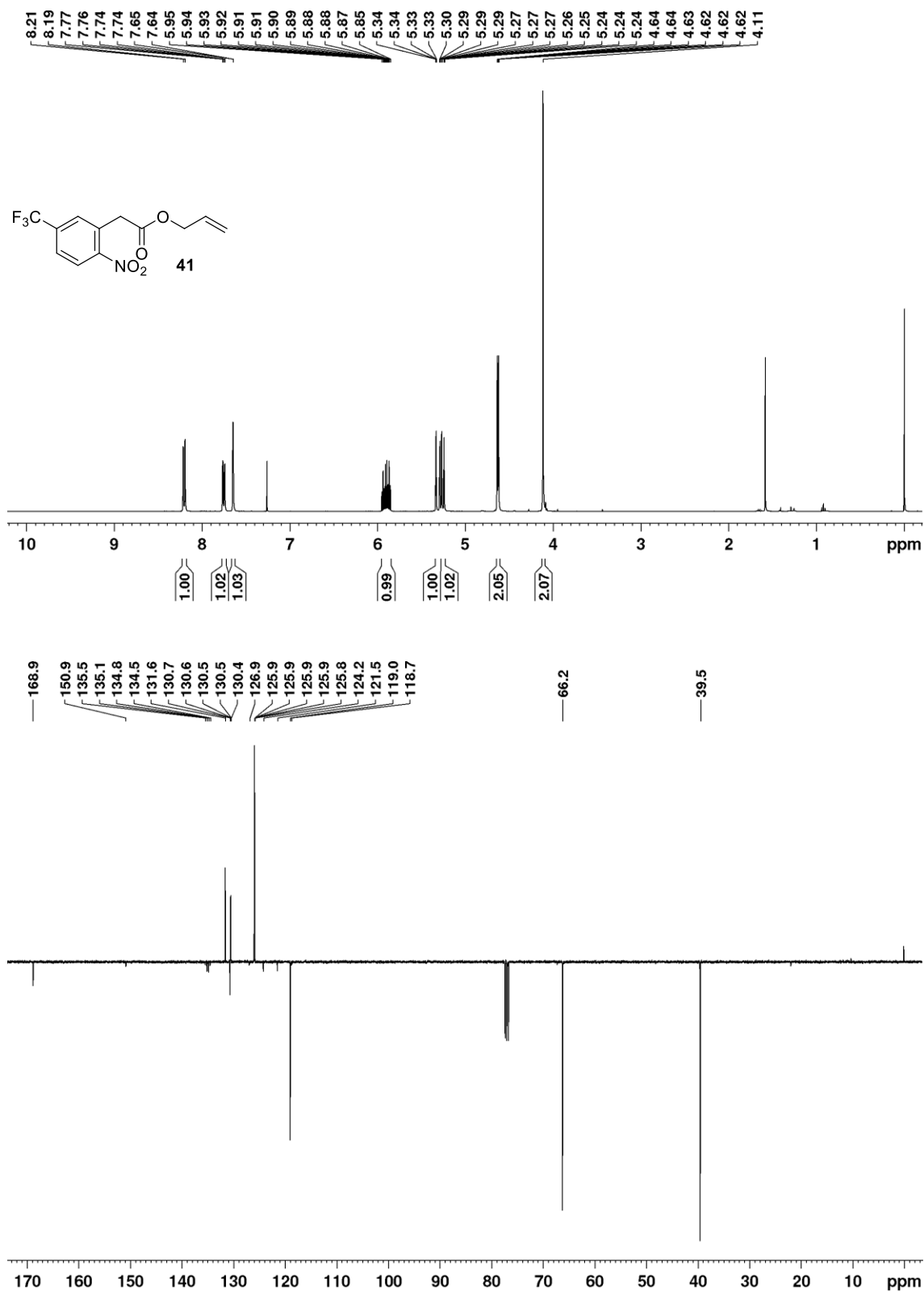
^1H (400 MHz, CDCl_3) and ^{13}C APT (101 MHz, CDCl_3) NMR spectra of **39**

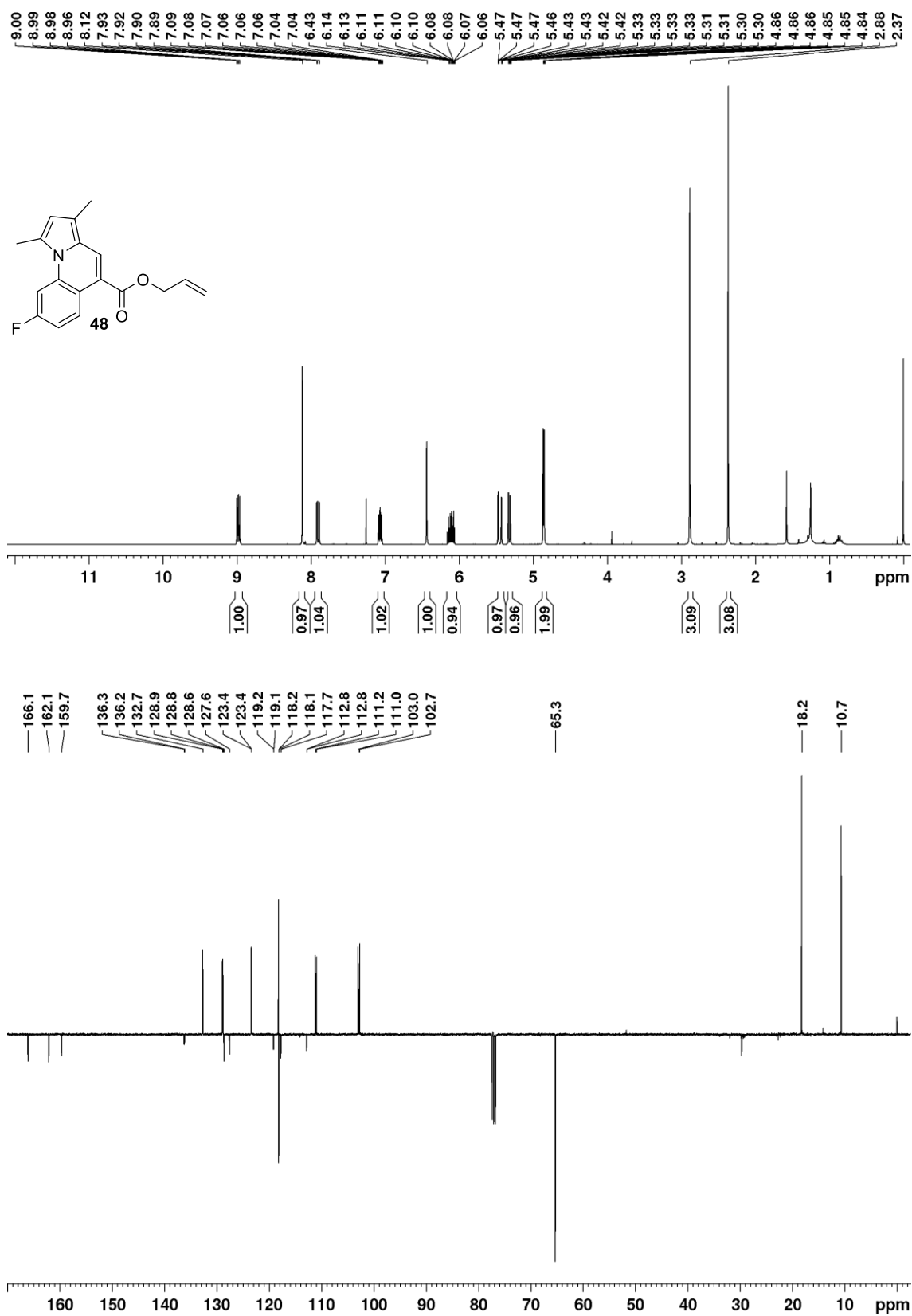


^1H (500 MHz, CDCl_3) and ^{13}C APT (126 MHz, CDCl_3) NMR spectra of **40**

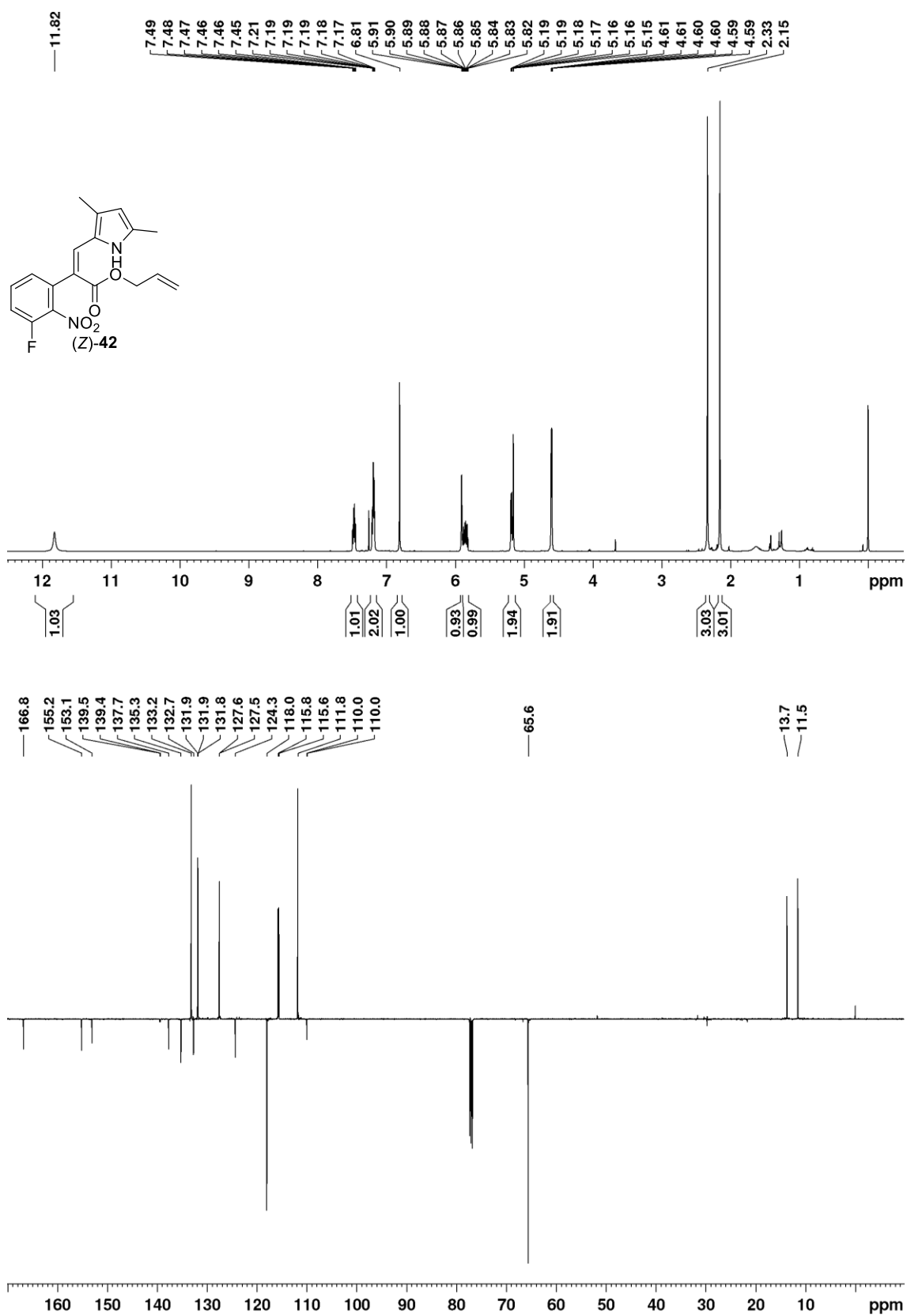


^1H (400 MHz, CDCl_3) and ^{13}C APT (101 MHz, CDCl_3) NMR spectra of **41**

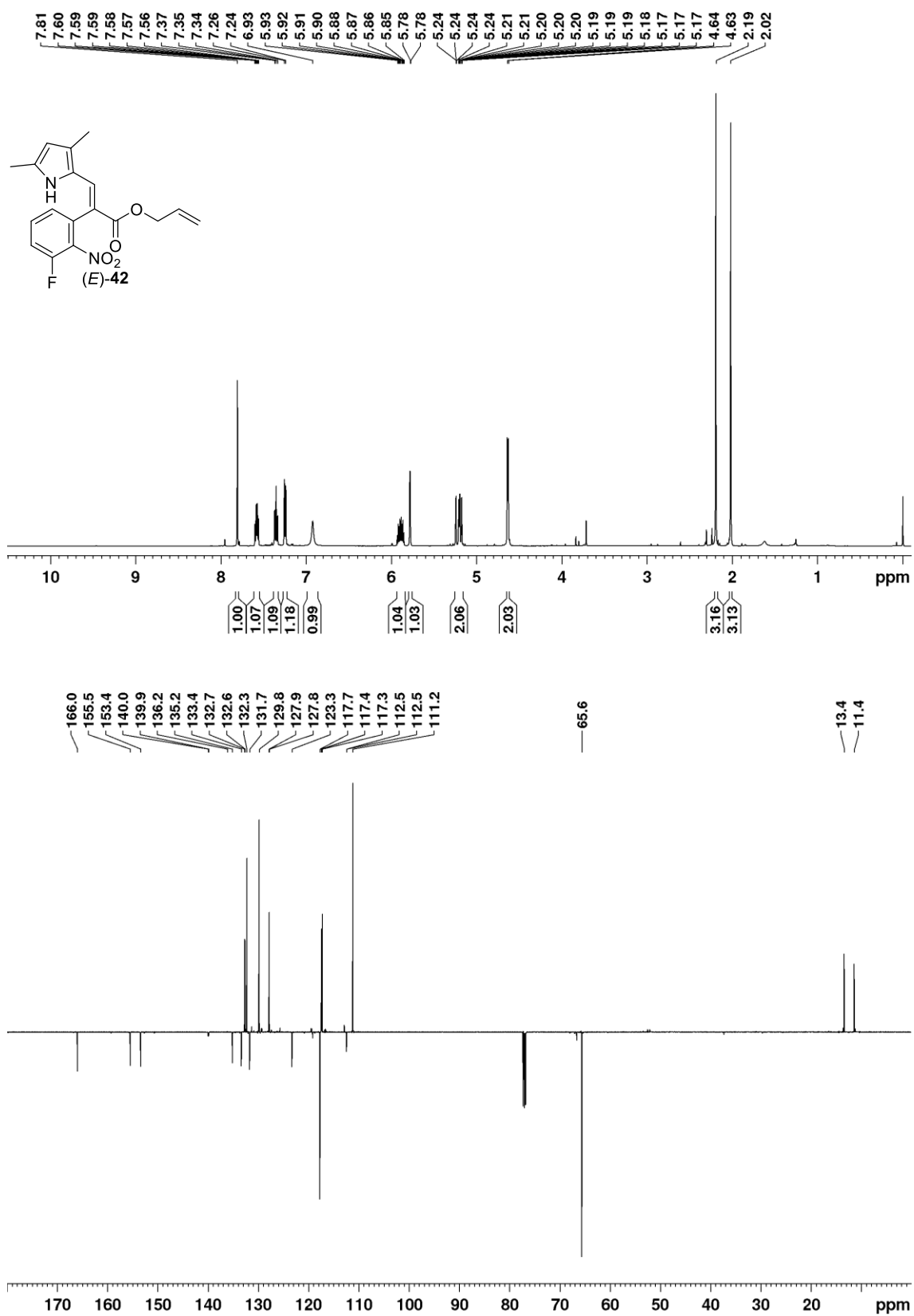


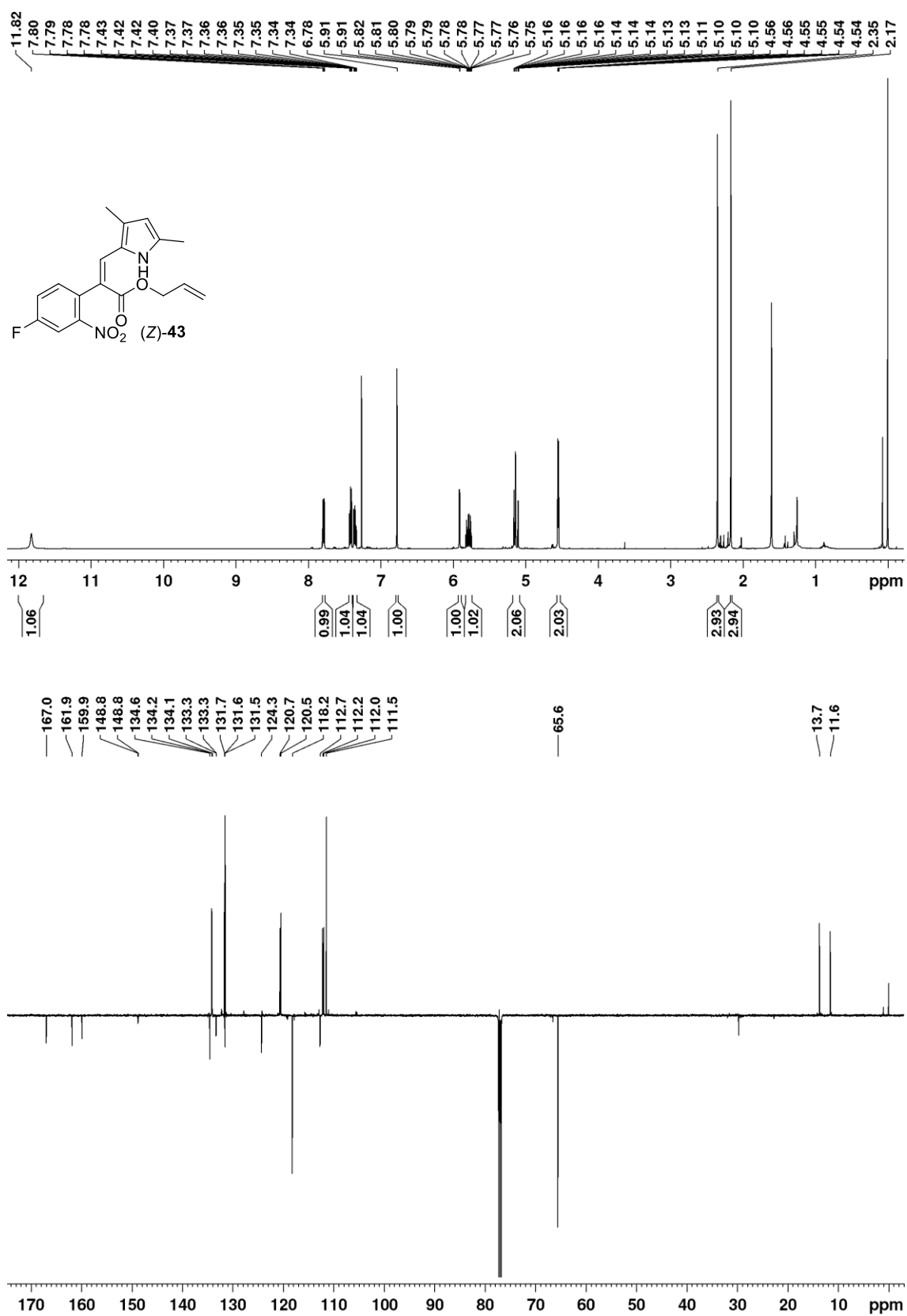
^1H (400 MHz, CDCl_3) and ^{13}C APT (101 MHz, CDCl_3) NMR spectra of **48**

^1H (500 MHz, CDCl_3) and ^{13}C APT (126 MHz, CDCl_3) NMR spectra of (Z)-42

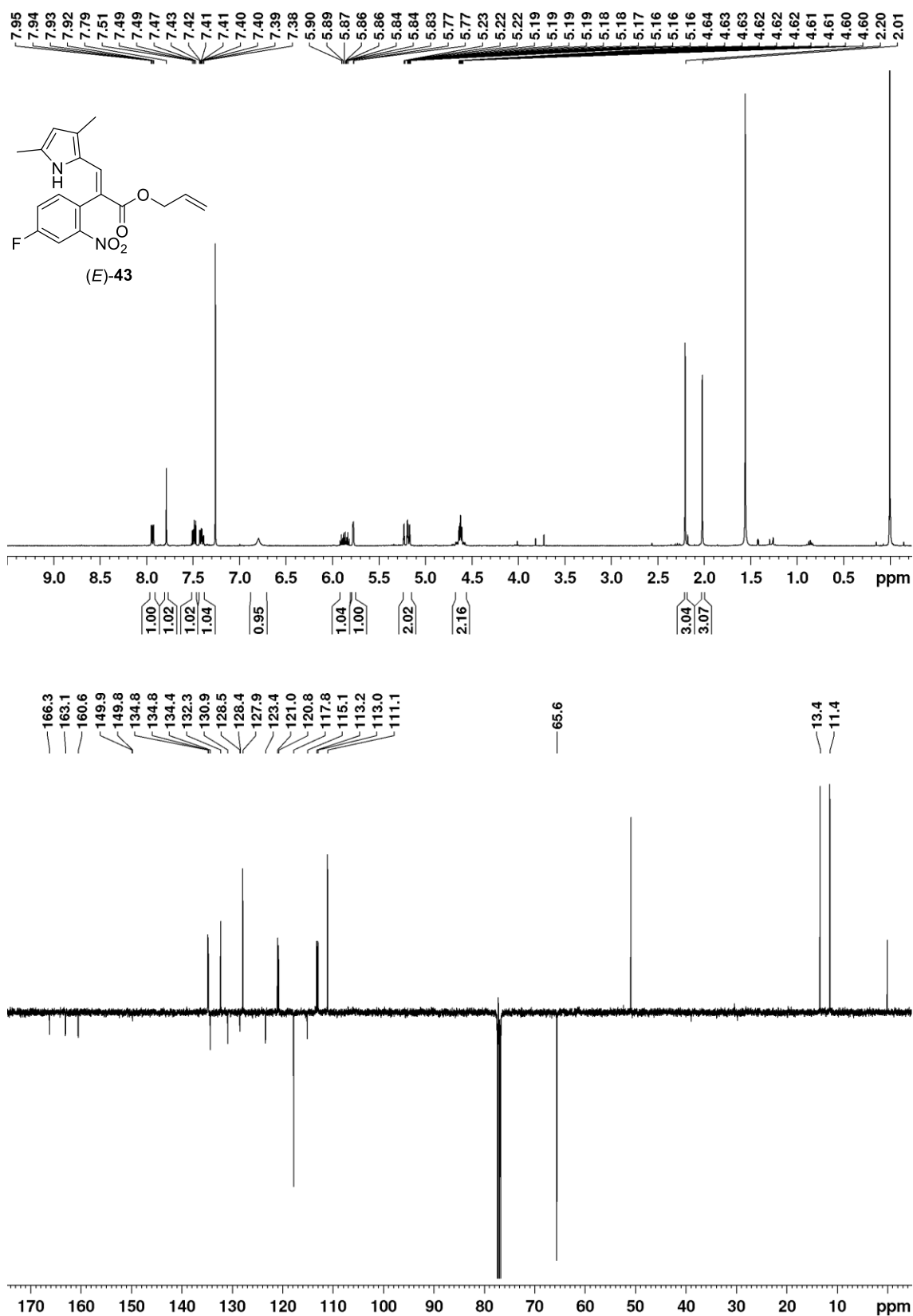


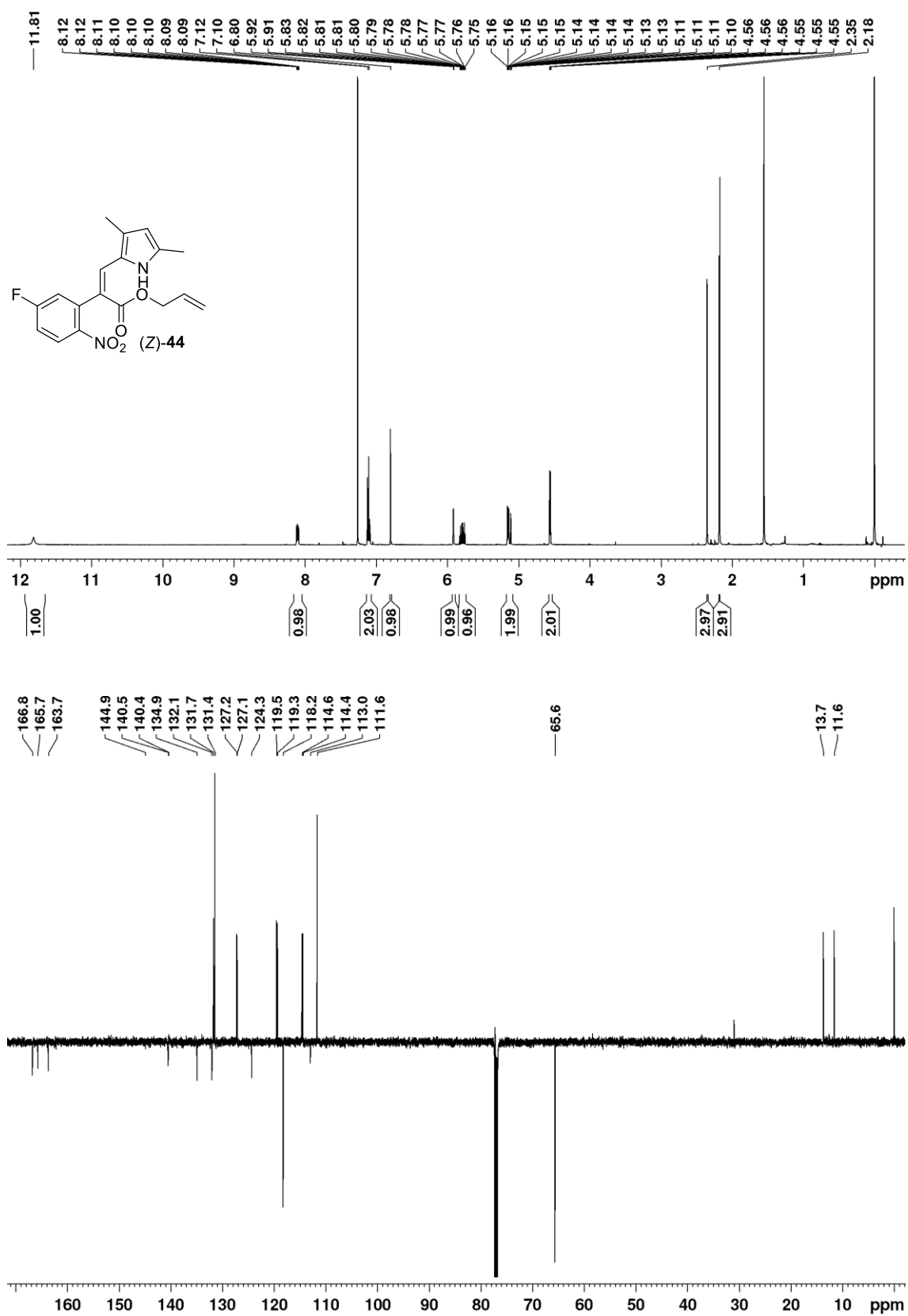
^1H (500 MHz, CDCl_3) and ^{13}C APT (126 MHz, CDCl_3) NMR spectra of (*E*)-**42**



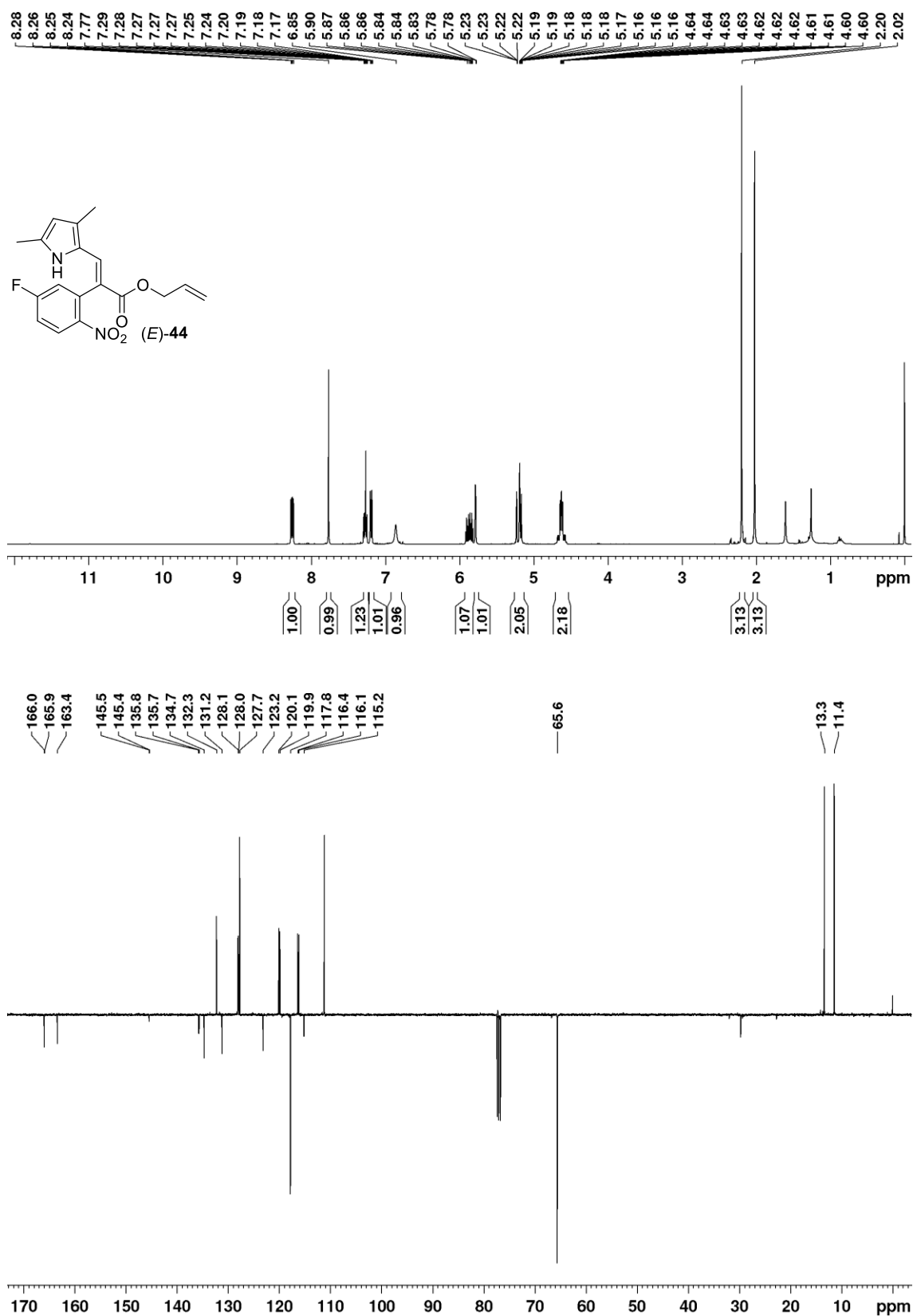
^1H (500 MHz, CDCl_3) and ^{13}C APT (126 MHz, CDCl_3) NMR spectra of (Z)-43

^1H (400 MHz, CDCl_3) and ^{13}C APT (101 MHz, CDCl_3) NMR spectra of (*E*)-**43**

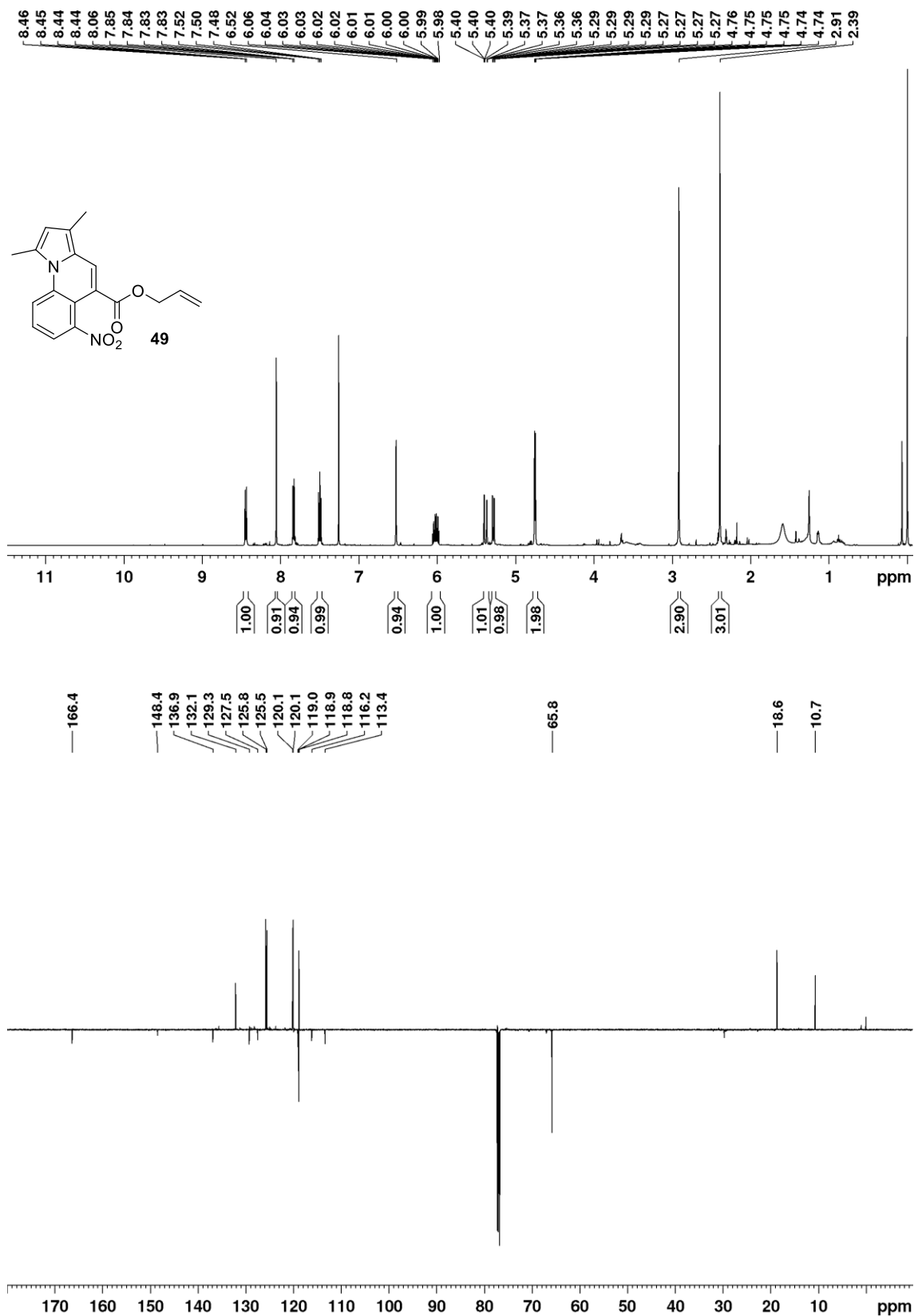


^1H (500 MHz, CDCl_3) and ^{13}C APT (126 MHz, CDCl_3) NMR spectra of (Z)-44

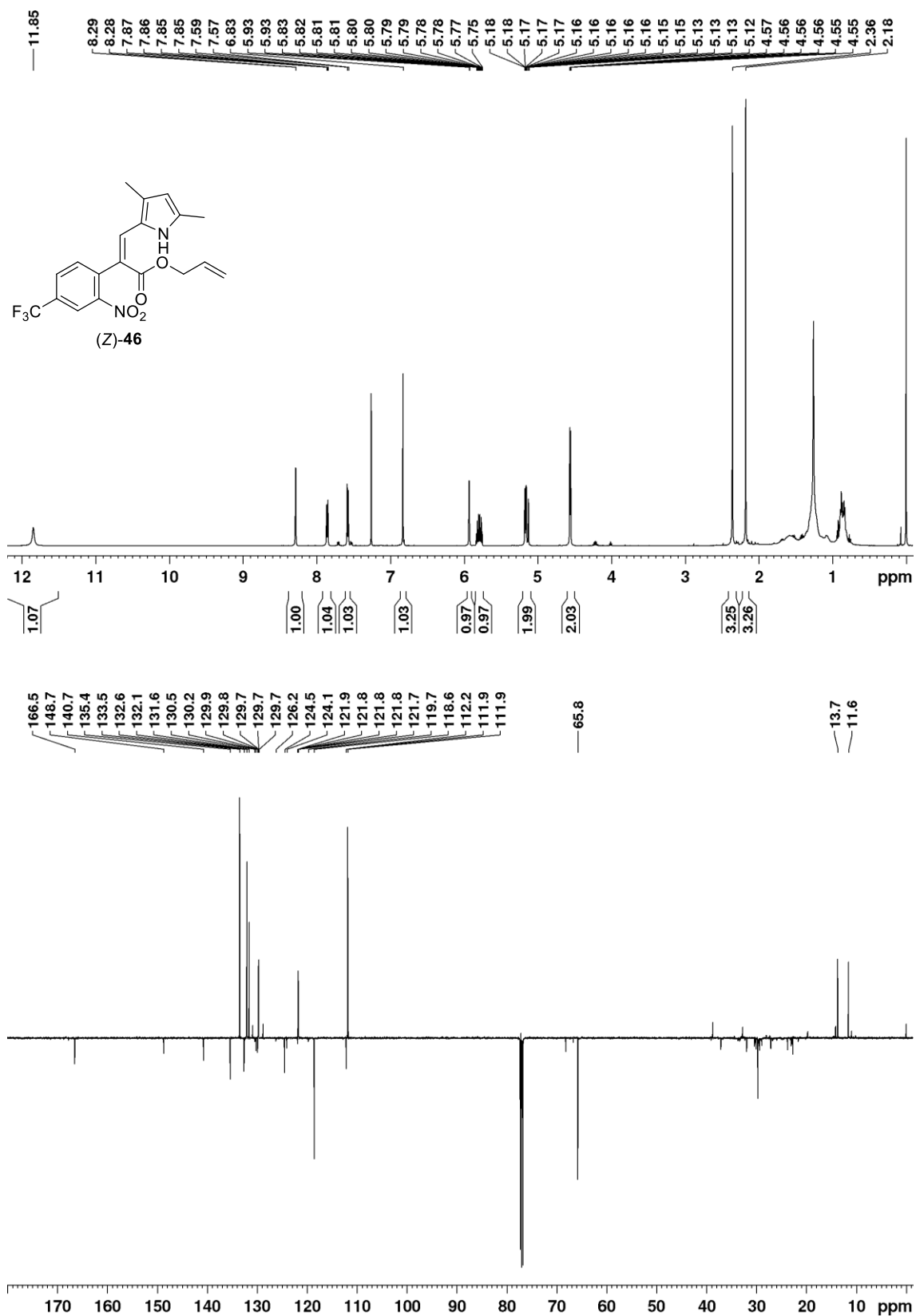
^1H (400 MHz, CDCl_3) and ^{13}C APT (101 MHz, CDCl_3) NMR spectra of (*E*)-**44**



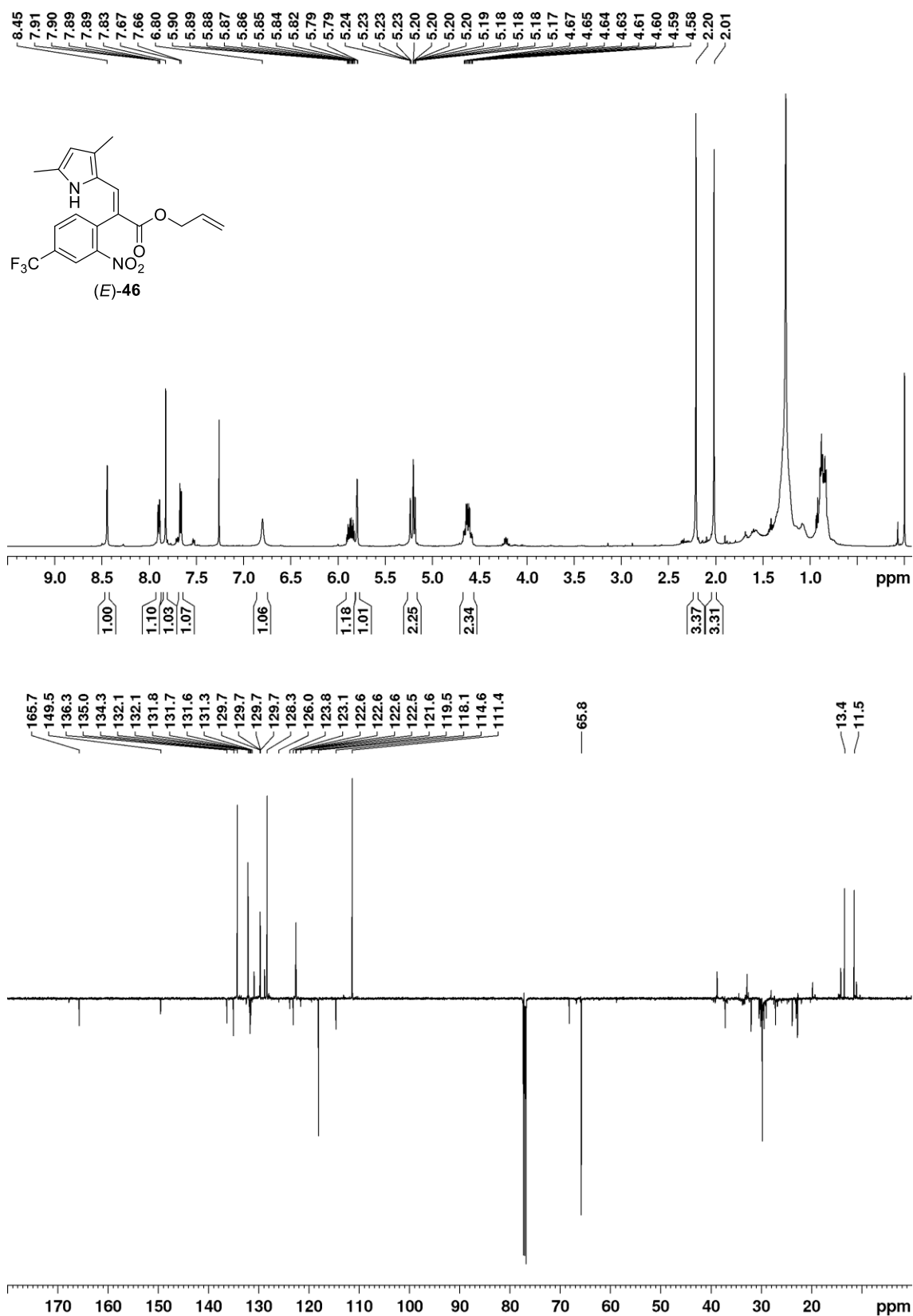
^1H (500 MHz, CDCl_3) and ^{13}C APT (126 MHz, CDCl_3) NMR spectra of **49**



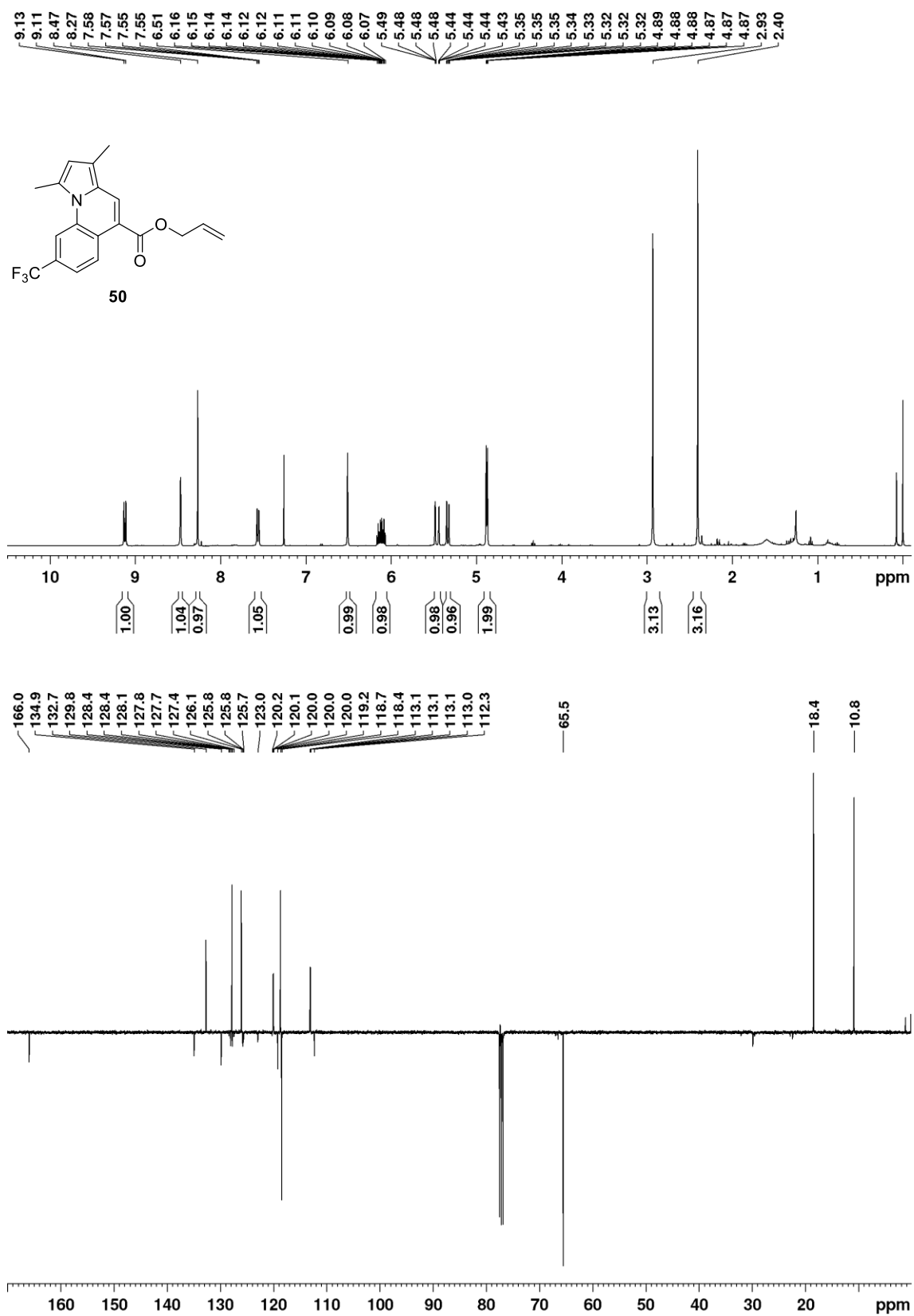
^1H (500 MHz, CDCl_3) and ^{13}C APT (126 MHz, CDCl_3) NMR spectra of (Z)-46



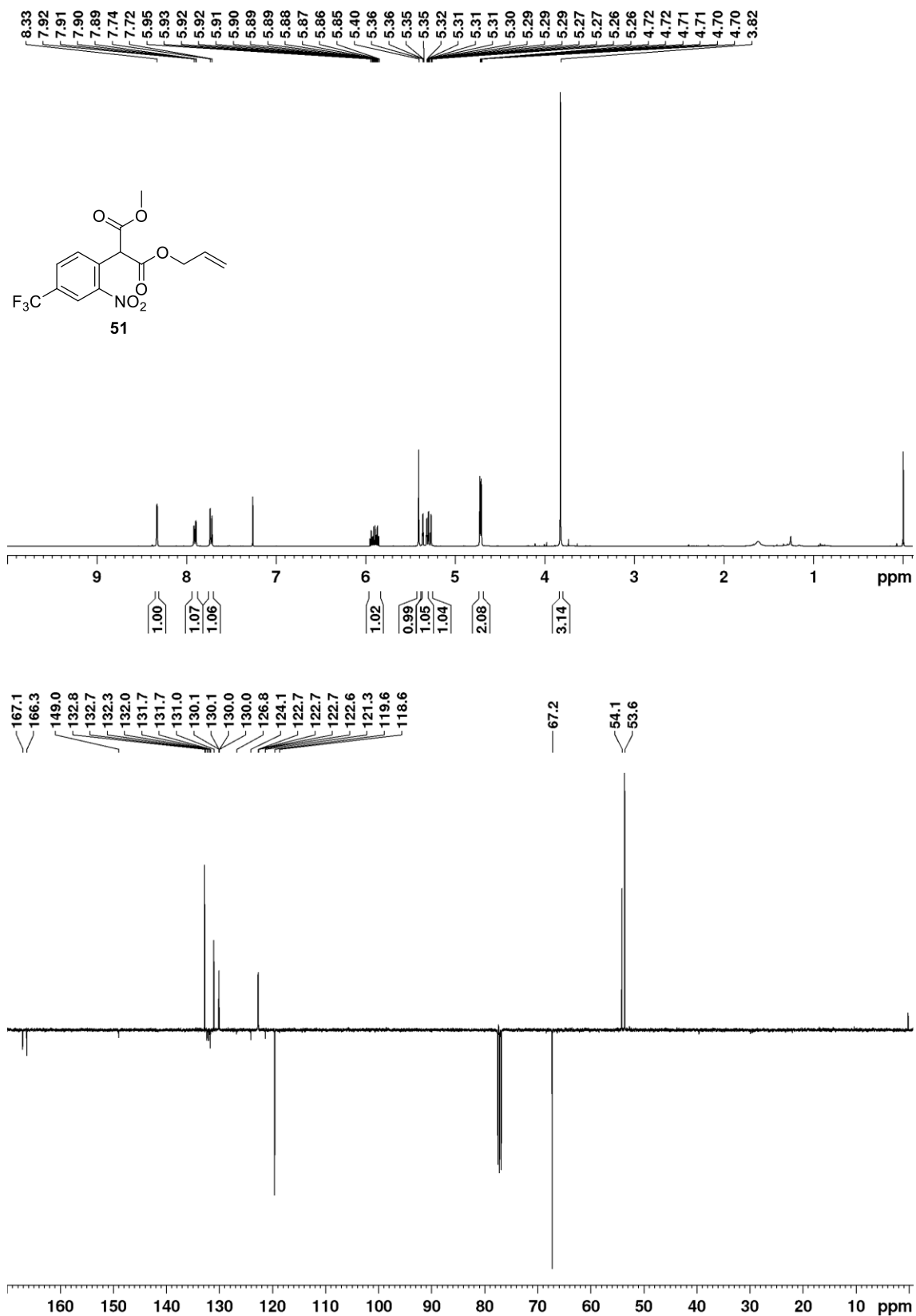
^1H (500 MHz, CDCl_3) and ^{13}C APT (126 MHz, CDCl_3) NMR spectra of (*E*)-46



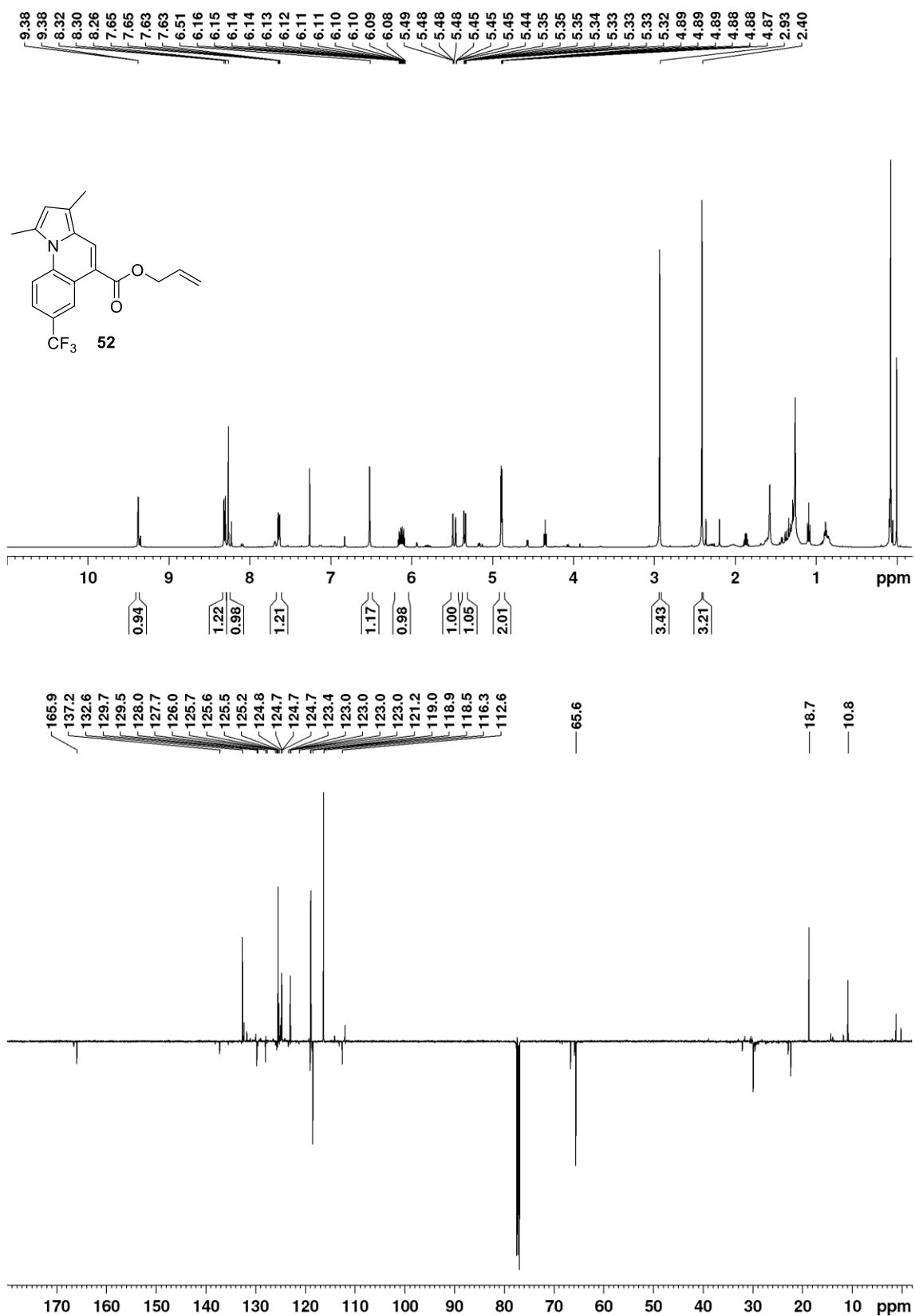
^1H (400 MHz, CDCl_3) and ^{13}C APT (101 MHz, CDCl_3) NMR spectra of **50**



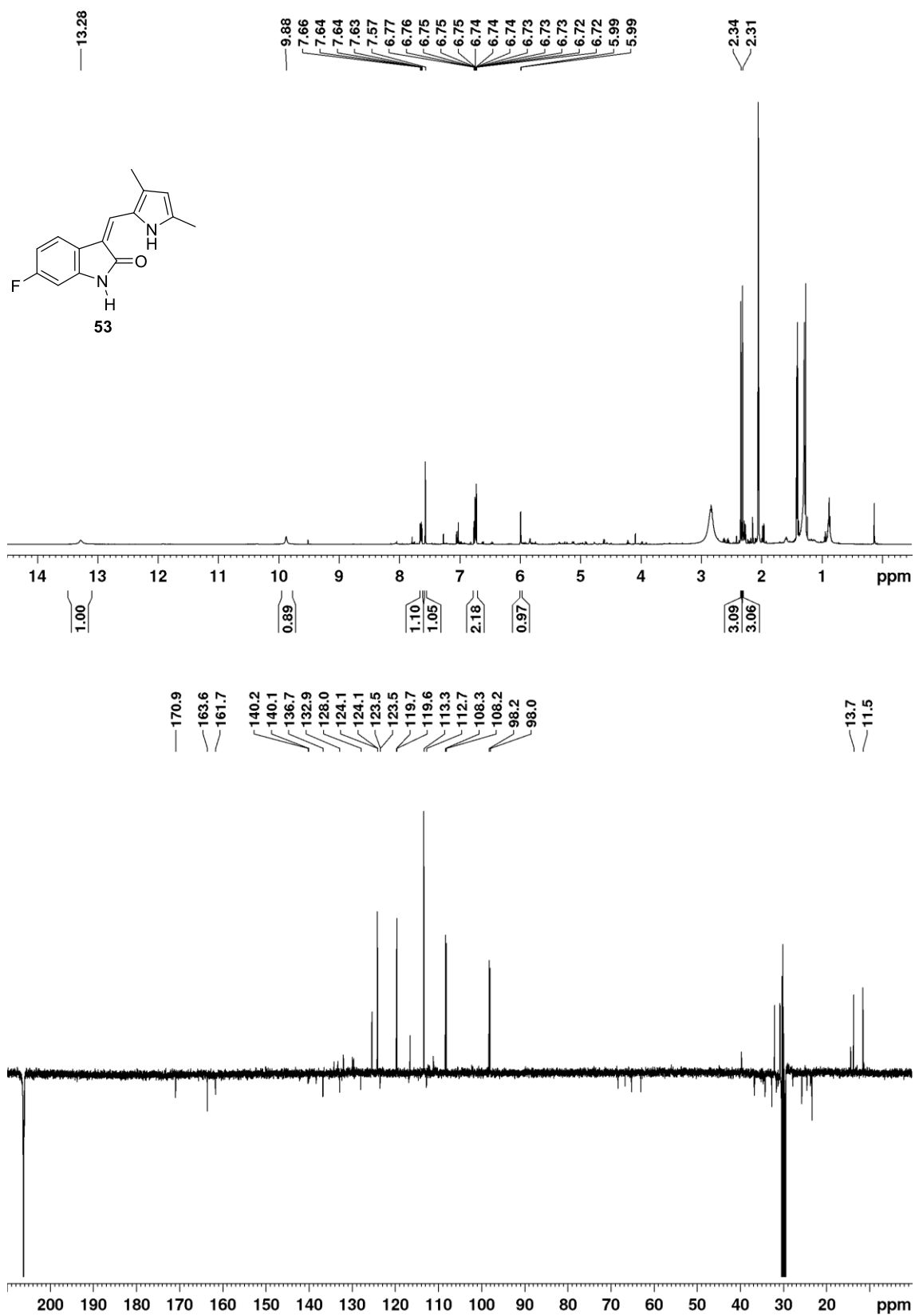
^1H (400 MHz, CDCl_3) and ^{13}C APT (101 MHz, CDCl_3) NMR spectra of **51**



^1H (500 MHz, CDCl_3) and ^{13}C APT (126 MHz, CDCl_3) NMR spectra of **52**



^1H (500 MHz, d_6 -Acetone) and ^{13}C APT (126 MHz, d_6 -Acetone) NMR spectra of **53**



^1H (400 MHz, d_6 -Acetone) and ^{13}C APT (101 MHz, d_6 -Acetone) NMR spectra of **54**

